3rd International Workshop on Coal Pillar Mechanics and Design

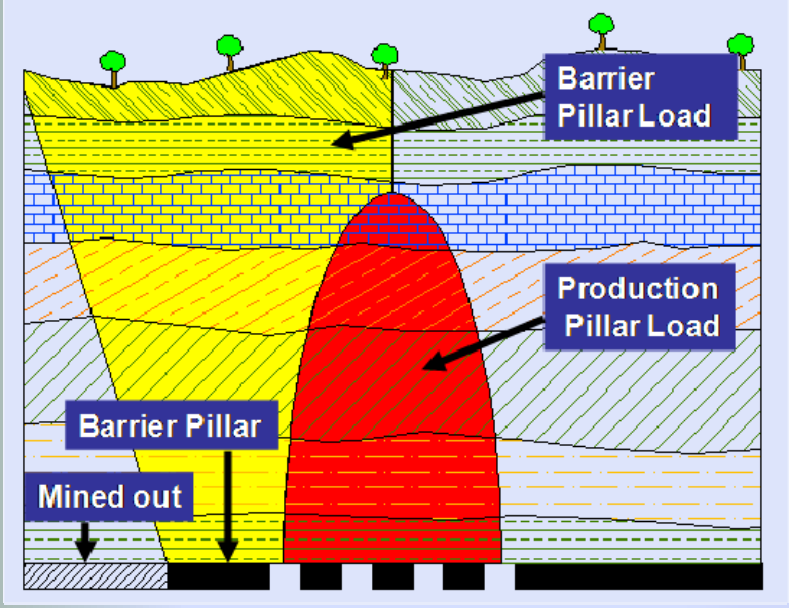

Morgantown, WV
July 26, 2010

Sponsor:

U.S. National Institute for Occupational Safety & Health

TABLE OF CONTENTS

Analytical Design Procedure Using the Wilson Equation

Vincent A. Scovazzo, Director of Geotechnical Services
John T. Boyd Company
Richland, WA

INTRODUCTION

The analytical pillar design procedure employing the Wilson equation is based on the site-specific material strength of the floor, pillar, and roof rock. Stable pillars so designed will sometimes be larger than those designed using empirical methods thus providing more stability or at other times smaller than empirically designed pillars thus conserving natural resources. Presented here is a detailed procedure for the analytical design of soft rock pillars using the Wilson equation. An example of this procedure is presented that uses data from a mine in the Owl Seam in Southern Appalachia. These Owl Seam pillars are now in use and are performing as expected. Also addressed is an assessment of the Dr. Scovazzo's analytically designed pillars based on pillar performance data gathered by Dr. Mark in the Southern Appalachian Coal Field.

PILLAR DESIGN PROCEDURE

Because of the reliance of analytical designs on accurate mechanical properties and the potential variation of rock and coal material properties that can be introduced at several stages of drilling, sample shipping, and testing, the highest standards must be adhered to during these steps. The design procedure includes the following steps:

1. Drilling, logging, selecting, preservation, and shipping of core samples.
2. Laboratory mechanical testing of roof, pillar, and floor rock.
3. Analysis of test results and development of failure envelopes.
4. Development of a site specific pillar strength equation based on the Wilson equation.
5. Load assessment and pillar design.

The importance of accurate determination of rock and coal mechanical properties in analytical design cannot be emphasized enough. To that end, drilling, sampling, and testing will be covered here in detail.

GEOTECHNICAL SAMPLING

Geotechnical drilling, sampling, and testing must adhere to the American Society for Testing and Materials (ASTM) and International Society of Rock Mechanics (ISRM) standards. These procedures help maintain the natural moisture and mineralogy of the samples, reduce breakage during drilling, sampling, and shipping, and minimize confusion in the laboratory.

The sample diameter must be NX or HQ size core recovered by wire-line split barrel. The objective is to minimize core breakage during drilling and core extraction. The core barrel containing the core should not be removed from the hole until the geologist is present and ready to log the core. Logging of the core should take place immediately and quickly and documented with photographs. The surface of the samples must not be allowed to dry, thus constant wetting of the samples is required.

A qualified geologist should geologically and geotechnically log the core and select samples for testing. Besides rock type and geologic description, the log must include such data as hardness, joint roughness coefficient (JRC), rock quality designation (RQD), percent recovery, gouge and filling type and hardness, degree of weathering, discontinuity types and spacing, all to the ISRM standards (ISRM, 1974).

The mechanical properties of a rock type can vary across a mine block and vertically through the sequence because of the different sediment sources and depositional environments that existed for rock above and below the seam. As a result, sandstone above and below the seam will not have the same mechanical properties. This variation of mechanical properties from above and below the seam is true for all other rock types. Thus, rock samples for testing should be selected from holes (a minimum of three holes) located throughout the reserve and throughout the drill hole.

Generally, 15 core samples, three times longer than the core diameter, should be obtained for each rock type found in the roof, pillar, and floor. Core samples should be obtained from the coal and partings, as well as from 15 m (50 ft) above the top of coal to 6 m (20 ft) below the base of the coal. In thick seams, samples should be obtained from each coal ply or bench.

The samples should be preserved and shipped to a laboratory in accordance with the highest standards. Samples from the core selected for testing should be immediately wrapped in plastic or otherwise sealed to prevent moisture loss and to strengthen

the core for shipping. Plastic core sleeves can be used but these sleeves have the disadvantage of not strengthening the sample. The borehole number, sample number, and depths (to and from) must be marked clearly on the plastic. The sample location should be noted on the geologic/geotechnical log and also logged into a sample inventory sheet which includes the borehole number, tube number, sample number, depths, and lithologic description.

The sealed core should be placed in a PVC or similar pipe cut to 1.2 m (4 ft) lengths or less (0.85 m (2.8 ft) if 55 gal drum is used for crating) with packaging material placed around the sample to cushion and stabilize the sample within the pipe. Filler material between samples and at the ends of the pipe is needed to prevent the samples from shifting and to allow the laboratory to saw off the end caps without damaging the sample. PVC end caps are then glued to both sides of the pipe. The borehole number, tube number, sample numbers, and depths of all the samples contained in the pipe should be marked clearly on the pipe.

Four to six of these pipes containing samples should be placed in a crate for shipping. This crate may need to be constructed if commercial crates cannot be obtained. A common substitute is a 55 gal steel drum. Once a crate is full and the pipe secured from shifting, it is to be shipped immediately to the lab without waiting for additional crates to be filled. Storage of the pipes and crates that contain core should be out of the weather in a cool, temperature controlled environment.

TESTING PROGRAM

A typical minimum testing program is illustrated in Table 1. The confining stress, s_3, finally selected for testing will depend on the maximum depth of the reserve or mine block. Typically the maximum confining stress selected is 3.5 to 4 times the overburden load to account for the confining stress to be experienced at the pillar core. Test programs normally change once drilling begins, and continue to change throughout the testing phase. These changes are due to different rock types being encountered than anticipated, inability to recover correct core lengths, scatter in the test data, etc.

Emphasis should be placed on completing the triaxial tests first, as uniaxial tests are not needed to determine the failure envelope. Also, results of the uniaxial compressive strength test on rock are commonly scattered. The scatter, in large part, is due to the flaws within the rock sample and end effects, especially for cube samples. Fortunately, "…the average strength of triaxial confined rock specimens is much greater than the unconfined specimen strength, which can be more important to pillar strength (Able, 1988)." and triaxial tests are more repeatable and accurate because end effects and flaws within the sample have less of an effect on the final results (ASTM, 1966).

Because of the difference in material properties between pillar, roof, and floor materials, the coal-floor and coal-roof contacts shear once mining occurs and stress changes take place across these contacts. For these reasons, residual triaxial strength is used in the Wilson Equation. Fortunately, residual triaxial strength test results are highly repeatable compared to intact triaxial and, of course, uniaxial test results, as illustrated in Figure 1.

The selection of a laboratory is paramount as few laboratories are capable of both high confinement and the ability to complete a residual test. In the United States, the laboratory should be Army Corps of Engineers certified.

DEVELOPMENT OF FAILURE ENVELOPE

There are only a few failure envelopes that match rock and coal behavior and these are well defined in the literature. Rock and coal at the confinements needed for pillar design, on rare occasions, will match the Mohr-Coulomb failure envelope (Hoek and Bray, 1981).

$$\tau = C + \sigma_n \tan\phi$$
$$\sigma_1 = \sigma_c + \sigma_3 \tan\beta$$

where τ is the shear strength at a normal stress of σ_n, C is cohesion ϕ is the internal friction angle, σ_c is the uniaxial compressive strength, σ_1 is the triaxial compressive strength at a confinement of σ_3, and $\tan\beta$ is the Triaxial Stress Factor. However, at high confinement, coal and most rock strengths are not linear. Almost all rock, and sometimes coal, match the Hoek and Brown failure envelopes (Hoek and Bray, 1981):

$$\sigma_1 = \sigma_3 + \sqrt{m\sigma_c\sigma_3 + s\sigma_c^2} \qquad \text{compression equation}$$

$$\tau = A\sigma_c\left(\frac{\sigma_n}{\sigma_c} - T\right)^B \qquad \text{shear equation}$$

where σ_t is the tensile strength, and m, s, A, T, and B are curve-shaping parameters. Coal rarely matches the Hoek and Brown failure envelope for reasons discussed by Barron and Young (1992). However, several failure envelopes have been developed for the compressive strength of coal, including;

$$\sigma_1 = \sigma_c\left(1 - \frac{\sigma_3}{\sigma_t}\right)^R \qquad \text{Carter failure envelope}$$

$$\sigma_1 = B\sigma_3^{1-a}\sigma_c^{\ a} + \sigma_3 \qquad \text{Ramamurthy failure envelope}$$

$$\sigma_1 = K\sigma_3^{1-A}\sigma_3^{\ A} + \sigma_c \qquad \text{Bieniawski failure envelope}$$

all as presented by Bieniawski (Bieniawski and Kalamaras, 1993), and where R, B, a, K, and A are curve-shaping parameters. The author's experience has shown that the Carter failure envelope more frequently matches the coal test data.

Table 1. Test Program Example.

Rock Type	Number of tests			
	Uniaxial compressive	Intact and residual triaxial compressive		
		@ s_3 = Maximum/4	@ s_3 = Maximum/2	@ s_3 = Maximum
Roof				
Rock Type 1	3	3	3	3
Rock Type 2	3	3	3	3
Rock Type 3	3	3	3	3
Pillar				
Coal Ply 1	3	3	3	3
Parting Type 1	3	3	3	3
Coal Ply 2	3	3	3	3
Coal Ply 3	3	3	3	3
Floor				
Rock Type 1	3	3	3	3
Rock Type 2	3	3	3	3
Rock Type 3	3	3	3	3

Curve fitting test data to failure envelopes is time consuming but the following should assist in this matter:

- Curve fitting for the residual failure envelope should match U.S. Army Corp of Engineers standards (1970) that 2/3 of the test results lay above the failure envelope. The intact failure envelope should be best fit as the intact envelope will generate parameters needed to develop the residual failure envelope.
- For rock, first curve fit the intact results to the Hoek and Brown compression equation as the developed uniaxial compressive strength, σ_c, will be needed for subsequent failure envelopes. Start by using the suggested curve fitting parameters for the rock type being analyzed as presented by Hoek and Bray (1981).
- Use the developed intact uniaxial compressive strength from the intact curve fit to develop the residual Hoek and Brown compression equation. The curve fitting parameters of *m* and *s* developed during this step are used to calculated curve fitting parameter *T*[4].

$$T = 0.5\left(m - \left(m^2 + 4s\right)^{0.5}\right)$$

- Using the residual *T* and the developed uniaxial compressive strength, σ_c, develop the residual Hoek and Brown shear strength equation.
- Once all residual shear curves are developed for all the rock and coal, each shear curve in the floor is compared to the others and to that of the coal so that the weakest rock in residual shear is selected to represent the floor shear strength. A comparison is also made with the roof rock shear strengths.
- Coal residual strength test results are used to develop the residual compression failure envelope equation.

These curve fitting parameters are entered in the Wilson pillar equation and pillar strength is calculated. The resulting equation will need to be integrated. However, such integrations are time consuming and, depending on the failure envelope equations used, may not be possible to integrate to a closed form. The author uses MathCAD software (MathSoft, Inc) for this integration. Integrating this equation produces a stress profile which occurs within the pillar from the pillar edge to its core. For this equation to generate the load carrying capacity of the pillar, the Wilson equation will need to be double integrated. Double integrations of this equation have proven to be problematic, and until software is developed for this type of double integration, the author imbeds MathCAD into an Excel (Microsoft, Inc.) spreadsheet producing a matrix of the carrying stress which is used to developed pillar strengths.

THE WILSON PILLAR EQUATION

The Wilson equation is found as equation (3) in Wilson and Ashwin (1972):

$$\left(\sigma_H + d\sigma_H\right)ml - \sigma_H ml = d\sigma_H ml$$

where *l* and *dy* are the unit length and width of the element, *m* is extraction height, and σ_H is the horizontal stress created by Poisson's and other effects within the pillar, as illustrated in Figure 2.

Over distance *dy* the horizontal (confining) stress increase is defined by:

$$dy = d\sigma_H ml$$

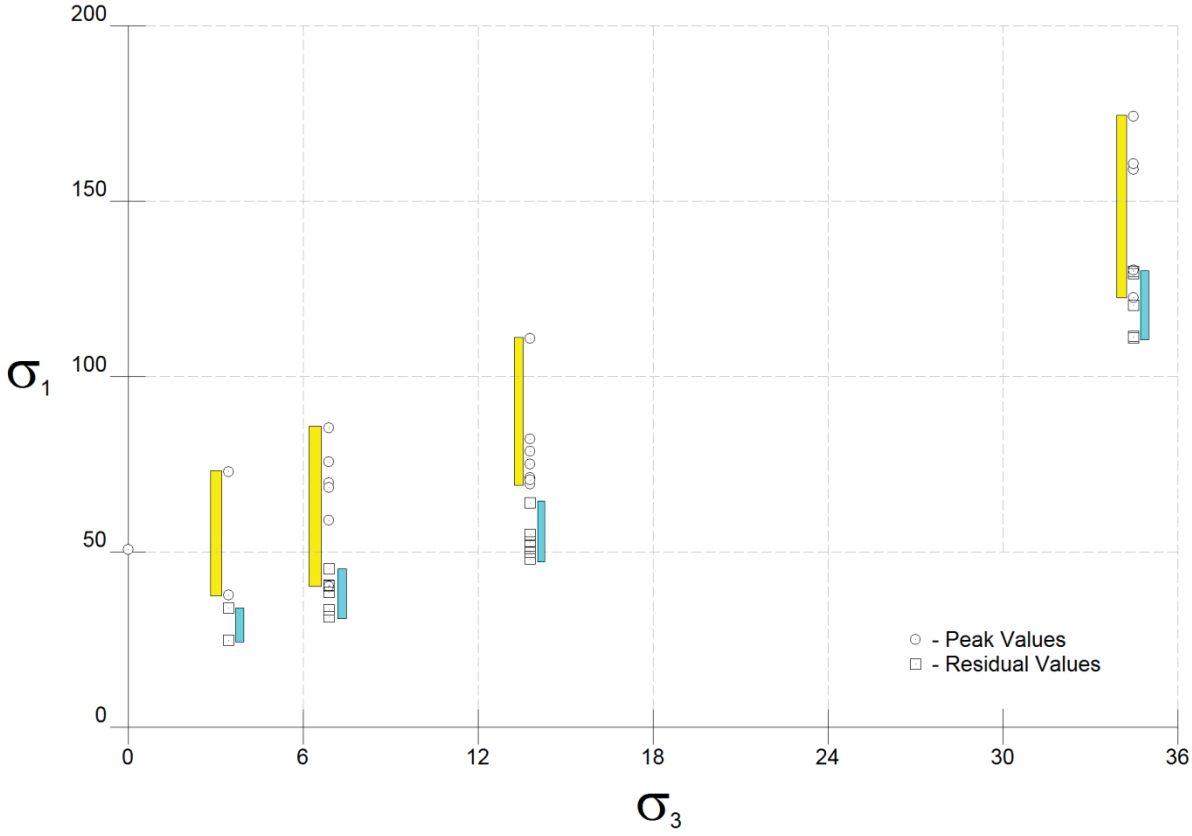

Figure 1. Intact and Residual Confined Compressive Strength for Owl Seam Roof Shale Test Results Showing Scatter.

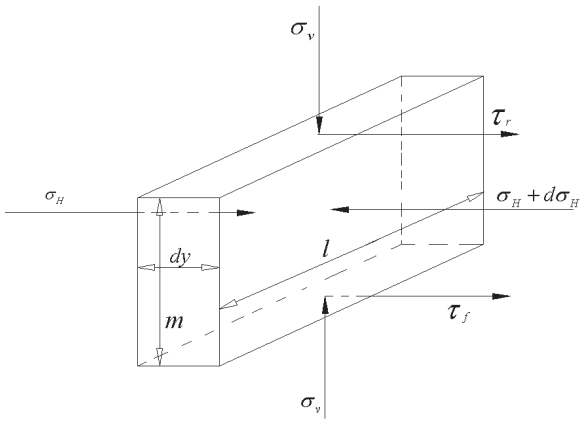

Figure 2. Free Body Diagram of a Pillar Slice, After Wilson and Ashwin[8].

This horizontal stress is resisted by the shear strength of the top and bottom of the pillar, τ_r and τ_f, where *r* and *f* are subscripts representing the material property at the roof and floor of the pillar (compare to equation (4) in Wilson and Ashwin (1972)). Thus,

$$(\tau_r + \tau_f) l dy = d\sigma_H m l$$
$$(\tau_r + \tau_f) dy = d\sigma_H m$$
$$dy = m \frac{d\sigma_H}{(\tau_r + \tau_f)}$$

Setting the integration:

$$y = m \int_{\sigma_c}^{\sigma_{max}} \frac{d\sigma_H}{\tau_r + \tau_f} d\sigma_v$$

where *y* is the distance from the rib of the pillar and σ_v is the vertical stress in the pillar at *y*. Note that the confining stress (σ_H) input in this equation is a derivative. This equation generates a

stress profile from the pillar edge, which has the strength of σ_c, the residual compressive strength of coal, to the core of the pillar which supports a vertical stress of σ_{max}. The vertical stress, σ_v, varies as the location, *y*, varies, see Figure 3.

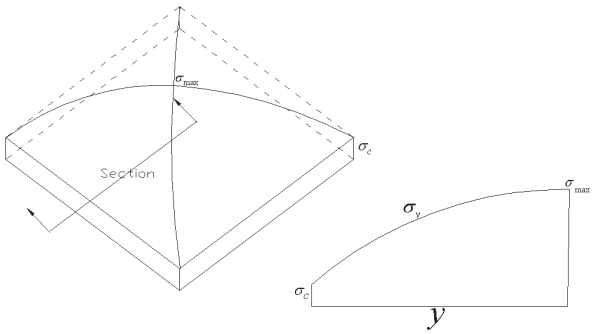

Figure 3. Stress Profile in a Soft Pillar.

The derivative of the Carter and Mohr-Coulomb equations are:

$$d\sigma_H = -\frac{\sigma_t}{R\sigma_c}\left(\frac{\sigma_v}{\sigma_c}\right)^{\left(\frac{1}{R}-1\right)} d\sigma_v \qquad \text{for Carter}$$

$$d\sigma_H = -\frac{1}{\tan\beta} d\sigma_v \qquad \text{for Mohr-Coulomb}$$

Assuming the coal's residual failure envelope matches the Carter equation, that the roof rock residual failure envelope matches the Hoek and Brown equation, and that the floor rock residual failure envelope matches the Mohr-Coulomb equation, the resulting Wilson equation form would be:

$$y = m\int_{\sigma_c}^{\sigma_{\max}} \frac{-\frac{\sigma_t}{R\sigma_c}\left(\frac{\sigma_v}{\sigma_c}\right)^{\left(\frac{1}{R}-1\right)}}{A_r\sigma_r\left(\frac{\sigma_v}{\sigma_r}-T_r\right)^{B_r} + C_f + \sigma_v \tan\phi_f} d\sigma_v$$

On occasion, and more commonly in the floor, the residual failure envelopes for one rock type will be weaker than the other rock types at low normal stress but will switch at higher normal stress. If these two rock types are thin layers in the floor, the pillar may spread in one rock type then switch to another. This can be handled by the Wilson equation. The normal stress at the intersection of the two failure envelopes can be taken as σ_{ni}. If this occurs in the floor for material types *1* and *2*, then the Wilson equation takes the form of:

$$y = m\left(\int_{\sigma_c}^{\sigma_{ni}} \frac{d\sigma_H}{\tau_r + \tau_{f1}} d\sigma_v + \int_{\sigma_{ni}}^{\sigma_{\max}} \frac{d\sigma_H}{\tau_r + \tau_{f2}} d\sigma_v\right)$$

Of course, this can occur in both the floor and roof for any number of materials *1*, *2*, *3*, … which will require adding components to the Wilson equation, σ_{ni}, $\sigma_{n(i+1)}$, $\sigma_{n(i+2)}$, … .

Another example of this equation's flexibility is its ability to handle a squeezing floor, within reason, by predicting the reduced pillar strength using the following modification:

$$y = m\int_{\sigma_c}^{\sigma_{\max}} \frac{d\sigma_H}{\tau_r - \tau_f} d\sigma_v$$

SAFETY FACTOR, REVIEW, PILLAR LOADING, AND PILLAR FOUNDATION

The author recommends a safety factor of 2 for the Wilson equation if testing and loading is understood, but this value can be as high as 2.5 to 3 for bump conditions and higher if loading conditions or material strengths are not well known.

Throughout the design process, the designer should review his results and determine, most importantly, if the resulting equation represents the observed behavior of the pillar. For example, the reviewer would note if movement is occurring in the coal or in the rock of the floor; or if spalling is occurring and whether this is included in the design, etc.

Important to the design of a pillar is knowing the load on the pillar. Pillar loading is beyond the scope of this paper but most of the time, the author employs equal area loading or uses LaModel (Heasley and Chekan, 1998) to estimate the load. Since a great deal of load predicted by equal area loading would actually be transferred to the coal block or barriers, using equal area loading offers redundancy. In high extraction settings, a transfer load is applied, either as recommended by Mark (1992) or by Able (1983). For designs that are more complicated, LaModel is used to calculate loads and for particularly complicated conditions ANSYS[1] is employed.

The Wilson equation only addresses pillar strength; a pillar foundation strength analysis needs to be completed before final pillar dimensions are recommended.

AN EXAMPLE

The Owl Seam (aka Taggart, Nosben, Upper Elkhorn, 34 Inch, and Upper Cedar Grove) is extensively mined in Kentucky and Virginia. The test results data base for this seam is to a point where trends can be defined across the region and blocks of similar behaving pillars have been delineated and separate pillar recommendations for each block have been completed. One such block is an area of strong floor. The following is the pillar design procedure used for this block.

[1] ANSYS, Inc., 275 Technology Drive, Canonsburg, PA

After drilling and testing, the strength data was analyzed to develop material properties for all the rock types in the immediate vicinity of the Owl Seam including sandstone, sandy shale, and shale in the roof and floor and the coal and binder (shale) in the seam. In the roof and floor, the shales were the weakest materials and the coal is the weakest in the seam. Figure 4 and Figure 5 show the curve fitting of the Hoek-Brown Failure criterion for the residual test results of the shale in the roof and floor of the Owl Seam.

Mark-Bieniawski Equation (blue dashed line). This is one of the few occasions where there is a close match between the results of these two equations.

MathCAD solves for the vertical stress, σ_y, at several points, y, from pillar edge to pillar center, producing an array of y(k) verses smax(k). Unfortunately, MathCAD or other programs cannot solve the double integration needed to calculate the pillar strength from the Wilson stress profile so the array generated by MathCAD for

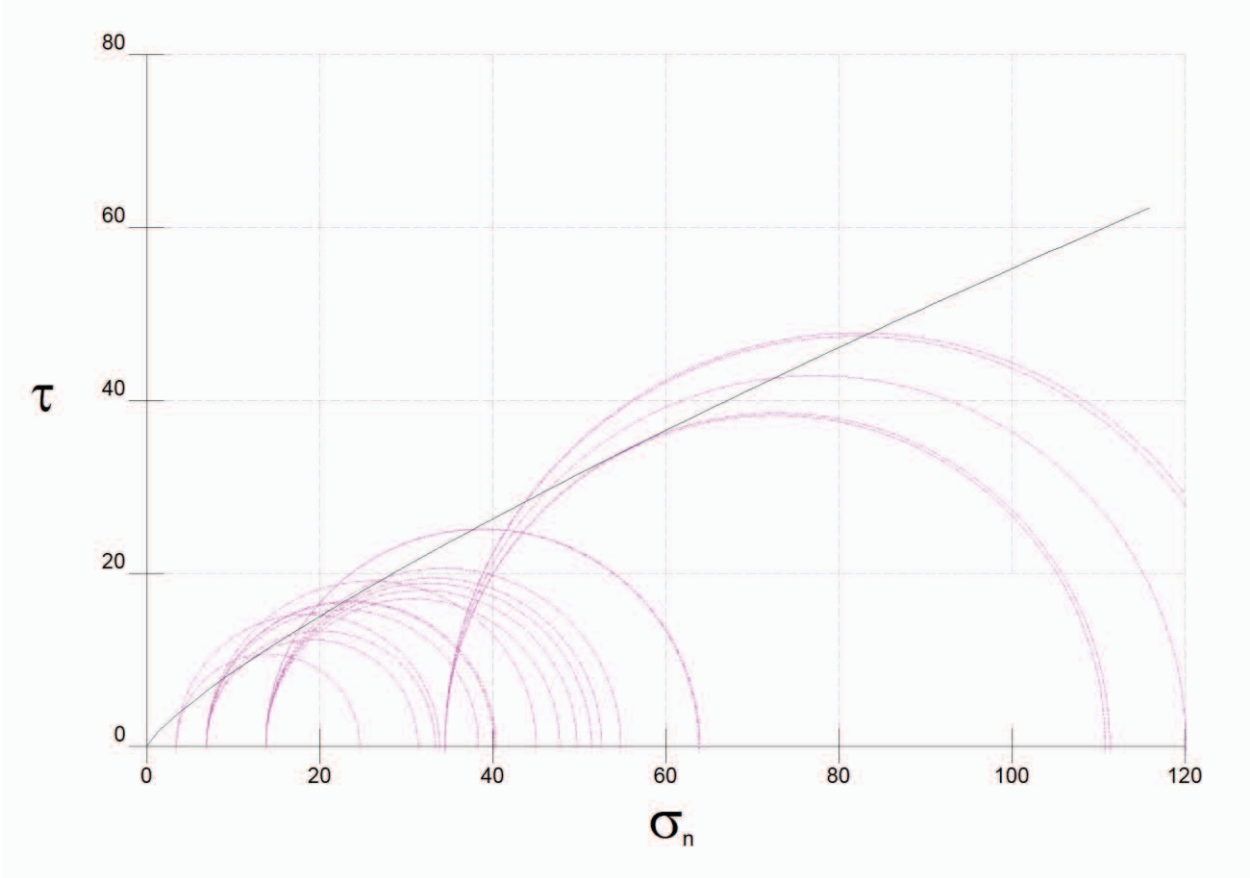

Figure 4. Shear Strength Plot of Owl Seam Roof Shale Residual Test Results and Hoek-Brown Failure Envelope.

Similarly, the curve fitting of the Carter and Hoek-Brown Failure criterion for the residual test results for the Owl Seam are shown in Figure 6 and Figure 7. Figure 7 shows that the shear strength of the Owl Seam coal is far less than the shear strengths of the surrounding shales, therefore failure and movement at the roof-pillar and pillar-floor contact will occur in the coal. Because of this, only coal parameters will be used in the Wilson pillar equation. Figure 8 is a screen shot of a MathCAD worksheet used to integrate the Wilson equation. Note that roof (*r*) and floor (*f*) parameters use the Hoek-Brown values for the Owl Seam.

Figure 8 shows the plot of the stress profile for both the Wilson Pillar Equation using Owl Seam data (red continuous line) and the

the Wilson equation is exported to an Excel worksheet as shown in Figure 7. This spreadsheet can calculate the pillar strength for any width, length, or cross-cut angle. The inby and outby crosscut angle can be different.

Figure 8 shows the strength of a square pillar 45 m on a side with 90° crosscut angles to be 136,413 MN. Employing the recommended safety factor of 2 results in a pillar strength of 68,206 MN. The corresponding Bieniawski calculated strength for the same pillar is 109,731 MN and using the recommended stability factor of 1.5 results in a pillar strength of 73,154 MN. In this atypical case, the Bieniawski equation results in a smaller pillar design than the Wilson equation.

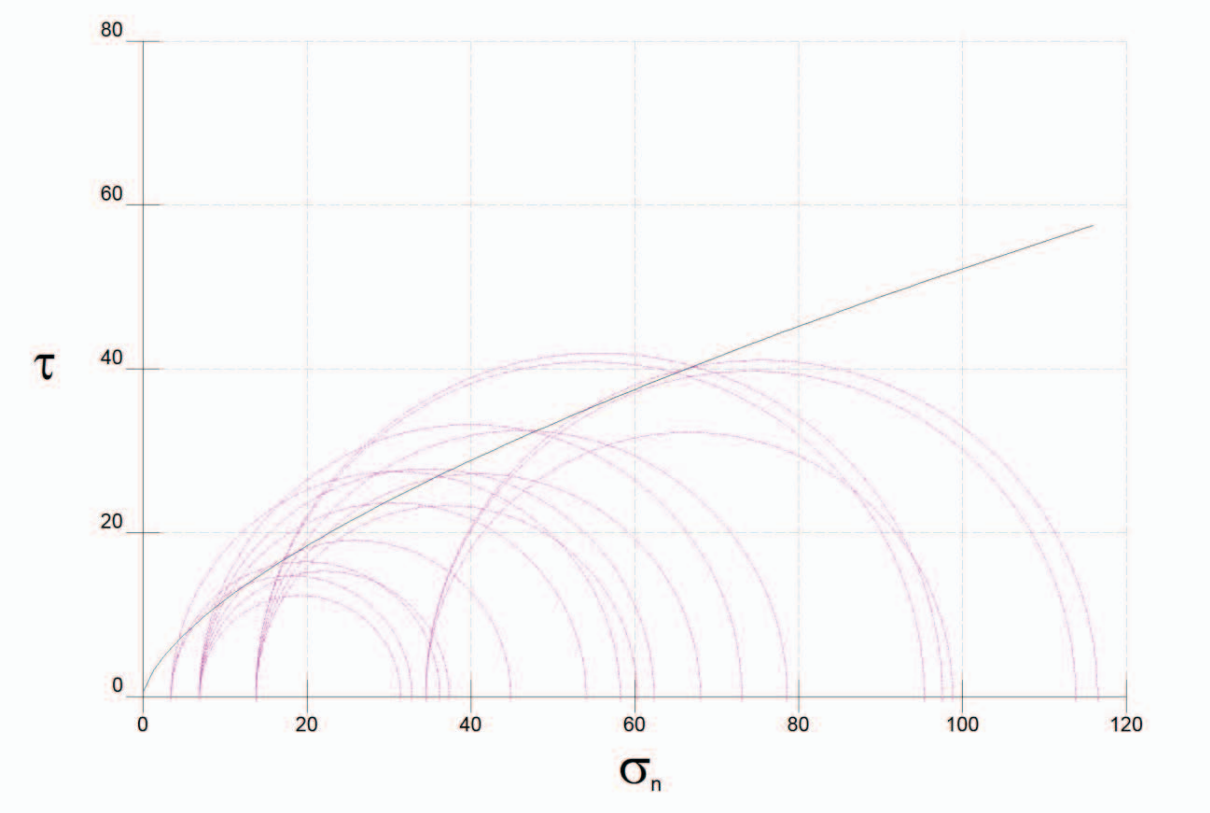

Figure 5. Shear Strength Plot of Owl Seam Floor Shale Residual Test Results and Hoek-Brown Failure Envelope.

DOES IT WORK

Dr. Christopher Mark of NIOSH gathered data on 63 pillar cases in Southern Appalachian Coal Fields. These cases were taken from 11 different mines. The author, using the analytical design procedure presented above, has designed pillars at 10 of these mines. Dr. Mark classified these pillar cases as "satisfactory" or "failed." Of the 20 cases not designed by the author, only 55% of the pillars were classified as satisfactory (11 cases).

Of the 43 cases that were designed by the author, successful cases (39) made up 91%. The following where NIOSH's reason for classifying the 4 remaining cases as failed:

- 2 bumped
- 1 squeezed
- 1 because the mine left pillars during retreat.

The two bump cases occurred in the same mine. The conditions in which these and other bumps occurred at this mine were analyzed and new successful pillar designs were undertaken to be used in areas where these conditions reoccurred.

For the squeeze case, this pillar was designed using the procedure for squeezing floor as discussed above and the pillar is stable. For the left pillar case, these pillars were left in place, at the author's request, to absorb the stress of pillars left in a mine above. In this reassessment of pillar success, of the 43 cases that were designed by the author, successful cases (41) made up 95%.

The conclusions are that the analytical design procedure is highly successful approach to designing pillars, and that when the performance proves to be unsatisfactory the conditions can be evaluated and the Wilson pillar equation adjusted to determine a stable redesigned pillar.

REFERENCES

Able, John F. Jr. (1988). Soft Rock Pillars. Geotechnical and Geological Engineering, Springer Netherlands, pp 215-248.

Able, John F. Jr. (1983). Rock Mechanics Handouts for MN 321.

ASTM (American Society for Testing and Materials) (1966). Testing Techniques for Rock Mechanics. STP 402, Philadelphia, PA, p. 209.

Barron, K. and Yang, T. (1992). Influence of Specimen Size and Shape on Strength of Coal. Proceedings of the Workshop on Coal Pillar Mechanics and Design, U.S. Bureau of Mines IC 9315, pp. 5-24.

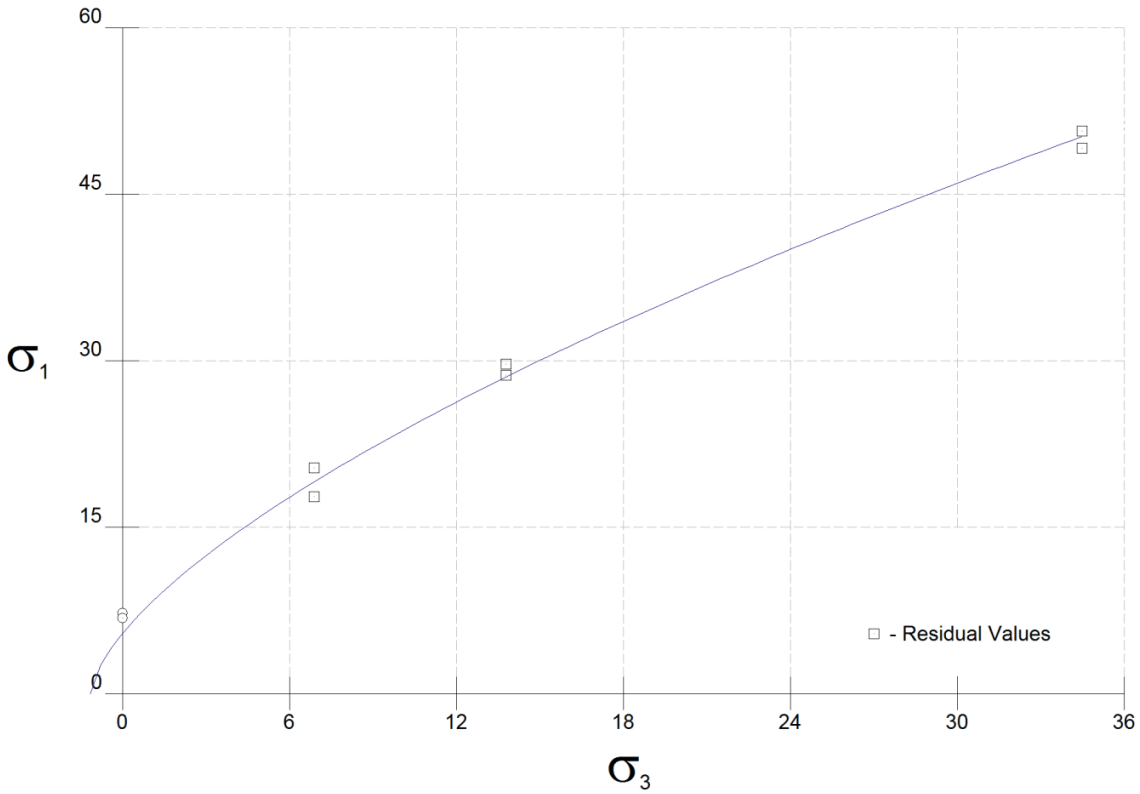

Figure 6. Residual Confined Compressive Strength for Owl Seam Test Results with Carter Failure Envelope.

Bieniawski, Z.T. and Kalamaras, G.S. (1993). A Rock Mass Strength Concept for Coal Seams. Proceedings of the 12th International Conference on Ground Control in Mining, Morgantown, WV, pp. 274-283.

Heasley, K.A. and Chekan, G.J. (1998). Practical Stress Modeling for Mine Planning. Proceedings of the 17th International Conference on Ground Control in Mining, Morgantown, WV, pp. 129-137.

Hoek, E. and Bray, J.T. (1981). Rock Slope Engineering. Institution of Mining and Metallurgy, London.

ISRM (International Society of Rock Mechanics) (1974). International Society of Rock Mechanics, 1974-1978. Commission on Standardization of Laboratory and Field Testing, Suggested Methods, Pergamon Press Ltd, Great Britain.

Mark, C. (1992). Analysis of Longwall Pillar Stability (ALPS): An Update. Proceedings of the Workshop on Coal Pillar Mechanics and Design, U.S. Bureau of Mines IC 9315, pp. 238-249.

U.S. Army Corp of Engineers (1970). Engineering and Design. Engineer Manual 1110-2-1902, Washington D.C., pp. V888-21, see page 13.

Wilson, A.H. and Ashwin, D.P. (1972). Research into the Determination of Pillar Size. The Mining Engineer, *131.9*(141):409-417, Institution of Mining Engineers, London.

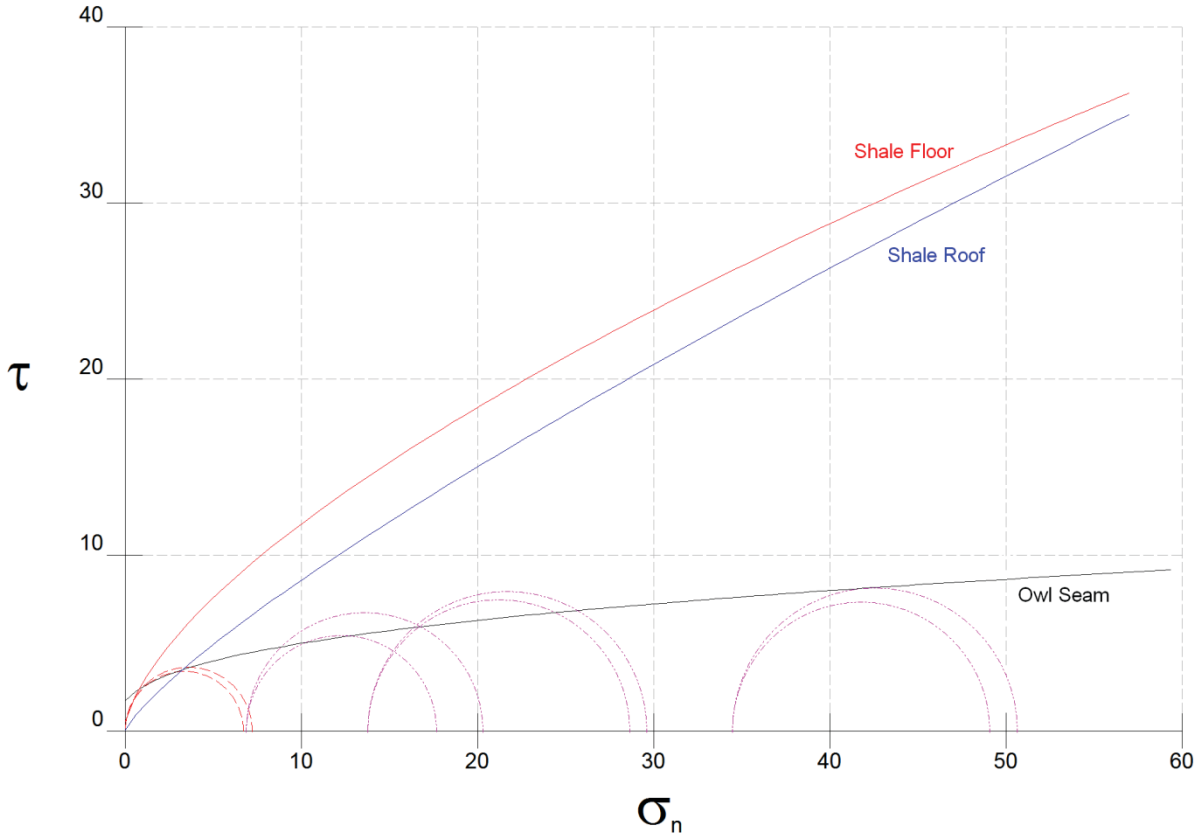

Figure 7. Shear Strength Plot of Owl Seam Residual Test Results and Hoek-Brown Failure Envelopes for Coal and Shale.

$\sigma_r := 6.76$ $\quad \sigma_c := 5.4$ $\quad \sigma_f := 6.76$

$A_r := 0.630$ $\quad \sigma_t := -1.155$ $\quad A_f := 0.630$

$T_r := -0.0747$ $\quad R := 0.65$ $\quad T_f := -0.0747$

$B_r := 0.350$ $\quad B_f := 0.350$

$m := 2$

$n := 100$

$D := 5$

$k := 0..n$

$\sigma_{max}(k) := D \cdot k + \sigma_c$

$$y(k) := m \cdot \left[\int_{\sigma_c}^{\sigma_{max}(k)} \frac{-\frac{\sigma_t}{R \cdot \sigma_c} \cdot \left(\frac{\sigma_v}{\sigma_c} \right)^{\left(\frac{1}{R} - 1 \right)}}{A_r \cdot \sigma_r \cdot \left(\frac{\sigma_v}{\sigma_r} - T_r \right)^{B_r} + A_f \cdot \sigma_f \cdot \left(\frac{\sigma_v}{\sigma_f} - T_f \right)^{B_f}} d\sigma_v \right]$$

$S_1 := 6.2$

$$\sigma_v(k) := S_1 \cdot \left[0.64 + 2.16 \cdot \left(\frac{y(k)}{m} \right) \right]$$

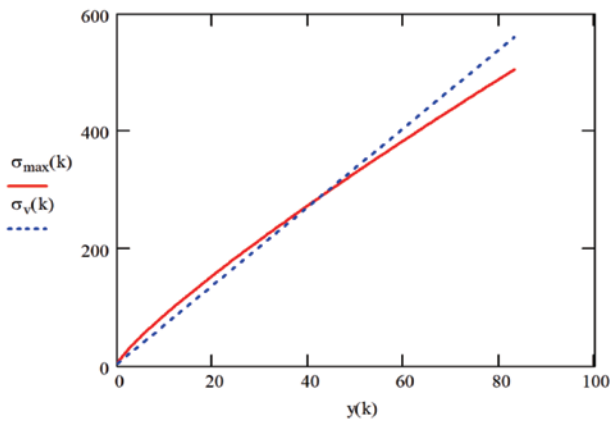

Figure 8. Screen Shot of Mathcad Analysis of Owl Seam Pillar Strength Using Wilson Pillar Equation, note plot of Wilson Stress Profile versus Mark Bieniawski Stress Profile.

y(k), metres =	0	0.438	0.923	1.442	1.986152	...	20.927	21.72	22.518	23.32	24.127	...
smax(k), MPa =	5.4	10.4	15.4	20.4	25.4	...	160.4	165.4	170.4	175.4	180.4	...
Strength per slice, MN (length) =		154.2	273.2	395.7	518.2372	...	490.06	304.12	102.08	-116.29	-351.22	...
Strength, MPa (length) =		154.2	427.4	823.1	1341.319	...	33697	34001	34103	33987	33636	...
Strength per slice, MN (width) =		154.2	273.2	395.7	518.2372	...	490.06	304.12	102.08	-116.29	-351.22	...
Strength, MPa (width) =		154.2	427.4	823.1	1341.319	...	33697	34001	34103	33987	33636	...
Strength per slice, MN (length) =		154.2	273.2	395.7	518.2372	...	490.06	304.12	102.08	-116.29	-351.22	...
Strength, MPa (length) =		154.2	427.4	823.1	1341.319	...	33697	34001	34103	33987	33636	...
Strength per slice, MN (width) =		154.2	273.2	395.7	518.2372	...	490.06	304.12	102.08	-116.29	-351.22	...
Strength, MPa (width) =		154.2	427.4	823.1	1341.319	...	33697	34001	34103	33987	33636	...
Total Strength, MN =		616.7	1709.6	3292.3	5365.278	...	134788	136004	136413	135948	134543	...
Width to slice, metres =	0.0	0.9	1.8	2.9	4.0	...	41.9	43.4	45.0	46.6	48.3	...
Angle of first crosscut	90	second	90									
Pillar Length, m =	45											
Pillar Width, m =	45											

Figure 9. Screen Shot of Spreadsheet Used to Calculate Pillar Strength Based on the Stress Profile.

The In–Situ Pillar Strength and Overburden Stability in U.S. Mines

Hamid Maleki, President
Maleki Technologies, Inc.
Spokane, WA

ABSTRACT

Prudent design of coal pillars in any mining system requires an estimation of in-situ pillar strength, overburden lateral load transfer capability, and a failure criterion. Pillar strength is typically determined using one of several different empirical pillar strength formulas. For coal reserves in the U.S., a new pillar design method was proposed based on extensive U.S. field measurements in underground mines (Maleki, 1992) which accounted for confinement effects. Field measurements in seven U.S. seams indicated highest strength for some Utah mines where the coal seam developed high confining stresses. Lower strength was measured in structurally controlled seams. This method is expanded here including the data from the weaker tertiary coal measure rocks and lower confinement for pillars with low width-to-height ratios.

The determination of how much load a pillar is expected to take is partially dependent on the ability of overburden to transfer load laterally; this is useful for selection of panel width and barrier pillars size in select mining applications where long-term stability is required in conservative designs. In caving mining systems, caving of the strata is influenced by geologic, mining and stress conditions and the released energies influence how the pillars react at loads approaching pillar strengths. Overburden deformation and caving mechanisms are analyzed in this paper in multi-panel extractions to enhance the understanding of load transfer, seismicity and coal bump control in deep western U.S. operations.

INTRODUCTION

Prudent design of coal pillars in any mining system requires an estimation of in-situ pillar strength, overburden lateral load transfer capability, and failure criteria. Pillar strength is typically determined using one of the empirical pillar strength formulas which are either based on laboratory testing (Bieniawski, 1968; Salamon et al., 1967; Van der Merwe, 2002) or theoretical considerations (Bieniawski, 1968; Wilson, 1972). These empirical methods are useful for preliminary investigations but lack provisions for including site-specific conditions including layered coal, confinement stress, and groundwater conditions among other factors.

For coal reserves in the U.S., a new triaxial strength method was proposed based on extensive U.S. field measurements in underground mines (Maleki, 1992) which accounted for confinement effects. Field measurements in seven U.S. seams indicated highest strength for some Utah mines where the coal seam developed high confining stresses including Blind Canyon, Rock Canyon, Upper Hiawatha and Sunnyside (Maleki, 1995; Maleki et al., 2003). Lower strength was measured in structurally controlled seams where presence of partings and cleats effectively reduced the confining stress and contributed to time-dependent softening (including Hiawatha Split, O'Conner, Harlan, Pittsburg, D and B seams). The method was based on long-term observations, geotechnical monitoring, and back analyses of stresses that caused pillar failure in eight mines and seven coal seams in the United States. This method is expanded here including the data from the weaker tertiary coal measure rocks of a new study site at shallow cover and lowest confining stress.

In development panels, the determination of how much load a pillar is expected to take is partially dependent on the ability of overburden to transfer load laterally. The load transfer distance (LTD) is an important consideration for selection of panel widths and barrier pillar designs. It is the maximum distance that the overburden can transfer loads. By limiting panel width below a distance equal to twice the LTD, the operator could prevent full tributary loading of pillars if desired (for design of mains and highwall miner panels, for instance). To avoid any load transfer toward the next panel in conservative designs, the barrier pillar should be wider than the LTD. Because the LTD is depth dependent, wider panels can be protected by the pressure arch at higher depth but narrower panels are required at shallow cover near the outcrop. This is particularly important for highwall miner panels where panels are driven typically at low cover near the highwall face. Pillar stability near the free highwall face is further compromised by reduced confinement effects perpendicular to the highwall face.

Critical to the design of a caving mining system is an understanding of load transfer through the caved zone (gob) and the influence of site-specific depositional and structural conditions. While caving has been favorable in some mines, a lagging, cyclical cave has contributed to excessive load transfer toward panel boundaries and major seismicity in

many western U.S. mines, including some operations in Utah. Because of challenges in placing instruments in the gob, a good understanding of cave progression toward the surface in single- and multiple-panel geometries is missing, creating challenges in the prudent application of models for development of mine designs. Considering limitations in measurement technologies, manpower, and costs, some ground control engineers have tried to collect information at panel boundaries where inelastic material behavior under high-stress conditions makes interpretation of the results very difficult. Popular empirical methods (Mark, 1990) are useful but simplistic under British and U.S. strata conditions when using an average cave angle of 15º to 21º, approximating the shape and condition of the pressure arch influencing load transfer (Maleki, 1990).

In this paper, the author identifies geotechnical factors influencing pillar strength and overburden stability, emphasizing the role of horizontal stress and the heterogonous nature of the coal among other factors. The usefulness and limitations of popular empirical methods are presented, while proposing a new empirical method for accounting for confinement influence on pillars for U.S. coal seams including a new lower bound for some weaker tertiary strata at a recent study site. Overburden deformation and caving mechanisms are analyzed in multi-panel extractions to enhance the understanding of load transfer, seismicity and coal bump control in deep western U.S. operations.

LOAD TRANSFER AND PANEL DESIGNS

Two diverse design approaches may be considered for design of mining layouts, although other intermediate approaches are common: (1) use of narrow panels protected by the pressure arch separated by relatively wide barrier pillars (or stable, abutment pillars in case of longwall mining) and (2) use of wide panels (exceeding the pressure arch) where favorable caving is anticipated. The first conservative design approach is most suitable for deep room-and-pillar mines or mines with lagging cave conditions where sudden release of energy accumulated in stiff stratigraphic units could increase the geotechnical risks of violent failure. The second approach requires a jointed, laminated overburden with favorable caving characteristics in mines where side-by-side full extraction is carried out without any significant barrier pillars.

To apply the pressure arch concept, one needs to measure it under site-specific geologic conditions. Direct measurement of the pressure arch width is, however, very challenging in coal mine environments (Maleki, 1981) and limited to a single measurement in a Wasatch Plateau Utah mine, operating under the Castlegate Sandstone. The mine utilized the room-and-pillar retreat mining system (Maleki, 2006). This measurement is significant in that it contradicted common mining misconceptions (based on underground observations or empirical methods) regarding rapid cave progress toward the surface. The pressure arch width is shown to be two times wider than reported values by Holland (1963) confirming the long load transfer capabilities of massive stratigraphic units in many western U.S. mines.

Figure 1 presents an empirical formula proposed by Holland (1963) and additional measurements obtained by the author. In this figure, the author has shown an upper bound suitable for many Utah mines based on these unique pressure measurements in the gob of the Utah mine (Maleki, 1981) and analyses of other overburden collapse mechanisms at other sites. Other factors favoring long load transfer distances in the west are lack of well developed jointing at some mines and the presence of a moderate horizontal stress field promoting the stability of the pressure arch. Obviously the LTD for many mines fall within the lower and upper bounds and influenced by site-specific geologic conditions.

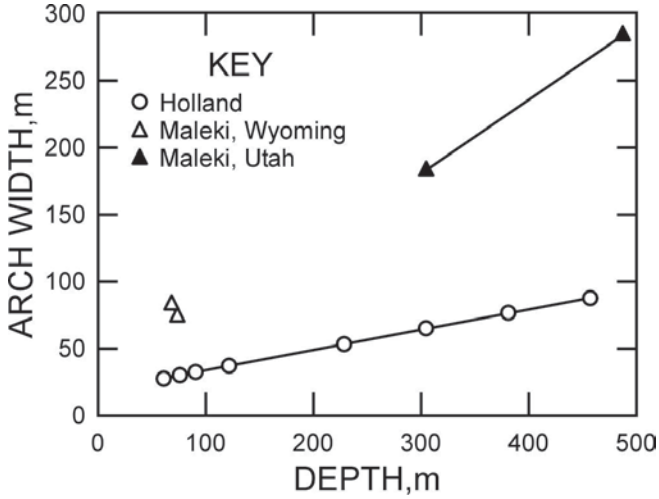

Figure 1. Pressure arch width vs. depth.

From a practical point-of-view, the pressure arch concept has useful implications for design of caving mining systems and stiff overburden environments. Under a competent roof, western U.S. operations generally use barrier pillars between room-and-pillar panels or sometimes in longwall mines for coal bump control (Maleki, 1995). As the excavation width is increased in the second and third panels, geotechnical risks are generally increased due to additional static stress and dynamic loading associated with collapse of the pressure arch and failure of stiff, stratigraphic units toward the surface. Because room-and-pillar mines have less tolerance for static and dynamic loads than fully mechanized longwalls, it is a common practice to leave an isolating barrier pillar between panels to moderate stress levels and seismicity by extracting individual panels under the protection of the pressure arch. To expand the practice to deep longwall mines operating under stiff stratigraphic units, Maleki (1995) proposed to leave large blocks of coal in place to reduce coal bump potential where all other attempts to control coal bumps fail.

Case studies presented by this author (Maleki, 2006) clearly demonstrate the role of barrier pillars for stability control in multi-panel extractions. At the Wasatch Plateau Utah mine measurement site, for instance, the operator attempted to eliminate barriers in the room and pillar operation by splitting access chain pillars on retreat so that mining could take place continuously from one panel to another. Because the cave was shown to be very limited in the first panel, mining conditions remained acceptable in general, under the protection of the pressure arch. Significant stress was transferred to the second panel as the total extraction width exceeded the pressure arch width during the extraction of the second panel.

Attempts to mine with no barriers were not successful and caused concentrations of stress at the tailgate/ bleeder corner. Because of higher geotechnical risks in room-and-pillar retreat

systems, the operator eventually switched to a longwall method using a stable gate-road pillar system. Maleki (2003) present geotechnical data from another application mining under stiff overburden and lagging cave conditions where the operator successfully left barriers at strategic locations to control seismicity.

Other geotechnical measurements clearly relate mining conditions in multi-panel extractions to the cavability of the overburden units where side-by-side longwall mining took place. In one Utah mine, the author examined direct measurements of side-abutment stresses during multi-panel extraction in a longwall block consisting of seven panels. Together with detailed underground observations during the extraction of all seven panels, geologic mapping, and subsidence measurements, the author presented evidence of the relief of side-abutment stress after the collapse of the pressure arch after the extraction of the third panel where caving was favorable at moderate depth of cover (Figure 2).

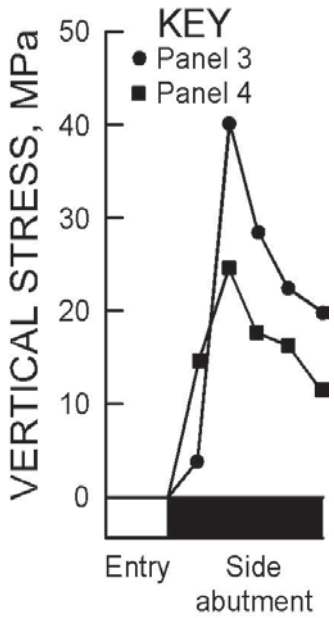

Figure 2. Side-abutment measurements.

On the contrary, monitoring seismicity and subsidence over another seven-panel longwall block at a Utah mine were used to indicate a possible increase in side-abutment stress even after supercritical width was achieved. The mine used 720-ft wide panels and 30-ft wide yielding pillars. These east-west oriented panels were retreated from south toward north. The increase in side-abutment stress was suspected because of an increase in mining-induced seismicity and more difficult mining conditions as mining continued toward higher overburden depths to the north of the block. Figure 3 compares the subsidence development curve and measured seismicity during extraction of the seven panels. In this figure, the author has normalized seismic frequency per unit length of retreat. Maximum recorded event magnitude is also shown for each panel. In addition, both raw data and filtered events are included to homogenize data collected at different times.

The number of seismic events generally increased as the excavation was widened by mining in subsequent panels,

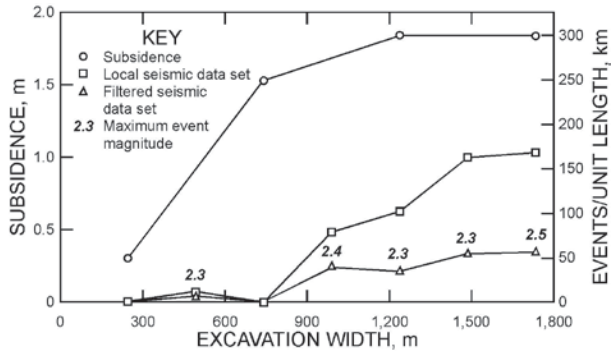

Figure 3. Subsidence development curve and seismic event history.

confirming the progression of a cave zone toward higher stratigraphic units. An exception to this trend was noted during extraction of the third panel, where the excavation width (current and previous panel) exceeded 2,000 ft. Subsidence reached 5 ft, but no seismicity was reported. This abnormal pattern was possibly caused by limitations of the regional seismic network being operated by the University of Utah at this time. Note the higher number of events recorded as mining expanded to the north. This was not due just to an increase in cover, but was also influenced by better resolution of the seismic array after additional monitoring stations were installed in that area. With the higher cover to the north, longwall abutment stress increased significantly, with a resultant increase in event magnitude. The increased seismicity and bouncing experienced at this site to the north in supercritical excavations are indicative of a lagging cave and perhaps an improper direction of retreat from low to high overburden depths (Maleki, 1995).

IN SITU PILLAR FAILURE MECHANISMS

The strength of a coal pillar depends on the vertical stresses that can be transmitted through the coal measure strata including the coal, roof and floor. As pillar stresses increase during retreat mining, failure may be initiated within the seam or at weak surrounding strata including bedding planes with low shear strength properties. Depending on the depositional and structural setting in a mine, it is possible to have a combination of two or more of these mechanisms. Figure 4 presents typical failures caused by excessive vertical stresses. Mines with excessive horizontal stresses (Baron, 1983) are excluded from this analysis because the focus is on vertical stress-induced pillar stability problems.

Figure 4A presents typical roof stability problems caused by excessive pillar loading. In this case, high vertical stress concentrations caused lateral movement of a claystone layer in the mine roof, which bent roof bolts (Figure 5) and contributed to the failure of the top coal and the ribs. Extensive measurements and numerical modeling revealed pillar stresses exceeding 3,000 psi which approached the strength of the coal pillar (Maleki, 1981).

Figure 4B illustrates schematically gradual pillar failure in a structurally controlled coal seam including three sets of cleats and bedding planes. This failure was associated with gradual rib slabbing (buckling) and the propagation of failure toward the pillar

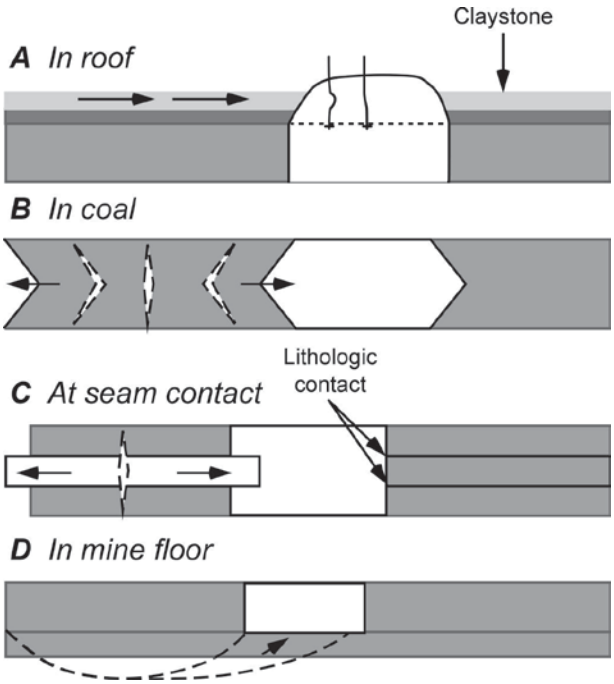

Figure 4. Failures caused by excessive vertical stresses: A, In roof; B, in coal; C, at seam contact; D, in mine floor.

Figure 5. Typical roof fall caused by excessive pillar loads.

core. Lateral dilation measurements, where available in a pillar, are sensitive indicators of pillar yielding and can be used to verify pillar unloading (Maleki et al., 2003).

Figure 4C illustrates failure originating at seam contacts, such as bedding planes or rock splay contact planes. Confining stresses cannot be fully developed under such conditions. In these mines, pillar dilation was facilitated along favorable low-friction contact planes, which contributed to pillar failure at moderate stress levels. Figure 6 shows rib conditions for one study site in Kentucky.

Figure 4D presents development of failure in a mine floor and formation of excessive heave in a mine with a strong coal seam,

Figure 6. Pillar failure influenced by partings within the seam.

a strong roof, and a weak floor. Failure in the mine floor created tensile zones within the pillar, contributing to pillar failure. Detailed geotechnical measurements and three-dimensional stress analyses supporting this assertion are presented elsewhere (Maleki and Hollberg, 1995).

These simple descriptive mechanisms are important in recognizing that pillars are taking excessive loads and for taking remedial action in the early stages of mine life. Based on these descriptive guidelines, pillar failure mechanisms can be identified and used for modeling in situ pillar behavior.

IN SITU PILLAR STRENGTH

For coal seams in the U.S., a new method of pillar design was proposed based on extensive U.S. field measurements in underground mines (Maleki, 1992) while accounting for confinement effects or lack of it where weak bedding planes are present near the seam. The importance of confined strength was highlighted using both laboratory split-platen measurements (Maleki, 1981) and field measurements of changes in both vertical and horizontal stress (Maleki, 1995). The work dealt with specific failure mechanisms and post-failure pillar characteristics, an important requirement for yield pillar designs. More recently numerical studies have been completed to study the role of weak bedding planes on reducing confining stress in the roof and pillar and thus effecting strength and strata behavior (Morsy and Peng, 2003; Maleki et al., 2001).

Average peak vertical stresses on pillars were calculated on the basis of back-analyses of stresses causing pillar failures using numerical modeling, and a review of studies of pillar load monitoring conducted by the U.S. Bureau of Mines and MTI (Maleki et al., 2003). These studies involved the use of borehole pressure cells, vibrating-wire strain gauges, and, in a few cases, overcoring stress measurements. Pillar failure was verified both through analyses of geotechnical data including both stress and pillar dilation and numerical modeling for some cases. The focus was to determine in-situ triaxial peak strength for individual coal seams and estimates of yield zones within the ribs using detailed

measurements. Average pillar strength was then determined using the area under the load curve.

Additional insights were gained recently based on back analyses of stresses associated with local and regional failures over a large number of highwall mining panels while producing a lower bound pillar strength formula for weaker tertiary coal of the study site. The work highlighted the importance of geologic, mining and design factors including (1) the heterogeneous strength properties of multi-layered benches forming the thick seam (5m or 16-ft), (2) lower pillar confinement close to the highwall face and in pillars with low width-to-height ratio. These effects are analyzed here using a two-dimensional, finite-difference code (Fast Lagrangian Analysis of Continua or FLAC, Itasca 2006). It is suitable for addressing heterogeneous coal seam subject to triaxial stress condition using the Mohr-Coulomb criteria.

The analyzed geometry consisted of half of a web pillar and heterogeneous material properties. By using lines of symmetry on the sides of the model, the author has assumed an indefinite number of pillars typical for wide highwall miner panels consisting of 20 openings. Pillar stress is maximum discounting for any arching effect in this model. These analyses were completed to study stress distribution within the pillars and to calculate the pillar SF (safety factor) while accounting for horizontal stress and exact pillar geometries (or width-to-height ratio) on a mechanical basis. The focus was on the stability of the pillars toward the center of a panel while considering heterogeneous coal strength, and confinement effects near the initial collapsed panels.

Two conditions were compared: (1) homogenous vs. layered coal seams and (2) full pillar confinement for a typical section about mid-length of highwall mining of panels (plane strain) vs. reduced confinement near the highwall face simulated using plane stress solutions. Safety factor values were post processed from elastic stress solutions. The Mohr-Coulomb strength parameters, cohesion and friction angle, used in the post processing were obtained from available site specific geotechnical testing.

Figure 7 compares horizontal stress distribution for the central zone panels, and shows the importance of including layered properties for the calculation of horizontal stress and SF (safety factor) where applicable. For the analyzed pillar with width-to-height ratio of 0.7, horizontal confining stresses are small but remain compressive for homogeneous seam properties. On the contrary, tensile stress forms within the pillar as layered structure is included within the seam. The tensile stress is induced by the contrast of the stiffness between coal layers. This reduces pillar SF along stiffer layers below 1.0. Since tensile strength is low (0.05-0.14 MPa), tensile slabbing may contribute to pillar failure.

Figure 8 presents the calculated average web pillar SF for typical pillar width-to-height ratios and far-field stress conditions in select study areas. Assuming full confinement effects, pillar stability is reduced at greater depths because of higher concentration of vertical stress in high extraction panels.

Near the highwall face, pillar confinement is reduced and thus pillar SF is also reduced. The reduced confinement effects are simulated conservatively by assuming plane stress conditions at 75-m of depth. It is interesting to note that pillar stability is lowest for the plane stress conditions and thus most realistic pillar

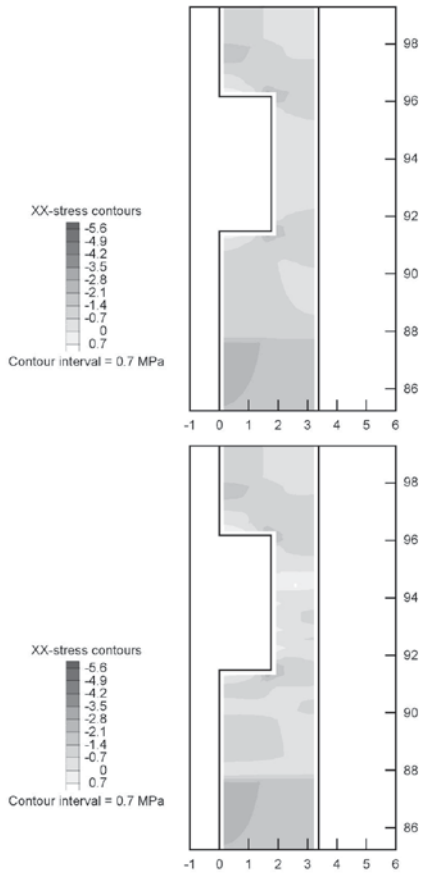

Figure 7. Compared horizontal stress distribution for homogenous and layered seams.

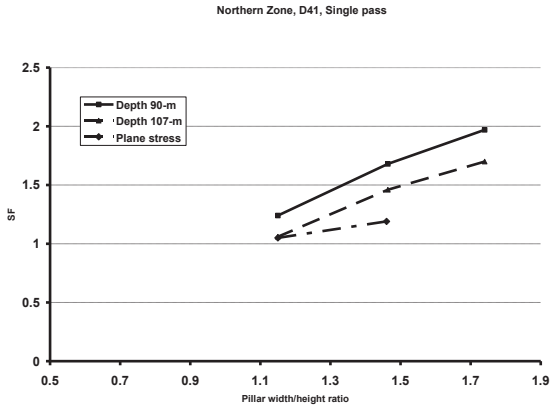

Figure 8. Average pillar SF for typical mining geometries and analyzed conditions.

designs should consider reduced pillar stability near the highwall face. Subsidence contours (excluded from this paper) clearly show higher subsidence forming at shallow areas than at deeper portion of panels. Among contributing factors are (1) reduced confinement and pillar strength and (2) lower overburden ability to arch at shallow cover (Figure 1). Three dimensional stress analyses are planned to verify plane stress assumptions.

By considering data from weaker geologic conditions of this site, the author has included a lower bound for structurally influenced multi-layered coal at shallow depths (Figure 9). The formulations reflect non-linear behavior (Maleki, 1992) and the pillar strength is capped based on field measurements that showed coal pillars can sustain maximum stresses between 17 and 32 Mpa (2,500 to 4,700 psi) depending on structural and confining effects. Beyond these stress levels, stability problems may occur as a result of failures in the roof, seam, and floor and thus a conservative cap has proven to be prudent, reducing the need to use very high factor of safety for pillars with high width-to-height ratio.

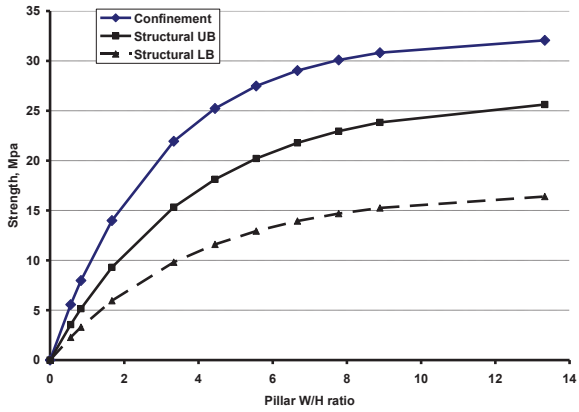

Figure 9. Updated in-situ pillar strength for different width to height ratios.

In selection of an in-situ strength curve for new applications, the user needs to consider historic measurements in select U.S. coal seams (Maleki, 1992) while including site-specific analyses of geologic conditions, laboratory strength and stress regime. For instance, a strong coal under high confinement stresses may locally become weaker at fluvial channel boundaries as slickensided features or weak bedding planes come in contact with the seam. A structurally controlled strength thus is considered more conservative for those areas than confinement control strength.

CONCLUSIONS

Site specific analyses presented in this paper clearly have identified the influence of geologic and geometric factors on pillar and overburden stability, including: (1) the heterogeneous strength properties of multi-layered benches in thick seams, (2) the importance of effective confining stresses in-situ on pillar strength, and (3) high arching ability of massive stratigraphic units in the western US mines influencing load transfer, seismicity and barrier pillar designs.

The in-situ strength method originally proposed by this author is enhanced by including data from weaker tertiary coal, including a lower bound for structurally influenced multi-layered coal at shallow depths. The formulations reflect non-linear behavior (Maleki, 1992) and the pillar strength is capped based on field measurements that showed coal pillars can sustain maximum stresses between 17 and 32 Mpa depending on structural and confining effects. Beyond these stress levels, stability problems may occur as a result of failures in the roof, seam, and floor and thus a conservative cap has proven to be prudent.

Two diverse design approaches are presented which consider lateral load transfer capability of the overburden and site specific cave conditions. Geotechnical measurements are used to highlight long load transfer capability and variable cave conditions in many U.S. mines.

REFERENCES

Baron, K. (1983). An Analytical Approach to the Design of Pillars in Coal. Canada Center for Mineral and Energy Technology.

Bieniawski, Z.T. (1968). The Effect of Specimen Size on Compressive Strength of Coal. Int. J. of Rock Mech. Min. Sci., pp. 325-335.

Holland, C. (1963). Pressure Arch Techniques. Mechanization, March, pp. 45-58.

Maleki, H. (2006). Caving, Load Transfer and Seismicity in Western U.S. Mines. Proceedings of the ARMS/USRMS, Paper 06-931, Colorado School of Mines, Golden, CO.

Maleki, H. (1995). An Analysis of Violent Failures in U.S. Coal Mines – Case Studies. Proceedings of the Mechanics and Mitigation of Violent Failure in Coal and Hard-rock Mines, Maleki, H., Wopat, P.F., Repsher, R.C. and Tuchman, R.J. (eds), U.S. Bureau of Mines, SP 01-95, pp. 5-26.

Maleki, H. (1992). In-Situ Pillar Strength and Failure Mechanism for U.S. Coal Seams. Proceedings of the International Workshop on Coal Pillar Design and Mechanics, Santa Fe, New Mexico, U.S. Bureau of Mines IC 9315.

Maleki, H. (1990). Development of Numerical Modeling Procedure for Coal Mine Stability Evaluation. Proceedings of the 31st Rock Mechanics Symposium.

Maleki, H. (1981). Coal Mine Ground Control. Ph.D. Dissertation, Colorado School of Mines, Golden, CO.

Maleki, H., Dubbert, J. and Dolinar, D.R. (2001). Rock Mechanics Study of Lateral Destressing for the Advance-and-Relieve Mining Method. Proceedings of the 22nd International Conference in Ground Control in Mining, Morgantown, WV, pp. 105-113.

Maleki, H. and Hollberg, K. (1995). Structural Stability Assessment through Measurements. Proceedings of the ISRM Workshop on Rock Foundations, Tokyo, Japan.

Maleki, H., Olsen, R., Spillman, D. and Stevenson, M. (2003). Development of Geotechnical Procedures for the Analysis of Mine Seismicity and Pillar Designs. Proceedings of the 22nd International Conference on Ground Control in Mining, S.S. Peng et al. (eds), West Virginia University, Morgantown, WV, pp. 270-277.

Mark, C. (1990). Pillar Design Methods for Longwall Mining. U.S. Bureau of Mines IC 9247.

Morsy K. and Peng, S.S. (2003). New Approach to Evaluate the Stability of Yield Pillars. Proceedings of the 22nd International Conference on Ground Control in Mining, S.S. Peng et al. (eds), Morgantown, WV, pp. 371-381.

Salamon, M.D.G. and Munro, A.H. (1967). A Study of the Strength of Coal Pillars. J. of So. Afri. Inst. of Min. and Tech. *II B*:55-67.

Van der Merwe, M. (2002). A Linear Coal Model for South African Coal. Proceedings of the 21st International Conference in Ground Control in Mining, S.S. Peng et al. (eds), Morgantown, WV, pp. 98-104.

Wilson, A.H. (1972). An Hypothesis Concerning Pillar Stability. Min. Eng. (London) *131*:409-417.

The Unsw Pillar Design Methodology and Considerations for Using This and Other Empirical Pillar System Design Approaches

Jim M Galvin, Professor
Galvin and Associates
Manly, Australia

ABSTRACT

The UNSW Coal Pillar Design Methodology was developed in 1995 using the maximum likelihood statistical approach adopted by Salamon and Munro in the 1960s and extended to account for squat and rectangular pillars. The methodology is based on back analysis of field performance to derive linear and power versions of pillar strength formulae and to assign a probability of stability to the design outcomes based on these formulae. This paper reviews some of the considerations arising out of the application of the UNSW and other empirical pillar system design approaches. Issues canvassed include confidence limits associated with the strength of rectangular shape pillars, the scope of UNSW probabilities of stability, precautions in applying modified pillar design formulations based on relationships between pillar width-to-height ratio and pillar safety factor, the effects of water pressure on pillar load and stability in flooded workings, the applicability and limitations of civil engineering based floor bearing capacity formulae, and the confidence to be placed in experimental panels.

INTRODUCTION

The stability of pillar layouts is an interactive function of both the stability of the excavations and the stability of the natural support, or pillars, left between the excavations. Most safety and production difficulties related to instability of the pillar component of the mine layout can be attributed to one of three factors, namely:

- a design focus restricted to the strength of the pillar itself;
- the inappropriate application of a pillar design procedure to conditions outside of its intended purpose or operational range; and
- non-compliance with the mine design.

The safe and efficient design of the pillar component of a mine layout requires that consideration be given to:

- the pillars
- the pillar/roof interfaces
- the immediate roof strata
- the pillar/floor interfaces, and
- the immediate floor strata.

These five elements comprise what is known as the *pillar system*. They influence both the load carried by the pillars and the strength of the pillars. Since the early 1990s, there has been a research focus in Australia on coal pillar system design. One outcome has been the UNSW Pillar Design Methodology, which now finds extensive application. In all likelihood, this design procedure would have prevented all 18 known pillar failure events and a number of the pillar extraction mishaps that have occurred in Australian coal mines over the last 25 years. However, it has to be applied correctly and judiciously. This is not always the case, resulting in two collapses since 2001 in bord and pillar workings that were less than 2 years old. There is no one design procedure for all circumstances and it is important that end users do not misapply pillar design methodologies or push the limits of a pillar design procedure too far.

DEFINING PILLAR FAILURE

One of the complexities in designing pillar systems is that pillar strength, failure mode and post-failure behaviour are variable. Laboratory testing gives insight into how these factors are influenced by pillar width-to-height ratio, w/h (Figure 1). Field experience and numerical modelling confirm that width-to-height ratio affects the load-deformation behaviour of in situ coal pillars in a similar manner, albeit that the various stages of behaviour may be associated with different width-to-height ratios to those recorded in the laboratory.

In mining layouts comprising pillars of small width-to-height ratio, typically less than four, the volume of coal in the pillars is usually small in comparison to the volume of the surrounding voids. This factor and the slender nature of such pillars make them prone to rapid and total disintegration when their strength is exceeded.

As the width-to-height ratio increases, failure is more likely to develop over an extended period of time and the pillars become less deformable in their failed state. Pillar failure in conventional bord and pillar layouts may be arrested quickly and seam convergence restricted to low levels due to the voids surrounding the pillars becoming choked off by pillar dilation. As width-to-height ratio increases, the signs of pillar failure become less evident

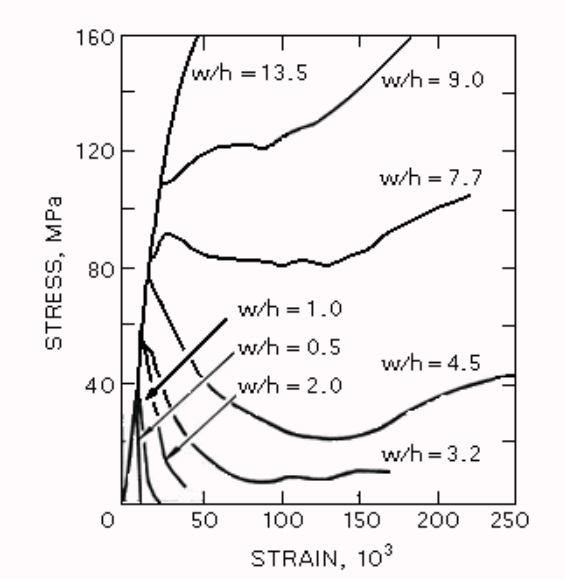

Figure 1. Influence of width to height ratio, w/h, on the strength and post failure behaviour of coal specimens as determined by laboratory testing (Das, 1986).

on the surface and are more likely to go undetected if the mine workings are no longer inspected from underground.

At higher width-to-height ratios, of the order of 8, instrumentation installed into the core of the pillar may be required to confirm that pillar failure has occurred. Ultimately, a point is reached where a failed pillar can support a load greater than its failure load, albeit that it may be more deformable than in its unfailed state. There is a body of opinion that, in competent roof and floor conditions, self generated confinement within a coal pillar will prevent it from failing under any practical working load once its width-to-height ratio exceeds 10. However, the increase in the overall load carrying capacity of a pillar with increasing width-to-height ratio can aggravate the occurrence of pressure bursts within the pillar, which can indirectly result in pillar failure.

UNSW PILLAR DESIGN METHODOLOGY

Two features distinguish the Salamon and Munro (1967) approach to determining coal pillar strength in South Africa. Firstly, it was based on back-calculating the *in situ* strength of a natural structural element from data representing field experience. Secondly, it assigned a probability of stability to the safety factor of a coal pillar. The database was comprised almost exclusively of square pillars and so the pillar strength formula only incorporates one of the plan dimensions of a coal pillar, Equation 1. The approach has proved extremely successful in designing over 2 million coal pillars in South Africa and remains largely unchanged today.

$$\sigma_{ps} = 7.2\frac{w_m^{0.46}}{h^{0.66}} \quad (MPa) \qquad (1)$$

Where:

σ_{ps} = pillar strength

w_m = minimum pillar width = w_1 for a square pillar (m)

h = pillar height (m)

The existence of this extensive experience and the lack of another widely tested method for estimating the strength of coal pillars encouraged Salamon et al. (1996) to test the approach under Australian conditions, resulting in the so-called UNSW Pillar Design Methodology. The Australian database includes rectangular and diamond shaped pillars and is restricted to cases where the roof and floor contacts and the surrounding strata played no role in the pillar failure. Engineering intuition suggests that the load bearing capacity of a rectangular pillar is somewhat greater than that of a square pillar of the same minimum width, because of the additional confinement that develops along the length of a rectangular pillar. However, mechanistic considerations suggest that this benefit will not materialise in pillars that have a small minimum pillar width height ratio (w_m/h), because failure will progress across the narrow dimension to the core of the pillar before the additional confinement is generated in the long dimension.

The UNSW researchers addressed these issues by invoking the concept of hydraulic radius (Wagner, 1980) to calculate an *effective pillar width* and applying it to the most general case of a parallelepiped shape pillar, Figure 2. They based their statistical analysis on the judgement that the effective pillar width only starts to come into play once w_m/h = 3, with the full benefit only materialising once w_m/h = 6.

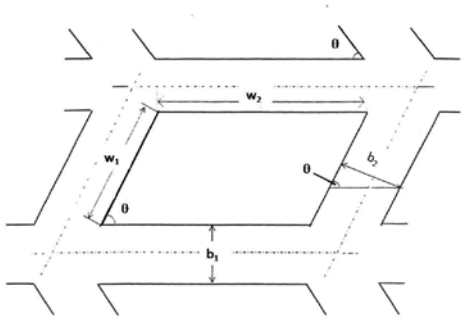

Figure 2. Definition of mining variables in the plane of the seam.

The UNSW research also incorporated the *squat pillar* extension of the Salamon and Munro pillar strength formula (Salamon, 1982), whereby 'squat' is defined by a width-to-height ratio above which pillar strength increases exponentially. The UNSW statistical back-analysis was based on the judgement that a pillar behaved as a squat pillar once w_m/h > 5. The following UNSW pillar strength formulae resulted:

$$Linear: \qquad \sigma_{ps} = 5.12\left\{0.56 + 0.44\left[\frac{w_m}{h}\right]\right\} \qquad (MPa) \qquad (2)$$

(Note: The linear formula is premised on minimum pillar width only)

Power:

$$\frac{w_m}{h} < 5: \qquad \sigma_{ps} = 8.60\frac{(w_m\Theta)^{0.51}}{h^{0.84}} \qquad (MPa) \tag{3}$$

$$\frac{w_m}{h} \geq 5: \qquad \sigma_{ps} = \frac{27.63\Theta^{0.51}}{w_m{}^{0.220}h^{0.110}}\left\{0.290\left[\left(\frac{w_m}{5h}\right)^{2.5} - 1\right] + 1\right\} \quad (MPa) \tag{4}$$

Where

$$w_m = w_1 Sin\theta$$

$$\Theta = \left[\frac{2w_2}{w_1 + w_2}\right]^{\frac{R-3}{3}}$$

Equation (4) comprises three components as shown in Equation (5).

$$\sigma_{ps} = k_2 V^a R_c^b \quad \Theta^a \quad \left\{\frac{b}{\varepsilon}\left[\left(\frac{R}{R_c}\right)^{\varepsilon} - 1\right] + 1\right\} \tag{5}$$

Base Power Strength Formula | Effective Pillar Width Multiplier | Rate of Strength Increase once $w_m > R_o$

Where:

V = pillar volume = $(w_m w_2)h$

R = w_m/h

R_o = the width-to-height ratio at which a pillar is considered to become squat (=5 for UNSW)

ε = A measure of the rate of strength increase once w_m/h exceeds R_o (=2.5 for UNSW)

The statistical confidence levels associated with these pillar strength formulae are shown in Table 1. The standard deviation for the UNSW linear pillar strength formula is greater than that for the UNSW power strength formulae, indicating that there is a lower confidence level associated with the linear formula. This is reflected in the higher safety factor required when applying this formula to achieve the same levels of confidence in a design outcome as when the power formulae are applied.

Table 1. Probability of failure associated with UNSW pillar design formulae.

Probability of Failure	UNSW Linear Formula	UNSW Power Formula
	Safety Factor	
8 in 10	0.84	0.87
5 in 10	1.00	1.00
1 in 10	1.30	1.22
5 in 100	1.40	1.30
2 in 100	1.53	1.38
1 in 100	1.62	1.44
1 in 1,000	1.85	1.63
1 in 10,000	2.09	1.79
1 in 100,000	2.33	1.95
1 in 1,000,000	2.57	2.11

CONSIDERATIONS RE UNSW METHODOLOGY

Effective Pillar Width

The procedure proposed by Salamon et al. (1996) for deriving effective pillar width is premised on a mechanistic understanding of pillar behaviour. However, the database of parallelepiped pillars used to derive the UNSW pillar strength equations is small. It includes 11 rectangular shaped pillars and only one diamond shaped pillar. In situations where pillar stability is critical, it is recommended that at this point in time, pillar design be based on the minimum dimension for pillar width.

Developments in mining technology and ground control strategies are resulting in a greater use of diamond shaped pillars. Additional caution is always required when dealing with pillars of this shape because of the propensity for the two acute corners of the pillar to be damaged by equipment, to spall along cleats or to fail under low levels of vertical stress. These effects can result in a significant reduction the load carrying area of a pillar whilst, at the same time, increasing the load acting on the remaining portion of the pillar. Average pillar stress may increase significantly. The effects on pillar stability are more pronounced on smaller pillars. The design of diamond shaped pillars should be premised on site inspections and consideration of the geotechnical environment and be followed up with site monitoring and performance review.

Empirical Data Regime

The fundamental rule that considerable care must be exercised if empirical relationships are applied outside the range of the data used in their derivation is particularly important when working with pillar strength formulae. The maximum width-to-height ratio of failed pillars in the Salamon and Munro (1967) database was 3.37. The UNSW database included one failed case at a width-to-height ratio of 8.16; otherwise the remaining 15 cases had a width-to-height ratio of ≤ 5.

Subsequently, cases of pillar failure in competent roof and floor conditions have been reported in South Africa for width-to-height ratios of around 4, and in the USA for width-to-height ratios up to 5. Additionally, the Investigation Report into the Crandall Canyon collapse in the USA in 2007 (Stricklin, 2008) concluded that overstressed panel pillars with a width-to-height ratio of almost 8 had failed over a distance of 800m within seconds and that the barrier pillars to the north and south also failed. The barrier pillar to the south had a width-to-height ratio of about 6.2 at the point

where failure was initiated, with failure then propagating through an area where the width-to-height ratio of the pillars exceeded 15.

There are a number of reasons which may account for the limited reported cases of pillar failures at width-to-height ratios exceeding about 5. These can be illustrated by considering a panel of square pillars having a width-to-height ratio of 8, where pillar width is 20 m and pillar height is 2.5 m. Based on the UNSW power formula, such pillars have a strength of the order of 21 MPa. The reasons include:

- Typical bord and pillar mining layouts do not generate the high loading regimes required to cause failure of pillar of high width-to-height ratio. In order to generate sufficient tributary load to fail the case study pillars at a depth of 100 m, bord width would need to be of the order of 38m (and greater if caving occurs). Safety and practical perspectives dictate against such layouts. At a depth of 400 m, the bord width required to generate the failure load is reduced to the order of 8.5 m, which is feasible as evidenced by Australian experience.
- The occurrence of total collapse of large width-to-height ratio pillars will be masked in conventional bord and pillar layouts because the bords will choke off, thereby arresting the failure and limiting seam convergence. In the 400 m deep case study, the effective total extraction mining height is 51% of the pillar height, say 1.25 m. This is a worse case approach and not representative of bord and pillar situations. Based on Holla (1987), it would result in maximum vertical displacements, tilts, tensile strains, and compressive strains of the order of 550 mm, 3 mm/m, 0.6 mm/m and 1 mm/m, respectively, at the surface. These are small subsidence effects that could easily go unnoticed, especially where the surface is undeveloped.
- Failure of pillars of large width-to-height ratio is more likely to be characterised by strain softening or strain hardening rather than total collapse. Therefore, failure may go undetected underground, particularly since the high pillar loading regimes are likely to have been generated by partial extraction of the pillars on retreat, restricting safe access back into these areas.

It is noteworthy that the UNSW case which failed at a width-to-height ratio of 8.16 and the Crandall Canyon case which failed at a similar width-to-height ratio were both associated with unusual mining layouts that resulted in exceptionally high pillar loads. The UNSW data point was the outcome of a research project concerned with validating that pillar size at depth could be based on an upper bound width-to-height ratio, regardless of working load. A panel of large pillars was formed at a depth of over 300 m and then reduced in size by trimming the sides off the pillars when retreating out of the panel. An extensive array of instrumentation was used to detect and confirm the onset of pillar failure in the backbye area of the mining panel. In the case of Crandall Canyon, the pillars were at a depth of 500 to 600 m and exposed to high abutment stress from pillar extraction and adjacent longwall mining operations. There are a number of other reports of high width-to-height ratio pillars failing but there is some doubt about the reliability of these reports as the poor condition of the perimeter of pillars may have been misinterpreted as indicating pillar failure.

Implications of field experience to date are:

- There is a lack of data to validate pillar strength once width-to-height ratio exceeds 5.

- The lack of failed cases at width-to-height ratios greater than 5 should not be interpreted to mean that coal pillars will not fail at higher width-to-height ratios.

Care also needs to be exercised at the lower end of the width-to-height ratio spectrum. As the width-to-height ratio reduces below 4, coal mass strength and geological structure have an increasing impact on pillar strength. Galvin et al. (1995) concluded that when geological features are present in pillars, empirical pillar strength formulae may overestimate pillar strength, especially at width-to-height ratios of less than 4. The researchers recommended that, due to the sensitivity of pillar strength to geological structure and to slight variations in pillar dimensions, a lower width to height bound of 2 be applied when using pillar strength formulae. Esterhuizen (1995) reached a similar conclusion in respect of geological structure and Madden (1990) in respect of a lower bound w/h ratio.

Methodologies such as that of Salamon and Munro or UNSW are not recommended for the design of highwall pillars, the width of which falls outside the empirical databases used to derive these formulae. The width-to-height ratio of very slender pillars is too small for pillar strength to be influenced by confinement and, in the absence of geological structure, their strength is governed primarily by material strength. Geological discontinuities, especially if they are inclined, have the potential to reduce pillar strength to a negligible value. Numerical modelling by Esterhuizen (2006) of slender pillars comprised of limestone, for example, indicated that pillar strength was reduced by as much as 70% in the presence of an inclined discontinuity.

Figure 3 illustrates an example of where the UNSW pillar strength formulae have been applied to highwall pillars. Clearly, highwall pillar strength is not predicted by the formulae. Further concerns arise with Figure 3 in that, in some instances, the upper bound, or limit line, shown in this figure is being assigned an equation and applied to the design of coal pillars. This approach is flawed because:

1. Mathematically, no sensible relationship can exist between width-to-height ratio and safety factor because safety factor is, itself, a function of width-to-height ratio. Any safety factor can be associated with a given width-to-height ratio value, as evident in Figure 3
2. The lower end of the limit curve is being determined on the basis of applying pillar strength criteria that do not apply to very small and slender highwall pillars.
3. The upper end of the limit curve is being determined on the basis of only one data point. There is no confirmed engineering reason why there could not be a range of safety factors associated with width-to-height ratios at this upper end, just as there are at lower width-to-height ratios. The lone data point may simply reflect a lack of bord and pillar mining layouts with the capacity to generate sufficient load to cause failure of such high width-to-height ratio pillars, and the difficulty in detecting failure in these circumstances.

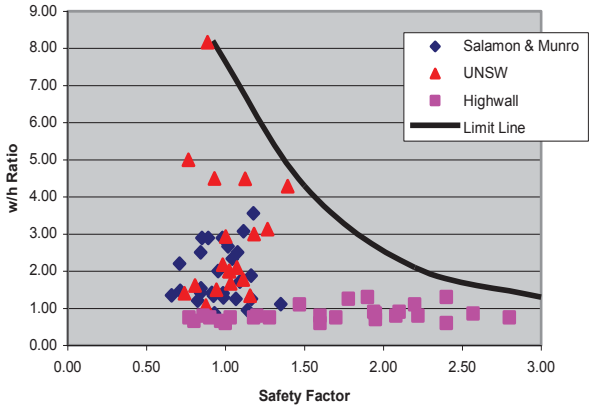

Figure 3. A w/h ratio versus safety factor relationship which is prone to erroneous interpretation.

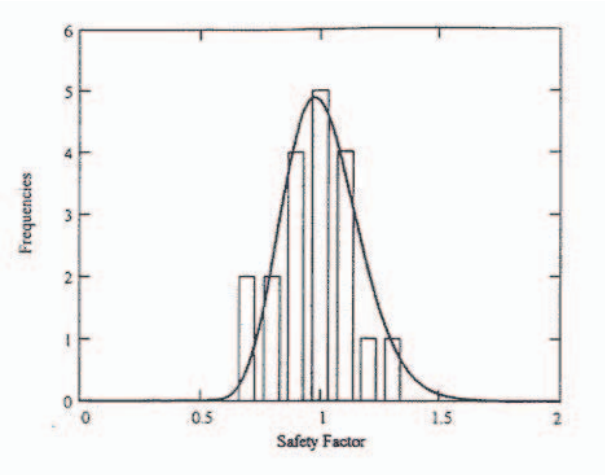

Figure 4. Histogram of frequency of failure versus safety factor constructed from the Australian database employing the UNSW power law formulae and utilizing the maximum likelihood method.

Probabilistic Relationships

Figures 3 and 4 show the distribution of safety factors for Australian failed pillar cases based on the UNSW power pillar strength formulae and tributary area load. The safety factors range from 0.74 to 1.39. This scatter reflects the approximations, assumptions and potential errors in the input data associated with this pillar design methodology. These include:

- approximating gravitational acceleration to 10 m/s^2;
- approximating the effective overburden density to 2500 kg/m^3;
- assuming pillar strength to be a function of only three parameters, namely coal material strength, pillar width and pillar height;
- assumed ramp up rate of effective pillar width;
- assumed width-to-height ratio of transition to a squat pillar;
- assumed rate of strength increase of squat pillars;
- assuming that all pillars in the database were subjected to full deadweight loading;
- computing pillar strength based on average pillar stress rather than the actual stress distribution within the pillar;
- natural variations in geological conditions and material properties between the sites from which the data was collected;
- variation in the effective load carrying area of the pillar edges associated with the excavation technique (hand mining, drill and blast, machine cutting);
- a database that may have included pillar failures in flooded workings, resulting in pillar load being less than tributary area load due to buoyancy effects;
- mining dimensions derived from plans which may not have accurately depicted the actual working dimensions;
- a database that is likely to be biased towards undersized rather than oversized pillars.

These uncertainties are catered for in the design process by the relationship between probability and safety factor. The higher the risk associated with an unsuccessful outcome, the lower the level of uncertainty that can be tolerated in the design process and, therefore, the higher the required design safety factor.

The solid line shown in Figure 4 has the shape of a 'normal' or 'Gaussian' distribution and is symmetrical about its mean. This is an assumed and purely theoretical distribution. It is but one of many possible mathematical functions that could be assumed to denote the shape of the distribution of safety factor versus frequency. Insufficient data hampered the evaluation of alternative distributions until 2006 when Salamon et al. (2006) repeated the analysis for a Weibull distribution and a Gamma distribution. These distributions were chosen because they also satisfied the mathematical properties required for the type of problem being analysed. The researchers found that the Weibull distribution produced significantly poorer quality outcomes than the lognormal distribution, whilst the Gamma distribution gave comparable qualities of fit and very similar fitting functions. It was concluded that the lognormal distribution gave reasonably robust and consistent results.

Table 1 shows that increasing the safety factor beyond 1.63 when using the UNSW power pillar strength formulae and beyond 1.85 when using the UNSW linear pillar strength formula, only has the potential to reduce the probability of failure by 1 in 1,000. However, as the consequences of failure increase, lower probabilities of failure could well be justified. It is not uncommon to design to probabilities of 1 in 1 million or greater when the consequences are very high, such as inrush of a tidal water body or derailment of a high-speed passenger train. Often, percentage extraction only has to be reduced marginally to achieve orders of magnitude reduction in risk.

In an attempt to produce more realistic estimations of safety factor, some practitioners have undertaken analysis of pillar system stability based on reducing the value of gravitational acceleration to 9.81 m/s^2, reducing the value of effective overburden density to account for buoyancy effects due to workings being flooded or to the overburden containing alluvial deposits, and reducing pillar load to compensate for an expectation that tributary area theory overestimates pillar load in the given circumstances. It needs to be appreciated that modifications represent changed circumstances to those for which the original relationship between safety factor

and probability of failure were derived. Hence, the original probabilities of stability may no longer be applicable.

Conversely, the statistical process for calculating the relationship between safety factor and probability of stability may include cases where the extraction dimensions were larger than the dimensions shown on the mine plan. Therefore, applying measurements obtained from old workings or making allowances for over-mining could be unnecessarily conservative in some cases because such variations are already reflected in the probabilities of stability.

It is also sometimes argued that a mining layout is more stable than predicted by statistical procedures based on tributary area load because, due to factors such as stiff roof strata, the pillars in the layout are not being subjected to full tributary area. Caution needs to be applied when adopting this argument. It gives rise to a counter argument when applied to the derivation of pillar strength formulae and probabilities of stability. Both Salamon and Munro and UNSW based the derivation of their pillar strength formulae on a criteria that the diameter of a panel of pillars, W, had to at least equal the depth of mining, H. This was thought to result in full tributary loading. It is now known that there are some mining environments included in both the South African and Australian databases in which mining span must exceed depth by a considerable margin in order to achieve full deadweight loading. Hence, it is logical to conclude that these data points may have contributed to pillar strength being overestimated by Salamon and Munro and UNSW.

Normally, this should be of no consequence because it is reflected in the probability of design success associated with any given safety factor. Similar considerations are associated with the application of numerical models to calculate the input load into design procedures such as the UNSW Pillar Design Methodology. Judgment and experience premised on sound geotechnical engineering principles are required.

SOME GENERAL CONSIDERATIONS

Pillar Stiffness

Probabilistic analysis of pillar stability is premised on the overall behaviour of panels comprising pillars that are regular in distribution and uniform in shape. Therefore, the pillars are of equal modulus (E), area (A) and height (h) and, thus, stiffness (EA/h) and so are assumed to share the load equally.

It is often the case that old workings comprise pillars that are irregular in shape and in distribution. It sometimes happens that in assessing the stability of these workings, the focus in placed on the smaller pillars in the layout because they are perceived to have the lowest safety factor. However, in reality, the safety factor of these pillars may be enhanced because they are surrounded by stiffer pillars. The stiffer pillars shield the softer pillars from load. For failure of the smaller pillars to occur, the surrounding larger pillars must first have failed. Once this occurs, there is little chance that the small pillars will remain stable. Therefore, when evaluating the stability of irregular pillar layouts, it is important to appreciate that:

- Probabilities of stability derived on the basis of tributary load theory may not apply.
- Larger pillars may be the weakest links in the system.

Similar consideration needs to be given to stiffness when assessing the stability of an individual pillar that is irregular in shape. Figure 5 shows a mining layout in which stubs have been driven in some pillars and diagonal cuts made through other pillars. The effect of driving a stub into a pillar can be visualised as resulting in three pillars of potentially different stiffness, namely, the fenders of coal to each side of the stub and the remaining remnant of the pillar. The stiffer remaining pillar segment will attract load.

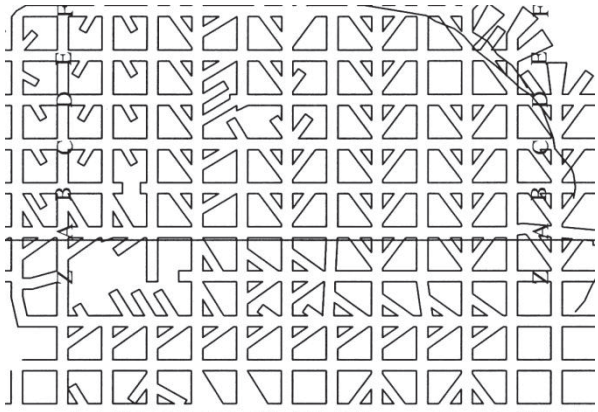

Figure 5. Layout of a panel in which the pillars failed.

Considerable judgment and experience premised on knowledge are required when computing the stability of a layout such as that shown in Figure 5. This layout was designed to be stable but failed as it was being mined. When the relative stiffness of the various portions of the pillar is taken into account, the UNSW Pillar Design Methodology yields an approximate probability of stability of only 70%.

Flooded Workings

Theoretically, the flooding of mine workings can impact on pillar load in two ways. At one extreme, all the surfaces of the mine workings could be visualised to be impervious (or sealed), in which case water pressure acting on the roof of the workings would function as a hydraulic jack to unload the pillars.

At the other extreme, the overburden may be fully saturated over the full water head. Archimedes principle applies and the overburden has buoyancy, reducing its effective density. If the workings are flooded to the surface, the average pillar working stress is only of the order of 60% of the tributary area stress. Obviously, this can have a significant positive impact on the stability of old workings. However, the other side of the equation must not be overlooked, namely the effect of water under pressure on pillar strength. Water can reduce pillar strength in a number of ways, including reducing friction on fracture planes and end contact surfaces and accelerate the weathering of clay rich materials that may be present in a pillar or the adjacent strata. Recent pillar collapses associated with the decision to allow the bord and pillar iron ore workings to flood in the Lorraine district of France is testament to this behaviour. On the other hand, flooding of old bord and pillar coal workings beneath the city of Newcastle

in NSW, Australia, over many decades appears to have had no effect on pillar strength, or at least to have been compensated by the associated pillar unloading.

Ultimate Bearing Capacity

The term 'foundation' can have two meanings in geotechnical engineering, one being the natural material on which the footing of a structure is founded, and the other being the footing itself. In this paper, a coal pillar is referred to as a 'footing' and the strata immediately above and below the pillar as 'foundations'.

There have been many attempts to apply civil engineering foundation principles to the design of coal pillar systems. These principles can be grouped under the following headings, of which ultimate bearing capacity is the focus of this paper:

- Settlement
- Ultimate Bearing Capacity
- Creep
- Swell

Most ultimate bearing capacity procedures are premised on laboratory scale testing, empirical models, and elastic and plastic theory relating to the behaviour of soils, sands and clays which are homogeneous to a depth of two to three times the width of the overlying footing. To date, these procedures have met with mixed and questionable success when applied to coal mining situations. Often, they have been applied to geotechnical conditions well outside those for which they were developed. In many instances, so called 'successful' design outcomes have been premised on novel failure mechanisms or on material properties and safety factors that have had to be unrealistically adjusted in order to replicate field performance.

There have been a number of collapses of mine workings due to foundation failure, some of which extended back into active working faces. In soft and weak environments or where one or more low cohesion and friction interfaces are present in the foundation, foundation failure can be time dependent. Therefore, the risk associated with the inappropriate application of an ultimate bearing capacity design approach may take many years to materialise, during which time extensive areas of vulnerable mine workings may have been formed. Hence, one needs to be aware of the limitations and uncertainties associated with bearing capacity formulae.

Classical ultimate bearing capacity theory assumes that rupture surfaces develop in the foundation material of a footing and the foundation fails in shear. Failure is generally considered to take one of three forms, namely:

1. Punch shear failure
2. Local shear failure
3. General shear failure

Materials that are practically incompressible and have finite shear strength fail in general shear and, therefore, this failure mode is of most relevance to the stability of coal pillar systems. The failure mode is characterised by well-defined slip surfaces that extend from one edge of the footing and daylight on the opposite side of the footing, Figure 6. As the material in Zone I moves down, plastic flow is initiated in Zone II. The overlying material in Zone III provides resistance to this displacement but once this is overcome, the shear failure planes extend to the surface and the material around the footing bulges. Figure 7 shows general shear failure of the floor adjacent to coal pillars.

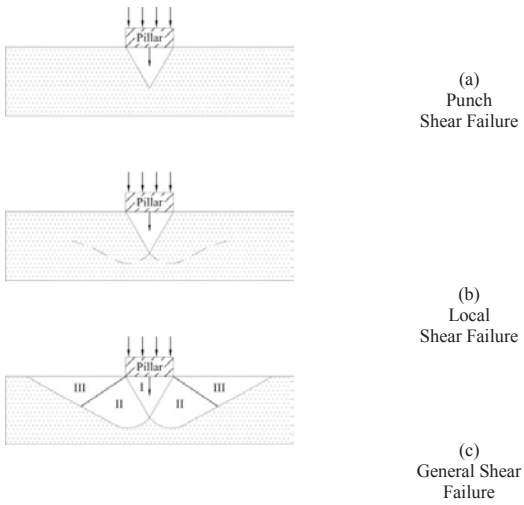

Figure 6. Three principal failure modes associated with bearing capacity failure (after Vesic, 1963).

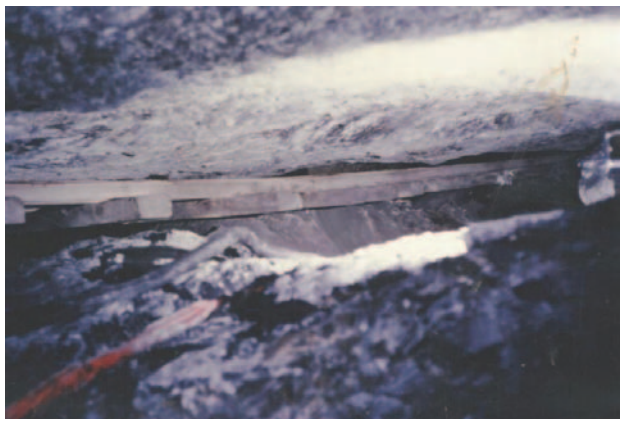

Figure 7. Foundation failure in 4.5m high bord and pillar workings, causing rail track to be pushed up to the roof.

If the thickness of a weak or soft foundation layer is limited, slip surfaces may not be able to fully develop. In this case, the foundation material can fail, shear on bedding planes and extrude laterally from under or over the footing, Figure 8. When this occurs in a coal pillar foundation, it subjects the pillar to lateral tension, which can result in open cracks developing from roof to floor through the full width of the pillar, Figure 9. The pillar failure mode moves from one of compressive failure under vertical load towards one of tensile failure under lateral load. The distinction between foundation failure and pillar system failure becomes blurred in these circumstances because both mechanisms may be active and interacting.

There is a myriad of bearing capacity formulae dating back to the mid 1850s. Those that find most application today are based on Buisman-Terzaghi bearing capacity equation (Terzaghi, 1943) for a uniformly loaded, infinitely long strip footing founded on a homogenous incompressible material, Eq 5.

$$q_u = cN_c + \gamma qN_q + \frac{\gamma wN_\gamma}{2} \quad (5)$$

Where

q_u = ultimate bearing capacity

N_c, N_q, N_y = bearing capacity factors which depend on the value of internal friction, φ

w = width of footing

γ = unit weight of soil

q = depth of footing beneath the surface

The bearing capacity of a foundation is least when it is fully saturated and in an undrained state, in which case $\phi = 0°$ and $N\gamma = 0$. In a mining environment in which the roadways have not been backfilled, flooded or affected by roof falls, the surcharge load of any material around the pillar can also be equated to zero; that is, q = 0. Hence, Eqn 5 reduces to one term, namely:

$$q_u = cN_cS_c \quad (6)$$

Several techniques have been proposed for estimating the ultimate bearing capacity of non-homogenous and anisotropic foundation materials. The more common which have been applied to mining environments on the basis that $\phi = 0°$ are summarised in Table 2.

In civil engineering, it is common practice to apply a safety factor of around 2 to bearing capacity design, increasing to 3 where additional uncertainty exists in the adequacy and reliability of field data or the bearing capacity formulae, or where the consequences of failure would be severe. Application of bearing capacity formulae by Ganow (1975) to the back analysis of floor heave in the coal mines of Illinois led to the conclusion that failure was occurring at a safety factor of almost 7. Seedsman and Gordon (1992) calculated a safety factor of 9.1 when they applied the bearing capacity formula of Mandel and Salencon (1969) for infinitely long pillars to rectangular and square pillars in the Great Northern Seam at Cooranbong Colliery. They concluded that this implied that cohesion had to be 1/8 of average laboratory value quoted by Seedsman and Mallet (1988) and 1/13 of the value measured at the site.

Further application of the Mandel and Salencon (1969) formula by Seedsman and Gordon (1992) to rectangular pillars of w_2/w_1 = 3.5 in the Great Northern Seam at Cooranbong Colliery and w_2/w_1 = 3.2 in the Fassifern Seam at Wyee Colliery produced safety factors of the order of 5 and 15, respectively. These safety factors were based on the most critical stability state of $\phi = 0°$. Seedsman and Gordon proposed an alternative model of bearing capacity failure as a means of avoiding unrealistic reductions in material properties whilst still employing classical bearing capacity formulae. This model was based on a number of assumptions, including that bearing capacity failure only occurred beneath the outer 1.5 to 2m rib zone of a pillar. However, the model could not account for behaviour at Wyee Colliery.

Mills and Gale (1993) and Mills and Edwards (1997) undertook more comprehensive studies involving 25 sites, of which 19 were located in the Great Northern Seam and 5 in the overlying Wallarah Seam in the Lake Macquarie region, the other being located in Illinois. Significant surface subsidence had occurred at 16 of these sites, many of which comprised a partial extraction layout whereby every alternate row of pillars had been extracted. Mills and Gale (1993) reported that bearing capacity theory predicted failure loads that were 4 to 5 times greater than those at which these pillar systems typically failed. In order to produce bearing capacity failure loads that corresponded with pillar loads, the researchers had to equate the properties of the claystone floor to a fully saturated clay in an undrained state ($\phi = 0°$). They found it difficult to conceive that claystone could have a friction angle even as low as 20° and were of the view that the claystone material under the pillars retained essentially rock-like properties. They went on to conclude that a classical bearing mechanism was not appropriate to explain the field behaviour, albeit that claystone behaviour was still involved in the pillar failure mechanism.

The high bearing capacity safety factors associated with the back analysis of unstable coal pillar events suggest that, with perhaps a few exceptions, classical bearing capacity mechanisms are not directly applicable to mining environments or if they are, the material strengths used in the analysis are grossly too high. Factors to consider include:

- Formulae derivation circumstances. The conditions under which the formulae were derived empirically are quite different to those applying in underground mining environments.
- Dimensional scale. The width of a pillar footing is typically an order of magnitude or more greater than a civil engineering footing. Similar to a coal pillar, this can change the confinement regime and, hence, the behaviour mode of the foundation.
- Load scale. The loads to which pillar foundations are subjected are typically at least one order of magnitude greater than those encountered in civil engineering.
- Multiple layered situations. The wider footing and higher loading regime encountered in mining extends the zone of influence of the footing, thereby increasing the likelihood that foundation response will be affected by the behaviour of multiple layers of strata. It is likely that these multiple layers will contain a variety of materials, some with contrasting mechanical properties. Classical bearing capacity formulae do not explicitly account for these situations. Implicit approaches, such as calculating effective material propertiesof a number of layers and inputting these values into classical bearing capacity formulae, can fail to give proper consideration to behaviour being modified or controlled predominantly by specific layers.
- Interaction between footings. The footing width to spacing ratio in a mining environment is about the inverse of that

Table 2. A selection of bearing capacity formulae which have found application in underground coal mining for the case of Φ= 0°.

	Pillar Shape	Ultimate Bearing Capacity (q_u)	Modification Factors
Classical: **(Buisman-Terzaghi)** • Single homogenous layer	Strip	$cN_c = 5.14c$	$N_c = 2+\pi = 5.14$
Classical: incorporating shape factors • Single homogenous layer		cN_cS_c	
	Square	$cN_c\left[1+\frac{N_q}{N_c}\right] = 6.168c$	$N_c = 5.14$ $\frac{N_q}{N_c} = 0.2$
	Rectangular	$cN_c\left[1+\left(\frac{w_1}{w_2}\right)\left(\frac{N_q}{N_c}\right)\right]$ $= c\left[5.14+1.028\left(\frac{w_1}{w_2}\right)\right]$	
Mandel & Salencon (1969) Soft layer over a layer of infinite rigidity and strength.	Strip	$cN_cF_c = 5.14\ c\ F_c$	$N_c = 5.14$ w_1/t / F_c: ≤ 1.41 / 1; 2 / 1.02; 3 / 1.11; 4 / 1.21; 5 / 1.30; 6 / 1.4; 8 / 1.59; 10 / 1.78; Thereafter: $N_cF_c \cong (\pi+1+0.5\ w_1/t)$
Brown & Meyerhof (1969)		cN_m where N_m is a function of c_2/c_1	
• Soft layer overlying a stiffer layer • c_1, t_1 = cohesion and thickness of top layer, • c_2, t_2 = cohesion and thickness of bottom layer	Strip	$c_1\left[4.14+1.1\left(\frac{w_1}{t_1}\right)\right]$ $for\ \frac{w_1}{t_1}>0.9$	
	Square	$\cong c_1\left[5.05+0.66\left(\frac{w_1}{t_1}\right)\right]$ $for\ \frac{w_1}{t_1}>1.5$	Derived for a circular footing of diameter w_1.
• Stiffer layer overlying a softer layer • c_1, t_1 = cohesion and thickness of top layer, • c_2, t_2 = cohesion and thickness of bottom layer	Strip	$1.5\left(\frac{t_1}{w_1}\right)c_1 + 5.14\,c_2$	
	Square	$\cong 3.0\left(\frac{t_1}{w_1}\right)c_1 + 6.05\,c_2$	Derived for a circular footing of diameter w_1.

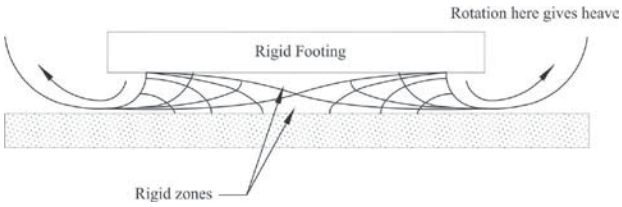

Figure 8. Bearing capacity failure of a thin layer (after Mandel and Salencon, 1969).

Figure 9. Extrusion of a soft and weak floor material from under a pillar, causing open vertical cracks to develop through the full width of the pillar because of induced lateral tension.

in a civil engineering environment, thereby giving rise to a much greater potential for interaction between footings. Interaction may provide confinement to the foundation zone of an adjacent pillar, retarding the development of shear failure and resulting in an increase in bearing capacity. Benefits are difficult to quantify in the field but laboratory studies of strip footings by Stuart (1962) and West and Stuart (1965) showed that bearing capacity started to increase once the distance between footings was less than 3 times the footing width.

- Material properties. It is neither practical nor economically feasible to determine material properties to the same level of detail or accuracy in a mining environment as it is in a civil engineering environment. Site access is severely limited by depth, the vertical extent over which properties need to be determined is an order of magnitude greater and the number of different materials of interest in these zones is likely to be considerably greater. The lateral extent of the area affected by a layout of pillar footings can be 2 or more orders of magnitude greater.
- Unloading of confining material. Mining results in an unloading of the constraining material surrounding a pillar foundation.
- Discontinuities: Due to the large scale of mining environments, coal pillar foundations are likely to contain discontinuities. The reduction in shear strength associated with discontinuities in not accounted for in bearing capacity formulae.
- Scale effects on strength: Bearing capacity theory does not account for reduced average shear strength along failure slip planes as foundation size increases.
- Groundwater and flooding: Water can affect all three components that determine bearing capacity. The 'cN_c' component is affected because the shear strength of soft and weak rock and soil materials may be reduced significantly in the presence of water. For example, the unconfined compressive strength of selected, wet, coal-bed floor strata has been found to be only 26 to 40% of that in its dry state (Bieniawski, 1987). If the foundation material is saturated, the 'γqN_q' component has to be based on effective material weight, γ', (γ - γ_{fluid}) to account for buoyancy effects. When workings become flooded, a surcharge load to the roof and floor surfaces of the foundations, in which case the '$\gamma wN\gamma$' component may need to be included in bearing capacity calculations.
- Time. Rock mass properties can change over time in a mine environment, especially upon being exposed to moisture or sustained load.
- Footing construction. Pillar footings comprise natural, non-reinforced material that is riddled with vertical and horizontal defects (joints, cleat, bedding planes) and is of minimal tensile strength, whilst civil engineering footings are usually constructed of quality controlled, reinforced materials of higher tensile and compressive strength.

Making design distinctions between foundation failure mechanisms and accounting for how interaction between coal pillar footings and foundations affects these failure mechanisms appears to be unrealistic without the assistance of numerical modelling. Rather than relying on classical settlement and bearing capacity formulae, it would be more beneficial and reliable in mining circumstances to utilise numerical modelling to identify possible failure mechanisms and to undertake parametric studies to evaluate the sensitivity of design outcomes to uncertainties in input data and failure models. The value of this type of approach would be enhanced by integrating it with a stochastic modelling technique.

Experimental Panels

There is a history in the coal mining industry of pillar collapses arising from the adoption of mining layouts that were first trialled in a so-called 'experimental panel'. The collapse of Coalbrook Colliery in 1960 and a recent pillar collapse in Australia are examples. Three factors, in particular, impact on the confidence that can be placed in mining layouts trialled in experimental panels:

- Loading regime: The dimensions of a single experimental panel must be sufficiently large to generate the loading that the pillar system will experience when it is put into routine practice.
- Time: Typically, pillar layouts that are trialled in an experimental panel are motivated by a desire to maximise percentage extraction. This implies maximising pillar load. Because the strength of rock is time dependent, the final effects of this loading may not become apparent until well after the completion of the experimental panel.
- Probability of Failure: Consistent with maximising extraction, experimental panels are often designed to a minimum safety factor. A recent pillar collapse in Australia was associated with a layout designed to a safety factor of 1.2 on the basis of one successful trial in an experimental panel. This safety factor corresponds to a 1 in 10 chance of collapse, Table 1, which is considered a very high risk. Obviously,

there was a 90% chance that the experimental panel would not fail. Hence, one successful outcome is inadequate for providing any level of confidence in the design.

CONCLUSIONS

Statistically derived empirical pillar strength formulae which are supported by design confidence levels are powerful design tools when applied to the range of conditions utilized in their derivation. Extrapolation to other mining conditions can be very useful and insightful but it has to be undertaken with a considerable degree of care. The success of a design procedure should not be interpreted to mean that the design procedure is conservative. Many pillar failures have been associated with attempts to flout probability predictions. One off successful experimental panels are no measure of the reliability of a design procedure. Permanent pillar stability cannot be guaranteed and design must always be based on an assessment of the risks associated with any failure.

REFERENCES

Bieniawski, Z.T. (1987). Strata Control in Mineral Engineering. Rotterdam: Balkema. ISBN 90 6191 607 0.

Das, M.N. (1986). Influence of Width/Height Ratio on Post Failure Behaviour of Coal. Int. J. Min. 7 Geological Engineering, No. 4.

Esterhuizen, G.S. (1995). Rock Engineering Evaluation of Jointing in South African Seams and its Potential Effect on Coal Pillar Strength. Proceedings of the Conference on Mechanics of Jointed and Faulted Rock, Rossmanith (ed), Balkema, ISBN 90 5410 541 0.

Esterhuizen, G.S. (2006). An Evaluation of the Strength of Slender Pillars. SME Annual Meeting, Preprint 06-003.

Galvin, J.M., Hebblewhite, B.K. and Wagner, H. (1995). Pillar and Roadway Mechanics – Stage 2 – Design Principles and Practice. School of Mines, University of New South Wales, ISBN 0 7334 1338 2.

Ganow, H.C. (1975). A Geotechnical Study of the Squeeze Problems Associated with the Underground Mining of Coal. Ph.D. Thesis, University of Illinois, Champaign.

Holla, L. (1987). Subsidence Prediction in the Newcastle Coalfield. NSW Dept. of Minerals Resources.

Madden B.J. (1990). An Investigation into the Factors Affecting the Strength of Pillars in South African Coal Mines. Ph.D. Thesis, University of Witwatersrand.

Mandel, J. and Salencon, J. (1969). Force Portante D'Un Sol Sur Une Assise Rigide. Proceedings 7th International Conference Soil Mechanics and Foundation Engineering, Vol. 2.

Mills, K.W. and Gale, W.J. (1993). Review of Pillar Behaviour in Claystone Strata. Strata Control Technologies Consulting Report to Elcom Collieries and Coal and Allied, ELC0437 (Unpublished).

Mills, K.W. and Edwards, J.L. (1997). Review of Pillar Stability in Claystone Floor Strata. Sym on Safety in Mines. The Role of Geology. Eds. Doyle, Moloney, Rogis and Sheldon, University of New South Wales.

Salamon M.D.G. (1982). Unpublished Report to Wankie Colliery, Zimbabwe.

Salamon, M.D.G. and A.H. Munro. (1967). A Study of the Strength of Coal Pillars. J. Sth. Afr. Inst. Min. Metall. *68*:56-67.

Salamon, M.D.G., Galvin J.M., Hocking, G. and Anderson, I. (1996). Coal Pillar Strength from Back-Calculation. School of Mining Engineering, UNSW, Research Report RP 1/96.

Salamon, M.D.G., Canbulat, I. and Ryder, J.A. (2006). Seam-Specific Pillar Strength Formulae for South African Collieries. 50 Years of Rock Mechanics – Landmarks and Future Challenges. Proceedings of the 41st U.S. Rock Mechanics Symposium, Golden, CO, American Rock Mech. Assoc.

Seedsman, R.W. and Mallet, C.W. (1988). Claystones of the Newcastle Coal Measures. Final Report to NERDDC, Project 902.

Seedsman, R.W. and Gordon, N. (1992). Weak Claystone Floors and Their Implications to Pillar Design and Settlement. Proceedings of the 11th International Conference on Ground Control in Mining, Wollongong.

Stricklin, K.G. (2008). Report of Investigation. Fatal Underground Coal Burst Accidents, August - 16, 2007, Crandall Canyon Mine, MSHA, CAI-2007-15-17, 19-24

Stuart, J.G. (1962). Interference Between Foundations with Special Reference to Surface Footings on Sand. Geotechnique, Vol. 12.

Terzaghi, K. (1943). Theoretical Soil Mechanics. New York: John Wiley & Sons.

Vesic, A.S. (1963). Bearing Capacity of Deep Foundations in Sand. National Academy of Sciences, National Research Council, Highway Research Record 39.

Wagner, H. (1980). Pillar Design in Coal Mines. J. S. Afr. Inst. Min. Metall. *80*(1).

West, J.M. and Stuart, J.G. (1965). Oblique Loading Resulting from Interference Between Surface Footings on Sand. Proceedings of the 6th ICSMFE, Montreal, Vol. 3.

Stress Conditions and Failure Mechanics Related to Coal Pillar Strength

Winton Gale, Managing Director
SCT Operations Australia
Wollongong, Australia

ABSTRACT

The aim of this paper is to discuss the rock mechanics issues which can influence the strength of pillars in coal mines. The paper utilises stress change monitoring results, micro seismic monitoring results and computer modelling to assess the stress history about a chain pillar. The implications and fracture modes developed are discussed, with the outcome being that chain pillar strength can be significantly reduced by the stress path and changes in boundary conditions to the pillar when longwall extraction occurs. It is envisaged that this effect is contained in measured and empirical data bases, however, it is important to recognise the stress path process when applying results to various site conditions and mine layouts.

INTRODUCTION AND BACKGROUND

The aim of this paper is to discuss the rock mechanics issues which can influence the strength of pillars in coal mines. It builds on work carried out and presented previously (Gale, 1998; Gale, 1999) which presented the effect of surrounding strata on coal pillar strength characteristics. It is not the intention to provide any strength guidelines, but to provide a framework to assess the influences on pillar strength and the application of empirical or measured data to a particular site.

The strength of a pillar is basically determined by the magnitude of vertical stress which can be sustained within the strata/coal sequence forming and bounding it. The vertical stress developed through this sequence can be limited by failure of one or more of the units which make up the pillar system. This failure may occur in the coal, roof or floor strata forming the system, but usually involves the coal in some manner. The failure modes include shear fracture of intact material, lateral shear along bedding or tectonic structures, and buckling of cleat bounded ribsides.

In pillar systems having strong roof and floor, the pillar coal is the limiting factor. In coal seams surrounded by weak beds, a complex interaction of strata and coal failure will occur and this will determine the pillar strength. The strength achievable in various elements is largely dependent on the confining stresses developed. This indicates that, as confinement is developed in a pillar, the axial strength of the material will increase significantly, thereby increasing the actual strength of the pillar well above its unconfined value.

The strength of the coal is enhanced as confining stress increases toward the pillar centre. This increased strength is often related to the width/height ratio, whereby the larger this ratio the greater the confinement generated within the pillar. Hence squat pillars (high W/H) have greater strength potential than slender ones (of low W/H).

The results of that work have demonstrated that the peak strength of a coal pillar can be variable depending on the failure mode occurring about the pillar system. Peak strength of the system can result from:

i. fracture of the coal material of the pillar,
ii. fracture of the strata surrounding the coal seam,
iii. slip on weak bedding planes near the coal roof or floor which reduces the confinement characteristics within the coal pillar, or within the surrounding strata,
iv. or combinations of the above.

The strength properties of the same pillar system can also be different if the imposed stress field changes significantly. Such changes are typically caused by a change in boundary conditions to the pillar system which typically occur about chain pillars as extraction occurs adjacent to the pillar. In this case, the stress geometry changes and the confinement potential within the pillar changes significantly as a result of the caving in the roof strata adjacent the coal pillar. The typical effect is that the vertical stress increases and the lateral stresses reduce, thereby increasing the potential of the strata above the pillar to fracture and limit the strength characteristics of the overall pillar system. The overall strength of the system will then depend on the post failure strength of the fractured materials (coal or strata) and the confinement conditions within the system.

Therefore, the stress path history about a pillar is important. This is presented in Figure 1 which shows a generalised failure envelope for a rock or coal material and the potential effect of variation in the stress field which may occur. In certain situations, the strength will increase if the confinement increases, however if the confinement remains constant or reduces coincident with an

increase in the maximum stress, then the system can fracture and be limited to the post failure strength of the material. This concept is equally applicable to bedding planes and other structural features in the strata.

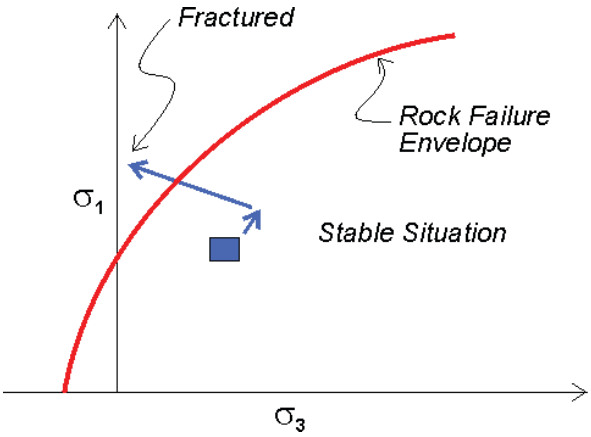

Figure 1. Stress path concept and rock fracture.

STRESS CHANGES AND ROCK FAILURE ABOUT LONGWALL PANELS

In order to assess the potential impact of stress path on pillars, in particular chain pillars, it is necessary to review stress changes and micro seismic monitoring undertaken about longwall panels.

Stress measurement and stress change monitoring has been conducted about longwall panels in Australia using 3-dimensional stress cells (CSIRO HI; ANZI) for over 20 years and has presented a good overview of the stress changes which occur about longwall panels (Gale and Matthews, 1992).

An example of this work and the typical results obtained at many sites obtained from industry funded research projects is presented below for a deep mine and a moderate depth mine, both in NSW.

The deep mine extracted the Bulli Seam at a depth of approximately 480 m at this site. The seam was surrounded by moderate to strong interbedded mudstone, siltstone and sandstone. The instrumentation layout is presented in Figure 2 and was established to monitor stress changes ahead and adjacent to a longwall panel. Three-dimensional HI stress cells were placed in the roof from approximately 2m to 20 m above the seam as presented in Figure 3. The results for the horizontal stress changes are presented in Figure 4 for the various heights into the roof relative to the distance of the longwall from the stress cells. Relief is shown as extensional arrows. The key outcome was that significant stress relief (50-100% of the virgin values) occurred ahead of the longwall faceline. This occurred up to 20 m above the coal.

The moderate depth mine site was from a depth of approximately 250 m and within interbedded mudstone and siltstone of weak to moderate strength. The site was within a pillar that was mined past on one side. Three dimensional stress cells were placed up to approximately 7 m above the roof in the central

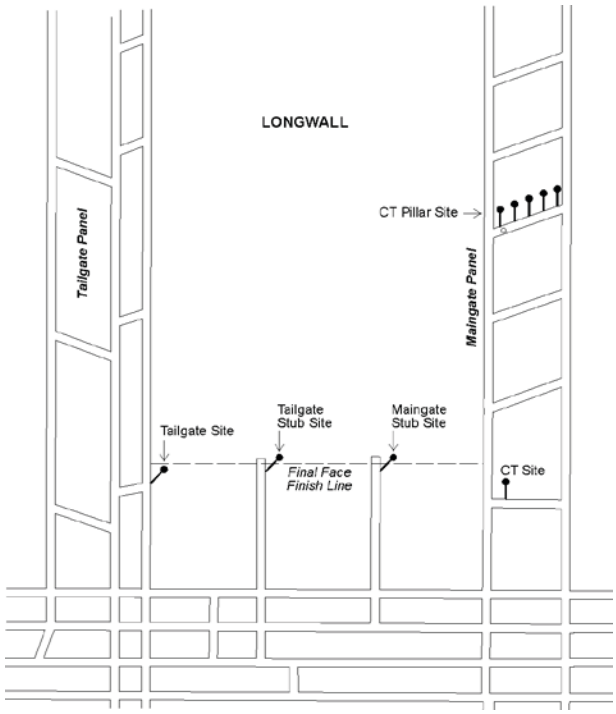

Figure 2. Longwall instrumentation sites.

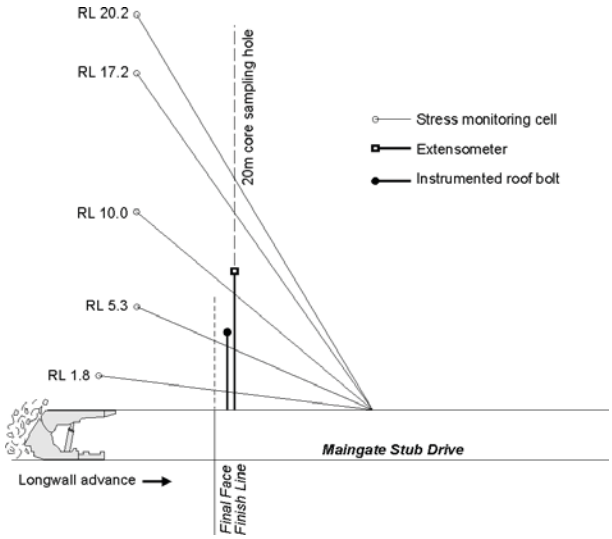

Figure 3. Stress cell placement array for maingate stub.

part of the pillar. The results are presented in Figure 5 in plan. The final situation is presented in Figure 6 as a section plan.

The results show that the vertical stress increases and the horizontal stress reduces significantly as the panel passes the site.

These results are typical of the sites and it was not uncommon for the ground about the cells to become overstressed and fracture.

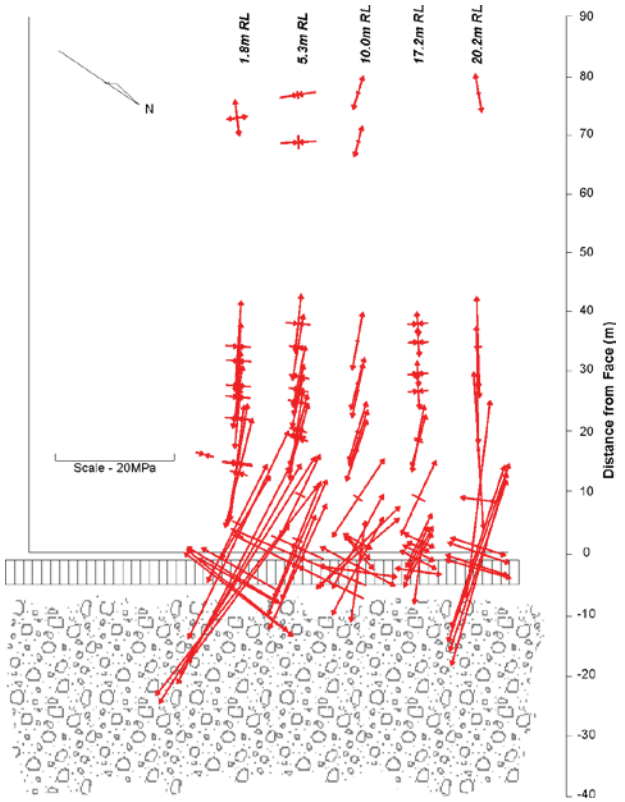

Figure 4. Horizontal stress changes monitored relative to face distance.

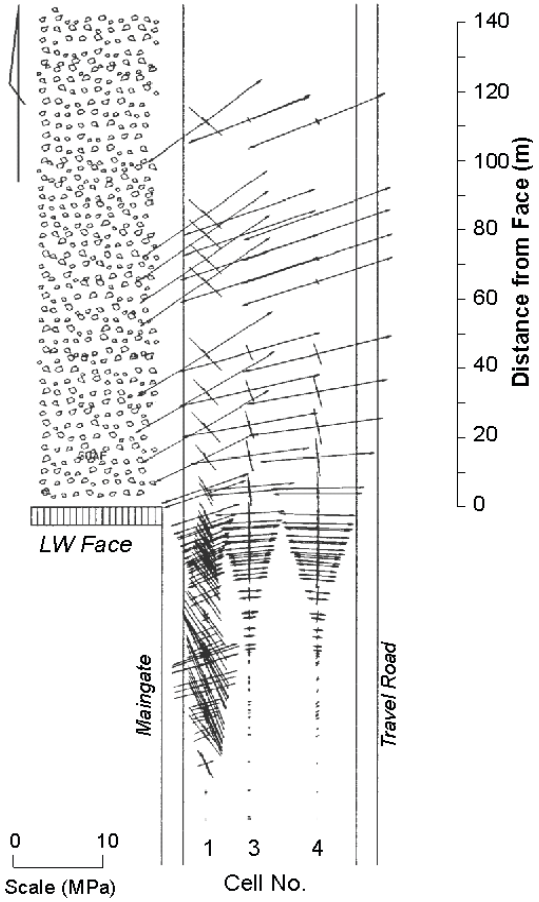

Figure 5. Stress monitoring data at a moderate depth mine.

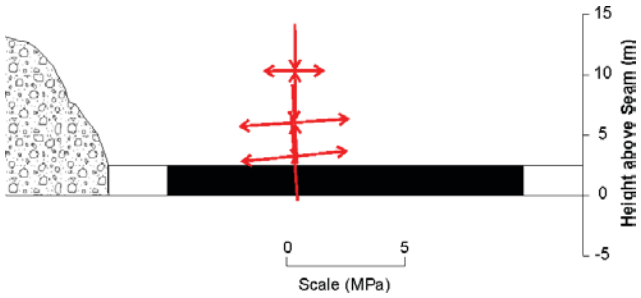

Figure 6. Section plan of stress changes.

The stress changes monitored demonstrate that the stress path is one where there is a high potential for rock failure to occur over solid ground adjacent to longwall panels.

The occurrence of fracture ahead of longwall panels is difficult to observe, however micro seismic monitoring allows location of such zones. Micro seismic monitoring results have been presented by many authors including Kelly et al. (1999), Ellenberger et al. (2001), Gale et al. (2001), and demonstrate that fracture within strata units ahead of the longwall panels occurs well ahead of the faceline in a range of strata materials ranging from weak to strong.

An example of the micro seismic distribution is presented in Figure 7 for the site at Gordonstone Mine (Queensland, Australia) and in Figure 8 for a Utah (USA) mine.

It was noted that the fracture within strata units may extend at least 50-100 m ahead of the face, however the greatest concentration is typically less than 30 m ahead of the face. The extent of fracture within the strata units need not cause complete "failure" of the rock mass but is likely to initiate as sporadic fractures within certain units which then increases in density and connection within the rock mass. Ultimately, networking of fractures is sufficient to cause "failure" of the rock mass. Failure is reached when the rock mass acts similarly to a test sample in that fractures are pervasive through the section.

The results presented above demonstrates that the stress path is a key consideration in assessing the strength of the pillar system about longwall panels as it has been demonstrated that fracture within the ground occurs above and below the coal well into the solid ground.

COMPUTER MODELLING OF THE PROCESS

Computer models of caving about longwall panels is undertaken by SCT Operations at a range of scales, from detailed caving about longwall shields to large scale caving of multiple panels. Large scale models of strata sections are undertaken with a metre square grid as a two dimensional cross section. The chain pillar strength characteristics in the large scale models reflect the stress path and material strength characteristics about the coal seam. The modelling process and input parameters are discussed in Gale and Tarrant (1997). The stress changes about the longwall panels

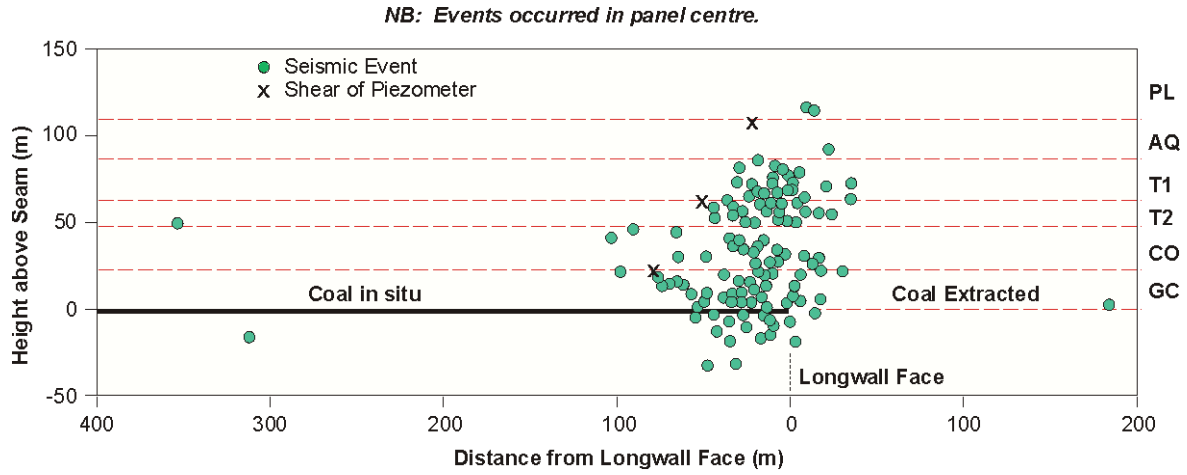

Figure 7. Micro seismic monitoring data from Gordonstone Mine.

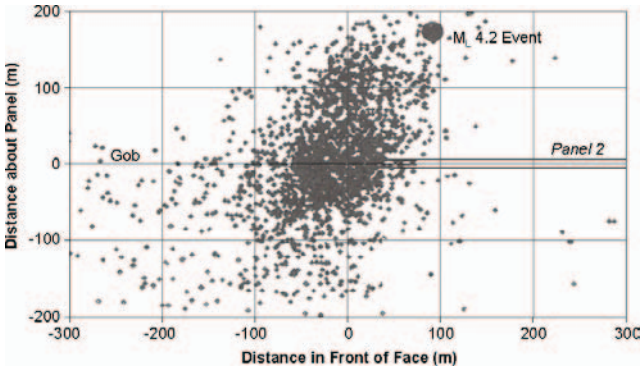

Figure 8. Micro seismic event locations in section relative to longwall face (after Ellenberger et al., 2001).

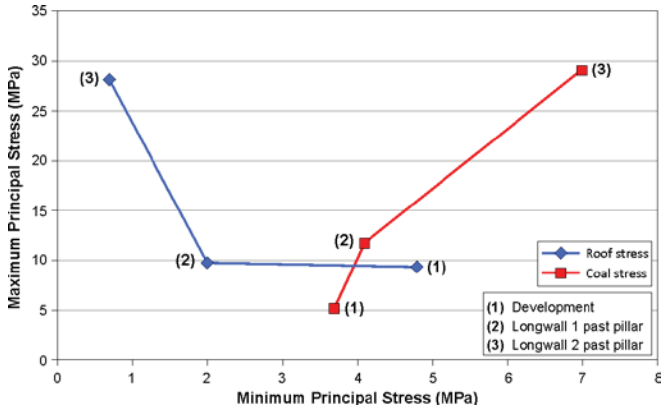

Figure 9. Stress path in and above the pillar for various longwall extraction boundary conditions.

are consistent with the monitoring data in that there is typically a vertical stress increase coincident with a horizontal stress reduction in the roof of the seam. This often causes fracture of the strata above the coal seam as part of the pillar yielding process. An example is presented in Figure 9 which shows the gross stress path above the pillar from development to extraction. The stress path presented represents "snapshots" for development, post Longwall 1 and post Longwall 2. The stresses used for this are the maximum and minimum principal stress at the centre of an 8 m coal pillar at mid pillar and one 5m above the coal.

This shows the overall stress path in the strata above the coal is consistent with the monitored results presented above, in that there is a stress path of increased maximum stress and a reduced minimum stress which is conducive to fracture of the rock materials. The stress path in the coal is different, whereby horizontal stress is developed in the coal pillar as a result of the additional vertical stress and lateral restraint at the seam floor level. The fracture distribution during mining adjacent to the pillar is presented in Figure 10 and shows fracture in the roof material over the ribside during the first pass and fracture above the pillar when fully isolated.

The material strength above and below the pillar is approximately 40 MPa and the in situ strength of the coal is modelled at 7.2 MPa. The width to height ratio of the pillar is approximately 6.2 relative to a 4.5 m extraction height. The contact surface of coal to roof and floor is representative of a moderate strength contact with slickensided characteristics. Bedding cohesion = 1MPa; Friction = 15°

The pillar strength and overburden vertical displacement resulting above the pillar is presented in Figure 11 which shows the yield characteristics of the system. The strength of the system relative to monitored data (Gale, 1999) is presented in Figure 12 and is consistent with expectation for such a system. It was noted that the horizontal displacement above the coal pillar in the immediate roof was greater than 500 mm toward the goaf, and the lateral (resisting) stress was minimal (less than 1 MPa) in the immediate 5-10 m above the roadway roof.

The same geological section modelled with different boundary conditions (and therefore stress path) will display very different pillar strength characteristics. A general overview of the boundary conditions is presented in Figure 13 for the case of a development pillar system and that of a chain pillar.

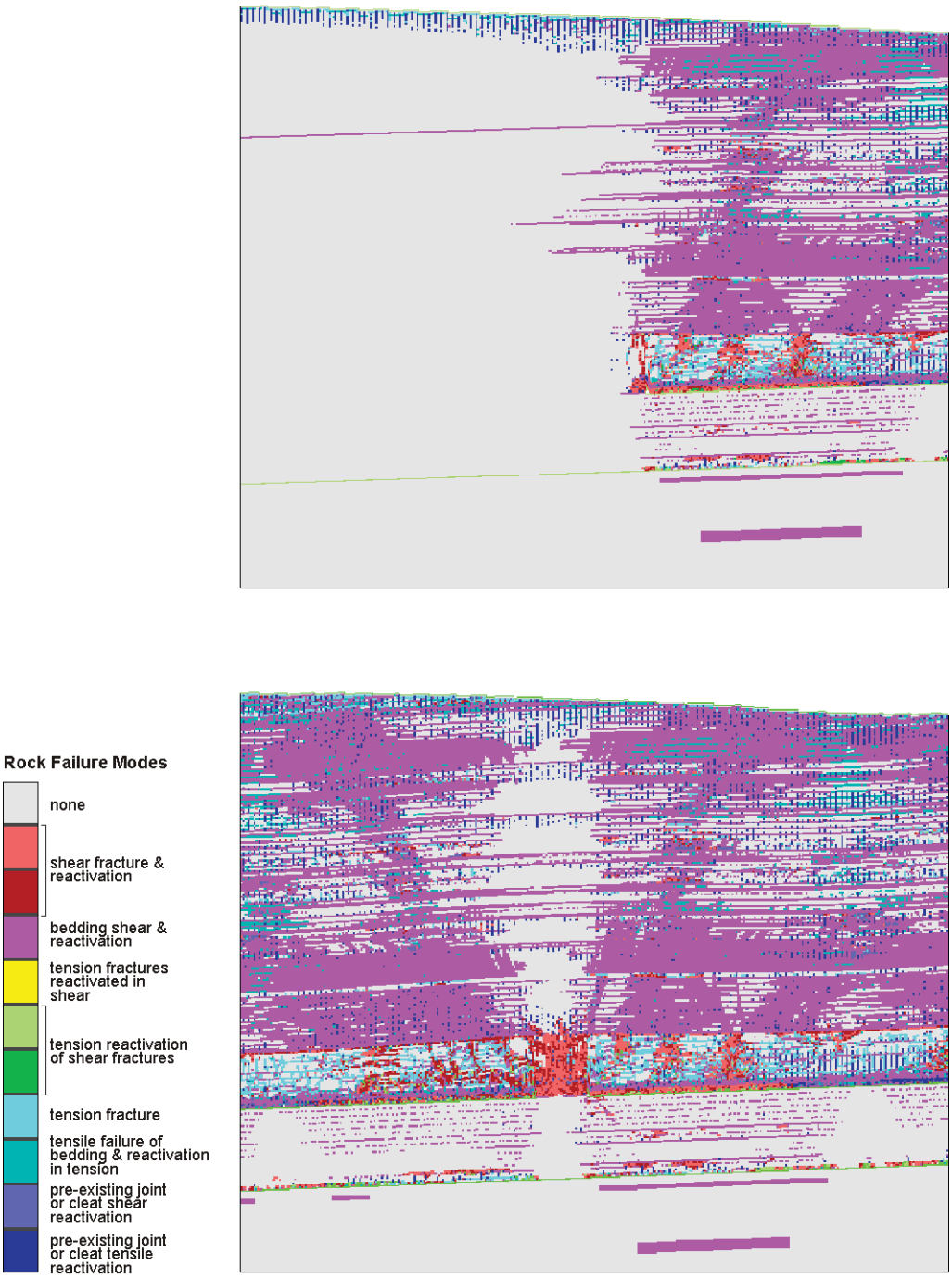

Figure 10. Fracture distribution in the pillar during longwall extraction.

It is likely that the pillar stress path will vary during loading history of a pillar, particularly for a thick coal or weak roof sequences. It is often noted that:

i. the pillar initially has a constrained boundary condition in the roof, floor and upper strata. This represents the maximum pillar strength potential;

ii. as load develops in the pillar lateral stress and shear stresses increase and fail bedding, floor and immediate roof strata. This changes the boundary condition and stress path within the pillar and reduces potential strength;

iii. once the pillar is adjacent and isolated in the goaf, the boundary conditions and stress path are changed again such that the immediate roof and upper roof are no longer restrained. This

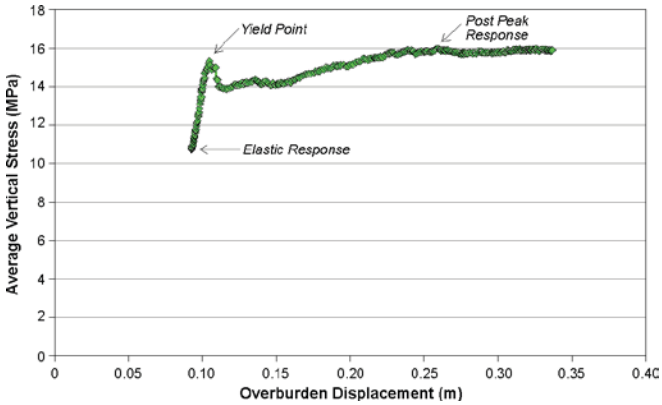

Figure 11. Pillar stress/convergence characteristics.

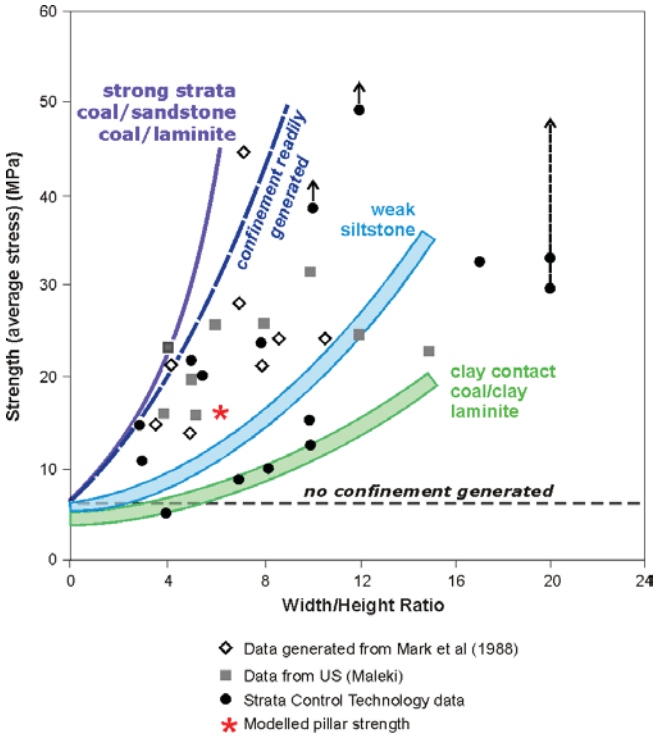

Figure 12. Pillar strength relative to measured data.

can cause fracture over the pillar of these units and limit the overall strength of the system.

The nature of the strata surrounding the seam will influence the strength achievable under each boundary condition, particularly that for development conditions (Gale, 1998). The strength will be further modified by the changing boundary conditions (stress path) during the loading history of the pillar. Therefore the overall performance and strength of a pillar is dependent on the ground conditions and the resultant boundary conditions of the pillar.

It would, therefore, be expected that the monitored strength and observed displacement characteristics of pillars would vary depending of the strata properties within the pillar system and the stress path it is subject to. It is considered that there would be a "scatter" in inferred strength properties within a large sample of measured data despite in situ coal strength being relatively uniform. In general, it is anticipated that much of the variations in stress path and pillar system strength are contained within empirical databases and measured databases which contain a proportion of single chain pillar results.

An important outcome is to be aware of geological characteristics of the pillar system and the stress path for a particular data point or set, so that the results can be applied at other sites under conditions which are representative of the data.

This has implications on the potential strength of development pillars and chain pillars (within the same pillar system) which are likely to have a different stress path history.

Development pillars are likely to experience significantly less variation in stress magnitude and geometry as barrier pillars are designed adjacent to the extraction panels to limit stress changes on the pillars. An important outcome of this is for barrier pillars to also act to limit ground displacements and changes to the boundary conditions of the mains pillars such that their full capacity can be realised. However, in some situations ground movements may extend significant distances from longwall panels which can contribute to long term roadway destabilisation. The stress changes anticipated for mains pillars would be primarily related to local effects such as roof falls and floor failure.

CONCLUSIONS

The strength characteristics of pillars are dependent on the strength properties of the strata surrounding the coal and the stress path or boundary conditions of the pillar system.

Main development pillars, distant from a goaf, have strength limited by geometry and the strength properties of the strata adjacent to the coal seam.

Chain pillars experience significant stress path changes during extraction operations and as such their strength is controlled by the strength properties of the strata adjacent to the seam, geometry, and a change in the boundary conditions about the pillar. The change in boundary conditions is caused by ground movement toward the goaf which changes the stress field and stress path experienced by the coal and surrounding strata. In such situations, fracture of the ground above the coal is likely. The combined impact of strata fracture and ground movement is to limit the strength of the pillar system. Failure of strata above and below chain pillars have been confirmed by micro seismic investigations and the stress changes have been confirmed by stress change monitoring.

It would be expected that the potential strength of a pillar system is greatest when distant from a goaf as the boundary conditions are constrained and conducive to developing confinement with additional loading. The limiting criteria would be the roadway deformation effects which may result from such additional loading.

Chain pillars will experience a transitional stage from the potential strength during development (constrained boundary conditions) to that when fully isolated in the goaf, as the boundary conditions change and the stress path changes. The potential strength of a pillar would be expected to reduce during the transitional stage.

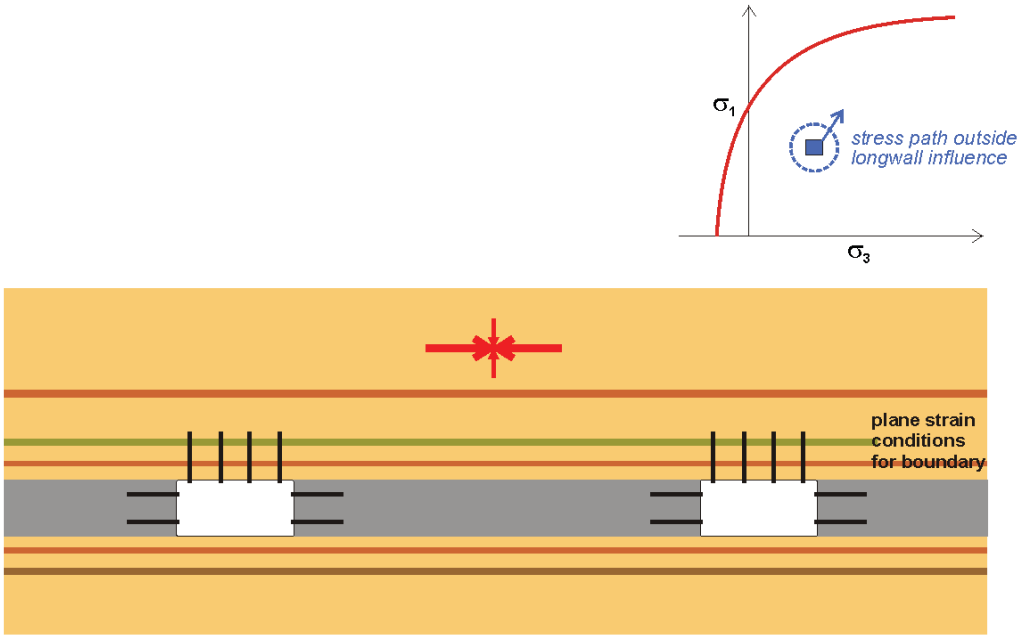

a) Development conditions.

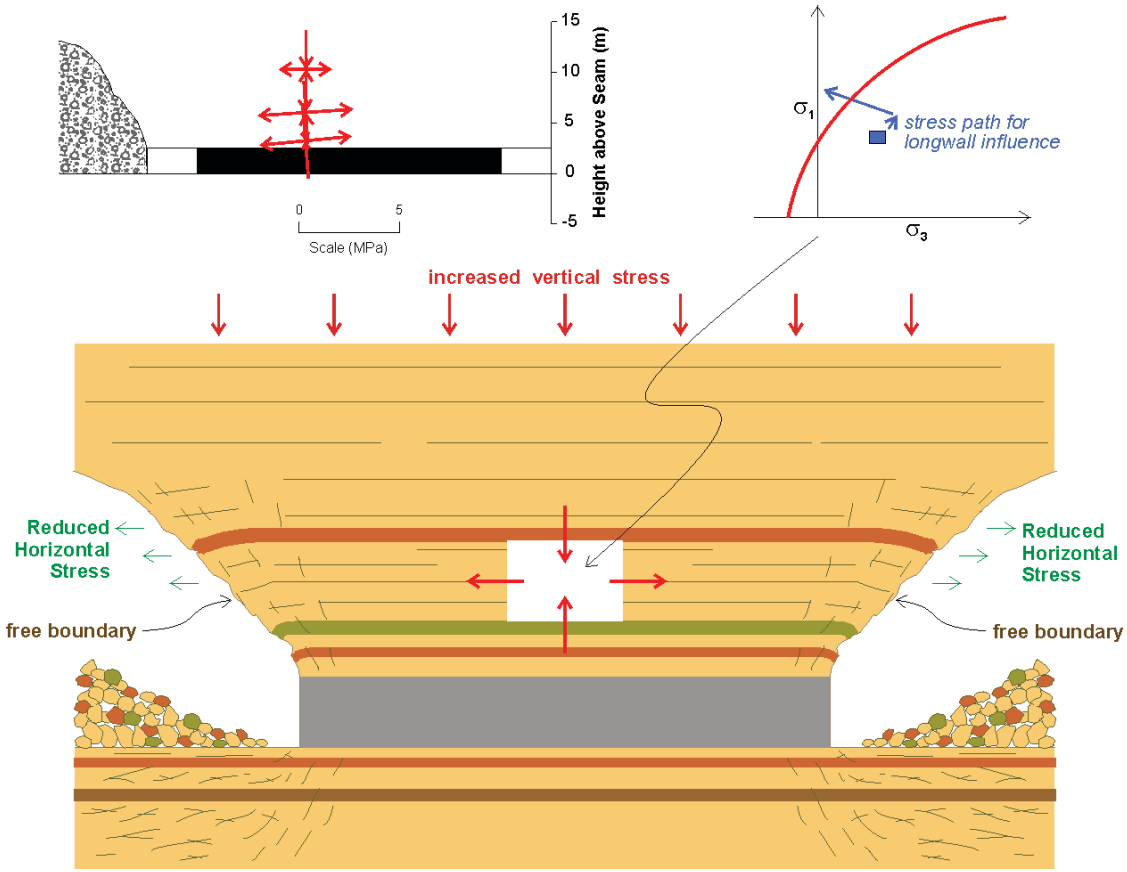

b) Longwall extraction conditions.

Figure 13. Boundary conditions and stress changes related to stress path for a pillar.

Roadway deformation effects can still be the main design criteria during this transitional stage.

REFERENCES

Ellenberger, J.L., Heasley, K.A., Swanson, P.L. and Mercier, J. (2001). Three-Dimensional Micro Seismic Monitoring of a Utah Longwall. Proceedings of the 38th U.S. Rock Mechanics Symposium, D.C. Rocks, pp. 1321-1326.

Gale, W. (1998). Coal Pillar Design Issues in Longwall Mining. Proceedings of 1st Australasian Coal Operators Conference (Coal98), February, University of Wollongong, pp. 133-146.

Gale, W. (1999). Experience of Field Measurement and Computer Simulation Methods for Pillar Design. Proceedings of the 2nd International Workshop on Coal Pillar Mechanics and Design in conjunction with 37th U.S. Rock Mechanics Symposium, Vail, CO, NIOSH IC 9448, pp.46-61.

Gale, W., Heasley, K.A., Iannacchione, A.T., Swanson, P., Hatherly, P. and King, A. (2001). Rock Damage Characterisation from Microseismic Monitoring. Proceedings of the 38th US Rock Mechanics Symposium, DC Rocks, Washington DC, *2*:1313-1320.

Gale, W. and Matthews, S. (1992). Stress Control Methods for Optimised Development and Extraction Operations. National Energy Research, Development and Demonstration Program, Report No. P282N.

Gale, W. and Tarrant, G. (1997). Let the Rocks Tell Us. Proceedings of the Coalfield Geology Council of NSW Symposium on Safety in Mines: The Role of Geology, Newcastle, NSW, pp. 153-160.

Kelly, M., Gale, W., Hatherly, P., Balusu, R. and Luo, X. (1996). New Understanding of Longwall Caving Processes: Microseismic Monitoring and Initial Computational Modelling at Gordonstone Mine. Proceedings of Symposium Geology in Longwall Mining, University of NSW, Sydney, pp. 153-161.

Assessment of Gate Road Loading under Deep Western U.S. Conditions

Tom Vandergrift, Senior Associate
David Conover, Senior Physicist
Agapito Associates, Inc.
Golden, CO

ABSTRACT

Currently accepted longwall abutment gate-road design criteria result in very large pillar sizes under deep cover. This leads to ventilation challenges, and makes it difficult for development to keep pace with longwall retreat. One of the most widely accepted gate-road pillar design approaches is the ALPS (Analysis of Longwall Pillar Stability) program. It has been speculated that ALPS overestimates the load transferred to the gate roads under deeper cover. A recent instrumentation program at a deep western U.S. longwall mine allowed for a direct comparison of measured side abutment loads and those assumed in ALPS. The results may help to explain why some pillars with low ALPS stability factors perform adequately, and may spur further research into more efficient gate-road design under deep cover.

INTRODUCTION

With western United States (U.S.) coal mine longwalls approaching 3,000 ft of cover, gate pillar design is becoming a critical issue with respect to both ground stability and longwall development requirements. Yield pillar designs have been successfully employed where the roof is sufficiently competent to withstand the large deflections associated with pillar yield. Under less competent roof, abutment pillars must be sized large enough to limit deflection to acceptable levels. However, abutment pillar sizing guidelines acceptable to the Mine Safety and Health Administration (MSHA) are largely based on eastern mining experience, and result in very large pillars at depth. In addition to limiting recovery and providing ventilation challenges, the development requirements associated with these large pillars make it very difficult for development to stay ahead of longwall retreat.

Faced with these circumstances, a mine in the western U.S. has undertaken a comprehensive geotechnical program, combining mine instrumentation with empirical design approaches and numerical modeling. Agapito Associates, Inc. (AAI) has been involved in this program since its inception. The mine is initiating longwall mining in a new district with maximum cover depths over individual panels ranging from 2,400 to 2,800 ft.

Instrumentation data from the geotechnical program appears to indicate that load transfer to the gate-road pillars is less than previously assumed. This may help explain why gate-road pillars with relatively low calculated stability factors have performed adequately at this mine. AAI has observed similar behavior at other western U.S. longwall operations. While the underlying mechanisms are not clear, the data presented herein contribute to the effort to quantify load transfer in deep western coal mines, and may generate interest in research to improve western U.S. gate-road design.

GATE-ROAD DESIGN PROCESS

In the early stages of planning for the new longwall district, the mining company considered both yield pillar and abutment pillar designs. Yield pillar designs have been found to be applicable under moderate to strong roof, generally where Coal Mine Roof Ratings (CMRR) are higher than 50 (DeMarco, 1994). Based on anticipated CMRR values in the 35 to 50 range, and on the performance of a gate-road yield pillar test area, it was the consensus of AAI and mine management that a yield pillar approach was unlikely to be successful. Therefore, the remainder of the design effort focused on various gate-road layouts consisting of abutment pillars.

One of the primary tools acceptable to MSHA for abutment pillar design is the Analysis of Longwall Pillar Stability (ALPS) program available from the National Institute for Occupational Safety and Health (NIOSH) (Mark, 1992). ALPS provides stability factors for longwall gate-road layouts by taking the quotient of pillar strength and pillar load for various mining geometries. Loads for development, headgate t-junction, bleeder, tailgate t-junction, and isolated gate-road pillars between gobs are estimated. Normally, the gate road is designed using the tailgate t-junction stability factor for the appropriate depth of cover over the gate road. Based on case history database analysis, it has been determined that there is an inverse relationship between allowable ALPS stability factors and roof strength (Mark et al., 1994). That is, roof quality and required pillar stability are related, with poor roof requiring larger pillars.

For the subject mine, using an input CMRR of 40, the recommended ALPS stability factor for design is 1.36. However, to achieve this stability factor for the depths where mining is planned, very large pillar sizes are required. For example, at a

design depth of 2,400 ft, two equal-sized square pillars on 262-ft centers are indicated; at a design depth of 2,800 ft, indicated center spacing increases to 279 ft. The potential conservatism of ALPS loading assumptions for deep cover (>1,250 ft) has been recognized by NIOSH and other researchers (Colwell et al., 1999; Chase et al., 2002; Heasley, 2008).

In an attempt to develop an alternative ALPS stability factor criterion for the mine, AAI back-calculated ALPS stability factors for various stable gate-road pillar configurations throughout the mine. Because portions of the mine are impacted by old workings above and below the currently-mined seam, pre-mining vertical stresses were estimated using LaMODEL boundary-element modeling. The pre-mining stress estimates were then converted to equivalent cover depths for input to ALPS. Figure 1 shows the actual stability factors corresponding to stable pillar configurations compared with the recommended value of 1.36. From Figure 1, a case can be made that the 1.36 stability factor criterion is too stringent, and that a lower stability factor, with smaller pillar dimensions, may prove satisfactory.

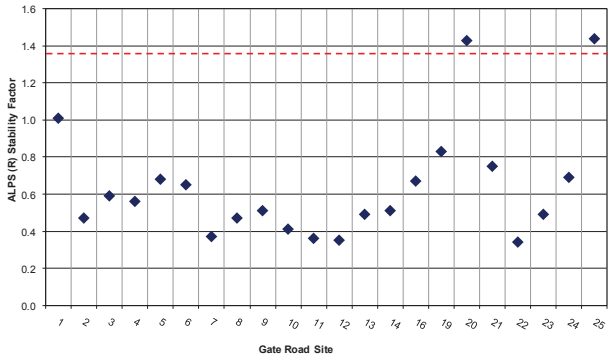

Figure 1. Minimum back-calculated ALPS stability factors corresponding to successful pillar designs.

After discussions with MSHA, the mine developed the first headgate in the new district using an ALPS stability factor criterion of 0.8. The tailgate, a former set of bleeders, had been driven previously. Even with this lower stability factor criterion, pillar sizes for the headgate are large, with entry and crosscut centers of 190 ft and 200 ft, respectively. The large entry centers have created ventilation challenges, requiring the use of ventilation curtains to divert air into the crosscuts. Even more problematic, development footage requirements (4.7 ft of development per foot of gate road) make it difficult for development to stay ahead of longwall retreat.

As mentioned, one possible explanation for the discrepancy between the successfully mined stability factors shown in Figure 1 and those recommended in ALPS may be an overestimation of gate-road pillar loading in ALPS. That possibility was explored through analysis of the instrumentation data.

INSTRUMENTATION PROGRAM AND DATA ANALYSIS

As part of a larger instrumentation effort, three instrumentation sites were developed in three different areas of a western U.S. longwall mine to measure vertical loads in the gate-road pillars and the adjacent panel. Table 1 lists the sites and their associated depth of cover and gate-road pillar dimensions. The longwall panel width associated with all three sites was approximately 800 ft.

Figure 2 shows a generalized layout map of the instrumentation that applies to all sites. Vertical loads were monitored using the encapsulated borehole pressure cells (BPCs) originally developed by the U.S. Bureau of Mines (USBM) and currently available commercially from various vendors. Data were captured using electronic transducers and data loggers. The instruments were installed before mining the first panel and monitored until after the face had passed the site. Site 1 is complete, as second panel mining is not planned. Sites 2 and 3 will continue to be monitored during mining of the second panel; however, the data for this study only applies to side abutment loads from first-panel mining.

Raw BPC data are commonly used to show the relative distribution of pillar loads, and load increases and pillar or rib yielding related to face passage. To directly compare pillar loading from the side abutment with the loading assumption in ALPS, a conversion of raw BPC data to ground stress is required. For each cell location, the BPC data consist of the hydraulic pressure of the fluid within the cell and tubing system, and are not a direct measurement of ground stress at the cell location. The theoretical behavior of the BPCs was developed through extensive investigations by USBM researchers, principally Dr. Paul Lu (1984) and Dr. Clarence Babcock (1986). The analysis techniques developed by these researchers differ in their application, and the instrumentation program was not completely compatible with all of the requirements of the two techniques. Specifically, the suite of instrumentation required to fully apply the Lu and Babcock methods is cost-prohibitive, so only vertically oriented BPCs were used. Therefore, an assumption regarding the horizontal change in pillar loading was required when applying both the Lu and Babcock methods. Nevertheless, the two techniques represent a reasonable approach to analyzing the BPC response and provide bounds for estimating the actual pillar loads. The following sections describe the theoretical basis for the ALPS calculations and the two BPC analysis methods.

Pillar Load Determination Using the ALPS Design Method

ALPS calculates pillar loads based on an estimate of the weight of overlying strata and assumptions regarding how much of that weight is supported by the gate-road pillars. The pillar load is normalized to a vertical slice oriented perpendicular to the gate road, and thus is expressed as a load per unit length (ft) and considered as a stress value (pounds per square foot or pounds per square inch). Figure 3 shows the general geometry of the vertical slice through the gate road. The weight of the rectangular area immediately above the gate road corresponds to the development load, and the weight of the triangular area adjacent to the gate road corresponds to the side load from the mined panel that is transferred onto the gate-road pillars. The pillar development loads also include the weight of overburden over the entries and are calculated using the tributary area method. Figure 4 shows details of the triangular areas representing the panel side loads. The size of the triangle is controlled by an abutment angle, the overburden depth, and the panel width. The abutment angle is an empirical value based on measurements taken in several mines, and the default, recommended value used in ALPS is 21°. The triangular shape is truncated for narrow (relative to the depth) panels as

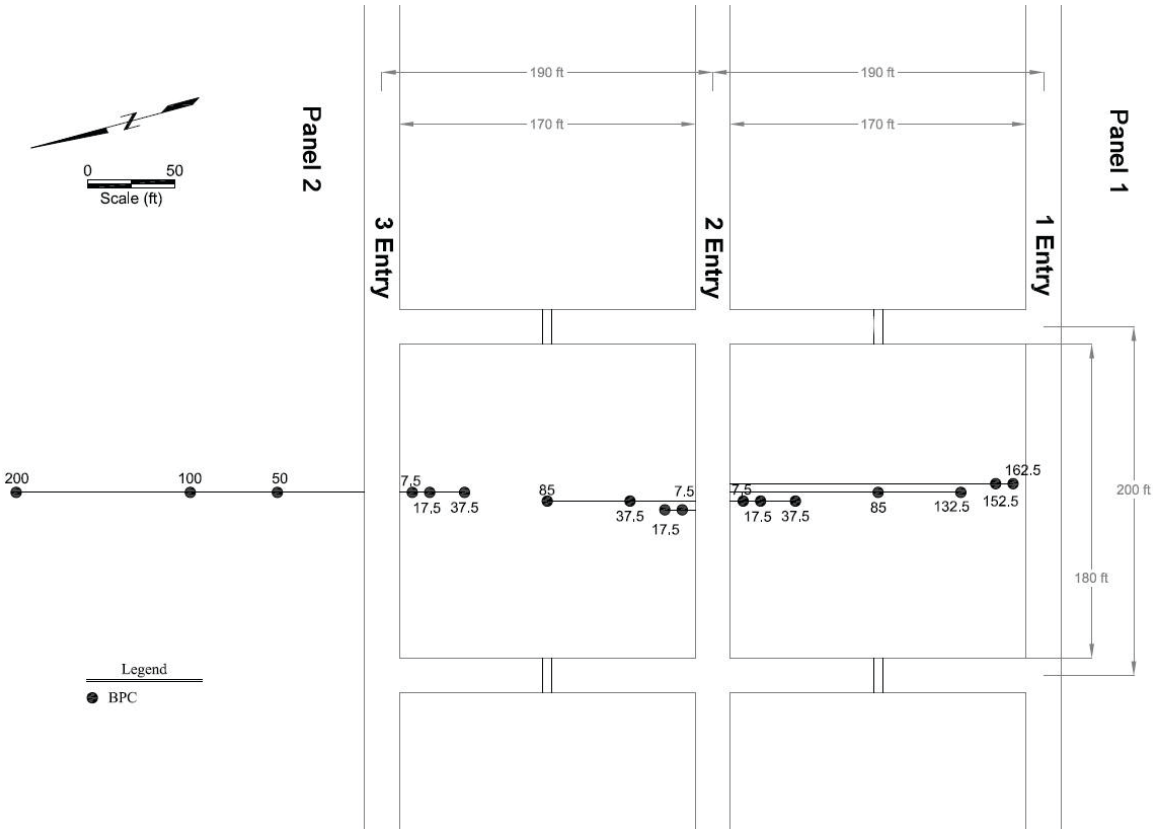

Figure 2. Generalized instrumentation layout.

Table 1. Test site summary.

Site	Depth of Cover (ft)	Pillar Centers (ft)
1	1,500	120 by 200
2	1,750	190 by 200
3	1,380	93 by 200

shown in the right-side portion of Figure 4. This situation is more common in deeper mines.

ALPS calculates loads separately for five production stages: Development, Headgate, Bleeder, Tailgate, and Isolated. Load for the development stage (before panel mining) consists of the tributary area load from the overburden directly over the gate road, with no side (panel) loads. The headgate stage (adjacent to the Panel 1 face) consists of the development load plus 0.5 times the side load from the first panel. The 0.5 factor was determined through numerical modeling analyses and accounts for non-uniform loading from the three-dimensional geometry at the headgate corner. The bleeder stage loading (gob on one side only) consists of the development load plus the full side load. The tailgate load (adjacent to the Panel 2 face) consists of the development load, the first panel side load and 0.7 times the second panel side load, again owing to the three-dimensional geometry at the tailgate corner. The isolated stage loading (gob on both sides) consists of the development load plus the side loads from both panels. The comparisons between field measurements and ALPS loading assumptions discussed later all correspond to a bleeder loading condition.

ALPS distributes the side load according to an exponential decay function, with most of the transferred load occurring on the pillar adjacent to the caved panel, and lesser load distributed on the pillars further from the panel and any un-mined adjacent panel or barrier. Figure 5 shows the shape of the distribution curve and the portion of load assigned to each pillar. The area under the curve is equivalent to the area under the side load triangle. The distance, *D*, was determined empirically by measuring the distance of the side abutment into the adjacent pillars and panel. ALPS uses the distribution to determine individual pillar loads for the headgate and bleeder stages. Insufficient data exist in the ALPS database to confirm that the load distribution is applicable to the tailgate and isolated cases, and therefore, a total pillar load rather than individual pillar loads are computed for these stages.

Regardless of the loading stage, the ALPS stability factor is defined as the ratio of the sum of the strengths of all pillars divided by the total load on the pillars. The method does not calculate stability factors for each pillar individually, thus a "yield-abutment" layout is considered identical to an "abutment-yield" layout. The method does not consider pillar yielding behavior; therefore, yield pillar designs are not accurately analyzed.

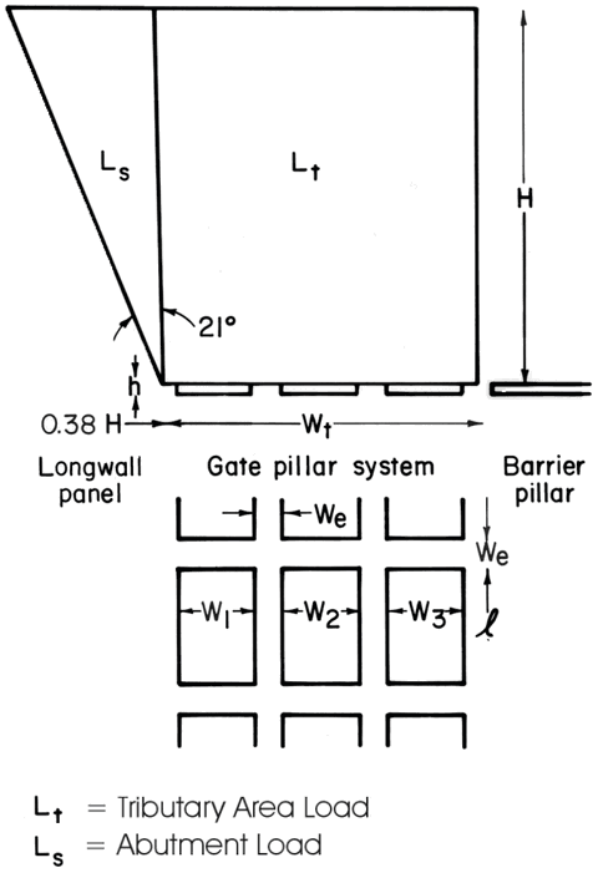

Figure 3. Development load geometry used in ALPS (Mark, 1992).

Analysis of BPC Pressures using the Lu Method

The Lu method relates the ground stress to BPC pressure by a linear relationship that considers the orientation of the cell relative to the vertical and horizontal stresses. The BPCs are directional, with greater sensitivity to pressures in the direction perpendicular to the flatjack and lesser sensitivity in the plane of the flatjack. To simplify the terminology, BPCs are commonly referred to by the orientation of the most sensitive direction, which is perpendicular to the plane of the flatjack. Thus, vertical BPCs are oriented with the flatjack horizontal, to measure vertical stresses, and horizontal BPCs are oriented with the flatjack vertical, to measure horizontal stresses. The Lu method defines the sensitivities as the relative areas of the flatjack in the direction of measurement, specifically, the sensitivity in the plane of the flatjack is 0.185 times the sensitivity in the plane perpendicular to the flatjack. Additionally, a response factor is used to account for behavior of the coal and the coupling between the coal and cell-encapsulating grout.

The method was originally developed to measure vertical and horizontal stresses in a coal seam using three cells: a vertical BPC, a horizontal BPC, and a Cylindrical Pressure Cell (CPC). A CPC is a cylindrical (non-directional) flatjack designed to measure the sum of the ground stresses. The cells were installed in specially prepared boreholes, pressurized to approximate virgin ground pressures, and allowed to stabilize to equilibrium pressures, to account for the inelastic nature of the coal. Equations were derived to determine the absolute ground stress using the three cell pressures. When a change to the mining layout occurred, such as passage of the panel, the cells were again allowed to re-stabilize to equilibrium and the post-mining stresses were determined.

From both a practical and cost standpoint, it quickly becomes prohibitive to install three cells at each measurement point. Therefore, a technique has been developed to estimate the vertical stress using vertical BPCs only and no horizontal BPCs or CPCs. This technique assumes that the horizontal stress is a constant fraction of the vertical stress. For this study, it was assumed that the horizontal stress is $\nu / (1 - \nu)$ times the vertical stress, where ν = Poisson's ratio. The general equation is:

$$P_v = w\,(N_v + S \times N_h)$$

where P_v = cell pressure of cell measuring vertical pressure (psi)

w = response factor (1.095 for coal)

N_v = vertical stress (psi)

S = ratio of cell flatjack side area to top area (0.185)

N_h = horizontal stress (psi)

By substituting the assumed horizontal stress ratio, the following simplified equation is obtained:

$$P_v = w\,\{1 + S\,[\nu / (1 - \nu)]\}\,N_v$$

For an average Poisson's ratio of 0.38, as determined through site-specific laboratory core testing, the equation becomes:

$$P_v = 1.22\,N_v$$

or

$$N_v = 0.82\,P_v$$

Thus, the vertical stress can be approximated as a constant fraction of the cell pressure.

Analysis of BPC Pressure Changes using the Babcock Method

The Babcock method only calculates the change in stress, as opposed to the Lu method, which calculates absolute stress levels. The method uses the initial and final pressures of BPCs oriented in orthogonal directions, generally vertical and horizontal. The general equation is:

$$S_v = [3/(8m)]\ln\left[\left(P_v/P_{v_0}\right)^3\left(P_h/P_{h_0}\right)\right]$$

where Sv = stress change (psi)

m = material constant $(4.348\,[(1 - \nu^2) / E]^{2/3})$

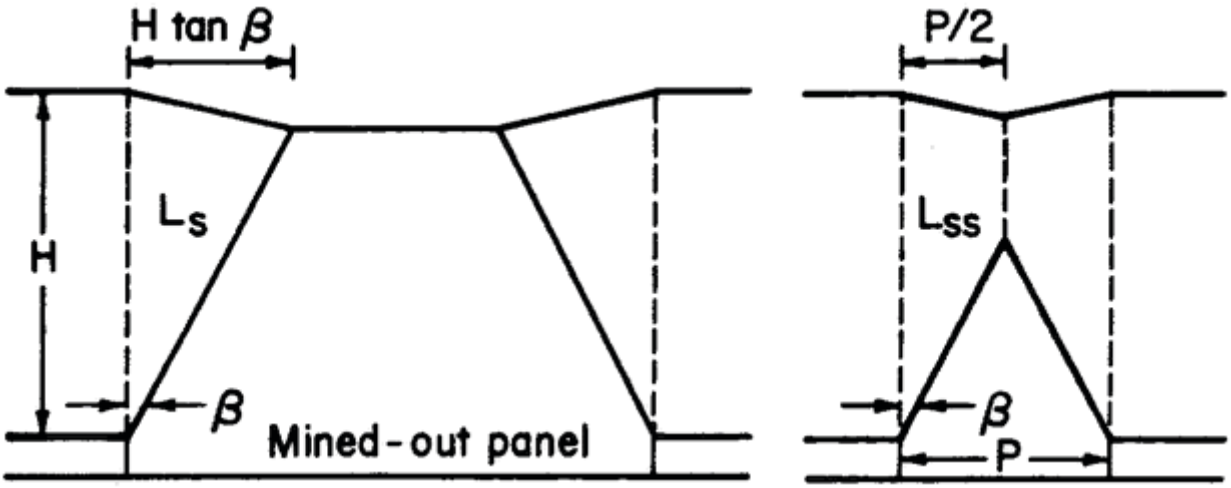

β = Abutment angle
H = Depth of cover
L_S = Side abutment for supercritical panels
L_{SS} = Side abutment for subcritical panels
P = Panel width

Figure 4. Panel side load geometry used in ALPS (Mark, 1992).

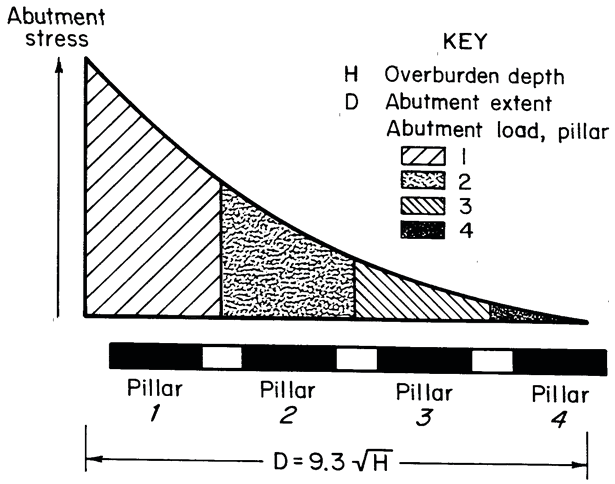

Figure 5. Side load abutment decay curve used in ALPS (Mark, 1992).

P_v = final cell pressure (vertical orientation)

P_{v_0} = initial cell pressure (vertical)

P_h = final cell pressure (horizontal orientation)

P_{h_0} = initial cell pressure (horizontal)

Again, the equation was modified based on the assumption that the ratio of the horizontal stress change to the vertical stress change was equal to ν / (1 – ν).

The two methods differ in the response factor between ground stress change and cell pressure change. The response for both methods depends on the ratio of horizontal to vertical stress. For a given stress ratio, the Lu method uses a constant response factor, whereas the factor for the Babcock method varies, depending on the absolute pressure (stress) magnitude. At higher pressures, the ground stress becomes less sensitive to cell pressure changes using the Babcock method. Figure 6 shows a comparison of the stress-to-pressure response factor for the two analysis methods.

Pressure Cell Measurements

Two types of plots were considered in evaluating the BPC data. Pressure versus time or pressure versus face position plots permit identifying the intervals in which loads are being transferred to the cells versus those intervals where the cells are in equilibrium. Pressure profiles for all cells across the gate road plotted for a given face position (time) show the distribution of load and are useful for comparing actual loads versus loads predicted by ALPS.

Figure 7 shows the variation of the converted BPC stress data versus face position of the first panel. In the figure, BPC pressures have been converted to vertical ground stress using both the Lu and Babcock methods, and the assumption that the horizontal stress

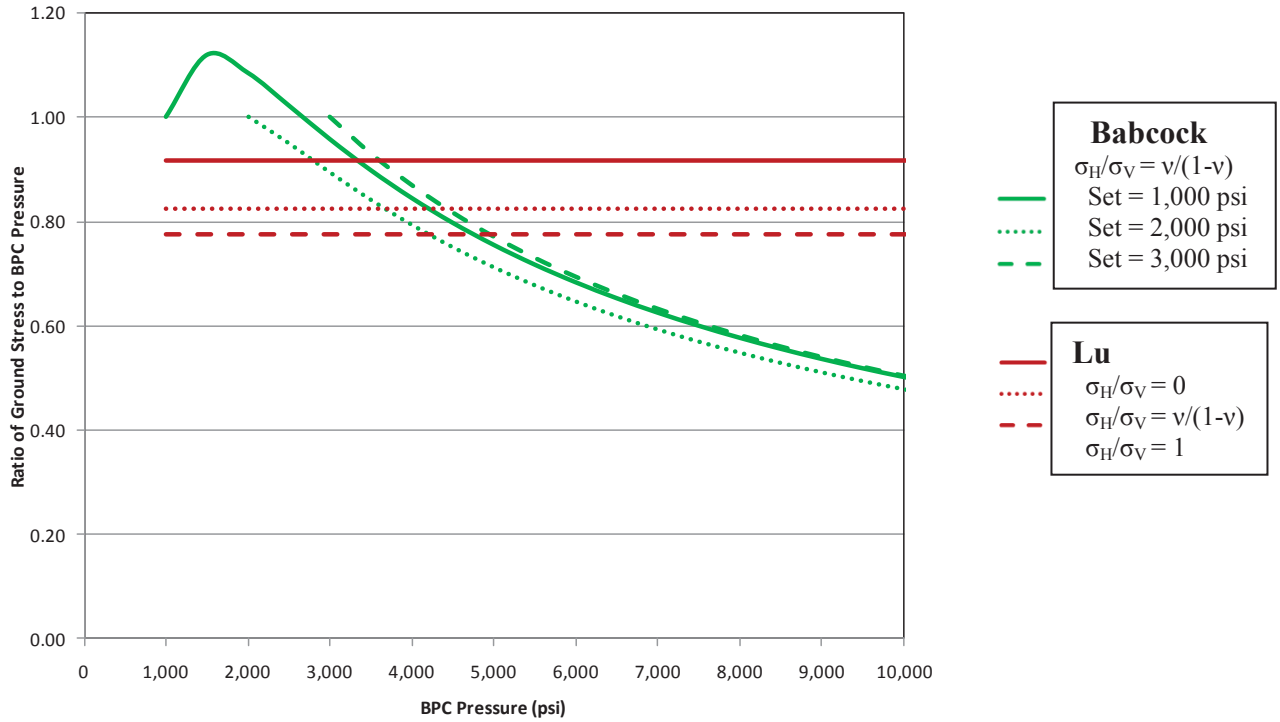

Figure 6. Comparison of BPC stress conversion factors.

is equal to the vertical stress times ν / (1 – ν). The plotted stress values are a weighted average of stresses from each cell based on an area of influence between adjacent cells. The average load increase can be compared to the difference between the ALPS bleeder and development loads.

COMPARISON OF ALPS ABUTMENT LOADING TO FIELD RESULTS

Cross-section plots were used to compare ALPS abutment load values to BPC stresses for both the Lu and Babcock analysis methods. Sections were plotted for the stable regions of Figure 7 for development (pre-face passage) and bleeder (post-face passage) conditions. Figure 8 shows the resulting sections for the three sites for BPC stresses converted using the Lu method and the previously discussed horizontal stress assumptions. For clarity, the stresses calculated using the Babcock method are not shown, but are generally less than the stresses calculated using the Lu method, and thus show an even greater discrepancy between BPC and ALPS results. The 21° ALPS curves also shown in Figure 8 were generated from the abutment decay distribution assumed in ALPS.

It is somewhat difficult to directly compare the ALPS and BPC results owing to inconsistent development loads. That is, although assumed accurate, the average BPC development stresses were about 90% to 95% of ALPS tributary area loads. Therefore, the analysis considered the relative (percent) increase of the final (bleeder) state to the initial (development) state. Table 2 lists the average loads on each pillar, the percent load increase for the individual pillars, and the average of both pillars. The load increases calculated by ALPS are significantly greater than those calculated from the pressure cell data. Briefly, the ALPS stress increases for the three sites are 105%, 74% and 121% (average 100%), whereas the corresponding increases for the Lu method are 23%, 65% and 51% (average 46%), and for the Babcock method are 16%, 39% and 37% (average 31%).

To obtain a smaller abutment load in ALPS that more closely agreed with the BPC results, the abutment angle was reduced such that the resulting average percentage load increase in ALPS matched the percentage load increase indicated by the BPCs. The resultant calculated abutment angles are shown in Table 2 and range from 3° to 16°. The ALPS abutment load decay curves for the smaller abutment angles are also shown in Figure 8. The BPC stress distributions and the modified ALPS abutment distributions represent different conditions, but are related in that the area under each is equivalent. The BPC stress distribution approximates the stress distribution in the pillars, including loads transferred from the entries and any yielded portions of the pillar. The ALPS distributions represent the side abutment load over a solid, elastic coal pillar. So, while it may appear that the 21° ALPS curves more closely correlate to the bleeder loading distributions, closer inspection reveals that for a given site, the area under the ALPS 21° curve is greater than the area under the BPC bleeder curves, while the area under the bleeder curves and adjusted ALPS curves are equivalent.

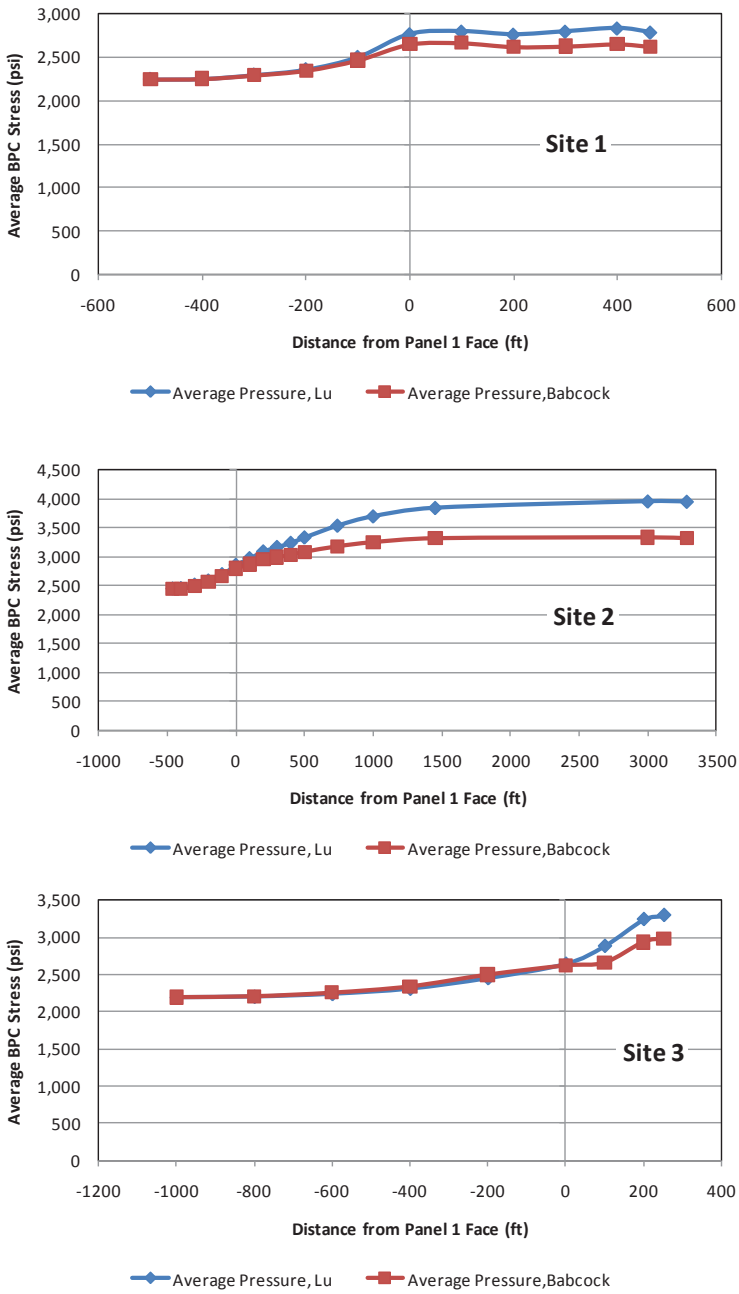

Figure 7. BPC stresses during panel 1 mining.

The fact that the BPC data show a more even loading of the two pillars compared to the ALPS distribution suggests that modification to the decay function or the abutment distance, *D*, may be warranted. However, data from the current study are insufficient to comment further.

CONCLUSIONS/IMPLICATIONS TO DEEP WESTERN MINE DESIGN

It is recognized that many elements of this analysis are imprecise and limited in scope, including the accurate conversion of cell pressures to vertical stress, limited BPC coverage within the pillars, pillar yielding effects, etc. In addition, current data are only available to comment on side abutment loading, and it remains to be seen whether the trends observed will persist through tailgate loading. However, it is evident that a large discrepancy exists between measured side abutment loads and those predicted in ALPS. The underlying mechanisms are not clear, but may be related to deep cover, stiff competent overburden, or both. This phenomenon has been measured by AAI at other western U.S. mines, and similar observations have been made by researchers in Australia (Colwell et al., 1999; Hill et al., 2008).

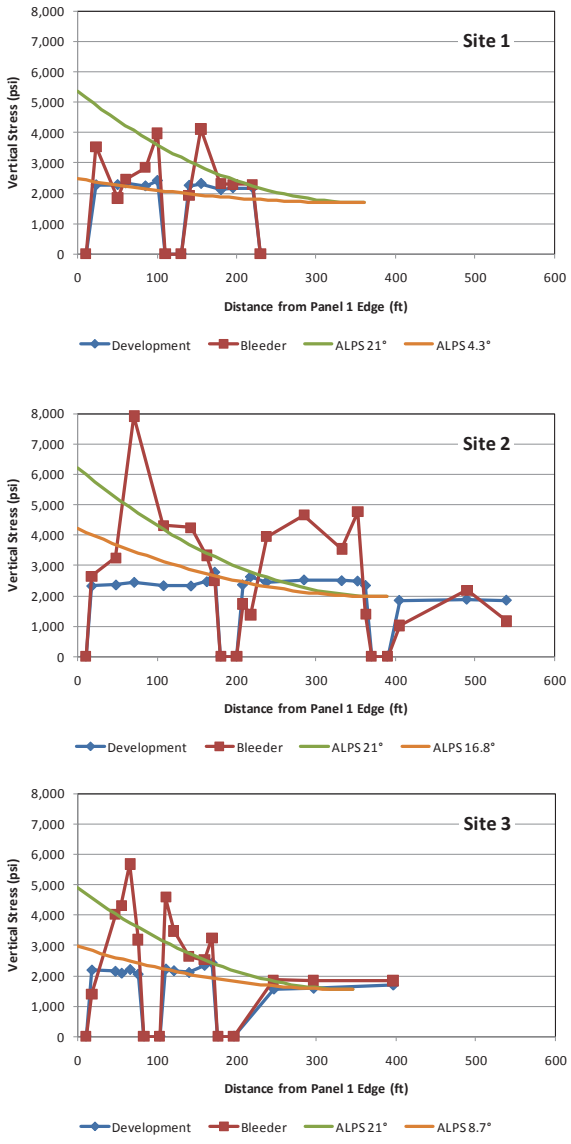

Figure 8. Comparison of BPC and ALPS pillar stresses.

If in fact ALPS underestimates gate-road loading under certain conditions, this would help to explain why pillar designs with lower-than-recommended ALPS stability factors perform adequately. The potential for successful application of lower stability factors under deep cover has been accounted for in the NIOSH ARMPS (Analysis of Retreat Mining Pillar Stability) program (Chase et al., 2002), but has not yet been incorporated into ALPS.

It is not the intent of this paper to suggest that alternate abutment angles be applied in ALPS. The ALPS technique has been developed and correlated to a large case history database using a constant 21° abutment angle. By modifying the input abutment angle, the tie to the database is broken. Rather, it is the authors' hope that further research will be conducted into abutment loading of deep western longwall gate roads, and the representation of such loads in ALPS, so that mining efficiency can be improved while maintaining ground stability.

REFERENCES

Babcock, C.O. (1986). Equations for the Analysis of Borehole Pressure Cell Data. Proceedings of the 27th U.S. Symposium on Rock Mechanics, University of Alabama, Tuscaloosa, AL, pp. 512-519.

Chase, F., Mark, C. and Heasley, K. (2002). Deep Cover Pillar Extraction in the U.S. Coalfields. Proceedings, 21st International Conference on Ground Control in Mining, Morgantown, WV, pp. 68-80.

Colwell, M., Frith, R. and Mark, C. (1999). Analysis of Longwall Tailgate Serviceability (ALTS): A Chain Pillar Design Methodology for Australian Conditions. Proceedings of the Second International Workshop on Coal Pillar Mechanics and Design, U.S. Bureau of Mines IC 9448, pp. 33-48.

DeMarco, M.J. (1994). Yielding Pillar Gate Road Design Considerations. Proceedings of the New Technology for Longwall Ground Control, U.S. Bureau of Mines SP 01-94, pp. 19-36.

Heasley, K. (2008). Some Thoughts on Calibrating LaModel. Proceedings of the 27th International Conference on Ground Control in Mining, Morgantown, WV, pp. 7-13.

Hill, D., Canbulat, I., Thomas, R. and van Wijk, J. (2008). Coal Pillar Loading Mechanisms and Progress in Pillar Design. Proceedings of the 27th International Conference on Ground Control in Mining, Morgantown, WV, pp. 235-240.

Lu, P.H. (1984). Mining-Induced Stress Measurement with Hydraulic Borehole Pressure Cells. Proceedings of the 25th U.S. Symposium on Rock Mechanics, Northwest. University, Evanston, IL, pp. 204-211.

Mark, C. (1992). Analysis of Longwall Pillar Stability: An Update. Proceedings of the Workshop on Coal Pillar Mechanics and Design, U.S. Bureau of Mines IC 9315, pp. 238-249.

Mark, C., Chase, F.E. and Molinda, G.M. (1994). Design of Longwall Gate Entry Systems Using Roof Classification. Proceedings of the New Technology for Longwall Ground Control, U.S. Bureau of Mines SP 01-94, pp. 5-18.

Table 2. Comparison of pillar load distribution.

Description	Site 1			Site 2			Site 3		
	Pillar 1	Pillar 2	Both Pillars	Pillar 1	Pillar 2	Both Pillars	Pillar 1	Pillar 2	Both Pillars
ALPS									
Development load (psi)	2,250	2,250	2,250	2,445	2,445	2,445	2,198	2,198	2198
Bleeder load (psi)	5,693	3,520	4,607	5,575	2,929	4,252	5,785	3,915	4,850
% increase	153.0	56.4	104.7	128.0	19.8	73.9	163.2	78.1	120.7
Lu									
Development load (psi)	2,039	1,980	2,010	2,288	2,386	2,337	1,933	2,007	1,970
Bleeder load (psi)	2,547	2,387	2,467	4,219	3,496	3,858	3,121	2,820	2,971
% increase	24.9%	20.6	22.8	84.4	46.5	65.1	61.5	40.5	50.8
Adjusted abutment angle	-	-	4.3	-	-	16.8	-	-	8.7
Adjusted bleeder load (psi)	2994	2524	2759	5215	2873	4044	3719	2926	3,323
Adjusted % increase	33.1	12.2	22.6	113.3	17.5	65.4	69.2	33.1	51.2
Babcock									
Development load (psi)	2,034	1,980	2,007	2,279	2,394	2,337	1,923	2,013	1,968
Bleeder load (psi)	2,396	2,261	2,329	3,478	3,003	3,241	2,618	2,772	2,695
% increase	17.8	14.2	16.0	52.6	25.4	38.7	36.1	37.7	36.9
Adjusted abutment angle	-	-	3.0	-	-	9.6	-	-	6.3
Adjusted bleeder load (psi)	2,768	2,441	2,605	4,094	2,700	3,397	3295	2,723	3,009
Adjusted % increase	23.0	8.5	15.8	67.4	10.4	38.9	49.9	23.9	36.9

Calibrating the LaModel Program for Deep Cover Pillar Retreat Coal Mining

Keith Heasley, Professor
Morgan M. Sears, Graduate Research Assistant
Ihsan B. Tulu, Graduate Research Assistant
Christian Calderon-Arteaga, Graduate Research Assistant
Larry Jimison, Undergraduate Research Assistant
Department of Mining Engineering
West Virginia University
Morgantown, WV

ABSTRACT

This paper reports on the results of the research work performed to develop and verify a standardized method of calibrating LaModel for deep-cover, pillar retreat. Initially, an in-depth evaluation of the critical input parameters for LaModel (the lamination thickness, the gob modulus and the coal strength) was performed. This evaluation identified a number of new parameter calibration procedures for making the program more accurate and effective. As these new input procedures were developed, they were implemented into various new "Wizards" in the LaModel program. Then to verify the "standardized" method for calibrating LaModel, 47 deep cover pillar retreat case histories from 11 different mines were analyzed with the new calibration procedures. As a result of this process, it was ultimately determined that if the LaModel user designs a deep cover pillar retreat section with the calibration method presented in this paper and keeps the safety factor above 1.40, then they should have a 90% chance of success (based on the given database analysis). This recommended calibration method and associated recommended safety factor represents a major milestone in the development of LaModel, since this is the first time that such recommendations have been made for use with the program.

INTRODUCTION

After the collapse of the Crandall Canyon Mine in Utah on August 6, 2007, several questions were raised concerning the accuracy of the currently available analysis tools and methods that can be used for the design of deep cover, pillar retreat mining sections (MSHA, 2008). One of the analysis tools that was used in the original design of the mine plan at Crandall Canyon was the LaModel boundary-element program. This program has a long history of successful application at coal mines in the U.S. and around the world. So, why was the mine design unsuccessful? As with any numerical method, the success and accuracy of the LaModel program is largely dependent on the accuracy of the input parameters. LaModel has default properties for most of the input parameters; however, these default properties were developed to give "reasonable" output for "average" mining conditions. To effectively design a specific mining plan and pillar layout well, the LaModel parameters need to be specifically calibrated to the unique conditions at the specific mine. The problem is that the process for calibrating LaModel for a specific mine site, and in particular a deep-cover pillar retreat mine, is not well established or standardized. Different users have developed different calibration processes that suit their particular application, and these various calibration processes have various degrees of success. What is needed is a "standardized" (documented and repeatable) method of calibrating LaModel that has been thoroughly evaluated and verified on actual case studies. This standardized or best practice calibration process for LaModel would greatly raise the quality of mine design in this country, and would allow both the designers and the evaluators to work with the same calibration process.

BEST PRACTICES FOR CALIBRATING LAMODEL

LaModel Introduction

The LaModel program is used to model the stresses and displacements on thin tabular deposits such as coal seams. It uses the displacement-discontinuity (DD) variation of the boundary-element method, and because of this formulation, it is able to analyze large areas of single or multiple-seam coal mines (Heasley, 1998). What makes LaModel unique among boundary element codes is that the overburden material includes laminations which give the model a more realistic flexibility for stratified sedimentary geologies and multiple-seam mines. Using LaModel, the total vertical stresses and displacements in the coal seam are calculated; and also, the individual effects of multiple-seam stress interactions and topographic relief can be separated and analyzed individually.

Since LaModel's original introduction in 1996, it has continually been upgraded (as need arose) and modernized as operating systems and programming languages have changed. The present program is written in Microsoft Visual C++ and runs in the windows operating system. It can be used to calculate convergence, vertical stress, overburden stress, pillar safety factors, intra-seam subsidence, etc. on single and multiple seams with complex geometries and variable topography. Presently, the program can analyze a 2,000 x 2,000 grid with 6 different material models and 52 different individual in-seam materials. It uses a forms-based system for inputting model parameters and a graphical interface for creating the mine grid. Also, it includes a number of "Wizards" for:

1. Calculating the lamination thickness based on the extent of abutment loading,
2. Calculating coal material properties based on a Mark-Bienawski pillar strength, and
3. Calculating gob properties based on expected gob loading

Recently, the LaModel program has been interfaced with AutoCAD so that it can now take AutoCAD maps of the pillar plan and overburden, and automatically convert these into the appropriate seam and overburden grids. Also, the output from LaModel can be downloaded into AutoCAD and overlain on the mine map for enhanced analysis and graphical display (Heasley, 2008).

The Calibration Process

When it was decided to make a standardized calibration process for LaModel, the next obvious question was: How to approach this? It was desired for the calibration process to be as realistic and accurate as possible; therefore, it seemed reasonable to base the process on field measurements, observations and/or empirically determined formula. Also, the time frame was limited, so it was necessary to utilize readily available, "standard", time-tested methodologies. At the same time as LaModel was being calibrated for deep-cover pillar retreat mining, the ARMPS program (by NIOSH) was also undergoing a similar review and calibration. As part of this review process, the overburden loading in ARMPS and LaModel were being compared and contrasted (Tulu et al., 2010). So, when searching for accurate, reliable techniques to use for calibrating LaModel, an obvious choice was to use the same techniques incorporated into the ARMPS and ALPS programs. These programs (and their underlying "empirical mechanics") have been verified against hundreds of case studies with good results. These programs are well known and frequently used in the industry, and have practically become design standards in many situations. Therefore, it was determined (at least for the first approach) to develop a process to calibrate LaModel to match the mechanics of overburden loading and pillar strength implemented in ARMPS and ALPS.

The Critical Input Parameters

In LaModel, the most critical input parameters with regard to controlling the mechanical response of the program and for calibrating with field data to accurately calculate stresses and loads, and therefore, pillar stability and safety factors are:

1. The Rock Mass Stiffness
2. The Gob Stiffness
3. The Coal Strength

During model calibration, it is critical to note that these parameters are strongly interrelated, and because of the model geo-mechanics, the parameters need to be calibrated in the order shown above. With this sequence of parameter calibration, the calibrated value of the subsequent parameters is determined by the chosen value of the previous parameters, and changing the value of any of the preceding parameters will require re-calibration of the subsequent parameters. The calibration derivation and recommended calibration process as it relates to each of these parameters is discussed in more detail below.

Calibrating the Rock Mass Stiffness

The stiffness of the rock mass in LaModel is primarily determined by two parameters, the rock mass modulus and the rock mass lamination thickness. Increasing the modulus or increasing the lamination thickness of the rock mass will increase the stiffness of the overburden. With a stiffer overburden:

1) The extent of the abutment stresses will increase,
2) The convergence and stress over the gob areas will decrease, and
3) The multiple seam stress concentrations will be smoothed over a larger area.

Rock Mass Modulus

When calibrating for good stress output and to match the ARMPS approach, it is recommended that the rock mass stiffness be calibrated to produce a reasonable extent of abutment zone at the edge of the critical gob areas. Since changes in either the modulus or lamination thickness cause a similar response in the model, it is logical and most efficient to keep one parameter constant and only adjust the other. When calibrating the rock mass stiffness, it has been found to be most efficient to initially select a rock mass modulus and then solely adjust the lamination thickness for the model calibration. It is recommended to determine the average rock mass modulus as a thickness weighted average of the elastic modulus of the overburden layers (Karabin and Evanto, 1999), or second best, to use the default rock mass modulus in LaModel. If the rock mass lamination thickness is calibrated to match the extent of the abutment zone as described below, then the choice of rock mass elastic modulus is not very critical to the final objective, since the lamination thickness will be adjusted as needed with regard to the elastic modulus to ultimately match the desired extent of the abutment zone.

Rock Mass Lamination Thickness

In calibrating the lamination thickness for a model based on the extent of the abutment zone, it would be best to use specific field measurements of the abutment zone from the given mine. However, often these field measurements are not available. As a substitute for measurements, visual observations of the extent of the abutment zone can often be used. Most operations personnel in a mine have a fairly good idea of how far the stress effects can be seen from an adjacent gob. (Note, for visually determining the abutment extent, the user is looking for the extent of the abutment zone from the full side abutment of a longwall or room-and-pillar gob area, not necessarily the distance outby the face where the front abutment zone is first observed. Also, if visually determining the extent of the abutment zone, the user should consider that the extent of the abutment zone as determined from sensitive field measurements as used in the derivation of equations 1 and 2 below is probably larger than what can be visually observed in the rib of the entries.)

Without any site specific field measurements or underground observations to guide the LaModel user, it is recommended to use the empirical information as implemented in ARMPS and ALPS. For instance, the ALPS program would indicate that, on average, the extent of the abutment zone (D, in feet) at depth (H, in feet) should be (Peng, 2006):

$$D = 9.3\sqrt{H} \tag{1}$$

Once the desired extent of the abutment zone has been determined, the next step is to calculate the lamination thickness that will match that abutment extent for that particular site. In the original development of LaModel (Heasley, 1998), an equation (2) was developed which gives the abutment stress magnitude (σ_l) for the laminated overburden model as a function of the distance (x) from the panel rib (also see Figure 1):

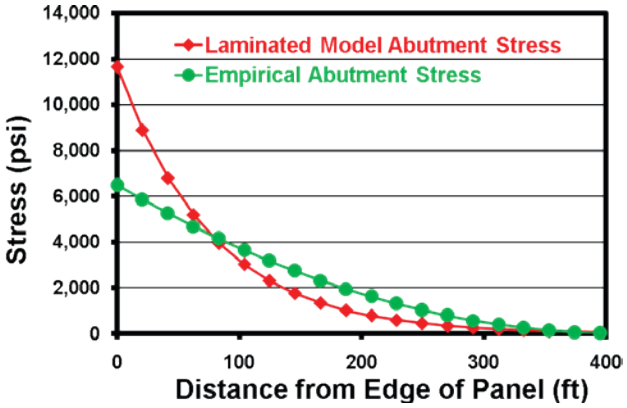

Figure 1. A comparison of abutment stresses from field measurements and LaModel.

$$\sigma_l(x) = q\frac{P}{2}\sqrt{\frac{2E_s}{E\lambda h}}\,e^{-\sqrt{\frac{2E_s}{E\lambda h}}x} \tag{2}$$

where:

q = the insitu stress

P = the width of the panel

E_s = the elastic modulus of the seam

E = the elastic modulus of the overburden

λ = a parameter of the laminated model

h = the seam thickness

In this equation, the insitu stress (q) is determined as:

$$q = \gamma H \tag{3}$$

where:

γ = the overburden density

H = the seam depth

and

$$\lambda = \frac{t}{\sqrt{12\left(1-\upsilon^2\right)}} \tag{4}$$

where:

t = the lamination thickness in the rock mass

υ = Poisson's Ratio of the rock mass

In equation 2, the panel is assumed to be open with no gob loading; therefore, the total abutment load is the full weight of the overburden for one half of the panel (qP/2). Also, equation 2 assumes the coal seam is perfectly elastic and there is no yield zone at the rib of the panel.

For the extent of the abutment stress given in equation 1, the empirically determined distribution of the abutment stress (σ_a) within the abutment zone has been found to be (Mark, 1992) (see Figure 1):

$$\sigma_a(x) = \left(\frac{3L_s}{D^3}\right)(D-x)^2 \tag{5}$$

where:

L_s = the total side abutment load

Based on the stress distribution generated by equation 5, it can be determined that essentially 90% of the abutment load should be within the distance ($D_{.9}$) from the edge of the panel (Mark and Chase, 1997):

$$D_{.9} = 5\sqrt{H} \tag{6}$$

To determine the distance from the panel edge which contains a given percentage (n) of the side abutment load for the laminated overburden model, first, the stress as defined by equation 2 needs to be integrated over the distance, x, to determine the load:

$$\int \sigma_l(x)\,dx = -q\frac{P}{2}e^{-\sqrt{\frac{2E_s}{E\lambda h}}x} \tag{7}$$

Then the fraction (n) of the total side abutment load (qP/2) which is contained in a given distance (D_n) can be determined as:

$$nq\frac{P}{2} = \int_0^{D_n} \sigma_1(x) = -q\frac{P}{2}e^{-\sqrt{\frac{2E_s}{E\lambda h}}D_n} + q\frac{P}{2} \quad (8)$$

Simplifying, by dividing through by the total abutment load (qP/2) gives:

$$n = 1 - e^{-\sqrt{\frac{2E_s}{E\lambda h}}D_n} \quad (9)$$

Then, solving for the abutment distance (D_n) for the given percent load (n) and substituting back in for λ, we get:

$$D_n = -\ln(1-n)\sqrt{\frac{E h t}{2E_s\sqrt{12(1-\upsilon^2)}}} \quad (10)$$

This equation (10) says that the extent of the abutment load is proportional to the square root of the rock mass modulus, seam thickness and lamination thickness and inversely proportional to the square root of the seam modulus.

Next, to determine the lamination thickness to use to get a given abutment distance with given rock and seam properties, equation 10 is solved for t:

$$t = \frac{2E_s\sqrt{12(1-\upsilon^2)}}{E h}\left(\frac{D_n}{\ln(1-n)}\right)^2 \quad (11)$$

Equation 11 shows that the lamination thickness (t) required to match a given abutment extent (D_n) is proportional to the square of the abutment extent, linearly proportional to the seam modulus and inversely proportional to the rock mass modulus and seam thickness. A comparison of the empirical abutment stress distribution and the matching laminated model abutment stress distribution as calculated by equation 11 at 90% load is shown in Figure 1.

One adjustment still needs to be made to equation 11 to use it in practice. For the original derivation of equation 2, the seam was assumed to be linearly elastic. Generally, this is not the case and there is some distance (d) of coal yielding at the edge of the panel. On the other hand, the field measurements used to determine the extent of the abutment stress in equations 1 and 6 naturally included the distance of the yielding zone in the measurements. Therefore, to use an abutment extent measured in the field for input to equation 11, the extent of the actual yield zone in the field needs to be subtracted from the field measurement to be more consistent with the derivation of equation 11. (This adjustment essentially neglects the amount of overburden load carried in the yield zone.) After making this yield zone adjustment to the extent of the abutment zone and substituting equation 6 for the distance of 90% load, an equation which determines the lamination thickness (t) that is required to match the field measurements for 90% of the abutment load is derived:

$$t = \frac{2E_s\sqrt{12(1-\upsilon^2)}}{E h}\left(\frac{5\sqrt{H}-d}{\ln(.1)}\right)^2 \quad (12)$$

Yield Zone Distance

In equation 12, the only parameter that is not necessarily known ahead of time is d, the extent of the yield zone. This value can be developed by running LaModel and observing the calculated yield zone for the given conditions. Or, to get a first approximation of the yield zone extent, one can find the point (x) into the pillar rib where the total load carrying capability of the coal rib is equal to the load distributed by the side abutment. First, to determine the load carrying capability of the coal rib, we start with the stress gradient implied by the Mark-Bieniawski coal strength formula (Mark, 1999):

$$\sigma_p(x) = S_i\left(0.64 + 2.16\left(\frac{x}{h}\right)\right) \quad (13)$$

where:

$\sigma_p(x)$ = peak coal stress (psi)

x = distance into the coal

S_i = insitu coal strength (psi)

h = pillar height

This equation is then integrated with respect to x and evaluated from the rib (x=0) to the distance x into the pillar to determine the total load carried by the edge of the pillar rib (see Figure 2):

$$\int_0^x \sigma_p(x)\,dx = S_i\left(\frac{1.08}{h}x^2 + 0.64\,x\right) \quad (14)$$

The load distributed by the side abutment for the laminated overburden model within the distance x was previously determined in equation 8. If these two loads are set equal, the following equation is determined:

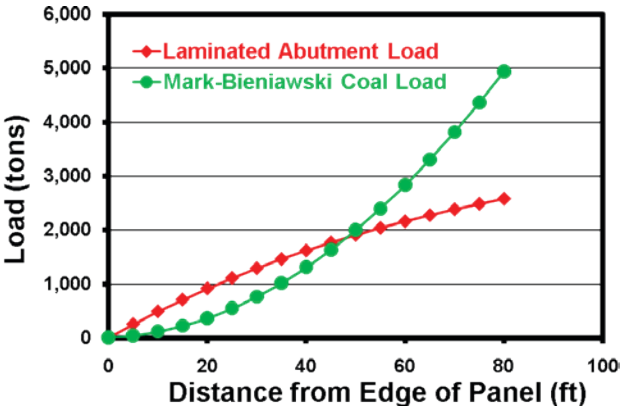

Figure 2. A comparison of laminated abutment load to the Mark-Bieniawski coal load.

$$-q\frac{P}{2}e^{-\sqrt{\frac{2E_s}{E\lambda h}}x}+q\frac{P}{2}-1.08\frac{S_i}{h}x^2-0.64S_ix=0 \qquad (15)$$

In the original derivation of equation 8, it was assumed that there was no gob and the total overburden load over half of the panel became the total abutment load. In the more general case, the gob is supporting some percentage of the overburden load and the remainder of the overburden load becomes abutment load. If the percentage of the total overburden load over the gob that becomes abutment load at the edge of the panel is (m), then 15 can be written as:

$$-mq\frac{P}{2}e^{-\sqrt{\frac{2E_s}{E\lambda h}}x}+mq\frac{P}{2}-1.08\frac{S_i}{h}x^2-0.64S_ix=0 \qquad (16)$$

The value of x which solves this equation is the distance into the pillar where the cumulative load applied by the laminated model is matched by the load carrying capability of the pillar. This is the point in Figure 2 where the loading curves cross and this value should give a reasonable estimate of the depth of the yield zone, d. Equation 16 is obviously non-linear and cannot be solved analytically; however, a numerical solution can easily be determined through using different trial values of x to find the zero point of the equation.

So, in summary, for determining the rock mass stiffness to use in LaModel, it is recommended to:

1) Determine the average rock mass modulus as a thickness weighted average of the elastic modulus of the overburden layers, or to use the default rock mass modulus in LaModel.
2) Then, determine the lamination thickness that matches the observed behavior (equation 11) or average field measurements (equation 12)
3) For estimating the depth of the yield zone at the coal rib of the abutment, use observations from the field or use equation 16

Implementation in LamPre3.0

To simplify applying the above protocols and equations in LaModel, a "Lamination Thickness Wizard" form has been added to the new LamPre 3.0 (see Figure 3). This wizard implements the previous equations in a user-friendly manner to assist the LaModel user in calibrating the lamination thickness as suggested above. In this wizard form, the user can enter a site specific value for the abutment extent determined from field measurements, observations, etc., or the user can check the box to the right ("Use the Suggested Value") and the empirically suggested value (as determined from equation 6) will automatically be entered for the extent of the abutment load to be used in subsequent calculations. Similarly, the user can enter a site specific value of the percentage overburden load on the abutment as determined from field measurements, observations, etc., or automatically use abutment load percentage as determined by a 21° abutment angle (as used in ARMPS), and the user can chose a yield zone distance measured or observed in the field or automatically use the value given by equation 16 above. Once all of the required input has been provided, the "Calculate" button at the bottom of the form is used to calculate the necessary lamination thickness (using equation 12).

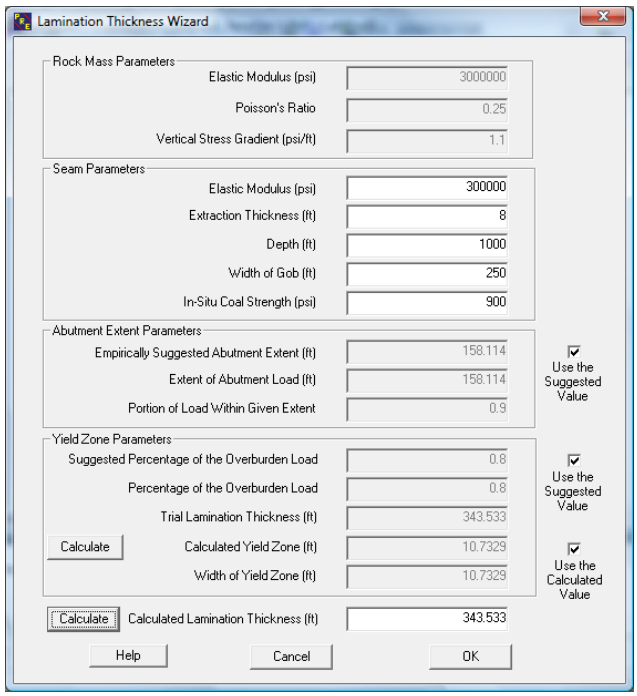

Figure 3. New Lamination Thickness Wizard in LamPre3.0.

Calibrating the Gob Stiffness

In a LaModel analysis with gob areas, an accurate stiffness for the gob (in relation to the stiffness of the rock) is critical to accurately calculating the overburden load distribution on the gob and abutment areas, and therefore the pillar stresses and safety factors. The relative stiffness of the gob determines how much overburden weight is carried by the gob; and therefore, not carried by the surrounding pillars. This means that a stiffer gob carries more load and the surrounding pillars carry less, while

a softer gob carries less load and the surrounding pillars carry more. In LaModel, the stiffness of the gob is primarily determined by adjusting the "Final Modulus" of the strain-hardening gob model (Heasley 1998) (see Figure 4). A higher final modulus gives a stiffer gob and a lower modulus value produces a softer gob material. Given that the behavior of the gob is so critical in determining the pillar stresses and safety factor, it is a sad fact that our knowledge of insitu gob properties is very poor For a calibrated LaModel analysis, it is imperative that the gob stiffness be calibrated with the best available information on the amount of abutment load (or gob load) experienced at that mine. It would be best to use specific field measurements of the abutment load (or gob load) from the mine in order to calibrating the gob stiffness. However, these types of field measurements are quite rare (and often of questionable accuracy). For estimating abutment loads or gob loads, visual observations are not very useful; and therefore, general historical measurements and/or empirical information are quite often the only available data.

Abutment Angle Gob Stress

To calibrate the gob stress in LaModel to match the mechanics of overburden loading implemented in ARMPS and ALPS, the abutment angle concept of overburden loading is used. In the abutment angle concept (see Figure 5), the amount of overburden weight within the abutment angle of the side of the panel is carried by the abutments (and the remaining load over the cave area is carried by the gob). In both ARMPS and ALPS, an average abutment angle of 21º was determined from an empirical database and is used to calculate the abutment loading. Using the abutment angle concept, the average gob stress ($\sigma_{g\text{-}av}$) for a supercritical panel (see Figure 5) can be calculated as:

$$\sigma_{g-av} = \left(\frac{H \times \gamma}{144}\right)\left(\frac{P - (H \times \tan\beta)}{P}\right) \qquad (17)$$

where:

β = Abutment Angle

Similarly, the average gob stress ($\sigma_{g\text{-}av}$) for a subcritical panel (see Figure 5) can be calculated as:

$$\sigma_{g-av} = \frac{P}{4}\left(\frac{1}{\tan\beta}\right)\left(\frac{\gamma}{144}\right) \qquad (18)$$

Note, equation 18, which is based on the abutment angle concept of gob loading, implies that the average gob stress for a subcritical panel (with an assumed abutment angle) is solely a function of the panel width, and not influenced by depth past the critical point.

Implementation in LamPre3.0

To get the LaModel user to consider the load distribution between the gob and the abutments and to simplify applying the above equations, a new wizard for defining the properties for the "Strain Hardening Gob" material has been added to the new LamPre 3.0. In this wizard, the user can enter a site specific value for the gob loading determined from field measurements, observations, etc., or the user can check the box to the right ("Use the Suggested Value") and the empirically suggested value (as determined from equation 17 or 18) will automatically be entered for the overburden load to be used in the subsequent calculations. Once all of the required input has been provided, the "Define Set" button at the bottom of the form, actually generates a two dimensional laminated model with the site specific geometry (depth, seam thickness, gob width, etc) and geo-mechanical properties (rock mass stiffness, coal properties, etc.), and iteratively determines the exact "Final Gob Modulus" which will provide the desired overburden load on the gob (in two dimensions).

Calibrating the Coal Strength

Accurate in situ coal strength is another value which is very difficult to obtain and yet is critical to determining accurate pillar safety factors. It is difficult to get a representative laboratory test value for the coal strength, and then scaling the laboratory values to accurate insitu coal pillar values is not very straightforward or precise. Other researchers (Mark and Barton, 1997) have found that it is more accurate to use empirically determined coal strength than to try and extrapolate laboratory test data to the field.

Mark-Bieniawski Pillar Strength Formula

Similarly, in LaModel, it is recommended to use the default coal strength of 900 psi in conjunction with the Mark-Bieniawski pillar strength formula as has been found to be optimum with ARMPS and ALPS (Mark, 1999):

$$S_p = S_i\left[0.64 + 0.54\left(\frac{w}{h}\right) - 0.18\left(\frac{w^2}{lh}\right)\right] \qquad (19)$$

where:

S_p = Pillar Strength (psi)

S_i = Insitu Coal Strength (psi)

w = Pillar Width

l = Pillar Length

h = Pillar Height

This formula also implies a stress gradient from the pillar rib that was previously presented as equation 13.

The 900 psi insitu coal strength that is the default in LaModel comes from the databases used to create the ALPS and ARMPS program and is supported by considerable empirical data. It is the author's opinion that insitu coal strengths calculated from laboratory tests are not more valid than the default 900 psi, due to the inaccuracies inherent to the testing and scaling process for coal strength. If the LaModel user chooses to deviate very much from

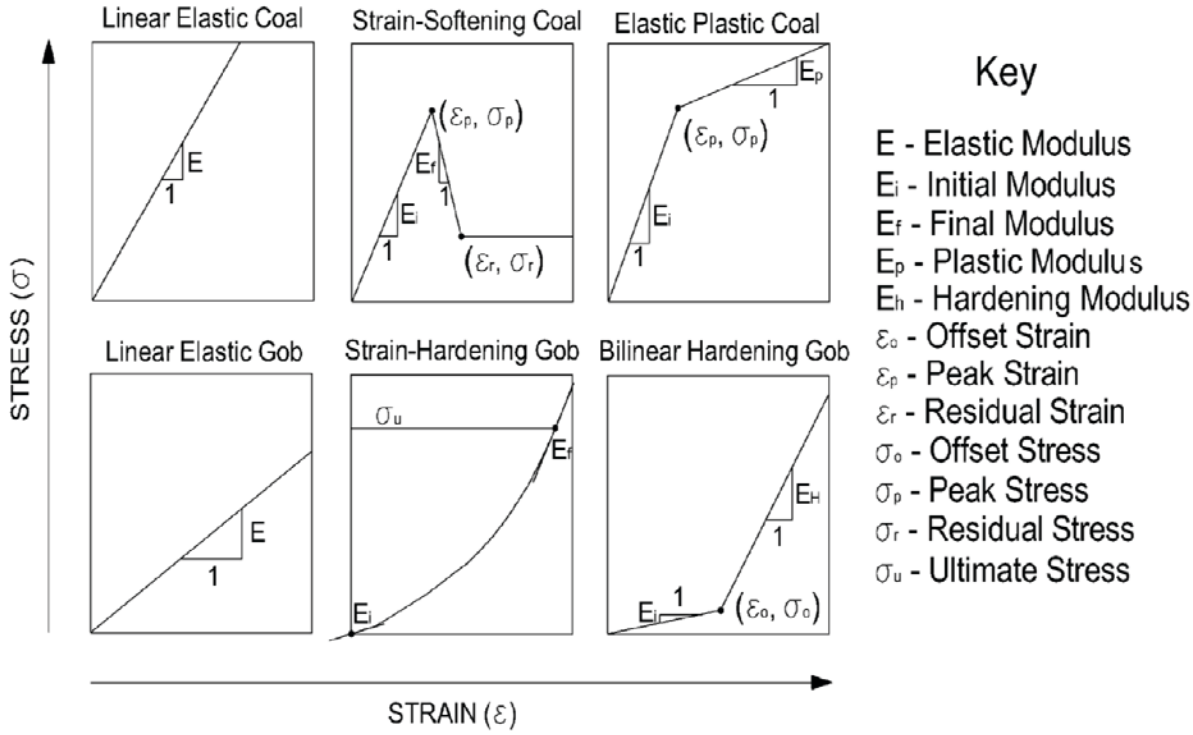

Figure 4. The six material models in LaModel.

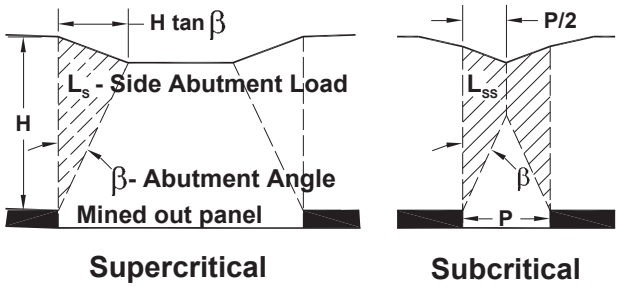

Figure 5. Conceptualization of the abutment angle.

the default 900 psi, they should have a very strong justification, preferably a suitable back analysis as described below or very accurate field measurements.

Back Analysis

If the user desires to improve upon the default average 900 psi coal strength, the best technique to determine a more accurate coal strength for LaModel is to back analyze a previous mining situation (similar to the situation in question) where the coal was close to, or past, failure. Back-analysis is an iterative process in which the coal strength is increased or decreased to determine a value that provides model results consistent with the actual measured/observed behavior. This back analysis should, of course, use the previously determined optimum values of the lamination thickness and gob stiffness. If there are no situations available where the coal was close to failure, then the back-analysis can at least determine a minimum insitu coal strength with some thought of how much stronger the coal may be. In the users' manual, a detailed example of back analyzing accurate coal strength is given.

Implementation in LamPre3.0

To numerically simulate a yield zone in LAMODEL, concentric rings of different materials are used against the openings and the material properties of the ribs are set such that the pillar yields from the rib inward. This type of yielding behavior matches that observed in the field (see Figure 7). In the last few years, a systematic technique for calculating these yielding coal properties based on the Mark-Bieniawski coal pillar strength formula (equation 19) and associated stress gradient (equation 13) has been developed. Essentially, for an element at the side of a pillar (such as A, C and E in Figure 7), the element average peak strength is equal to the stress at the midpoint of the element as determined by equation 13. For the corner elements, (such as B, D and F in Figure 7) which are needed to accurately approximate the Mark-Bieniawski pillar strength, the "pyramid-like" geometry produces an element average peak stress that is equal to the stress at the

point one third of the distance across the element as determined by equation 13.

In order to assist the user in implementing the Mark-Bieniawski pillar strength formula in LaModel, a new wizard for defining the properties for the "Elastic-Plastic for Coal" material has been added to the new LamPre 3.0 (see Figure 8). This coal wizard assumes an elastic, perfectly-plastic material model and uses the Mark-Bieniawski pillar strength formula to produce sets of realistic coal material properties for the yield zone at the edge of a pillar or longwall panel. In the new coal wizard, any number of yield sets with any number of yield zones (within the limits of the number of materials) can be defined. These yield zone properties are then automatically applied to the material grid in the grid editor.

DEEP COVER CASE HISTORY DATABASE

Database Overview

In order to help evaluate and verify a "standardized" method for calibrating LaModel, a database of deep cover retreat mining case studies was developed. For this database, NIOSH gathered the field data and mine maps, and provided them to the West Virginia University research team for analysis with LaModel. In the database there are 47 deep cover pillar retreat case studies from 11 different mines. Seven of these mines are in the Central Appalachian coal fields and 4 are in the Western coal fields. (These are the only areas in the United States where deep cover pillar retreat is presently being performed.) The depths at the case study sites ranged from 750 ft to 2200 ft with an average of 1256 ft. The extraction thicknesses at the case study sites went from a low of 3.6 ft to a high of 9.0 ft with an average of 6.9 ft. This is probably higher than the average seam thicknesses in the given mining areas, but for deep covering pillaring to be economically successful, a thicker coal is very helpful. The number of entries in the sections ranged from 3 to 13 with an average of 6.2 entries. Pillar widths ranged from 50 to 100 ft and crosscuts spacing ranged from 80 to 150 ft (center-center) with the average pillar size being 78 ft by 101 ft. The panel widths ranged from 160 ft to 940 ft with an average of 410 ft.

Thirty of the case studies included loading from a single side gob, while 14 of the panels only had an active gob, 2 of the sections had loading from two side gobs and one situation was development loading. Sixteen of the case study sites were considered failures, 28 were considered successful and 3 were considered marginal, or middlings. The NIOSH personnel made the determination of success or failure during their visit to the mine and conversations with the mine staff. A case study is considered a success when an entire panel was recovered without any significant ground incidents (Mark, 2009). Generally, the unsuccessful cases include (after Mark, 2009):

1) **Squeezes**, which are non-violent pillar failures that may take hours, days or even weeks to develop;
2) **Collapses**, which occur when large areas supported by slender pillars (w/h < 4) fail almost simultaneously, and;
3) **Bumps**, which are sudden, violent failures of one or more highly stresses pillars.

The database analysis does not specifically consider: the geology, the cut sequence, the specific coal strength or the type and amount of roof support.

ARMPS Analysis

The first analysis to be performed on each of the case studies was to calculate the ARMPS (2002) stability factor (Chase et al., 2002; Mark and Tuchman, 1997). These results are shown in Figure 9. For the 47 case histories, the ARMPS stability factors ranged from 0.33 to 1.55 with an average of 0.98. As can be seen in Figure 9, the stability factors cluster within a stability factor deviation of about 0.40 around the design line. There does not appear to be much separation between the successes and failures with a fairly equal number of each above and below the line (a few more successes above the line than below).

When examining these results it is important to consider how the case histories were obtained. For each failure, the mine typically retreated the panel until the active gob distance, depth of cover or some other factor became so adverse that the face was abandoned (for the reasons as discussed above). Therefore, these failures are just below the stability factor that was successful. For each of the failure points in the above plot, one can consider that all stability factors above that point were successful while all of the stability factors below that point were unsuccessful. Similarly, when a section was successful, the point with the deepest cover or most adverse conditions was analyzed to determine the minimum successful stability factor. Thus, for each of the success points in the above graph, one can consider all of the stability factors above that point to have been successful. So in essence, the points in Figure 9 plot the design curve between success and failure, and they do appear to track the present design curve fairly well. The vertical spread of these points essentially defines the magnitude of the uncertainty or "grey area" in the design line. This uncertainly appears to encompass a stability factor deviation of approximately ± 0.40 on either side of the design line. With an average stability factor of 0.98, this translates into a discrepancy of about 41%. Considering that the AMRPS analysis is performed for non-homogeneous, non-isotropic overburden and does not consider the specific: topography, geology, cut sequence, specific coal strength, or roof support, etc., this is a pretty good fit for the simplified geometric analysis implemented in ARMPS.

LaModel Analysis

Idealized LaModel Analysis

The next analysis that was performed on the database was to use LaModel with the calibration techniques described above to calculate a safety factor for each of the case studies. For the LaModel analysis, two different approaches were performed. In the first approach, what is called the "idealized" LaModel analysis, the LaModel grid was built to exactly duplicate the idealized mining plan simulated in ARMPS for each case study. The pillars were perfectly rectangular, the mine plan was rigidly organized and the overburden was set at a constant depth. To calibrate the input parameters for the models: the lamination thickness was set to match the expected abutment extent according to equation 12 using the Lamination Thickness Wizard (see Figure 3); the final gob modulus was set to provide a gob load that was consistent with a 21° abutment angle using equations 17 or 18 through the Strain

Hardening for Gob Material Wizard (see Figure 6), and the coal materials were set to provide a Mark-Bieniawski elastic-perfectly-plastic strength according to equation 19 using the Elastic-Plastic for Coal Material Wizard (see Figure 8). To calculate the safety factor for the idealized case study, the average stress-based pillar safety factor for the area within the ARMPS Active Mining Zone (AMZ) was used.

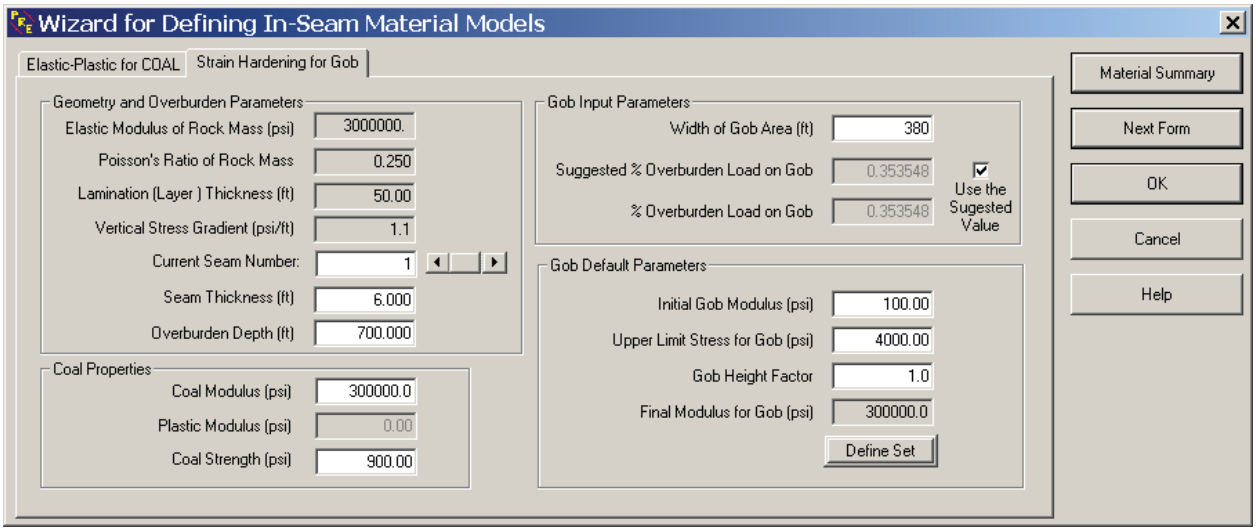

Figure 6. New wizard for calibrating the final modulus of the gob.

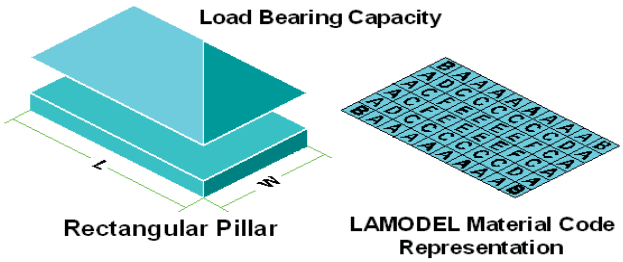

Figure 7 Schematic of pillar loading and material code representation.

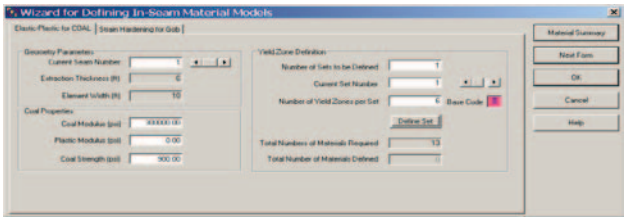

Figure 8 New wizard for defining Mark-Bieniawski coal properties.

The results of this idealized analysis are shown in Figure 10. For the case histories, the idealized LaModel safety factors ranged from 0.74 to 2.28 with an average of 1.39. Similar to the ARMPS analysis results, for each of the failure points in the above plot, one can consider that all stability factors above that point were successful while all of the stability factors below that point were unsuccessful. Similarly, for each of the success points in the above graph, one can consider all of the stability factors above that point to have been successful.

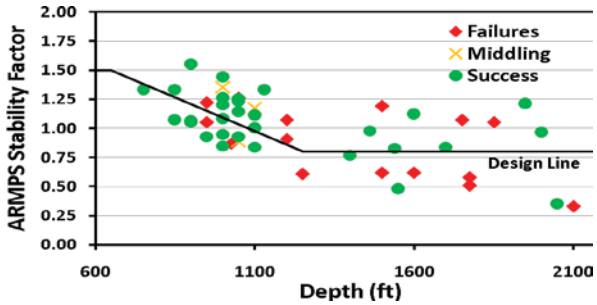

Figure 9 ARMPS 2002 stability factors for the case studies.

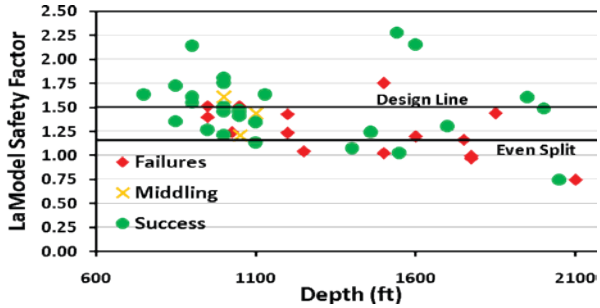

Figure 10 LaModel safety factors for the idealized case studies.

The area where the successful and failed designs overlap (the "grey area") appears to go from a safety factor of 0.75 to a safety factor of 1.75. This grey area encompasses a safety factor deviation of ± 0.50 on either side of a theoretical center line. With an average stability factor of 1.39, this translates into an uncertainty of about 36%. If a few outliers on the graph are not considered, the overlap appears to generally cover the area between a safety factor of 1.00 and 1.50, and encompasses a safety factor deviation of ± 0.25 on either side of a theoretical center line. This translates into an uncertainty of about 18%.

This 36% (or 18%) uncertainty (see Figure 10) shows that the idealized LaModel analysis does appear to provide a little more delineation between the successes and failures than the original ARMPS analysis. In the case studies, only 4 failures (and middlings) out of 19 (21%) occurred with an idealized safety factor above 1.5, and only one success out 30 (3%) occurred with an idealized safety factor below 1.0.

Dr. Chris Mark performed a logistic regression on the safety factor data from the idealized LaModel analyses. One of the first outcomes from his analysis was that the depth was not statistically significant. The analysis also determined that a safety factor of 1.16 best splits the successes and failures with 86% of the successes properly classified, 44% of the failures properly classified and an overall correct classification of 70%. The LROC value (which is a measure of the goodness of the fit somewhat comparable to the R^2 value in a linear regression) for the analysis was determined to be 0.746. Considering that the idealized LaModel results are from a geo-technical analysis that does not consider site specific factors such as: topography, geology, cut sequence, coal strength, and roof support, this is a pretty good fit.

Detailed LaModel Analysis

For the second approach to the LaModel analysis, what is called the "detailed" LaModel analysis, the LaModel grid was built directly from the mine map and included all of the typically abnormalities associated with retreat pillar mining: variable pillar sizes, variable panel width, variable surrounding rooms, variable pillar stumps, etc. Also, the true topography from the mine map was gridded into LaModel and used in the analysis. This "detailed" LaModel analysis was intended to simulate the true underground geometry and topography as closely as possible with LaModel. For the detailed analysis, the critical input parameters were calibrated exactly as for the idealized analysis using: the Lamination Thickness Wizard for determining the lamination thickness, the Strain Hardening for Gob Material Wizard for determining the final gob modulus, and the Elastic-Plastic for Coal Material Wizard for determining the coal materials. This approach resulted in the values of the critical input parameters being identical between the two LaModel analysis approaches. The safety factors for the detailed case study analysis were calculated in the same manner as for the idealized case studies, by using the average stress-based pillar safety factor for the area within the ARMPS (AMZ).

The results of this "detailed" LaModel analysis are shown in Figure 11. For the case histories, the detailed LaModel safety factors ranged from 0.85 to 2.14 with an average of 1.33. This spread is a little less than that for the idealized analysis, and as can be seen in Figure 11, the separation of the successes and failures was improved a bit with the detailed analysis. Including the real geometry and topography in the LaModel analysis changes the safety factors for the specific case studies about 11% on average with a range from 0% to 58%. One would hope that the more "detailed" analysis would have a tendency to lower the safety factors of the failures and raise the safety factors for the successes. For 11 out of 19 of the failures (or middlings), the safety factor was indeed reduced, but for 4 cases the safety factor was increased. However, for 10 out of 29 successful case studies, the safety factor was reduced; while for 8 of the case studies, the safety factor was indeed increased (11 stayed the same).

Examining the separation of the successes and failures as was done for the idealized analysis (see Figure 11) it can be seen that the bulk of the safety factors may have indeed become better separated. In fact, the detailed analysis brought one of the failures below the design line, although it took one of the middling cases to a higher safety factor. Looking at the graph in Figure 11, the area where the successful and failed designs overlap (the "grey area") appears to go from a safety factor of 0.86 to a safety factor of 1.50. This grey area encompasses a safety factor deviation of ± 0.32 on either side of a theoretical center line. With an average stability factor of 1.33, this translates into an uncertainty of about 24%.

This 24% uncertainty (see Figure 11) compares very favorably with the 36% uncertainty for the "idealized" analysis and the 41% uncertainty in the ARMPS analysis. It shows that the detailed LaModel analysis does indeed provide a better delineation between the successes and failures than either the idealized LaModel analysis or the ARMPS analysis. In the case studies, only 4 failures (and middlings) out of 19 (21%) occurred with an idealized safety factor above the design line at 1.40 (and 0 failures above a safety factor of 1.50). And only 1 success occurred with an idealized safety factor below 1.00. Overall, if a safety factor of 1.40 is used as a design objective, only 4 failures out of 47 case histories would be misclassified (or 8.5%).

A logistic regression on the safety factor data from the detailed LaModel analyses was performed by Dr. Chris Mark of NIOSH. Again, depth was found to not be statistically significant and the same safety factor value of 1.16 best splits the successes and failures. For the detailed analysis, the 1.16 safety factor successfully classifies 79% of the successes and 50% of the failures with an overall correct classification of 69%. The LROC value for the detailed analysis was 5% better at 0.791. Again, considering that the detailed LaModel results are from a geo-technical analysis that does not consider site specific factors such as: geology, cut sequence, coal strength, and roof support, this is a pretty decent fit

SUMMARY AND CONCLUSIONS

The research presented in this paper has produced a number of significant results that will undoubtedly raise the quality of mine design in the United States in the future, particularly for deep cover, pillar retreat coal mines. In the first part of this report, the protocols for a standardized LaModel calibration that simulates the "empirical mechanics" implemented in ARMPS and ALPS was rigorously developed. Essentially, for the standard calibration of the critical input parameters:

1. The lamination thickness is calibrated to match the expected abutment extent;

2. The final gob modulus is calibrated to an abutment loading that is consistent with a 21° abutment load angle; and
3. The coal material is calibrated to provide a 900 psi, Mark-Bieniawski pillar strength.

These calibration protocols have also been implemented into individual "Wizards" in LamPre3.0 in order to assist the LaModel user in quickly, easily and accurately producing a standard calibrated model.

Then, a database of 47 deep cover pillar retreat case studies was developed. With this database, the standardized LaModel calculation for deep cover pillar retreat mines was verified and calibrated. As a result of this process it was ultimately determined that if the LaModel user designs a deep cover pillar retreat section with the calibration method presented in this report and keeps the safety factor above 1.40, then they should have a less than a 10% chance of failure, or if the user keeps the safety factor above 1.50 they should have a 100% chance of success (based on the given database analysis). This recommended calibration method and associated recommended safety factor represents a major milestone in the development of LaModel, since this is the first time that such recommendations have been made for use with LaModel.

SUGGESTIONS FOR FUTURE RESEARCH

Having performed the analysis in this study, it is clear that the recommended LaModel approach (taken from the approach used by ALPS and ARMPS) for modeling and calibrating the lamination thickness and gob material presented in the report can still use improvement. The lamination thickness determined from the present calibration method appears to be a bit high, in particular for narrow panels. Equation 1, which defines the extent of the abutment loading, does not consider: the panel width, the seam thickness or the geometry. In any type of elastic or laminated overburden model, this does not make sense. Certainly, an improved formula for the abutment extent that accurately incorporates these factors should produce more accurate results. Also, the gob loading determined from the 21° abutment angle still produces too much loading in the section pillars for subcritical panels (Heasley, 2000). In the future, understanding the gob loading better, especially for deep cover situations, will help improve mine designs and result in safer mines.

REFERENCES

Chase, F.E., Mark, C. and Heasley, K.A. (2002). Deep Cover Pillar Extraction in the U.S. Coalfields. Proceedings of the 21st International Conference on Ground Control in Mining, Morgantown, WV, pp. 68-80.

Heasley, K.A. (2008). Some thoughts on Calibrating LaModel. Proceedings of the 27th International Conference on Ground Control in Mining, Morgantown, WV, pp. 7-13.

Heasley, K.A. (2000). The Forgotten Denominator, Pillar Loading. Proceedings of the 4th North American Rock Mechanics Symposium, Seattle, WA, pp. 457-464.

Heasley, K.A. (1998). Numerical Modeling of Coal Mines with a Laminated Displacement-Discontinuity Code. Ph.D. Dissertation, Colorado School of Mines, May.

Karabin, G. and Evanto, M. (1999). Experience with the Boundary-Element Method of Numerical Modeling to Resolve Complex Ground Control Problems. Proceedings of the 2nd International Workshop on Coal Pillar Mechanics and Design, NIOSH IC 9448, pp. 89-113.

Mark, C. (2009). Deep Cover Pillar Recovery in the U.S. Proceedings of the 28th International Conference on Ground Control in Mining, Morgantown, WV, pp. 1-9.

Mark, C. (1999). Empirical Methods for Coal Pillar Design. Proceedings of the 2nd International Workshop on Coal Pillar Mechanics and Design, NIOSH IC 9448, pp. 145-154.

Mark, C. and Barton, T.M. (1997). Pillar Design and Coal Strength. Proceedings of the New Technology for Ground Control in Retreat Mining, NIOSH IC 9446, pp. 49-59.

Mark, C. and Chase, F. E. (1997). Analysis of Retreat Mining Pillar Stability (ARMPS). Proceedings of the New Technology for Ground Control in Retreat Mining, NIOSH IC 9446, pp. 17-34.

Mark, C. and Tuchman, R. (1997). New Technology for Ground Control in Retreat Mining: Proceedings of the NIOSH Technology Transfer Seminar, NIOSH IC 9446.

Mark, C. (1992). Analysis of Longwall Pillar Stability (ALPS): An Update. Proceedings of the Workshop on Coal Pillar Mechanics and Design, U.S. Bureau of Mines IC 9315, pp. 238-249.

MSHA (2008). Fatal Underground Coal Burst Accidents August 6 and 16, 2007, Crandall Canyon Mine, DOL-MSHA, RI.

Peng, S.S. (2006). Longwall Mining, 2nd edition, Department of Mining Engineering, West Virginia University.

A Retrospective Assessment of Coal Pillar Design Methods

Daniel W Su, Sr. Geomechancial Engineer
Gregory J Hasenfus, Sr. Geomechanical Engineer
Coal Operations Engineering
Consol Energy Inc.
Canonsburg, PA

ABSTRACT

This paper demonstrates that numerical modeling can be used to predict in situ coal pillar strength, especially under non-ideal conditions where interface friction and roof and floor deformation are the primary controlling factors. It also illustrates that, despite their difference in approach, empirical, analytical and numerical pillar design methods have converged on fundamentally similar concepts of coal pillar mechanics. In addition, this paper attempts to cross-pollinate between the numerical and empirical methods, particularly for pillars in the "squat pillar" range. The combined numerical, empirical and analytical pillar design approach was employed in a Virginia coal mine to successfully control high longwall abutment stresses under deep cover.

INTRODUCTION

The strength of coal and coal pillars have been the subject of extensive research over the past 60 years, particularly over a 20-year span from the late 70's to the late 90's. Coal strengths determined in the laboratory as well as in situ typically increase with increasing specimen width-to-height (w/h) ratio and decrease with increasing specimen size. A number of empirical coal pillar strength formulas (Gaddy, 1956; Holland, 1964; Obert and Duvall, 1967; Salamon and Munro, 1967; Bieniawski, 1968) and analytical pillar strength formulas (Wilson, 1972; Barron, 1984) were proposed based on the shape and size effect derived from laboratory and in situ tests. These empirical and analytical coal pillar strength formulas were used by coal operators and regulatory authorities with varying degree of success. However, empirical pillar strength formulas may not be extrapolated with confidence beyond the data range from which they were derived, typically from pillars with w/h ratios of 5 or less (Mark and Iannacchione, 1992). Also, the empirical formulas treat the entire coal pillar as a single structure element to obtain an average pillar strength, often without consideration for roof and floor end constraints and subsequent interactions.

The importance of friction and end constraint on laboratory coal strength has been demonstrated by many researchers (Khair, 1968; Babcock, 1994). Brady and Brake (1968) reported that during a uniaxial compression test, the state of stress is triaxial within the specimen and biaxial at the free surface. In spite of this, the compressive strength obtained by testing a specimen with a diameter-to-length ratio (d/l) of 0.5 is approximately the correct uniaxial compressive strength. However, this is not true for test specimens having a d/l ratio greater than 0.5. Babcock (1990) also demonstrated that the state of stress, not the geometry, was responsible for the change in strength with the d/l ratio. In fact, specimens of coal, limestone, and sandstone with d/l ratios ranging from 1 to 8.5 were made to fail in compression at about the same stress for each rock type by removing end frictional effects with layers of PTFE. Panek (1994) also reported that lateral confinement generated by the end frictional effect may transform rock and coal samples from a brittle to ductile stage at relatively low width-to-height ratios. Bieniawski (1981) and Salamon and Wagner (1985) suggested that confinement generated by the end constraint of coal may increase more rapidly for width-to-height ratios greater than 5.

Practitioners and researchers alike, including Mark and Bieniawski (1986), Hasenfus and Su (1992), Maleki (1992) and Parker (1993) have noted the significance of roof and floor interactions on in situ pillar strength. To account for the apparent increase of pillar strength due to confinement at high w/h ratios, Bieniawski (1981) modified his original empirical formula for pillars with w/h ratios of 5 or more. Salamon and Wagner (1985) also proposed a squat pillar formula for use in South African coal mines to account for the rapid increase in pillar strengths at high w/h ratios. The squat pillar formula has been employed in South Africa with success (Madden, 1988). Wagner (1974) demonstrated that pillar stress within even a relatively small pillar near the peak load was highly non-uniform and that pillar failure was progressive. Wilson (1972) used similar progressive failure mechanism in the confined core concept of pillar strength, which assumed that coal follows a linear Mohr-Coulomb failure criterion. Barron (1984) later modified Wilson's assumption of exponential increase of horizontal confining stress by introducing the nonlinear Hoek-Brown criterion. This exponential increase of confining stress is also implied in the modified Bieniawski and the squat pillar strength formulas.

With increasingly powerful computing capabilities, and the increased commercial availability of sophisticated numerical modeling software, computer models have been used since the early 80's to study pillar strength and failure mechanisms

(Kripakov, 1981; Hsiung and Peng, 1985), although interface friction was not simulated in either case. Iannacchionne (1990) used the FLAC code to study the effect of interface slip on coal pillar strength and found that interface slip is the primary factor controlling the strength of in situ pillars. Su and Hasenfus (1996, 1997, 1999) employed the finite element modeling technique to predict in situ coal pillar strength under non-ideal conditions where interface friction and roof and floor deformation are the primary controlling factors. The predicted pillar strengths were in good agreement with field measurements over a wide range of width-to-height ratios. The effects of weak floor strata and rock parting on coal pillar strength were also evaluated.

HISTORICAL OVERVIEW OF COAL PILLAR DESIGN MODELS

Five coal pillar design model classifications can be defined according to decreasing reliance on empirical data and experience: empirical models, semi-empirical models, semi-analytical models, analytical models, and numerical models. Pre-1960 designs tend to rely almost exclusively on empirical models which were based only on past experience and observations. In the 60's, semi-empirical approaches to pillar design became very popular and they are still considered applicable for room-and-pillar designs under shallow to medium cover. The Hollad-Gaddy (1964), Obert and Duvall (1967), Salamon and Munro (1967), and Bieniawski (1981) formulas for coal pillar design are examples of this approach. Typically, these design formulas rely upon coal strength characteristics and empirically derived strength relationships for pillar size and shape. Rarely considered, however, are roof and floor conditions, pillar stress distribution, and in situ horizontal stress state, all of which affect pillar and entry stability.

Most of the models categorized as semi-analytical were developed to specifically account for high-extraction or longwall mining. Examples in this category include those advocated by Mark (1990) and Wilson (1981). Semi-analytical models typically account for abutment loading and abutment load distribution, and are thus more acceptable for longwall chain pillar design than semi-empirical models. One disadvantage of the semi-analytical model is that they are usually applicable only in areas where sufficient experience with the model and mining conditions has been attained. This is due to the model constraints and input assumptions, which often simplify the many geomechanical relationships that affect longwall development stability. As such, safety factor adjustments are often necessary. One example of this shortcoming is the inability of most semi-analytical models to adequately calculate pillar safety factors for longwall development under deep cover (>1,000 ft) in part because they tend to underestimate the effect of confinement on coal pillars with large width-to-height ratios.

The fourth model classification is purely analytical and relies almost entirely on geomechanical theories and principles. An example of this approach is that proposed by Salamon (1992). Although this approach does not rely upon empirical relationships, designs based on analytical models are usually oversimplified and cannot account for many geological and geometrical complexities.

The last category, the numerical model approach, can provide a more rigorous estimation of the longwall development design response and the corresponding safety factors. Numerical models can also be used to evaluate coal pillar strengths at various width-to-height ratios under a combination of roof, floor and in-seam conditions. In addition, they do not rely upon site-specific, empirically derived correlations and thus are better suited for coal pillar designs in new mining areas. The disadvantages to this approach include difficulties in material behavior simulation, reliance upon detailed, accurate input data, and the need for powerful computing capabilities.

USE OF FINITE ELEMENT MODELING IN PILLAR DESIGN

In the early to mid 1990's, numerical models were employed to study the effect of roof/coal and floor/coal interfaces on coal pillar behavior. While not attempting to suggest a new means of coal pillar design, Su and Hasenfus (1995, 1997) employed a sophisticated finite element technique to explore the effects of interface friction and in-seam and near-seam conditions on coal pillar strengths over a wide range of width-to-height ratios. Nonlinear pillar strength curves were first presented to relate coal pillar strength to width-to-height ratios under simulated strong roof and floor conditions (Figure 1). Confinement generated by the frictional effect at the coal-rock interfaces was demonstrated to accelerate pillar strength increase beginning at a width-to-height ratio of about 3. Thereafter, frictional constraint limitations and coal plasticity decelerate pillar strength increases beginning at a width-to-height ratio of about 6. The simulated pillar strength curve under strong roof and floor conditions compared favorably with measured peak strengths of five failed pillars in two southwestern Virginia coal mines (Figure 2) and is in general agreement with many existing semi-empirical and semi-analytical coal pillar design formulas at width-to-height ratios of 5 or less (Figure 1).

The finite element modeling technique has also been used to evaluate the effect of in-seam and near seam conditions, such a seam strength, rock partings, and weak floor rock, on in situ coal pillar strength. On a percentage basis, seam strength was found to have a negligible effect on the peak strength for pillars at high w/h ratios, since confinement generated by frictional effect is the controlling factor at high w/h ratios (Figure 3). Thus, for practical coal pillar design, particularly for pillars with w/h ratios greater than 5, exact determination of in situ coal strength becomes unnecessary. This is consistent with the findings of Mark (1990) and Mark and Barton(1996), who stated that meaningful results can be achieved with semi-empirical coal pillar strength formulas if an average seam strength value of 900 psi (6.2 MPa) is used for U.S. bituminous coal seams. They also suggested that pillar stability design is more reliable when a uniform seam strength is used to evaluate all cases.

Rock partings within the coal seam were found to have a variable effect on coal pillar strength, depending on the parting characteristics. A competent shale parting reduces the effective pillar height, thus increasing the w/h ratio and the ultimate pillar strength (Figure 4). Conversely, a weak claystone parting (drawslate) slightly decreases pillar strength. In addition, weak floor rocks may decrease the ultimate pillar strength by as much as 50% compared to strong floor rocks. Field observations confirm pillar strength reduction in the presence of weak floor rocks (Figure 5).

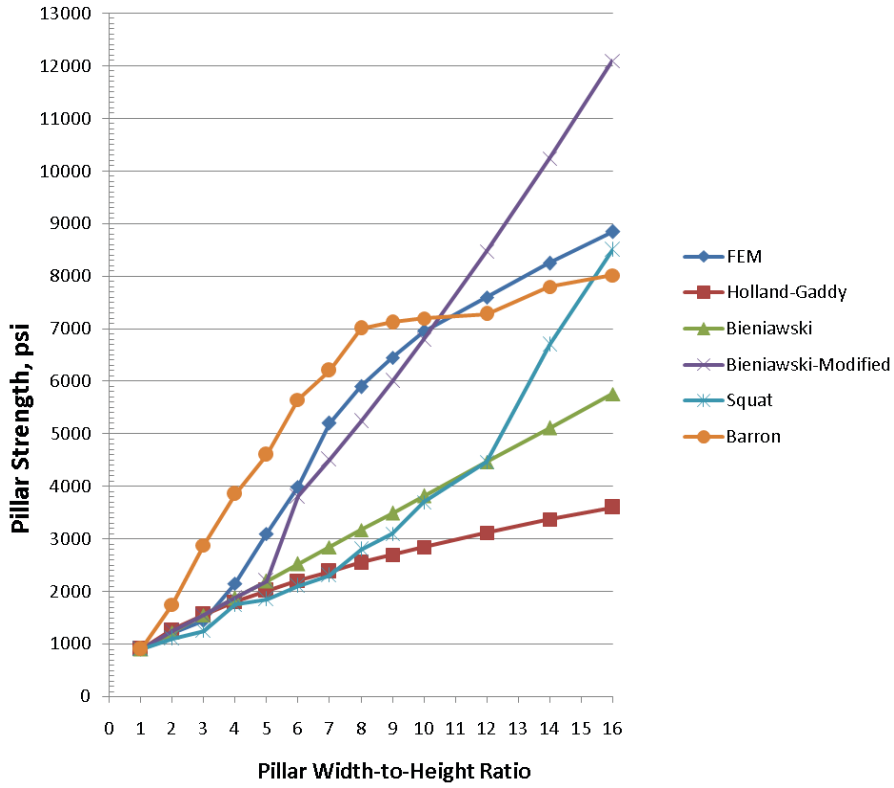

Figure 1. Pillar Strength versus width-to-height ratio – FEM versus semi-empirical and semi-analytical models.

PRACTICAL PILLAR DESIGN CONSIDERATIONS FOR DEEP COVER

Since many popular coal pillar design formulas are semi-empirical relationships that were developed under limited conditions, application of these formulas may be inappropriate when other factors not specifically addressed in these relationships are encountered. As demonstrated, pillar strength and therefore entry stability are extremely sensitive to the in situ characteristics of not only the coal, but also the adjacent and inclusive rocks that comprise the coal pillar system. Unfortunately, a single site-specific semi-empirical formula cannot accurately account for the variations of features that may significantly affect pillar and entry stability within a coal field or even a mine. However, it is neither practical nor efficient to develop site-specific semi-empirical formulas to account for all variations of roof, floor, and coal seam characteristics that may occur within a mine.

Over the past two decades, the Analysis of Longwall Pillar Stability (ALPS) and the Analysis of Retreat Mining Pillar Stability (ARMPS) have gained wide acceptance within the U.S. coal industry. Although proven to be applicable in many mines and mining regions, ALPS and ARMPS, which rely solely on the Bieniawski semi-empirical formula for pillar strength calculation, do not always provide accurate pillar strength for deep cover mines which typically employ coal pillars with high w/h ratios. For example, for the prevailing strong roof and floor conditions in the Virginia Pocahontas #3 Coalfield, ALPS and ARMPS significantly underestimate the peak pillar strength. As a result, stable pillar conditions will back calculate to a stability factor of about 0.7, which traditionally means 60% to 70% probability of failure. To rectify such a discrepancy, pillar strength curves derived from well calibrated finite element analysis could be incorporated into ALPS and ARMPS for calculating coal pillar strengths with high w/h ratios and varying roof, floor and parting conditions.

COAL PILLAR DESIGN : GROUND CONTROL AND VENTILATION PERSPECTIVES

The primary purpose of coal pillar design is to ensure that the coal pillars possess enough load bearing capacity compared to the expected loading condition with an appropriate safety factor. However, coal pillar design also significantly affects the ventilation aspect of high extraction mining, particularly longwall mining. For example, a typical 3-entry longwall gateroad, in most cases, must keep the middle entry (typically the track or travel entry) open behind the longwall face on the tailgate side to divert the air that crosses the longwall face to the bleeder system. Otherwise, the air that crosses the face must return outby through the tailgate, which may pull the gob air into the face area. It is important to remember that behind the tailgate T-junction, both outside entries are now part of gob, and the pillars are subject to maximum stress, the isolated abutment stress. Also, roof and floor stability in the middle entry depends not only on adequate pillar design, but also on the roof and floor characteristics and in situ horizontal stresses. It is this roof and floor stability that the pillar design intends to protect. However, the empirical, semi-empirical, semi-analytical, and analytical pillar design methods will have extreme difficulties dealing with the complex roof and floor geology as well as in situ horizontal stresses. On the other hand, numerical methods such as finite element analyses are better suited to address such complex roof and floor geology and in situ horizontal stresses.

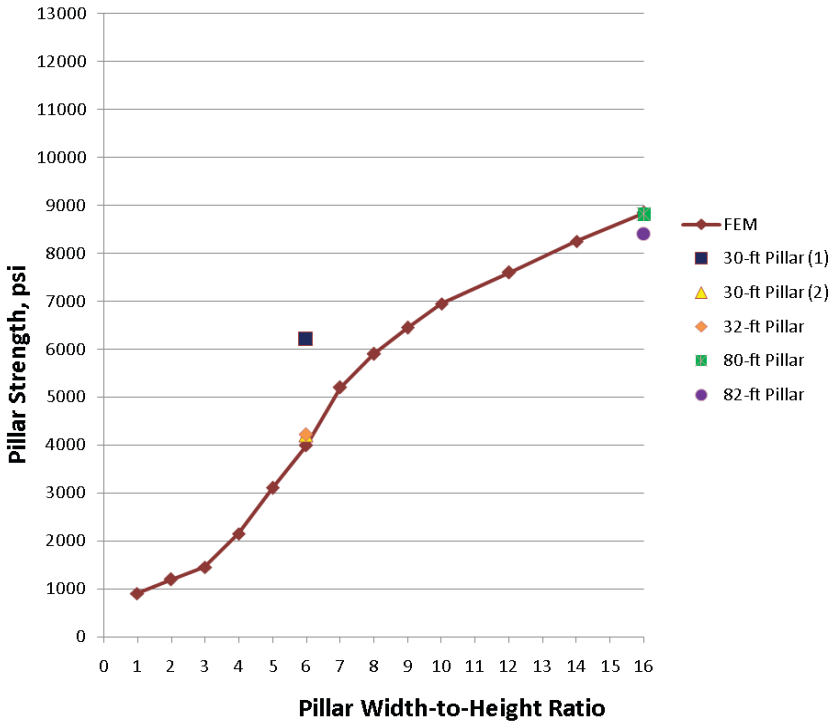

Figure 2. peak pillar strength comparison – FEM model versus failed pillars in a deep longwall mine.

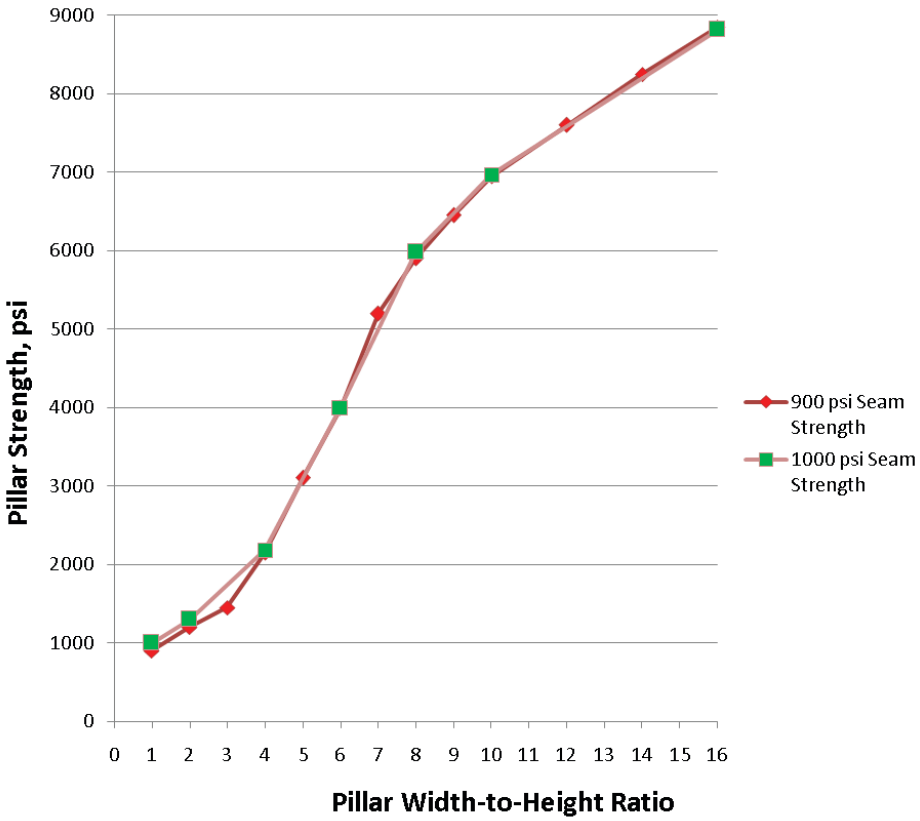

Figure 3. Effect of seam strength on pillar strength.

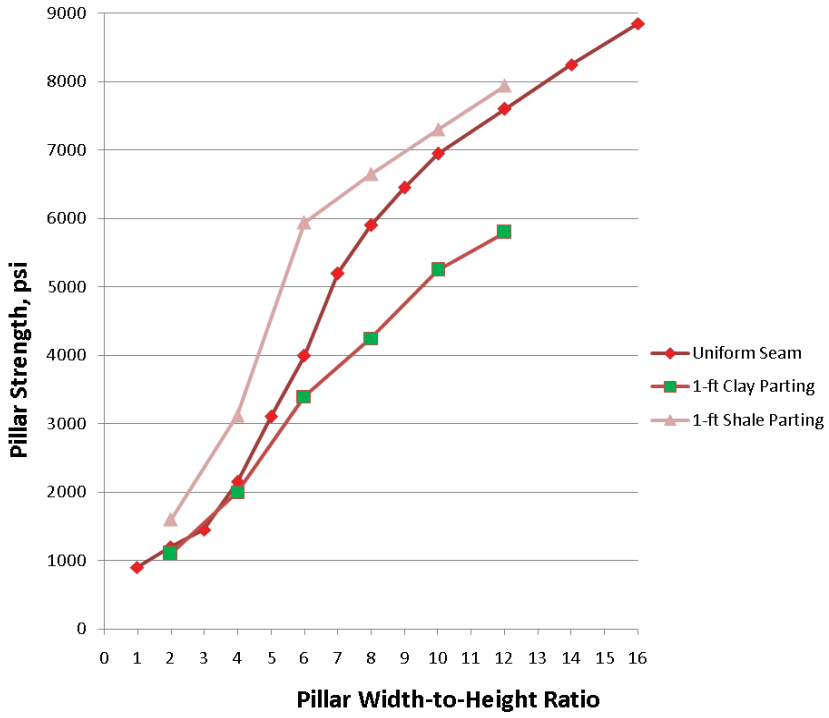

Figure 4. Effect of parting on pillar strength.

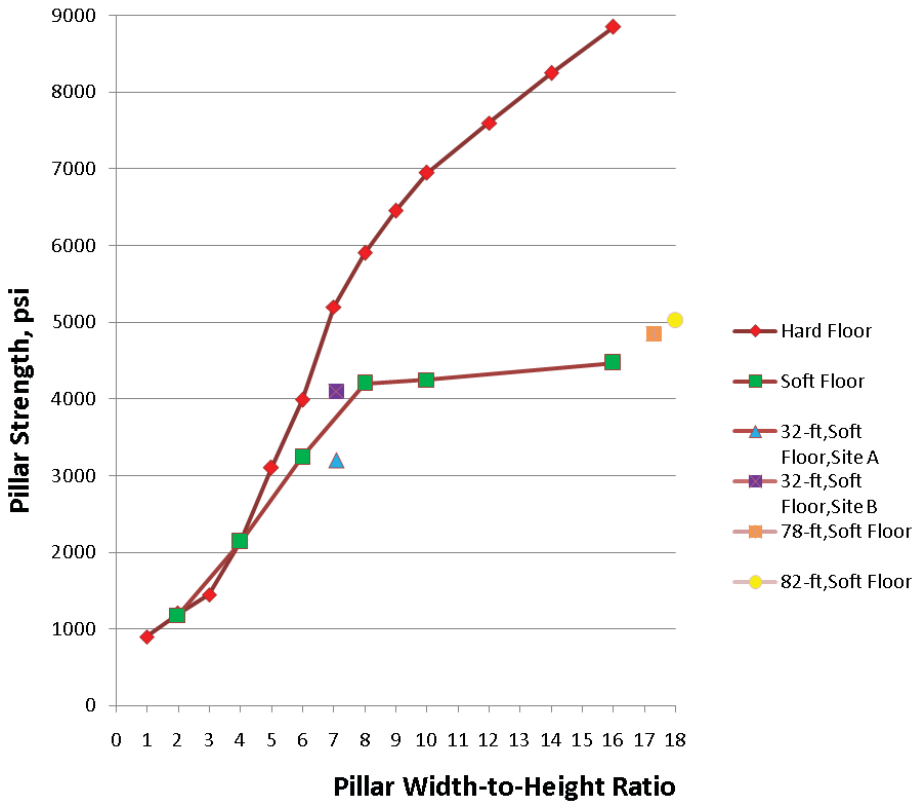

Figure 5. Effect of soft floor on pillar strength.

Figure 6 illustrates a comparison of pillar stresses calculated by finite element analysis and ALPS in a Pocahontas #3 seam longwall mine that employs a 4-entry longwall gateroad. Clearly, the strength of the 150-ft abutment pillar (w/h=25) as calculated by the finite element analysis is about 50% higher than that calculated by ALPS. Also, stresses and deformation of the roof and floor rocks calculated by the finite element analysis can be used to evaluate the required standing support capacity and yieldability to keep the #2 entry open behind the tailgate T-junction. In this case, a total of 15 in of convergence was estimated by the finite element analysis, which suggested that supplemental standing support would have to be yieldable up to 15 in. To this end, 30-in pumpable cribs were selected in part because they met both the capacity and yieldability requirements and were more efficient to transport and install. Ventilation surveys and in-mine observations confirmed the effectiveness of the 30-in pumpable cribs.

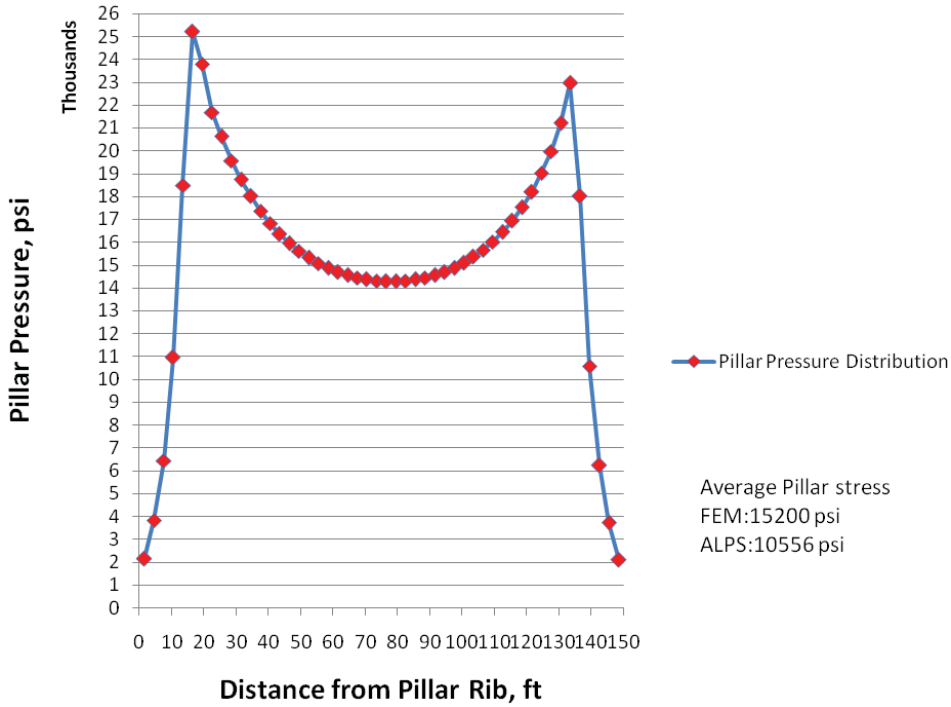

Figure 6. Pillar pressure distribution across a 150-ft wide pillar – FEM versus ALPS.

CONCLUSIONS

With the advance of interface friction modeling, finite element analysis has been demonstrated to provide reasonably accurate in situ coal pillar strength that takes into account the complex coal pillar failure mechanisms. Results from the analysis have indicated that interface friction and roof and floor deformation are the primary factors controlling the ultimate in situ coal pillar strength, particular for pillars with high w/h ratios. Nonlinear pillar strength curves were derived to relate the pillar strength increase to the w/h ratio. Confinement generated by the frictional effects at the coal/rock interfaces is shown to increase the pillar strength more rapidly at a w/h ratio of about 3. The nonlinear pillar strength curve for strong roof and floor conditions compares favorably with the measured peak strengths of five failed pillars in two southwestern Virginia coal mines and is in general agreement with many existing coal pillar design formulas at w/h ratios of 5 or less. However, for wide pillars, the finite element model predicts a higher in situ coal pillar strength than most accepted formulas. Consequently, use of the more conservative semi-empirical and semi-analytical formulas may lead to the employment of unnecessarily wide pillars or otherwise a lower estimated pillar safety factor.

Results from the finite element analysis also indicate that for coal pillars with high w/h ratios, the ultimate pillar strength is more dependent on the end constraints than on the coal strength. Such a conclusion, which is consistent with the suggestion by Mark (1990) and Mark and Barron (1996), reduces the significance of laboratory coal compressive strength test. For practical purposes, particularly for pillars with high w/h ratios, a seam strength of 900 psi (6.2 MPa) for all coal seams is adequate for use in the finite element analysis.

The finite element model results presented are not intend to suggest a new pillar design criterion. Rather, they are presented to emphasize the site-specific nature of coal pillar design and the importance of taking into account the interface friction. Semi-empirical, semi-analytical or numerical coal pillar design formulas or models should be calibrated and validated by site-specific measurements or obversational field studies whenever possible. Finally, proper longwall chain pillar design impacts not only the pillar and roof stability, but also the ventilation adequacy. With current emphasis on health and safety, effective roof control and ventilation can not be over-emphasized. Since finite element analysis is not designed to be used daily by engineers at the mine site, it appears that a cross-linkage of semi-empirical, semi-analytical and numerical pillar design methods may provide the ultimate coal pillar design medels for a variety of site-specific

conditions and can be comfortably used by engineers at the mine site.

REFERENCES

Babcock, C.O. (1994). Critique of Pillar Design Equations From 1833 to 1990. U.S. Bureau Of Mines IC 9398.

Babcock, C.O. (1990). True Uniaxial Compressive Strength of Rock or Coal Specimens are Independent of Diameter-to-Length Ratios. U.S. Bureau Of Mines RI 9316.

Barron, K. (1984). Analytical Approach to the Design of Coal Pillars. CIM Bulletin *77*(868):37-44.

Bieniawski, Z.T. (1981). Improved Design of Coal Pillars for U.S. Mining Conditions. First Conference on Ground Control in Mining, Morgantown, WV, pp. 13-22.

Bieniawski, Z.T. (1968). The Effect of Specimen Size on Compressive Strength of Coal. Int. J. Rock Mech. Min. Sci. *5*:325-335.

Brady, B.T. and Brake, W. (1968). An Elastic Solution of Laterally Constrained Circular Cylinder Under Uniaxial Loading. Proceedings of the 10th U.S. Symposium on Rock Mechanics, pp. 199-214.

Gaddy, F.L. (1956). A Study of Ultimate Strength of Coal as Related to the Absolute Size of the Cubical Specimens Tested. VPI Bulletin 49(10), Tables 6-10, Blacksburg, VA.

Hasenfus, G.J. and Su, D.W.H. (1992). A Comprehensive Integrated Approach for Longwall Development Design. Proceedings of the First Workshop on Coal Pillar Mechanics and Design. U.S. Bureau of Mines IC 9315, pp. 225-237.

Hsiung, S.M. and Peng, S.S. (1985). Chain Pillar Design for U.S. Longwall Panels. Mining Sciences And Technology *2*:279-305.

Holland, C.T. (1964). The Strength of Coal in Mine Pillars. Proceedings of the 6th Symposium On Rock Mechanics, Rolla, MO, pp. 450-456.

Iannacchione, A.T. (1990). The Effect of Roof and Floor Interface Slip on Coal Pillar Behavior.

Khair, A.W. (1968). The Effect of Coefficient of Friction on Strength of Mode of Coal Pillar. Ph.D. Thesis, West Virginia University, Department Of Mining Engineering, Morgantown, WV.

Kripakov, N.P. (1981). Analysis Of Pillar Stability on Steeply Pitching Seams using Finite Element Method. U.S. Bureau Of Mines RI 8579.

Madden, B.J. (1988). The Performance of Coal Pillars Designed to the Squat Pillar Formula. Proceedings of the 29th U.S. Symposium on Rock Mechanics, pp. 699-708.

Maleki, H. (1992). In Situ Pillar Strength and Failure Mechanisms for U.S. Coal Seams. Proceedings of the First Workshop on Coal Pillar Mechanics And Design, U.S. Bureau Of Mines IC 9315, pp. 73-77.

Mark, C. (1990). Pillar Design Methods for Longwall Mining. U.S. Bureau of Mines IC 9247.

Mark, C. and Barton, T. (1996). The Uniaxial Compressive Strength of Coal: Should it be used to Design Pillars? Proceedings of the 15th International Conference on Ground Control in Mining, Golden, CO, pp. 61-78.

Mark, C. and Bieniawski, Z.T. (1986). Field Measurements of Chain Pillar Response to Longwall Abutment Loads. Proceedings of the 5th Conference on Ground Control in Mining, Morgantown, WV, pp. 114-122.

Mark, C. and Chase F.E. (1993). Gate Entry Design for Longwall Using the Coal Mine Roof Rating. Proceedings of the 12th International Conference on Ground Control in Mining, Morgantown, WV, pp. 76-83.

Mark, C. and Iannacchione, A.T. (1992). Coal Pillar Mechanics: Theoretical Models and Field Measurements Compared. Proceedings of the First Workshop on Coal Pillar Mechanics And Design. U.S. Bureau Of Mines IC 9315, pp. 78-93.

Obert L, Duvall WI (1967). Rock Mechanics And The Design Of Structures In Rock. New York, NY , John Wiley And Sons, 650 Pp.

Panek, L. (1994). Scaling Mine Pillar Size and Slope With the F Function. SME Preprint 94-52, Littleton, CO.

Parker, J. (1993). Mine Pillar Design in 1993: Computers Have Become the Opiate of Mining Engineering, Parts I and II. Min. Eng. July: 714-717 and Aug:1047-1050.

Salamon, M.D.G. (1992). Strength And Stability of Coal Pillars. Proceedings of the 1st Workshop on Coal Pillar Mechanics and Design, U.S. Bureau of Mines IC 9315, pp. 94-121.

Salamon, M.D.G. and Munro, A.H. (1967). A Study of the Strength of Coal Pillars. J. S. Afr. Inst. Min. Metall. *68*: 55-67.

Salamon, M.D.G. and Wagner, H. (1985). Practical Experiences in the Design of Coal Pillars. Proceedings of the 21st International Conference of Safety in Mines Research Institutes, Sydney, Australia, pp. 3-9.

Su, D.W.H. and Hasenfus, G.J. (1999). Coal Pillar Strength and Practical Coal Pillar Design Considerations. Proceedings of the 2nd Workshop on Coal Pillar Mechanics and Design, NIOSH IC 9448, pp. 155-162.

Su, D.W.H. and Hasenfus, G.J. (1997). Effects of In-Seam and Near-Seam Conditions on Coal Pillar Strength. Proceedings of the 16th International Conference on Ground Control in Mining, Abstract, Morgantown, WV, pp. 282.

Su, D.W.H. and Hasenfus, G.J. (1996). Practical Coal Pillar Design Considerations Based on Numerical Modeling. Proceedings of the 15th International Conference on Ground Control in Mining, Golden, CO.

Wagner, H. (1974). Determination of Complete Load-Deformation Characteristics of Coal Pillars. Proceedings of the 3rd International Conference on Rock Mechanics, Denver, CO, pp.1076-1081.

Wilson, A.H. (1981). Stress And Stability in Coal Ribsides and Pillars. Proceedings of the 1st International Conference on Ground Control in Mining, Morgantown, WV, pp. 1-12.

Wilson, A.H. (1972). An Hypothesis Concerning Pillar Stability. Min. Eng. (London) *131*(141):409-417.

Numerical Modeling of Yielding Chain Pillars in Deep Longwall Coal Mines

Ugur Ozbay, Professor
Mining Engineering Department
Colorado School of Mines
Golden, CO

Salah Badr, Associate Professor
Mining Engineering Department
King Abdulaziz University
Jeddah, Saudi Arabia

ABSTRACT

This paper describes a numerical modeling methodology developed for investigating the behavior of yielding of chain pillars in deep longwall coal mines. The methodology is based on first calibrating the material properties of coal using an isolated pillar model and then translating the results to a deep two-entry longwall mine that uses yielding chain pillars. The calibration study results are validated against the commonly used empirical pillar strength formulae and published results of in situ coal pillar tests. A closer analysis of the calibration results show sudden cohesion drops within a region of about 1 to 1.5 mining height distance from the pillar sides as the width to height ratio of these pillars increase beyond 4. The longwall model incorporates two 240 m wide 1,000 m long panels at a depth of 600 m. The coal seam is modeled as a strain softening material to observe its response to loading in both pre- and post-peak states. The model allows monitoring of a width – height ratio 4 chain pillar responses while being subjected to development, headgate, and tailgate loading stages. Full stress-strain behavior of these pillars show that failure initiates within pillar sidewalls under development loading. During headgate loading, the failure propagates further into the pillar and initiates a stable yielding of the pillar. At the time of tailgate loading, the pillar is already in its residual strength state. The validity of the modeling methodology is discussed by comparing the results against the in situ stress measurements taken in an actual longwall mine with similar conditions.

INTRODUCTION

Compared to their shallow counterparts, longwall chain pillars at depth experience much more damage, even while they are being formed. Beyond depths of about 300 m, the vertical component of the virgin stress exceeds the unconfined strength of coal, causing sidewall failures in pillars and abutments. The degree and mode of these failures (violent or non-violent) are dependent on mining geometries, coal and overburden geology, as well as the mining depth. In deep mining conditions, the purpose of the yielding chain pillar design is to allow pillars to exceed their peak stress capacity in a non-violent manner while maintaining the required support pressure levels to assure safety and operability in the gateroads. Due to high mining depths and the complex nature of longwall mining geometry and geology, the traditional methods of safety/stability factor are not able to fully provide the necessary tools for the rock mechanical analysis of yielding pillars. To facilitate an acceptable approach to this three-dimensional problem, a numerical model of a deep longwall mine has been developed using the FLAC3D computer code (Anon, 2003). This code incorporates a plastic softening constitutive model, called strain softening, which can reasonably simulate brittle rock behavior by allowing load shedding in the post-peak state. The following sections describe the methodology developed for building a numerical model of a deep longwall mine and calibrating its material properties with the main objective of studying the response of yield pillars to the various loading stages encountered in longwall coal mines.

Calibration of Coal Strength Parameters

An important, yet difficult, part of building a numerical model of yielding pillars is the determination of a constitutive model and its parameters that best represent the coal seam being modeled. For modeling of the coal seam material, the study uses the strain softening constitutive model as implemented in FLAC3D. The determination of the strain softening parameters is based on the assumption that the two most commonly used pillar strength formulae of Salamon (1967) and Bieniawski (1984) are valid estimators of the in situ strength of coal pillars. The results obtained from the calibration studies are also compared to the complete in situ stress strain curves for coal pillars as determined by Wagner (1974).

For the calibration studies, a stand-alone FLAC3D model of a pillar is used. This model represents a square pillar in an extensively mined room and pillar panel – an environment where most of the data come from for the development of the two empirical pillar strength formulae mentioned above. For numerical convenience, full symmetry condition is assumed and only a half-quarter of a single pillar (1/8 of a pillar), together with its floor, is built as the numerical model. Figure 1 shows the numerical model geometry as it relates to a room and pillar panel layout. The pillar height is 1 m and the entry width is 6.5 m. The width of the pillar varies depending on the width/height ratio being considered for a particular case.

Development of post-peak parameters for the strain softening constitutive model in FLAC3D requires defining values for

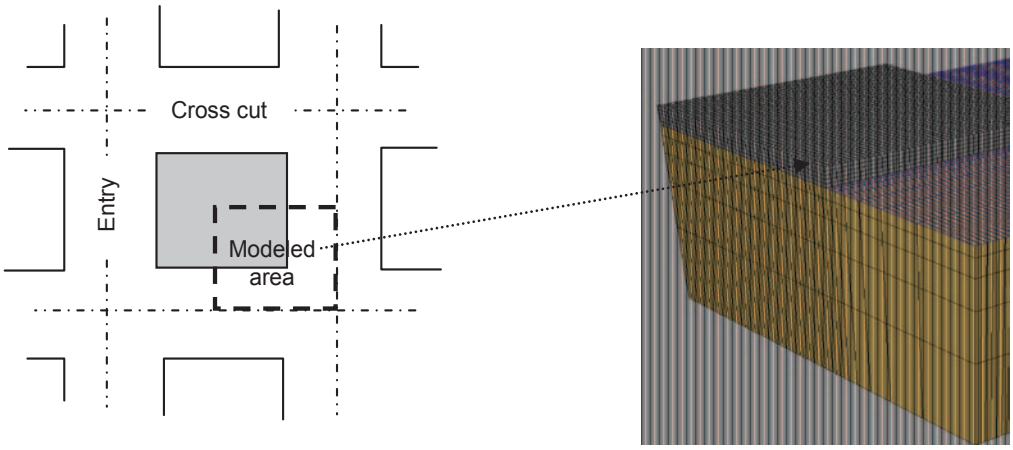

Figure 1. FLAC3D pillar model geometry as compared to room and pillar layout.

cohesion, friction angle, and dilation as function of strain. Using the cubic strength of coal (K = 6.2 MPa) as defined in Bieniawski (1984) pillar strength formula, and assuming that the mean internal friction angle of coal is 30°, the coal peak-cohesion is found to vary from 1.5 to 2.5 MPa depending on the cohesion drop rate during softening. There is no immediately available indicator for boundary values of cohesion drop rate for coal other than the studies by Badr (2004) which indicates a range of 35 to 100 MPa/ε_p (ε_p: plastic strain) as appropriate for calibration purposes. The residual cohesion is assumed to be a constant value of 5% of the average peak cohesion. Figure 2 shows the range of strain softening parameters used in the calibration studies.

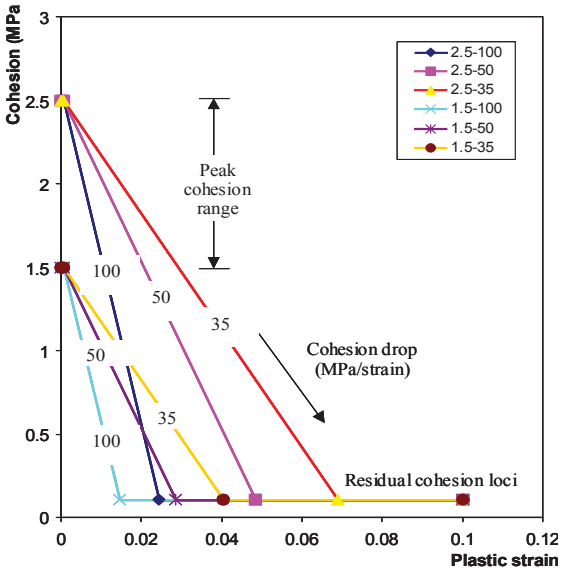

Figure 2. Range of cohesion and cohesion drop rate values used for the calibration simulations.

Calibration Against Commonly Used Pillar Strength Formulae

Calibration studies include four different width-height ratio pillars, specifically 1, 2, 3, and 4. For each w/h ratio, the numerical model is run with a particular combination of peak cohesion and cohesion drop rates, specified in Figure 2. The strength values as established from these models for different w/h ratios are plotted in Figure 3. These plots also include the strengths as predicted by the empirical pillar strength formulae. The plots indicate that the combination of peak cohesion of 2.2 MPa and cohesion drop rate of 50 MPa/ε_p is the best fit to the empirical strength formulae. This combination is used for the modeling of yielding chain pillars in the full longwall model described later in the paper.

Comparison of Calibration Against In Situ Pillar Test Results

There are only a few in situ complete stress–strain tests of pillars performed in the history of rock mechanics. In his tests, Wagner (1974) loaded coal pillars with constant displacements by a series of hydraulic jacks located in a horizontal slot cut at the pillar mid-height plane. This loading is similar to the loading boundary condition of the calibration model pillar described above. Three of the in situ test results published in Wagner's (1974) paper are used for the modeling methodology established above. Figure 4 shows the best fits of the model results to Wagner's in situ pillar complete stress-displacement curves. These plots result from using a cohesion – cohesion drop rate combination of 2.1 MPa and 20 MPa/ε_p. The cohesion drop rate in this case is smaller than that in the pillar strength formulae calibration case described previously. The difference is most likely due to the use of higher coal seam cube strength value of about 10.4 MPa in the Wagner's tests compared to 6.2 MPa in the pillar strength formulae.

Significance of Using Strain Softening as Opposed to Perfectly Plastic Model

To further investigate the effect of post-peak slope on pillar strength, additional models were run using classic Mohr-Coulomb (MC) and Mohr-Coulomb Strain Softening (MCSS) constitutive laws. The stress-strain curves obtained from eight different width height ratio models are given in Figure 5. As seen, the two forms of the MC constitutive law give significantly different pillar

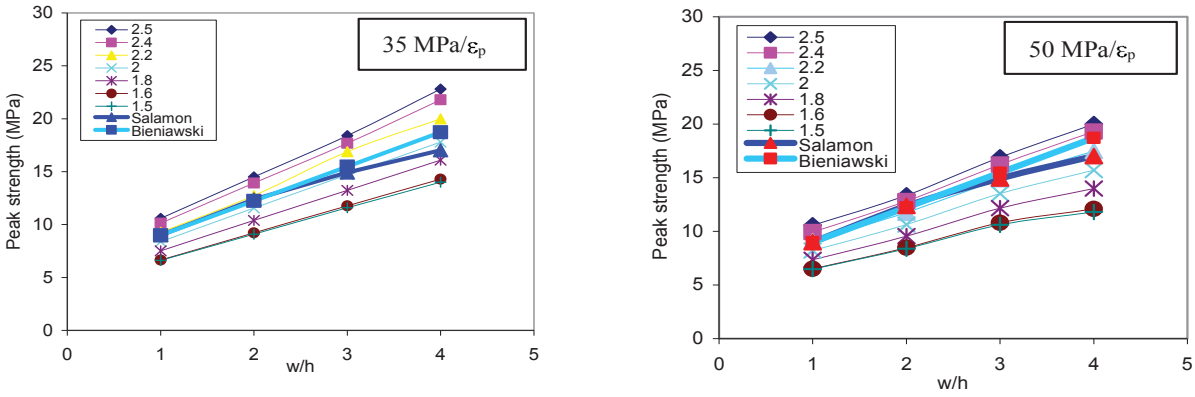

Figure 3. Comparison of modeled and empirical strength values.

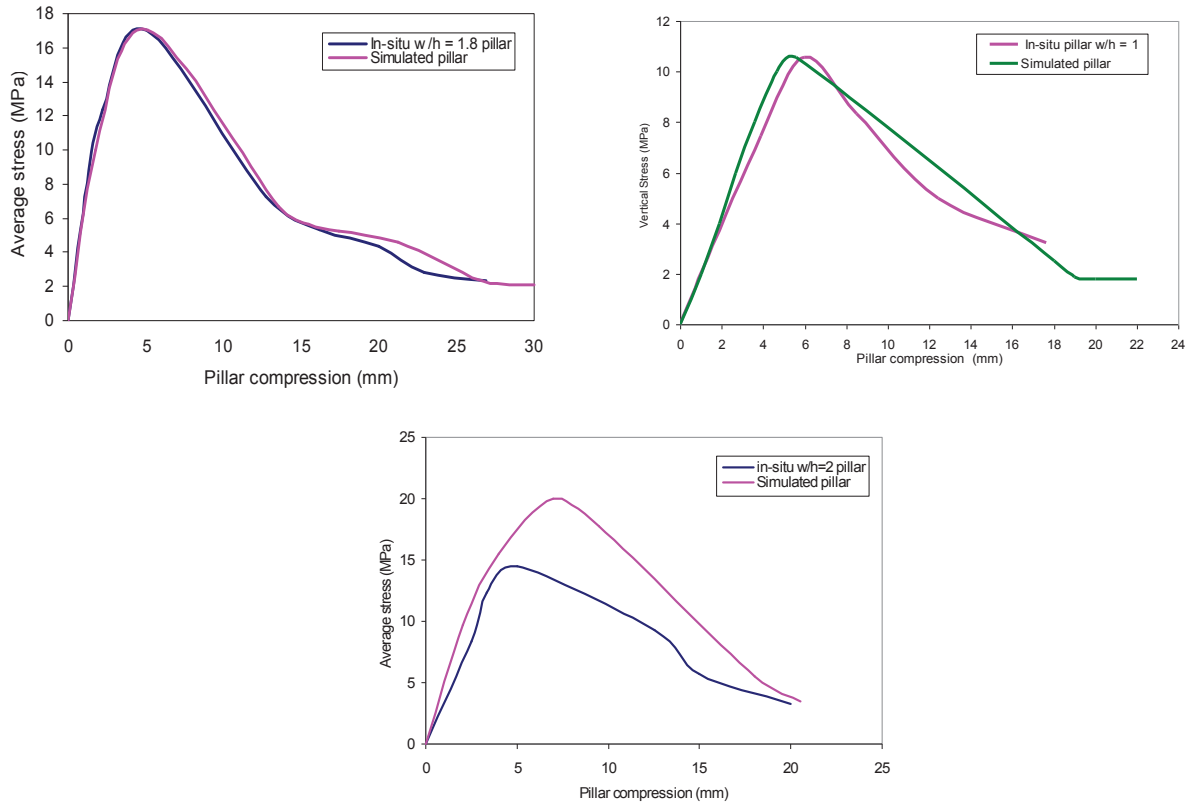

Figure 4. Comparison of modeled and Wagner's (1974) insitu pillar complete stress – displacement curves.

behavior. MC does not show softening and no clear strength can be defined for the pillars having width/height ratios of 3 or more. The MCSS pillars, on the other hand, have a downward slope and gradually transform to a non-softening mode as width/height ratio increases beyond 4.

Bump Proneness of Pillars as Function of Pillar Width/ Height Ratio

Another significant characteristic of the plots in Figure 5 is the appearance of a sudden drop in the softening post-peak curves as the pillar w/h ratio increases beyond 4. This sudden loss in resistance could potentially be interpreted as an "instability" or "bump", although it is not possible at this stage to prove this

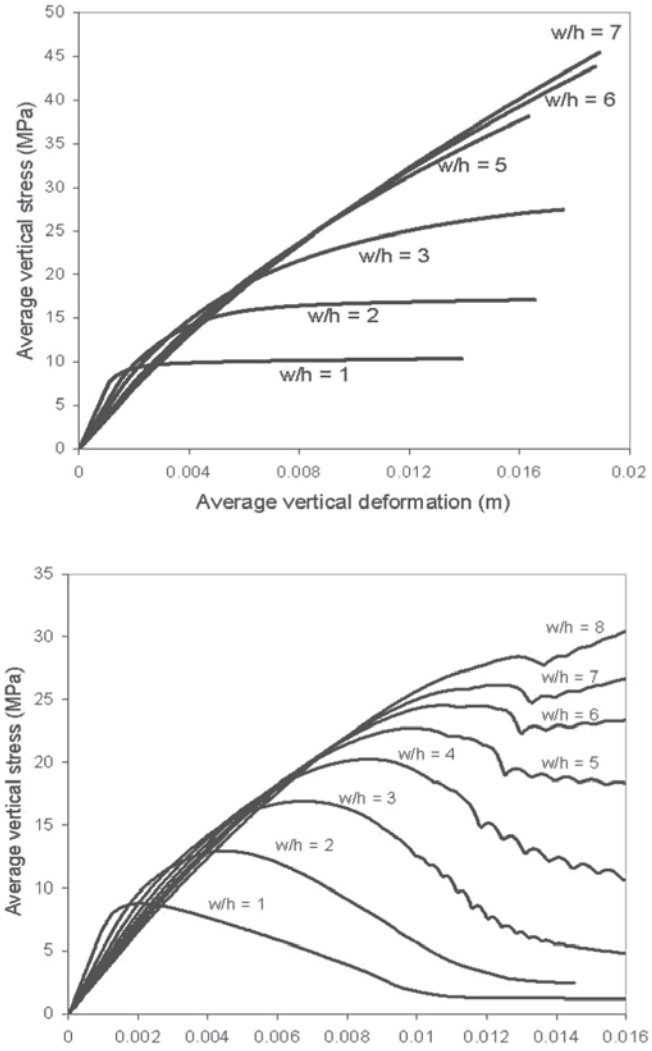

Figure 5. Comparison of complete pillar stress-strain curves obtained using Mohr-Coulomb (left) and Mohr-Coulomb Strain Softening (right) models.

contention against the field observations. However, the behavior is sufficiently interesting to warrant a closer look. Figure 6 shows the stress-displacement behavior experienced at each of the finite difference zones along the diagonal line placed from the pillar's corner edge to the pillar's center. The figure has results from one small and one large width-height ratio pillars having w/h=2 and w/h=6, respectively. All zones in the small w/h pillar experience relatively smooth softening while some of the zones of the large w/h ratio pillar show sharper and steeper reduction in load. These steep load reductions occur within about 1 to 1.4 m from the pillar corner. The curves relating to the zones further into the pillar appear smoother. Such distinguishable sharp stress drops are interpreted as signatures of instability, or a bump event, although unfortunately this supposition cannot be confirmed with certainty. The results from all of the w/h ratios models show that the pillars with width - height ratios 5, 6, 7, and 8 all show sudden stress drop in a region 1 to 1.4 m from the corner while the stress drop is smooth and continuous for width to height ratios 1, 2, and 3. The change over first appears on a smaller scale with w/h = 4 pillar. Assuming that the contention is valid, the implication is that the potential for bumping in coal pillar increase when their w/h ratio is greater than 4.

Full Longwall Model

Figure 7 shows the FLAC3D block used for the block used for the longwall modeling as well as the zoomed in details of the entries and chain pillars. The dark bands toward the center of the block are the regions of high mesh resolution where the two-entry gateroad is located. The symmetry conditions applied on the long sides of the block create a layout having one longwall panel on each side of the gateroad. The symmetry condition is also applied to the bottom of the block where the coal seam lies. The three layers of zones, each with 0.5 m height, located at the bottom of the block model the 3 m thick coal seam with the symmetry condition imposed to the bottom of the lowest layer. The block's height is 240 m but the mining depth can be set to a desired value by applying vertical stress tractions over the top plane. To save significant run times, only five evenly spaced cross cuts are placed in the gateroad.

With this geometry and boundary conditions, the model consists of two longwall panels, each on either side of the gateroad. The panel width and length of these longwalls are 240 m and 1,000 m, respectively. Vertical stresses added on the top of the block places the coal seam at 680 m depth. The 3 m thick coal seam is mined to its full height during extraction. The chain pillars consist of equally dimensioned small zones as depicted in the figure. The width of the pillars is 8 m and the entry and crosscut widths are both 6 m. The length of the pillars is 26 m. The dimensions of the finite difference zones comprising the pillars are 3 m, 1 m and 0.5 m in length, width and height, respectively. An interface plane is placed between the pillars and the roof and modeled as a Mohr-Coulomb material to account for pillar–roof contact conditions.

The model is brought to equilibrium elastically to achieve a lithostatic virgin stress state of 17 MPa at the seam level. Following the stress initialization, the coal seam is converted to strain softening material, wherein the strength parameters can be reduced as a function of plastic strain increment. Throughout all mining stages, the roof material remains elastic. The entry development is carried out by having the right entry leading the left entry by 9 m. Both entries advance with constant 3 m mining steps and the cross-cut is mined after the closest entry advances 9 m ahead. After each 3 m development cut, the model is brought to equilibrium before the next cut and the new stress and displacement are recorded.

Mining is carried out by first mining the right longwall panel and the left panel is mined after completion of mining in the right longwall. The longwall face advances initially with large cuts on one end, then gradually reducing to 3 m per cut within the 'core area'. After each longwall advance, the area behind the longwall face is converted to gob material.

A monitoring algorithm keeps a record of the stress and displacement histories for designated zones. The same algorithm also averages zone stress and displacement histories to develop pillar stress displacement curves.

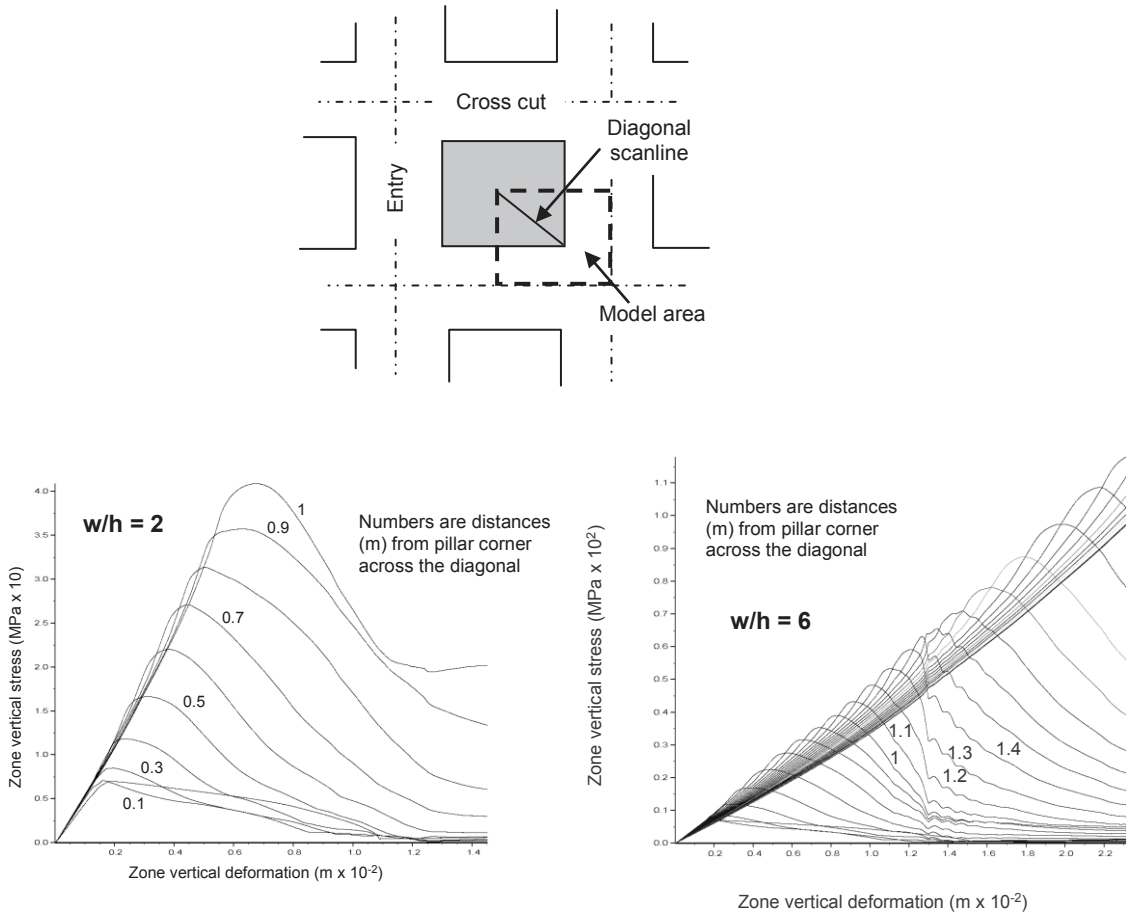

Figure 6. Stress-strain curves obtained at individual zones across the diagonal line at the pillar's center - plane.

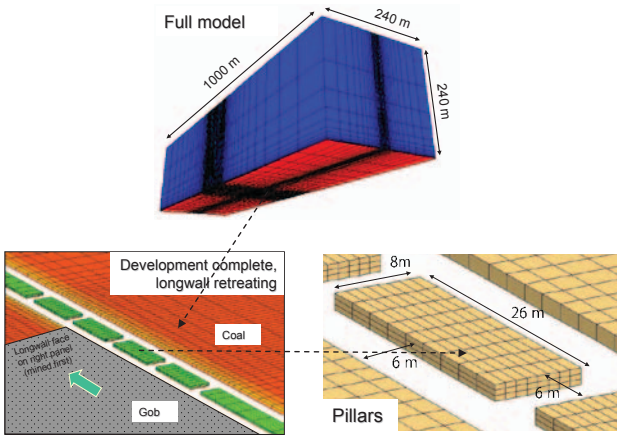

Figure 7. The longwall model used in the study showing FLAC3D model block (top), core area (left), and a chain pillar.

The coal seam has a peak cohesion of 2.2 MPa and a cohesion drop rate of 50 MPa/ε_p as determined from the parametric studies discussed earlier.

RESULTS OF LONGWALL MODELING

Development Mining

In the development mining stage, two entries and associated cross-cuts are introduced into the coal seam. The FLAC3D grid on the left in Figure 8 illustrates the method of measurement incorporated into the model for recording pillar responses as mining approaches and passes a selected pillar. The vertical stress and displacement affected on the pillar are captured at the zones along a scanline positioned across the pillar. As seen in the plots, Zone 8 at the edge of the pillar starts failing first as the leading entry approaches. This zone loses half of its strength as soon as it is exposed. On the lagging entry side, Zone 1 starts failing as the advancing development exposes it. Zones 2 and 7 experience some failure but at a smaller scale. The remainder of the zones experience less intense damage at the completion of development mining.

The average pillar stress along the scanline location resulted from the development mining is calculated by averaging the vertical stress of the zones along the scanline. In this particular case, the average stress reaches 22 MPa (3,191 psi) at the completion of the development (see Figure 9).

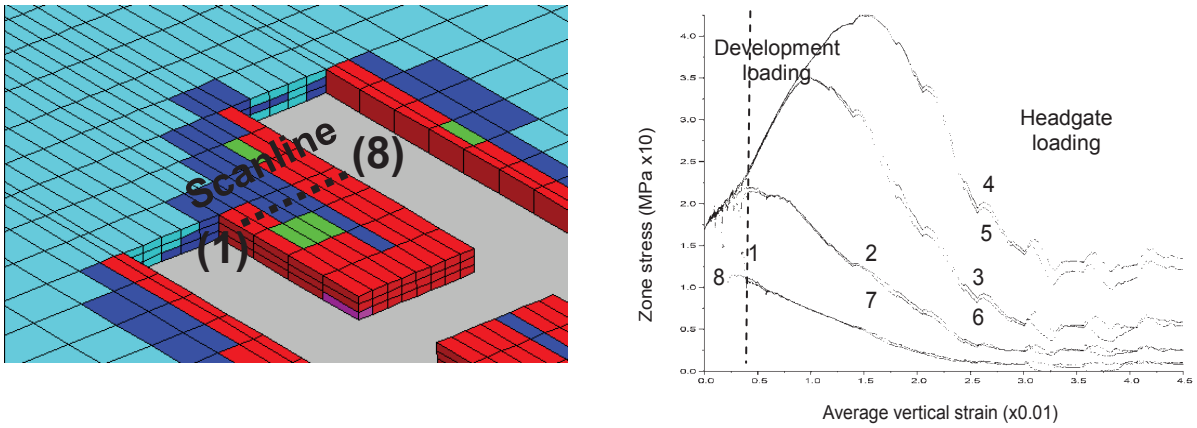

Figure 8. Development mining geometry (left) and pillar stresses recorded on the zones located along the scanline (right) during the development and headgate loading stages.

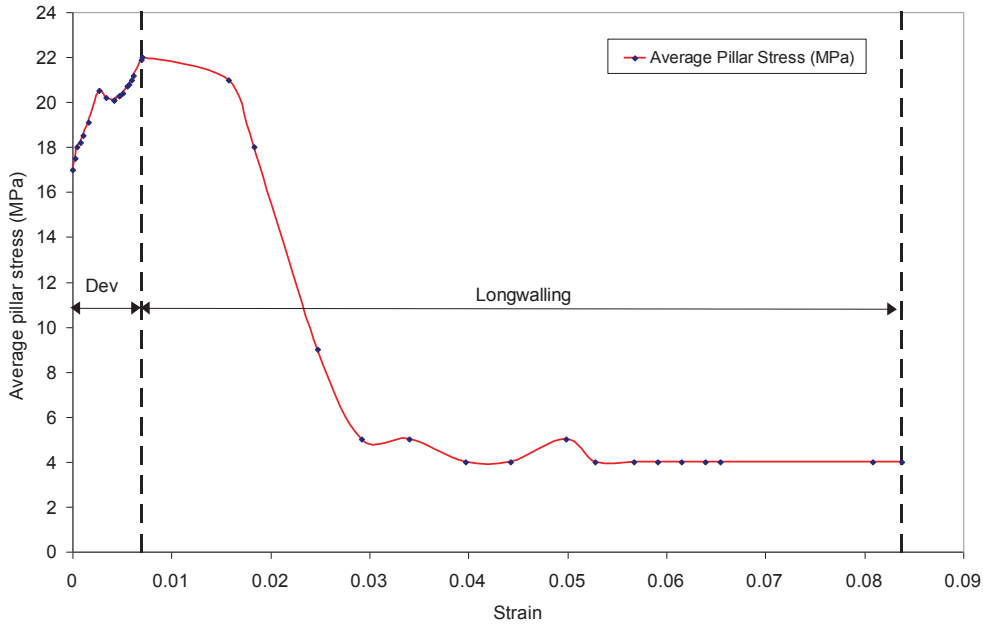

Figure 9. Overall stress-strain plot of the pillar in Figure 8 after completion of the first longwall.

Longwalling Stage

The longwall face advance starts initially as a 209 m (686 ft) long cut and then gradually reduces to 9 m cuts in the "core area". The chain pillars that remained in a hardening state at the completion of development start showing softening as the longwall face approaches (see headgate loading in Figure 8). The additional yielding starts when the longwall face is at about 150 m (492 ft) inby the pillar location. With the closer approach of the longwall, the failure propagates into the central zones in the pillar. Once the longwall passes the scanline position, all the zones on the scanline are at their residual strength. At this stage the central elements 4 and 5 have the highest and the two outmost zones, 1 and 8, have the lowest of residual strengths.

The overall pillar response to development and first longwall mining (headgate loading) is plotted in Figure 9 after averaging the zone stresses recorded along the scanline. The signatures of the development mining induced sidewall failures can be seen in the ascending part of the curve. The pillar's load exerting capacity reduces gradually down to 4 MPa (580 psi), which is substantial in terms of providing support to the roof strata. As such, the yielding chain pillar design in this particular case is considered successful under the conditions assumed for the model.

Gob Compaction Stresses

Figure 10 shows the gob stresses along the centerline of the first longwall at the completion of the first and second panels. The vertical stress build-up in the gob is 1.8 MPa after the first longwall and reaches 18 MPa (2,611 psi) after the completion of the second longwall, slightly higher than the vertical virgin stress magnitude of 17 MPa (2,466 psi).

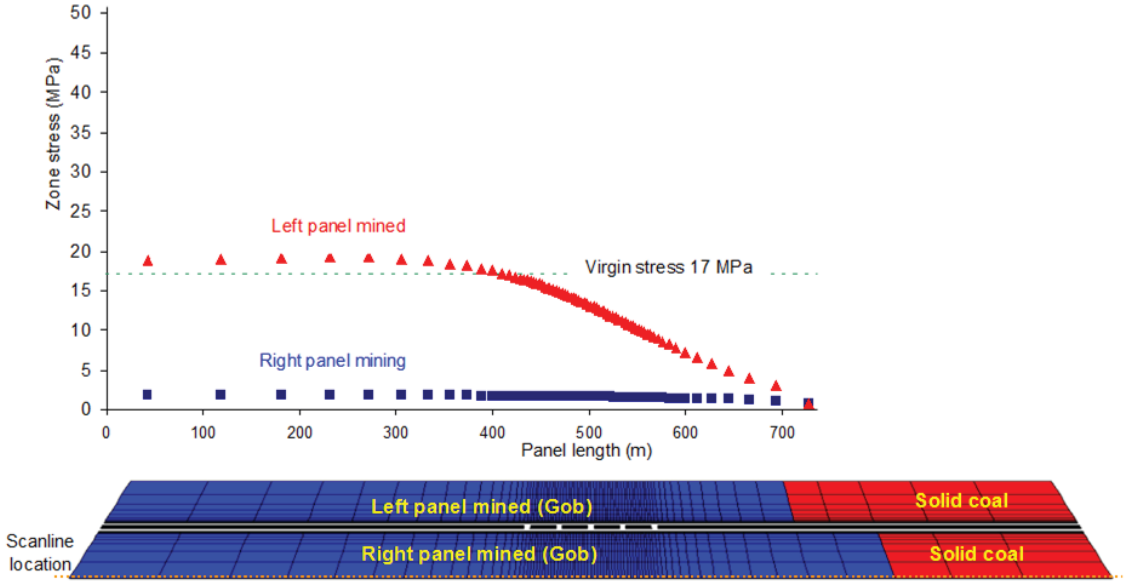

Figure 10. Gob and abutment stresses after completion of mining (right panel mined first).

Model Verification

The numerical model performance was verified with respect to in-situ stress measurements taken at a western U.S. longwall mine, for which the mine layouts are similar. In situ stress measurements were taken using Borehole Pressure Cells (BPCs) and the vertical closure data were obtained using borehole extensometers and roof to floor convergence meters installed in the entries and the cross-cuts. The pillar stress monitoring included three BPCs. Two of the BPCs were two meters from each side of the pillar, and the third was located at the center of the pillar. By averaging the BPC measurements, the relationship between averaged pillar stress and face position was determined and compared to corresponding results from the FLAC3D model.

The model predicted and in situ measured average vertical stresses are plotted as a function of the distance from the face in Figure 11. As depicted by this figure, the start of stress relief reported by BPCs is much earlier than that predicted by the model. However, the longwall position at the onset of maximum change in stress relief given by the model and instrumentation differs only by a few meters. The rates of the stress reduction given by the two methods as the longwall passes the measurement point also compare well.

CONCLUSION

The finite difference code FLAC3D appears to have significant potential for conducting detailed studies of several rock mechanics aspects of longwall coal mining at depth. The strain-softening constitutive model that comes with this code gives encouraging results in modeling of post-peak behavior of coal, in particular in the context of yielding coal pillars. Isolated pillar modeling studies emphasize the importance of post-peak material properties and width-height ratio in defining pillar strength and stability in post-peak state. With regard to yielding chain pillars, preliminary results show increased instability (potential bump proneness) as pillar width height ratio increases beyond 4.

The verification studies show reasonable comparison between the model results and in-situ measurements, suggesting a general validity of the methodology introduced. Further studies, such as back analyses of dynamic failures in coal mines, preferably by incorporating discrete element modeling, are needed to advance the methodology for conducting additionally realistic mechanistic analyses.

REFERENCES

Badr, S.A.E. (2004). Numerical Analysis of Coal Yield Pillars at Deep Longwall Mines. Ph.D. Thesis, Colorado School of Mines, Golden, CO.

Bieniawski, Z.T. (1984). Rock Mechanics Design in Mining and Tunneling. A.A. Balkema.

Itasca Consulting Group, Inc. (2003). FLAC3D – Fast Lagrangian Analysis of Continuum in Three Dimensions. User's Manual, Minneapolis, MN.

Salamon, M.D.G. (1967). A Study of the Strength of Coal Pillars. J. S. Afr. Min. Metall, *68*:55-67.

Wagner, H. (1974). Determination of the Complete Load-Deformation Characteristics of Coal Pillars. Proceedings of the 3rd Congress of International Society of Rock Mechanics, pp. 1076-1081.

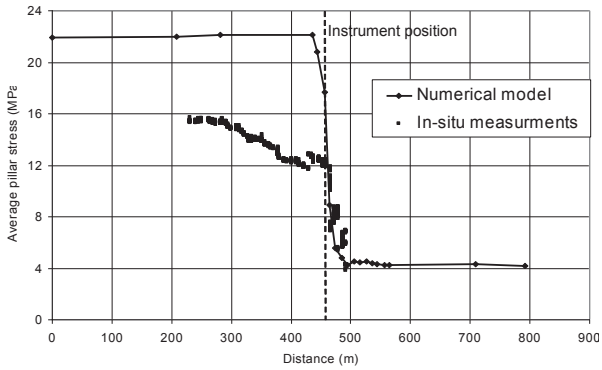

Figure 11. Modeled and in situ pillar responses to approaching longwall face.

Pillar Stability and Coal Bumps – Case Histories of Retreat Mining in the Thick Overburden and Multiple Seam Environment of Appalachia

David Newman, President
Appalachian Mining and Engineering, Inc.
Lexington, KY

ABSTRACT

Multiple seam underground coal mining under deep overburden is ubiquitous in Southern Appalachia. Many coal properties have from two to ten or more economically mineable coal seams with overburden ranging between 1,000 and 2,200 ft. Ground control engineering and mine planning may require incorporation of undermining and/or overmining where the geometry of the abandoned mine(s) is frequently incongruous with modern mining methods and layout. The overburden and interburden commonly consists of strong rock, sandstone, and sandy shales with a lesser percentage of weak shales, claystone, mudstone, and fireclay. Strong competent strata are beneficial to roof conditions on advance but frequently are detrimental to the ability to initiate caving.

The mine operator is confronted with two options, "pillar on advance" by driving panels with small pillar centers without secondary recovery or to develop panels with pillar centers amenable to full retreat mining. The "Christmas tree" retreat mining plan has many variations. It is popular because it provides multiple cuts from a single entry as portions of one or two pillars are mined simultaneously. Successful retreat mining in Appalachia requires a balance between the cut sequence, sizing of the panel pillars, barrier pillars, and "push-out" stump, a thorough understanding of the overburden geology, and consideration of the effect and the influence of abandoned mines in underlying or overlying seams.

INTRODUCTION

Room-and-pillar mining is the most commonly employed underground mining method in Southern Appalachia. The combination of highly variable geology and above drainage mining constrain the majority of coal reserves into irregularly shaped polygons that are not amenable to longwall mining. Room-and-pillar mining is easily adapted to rapidly changing geologic and mining conditions. The typical room-and-pillar panel is five to seven entries wide and 3,000 ft to 4,000 ft in length. A room-and-pillar panel is small in comparison to longwall panels that commonly range between 1,000 and 1,400 ft in width and 10,000 ft and 20,000 ft in length. Multiple room-and-pillar panels are developed from a submain and share a common "wrap-around" bleeder or are connected to a parallel submain that is used as a bleeder. A room-and-pillar panel is normally developed and retreated in one to three months. This is contrasted with six months to one year for gateroad development followed by an approximately equal time for longwall panel extraction. A commonality between room-and-pillar and longwall mining is that secondary recovery is important to ensuring high resource recovery and economic return. The recovery in a room-and-pillar panel is highly variable, ranging between partial and full pillar extraction. Partial extraction involves one or more cuts being taken from the pillar to leave a remnant that is capable of supporting the overburden stress. In partial extraction, a series of parallel cuts (slabbing) may also be taken along the panel perimeter. The objective is to remove coal while maintaining the roof stability. Roof falls may occur within the unsupported cuts, but the intent is to preserve the integrity of the entries and crosscuts as the panel is retreated.

Full pillar extraction is intended to promote roof caving and collapse behind rows of wood timbers or sets of hydraulic mobile roof supports (MRS). Although the use of MRS units was initially relegated to mining heights in excess of 7 to 8 ft, low seam units are available for mining heights to 3.50 ft. Full pillar recovery requires that sufficient cuts to be taken from the pillar so that the remnants left at the upper and lower end of the pillar crush out, enabling the roof to collapse. Parallel cuts into the panel perimeter are taken similar to that practiced in partial pillar extraction.

The danger associated with full pillar extraction is well known and documented in Mine Safety & Health Administration (MSHA) accident reports and by NIOSH researchers (Mark et al., 2009). MSHA has attempted to reduce the hazards through the implementation of NIOSH research (Mark and Zelanko, 2001, Hensley 1997, Mark and Chase, 1997). The key objectives include the following:

- use of MRS units where mining height permits,
- placement of longer bolts and/or supplementary roof support, (cable bolts) in the intersections of panels to be retreat mined,
- characterization of immediate roof stability using the CMRR,

- ❖ standardizing retreat panel, panel pillar, and barrier pillar design using ARMPS,
- ❖ designing the inby and outby remnant portions of the pillar to promote stability during pillar recovery, and
- ❖ requiring MSHA Technical Support review of ground control plans where retreat mining is to be practiced under greater than 1,000 ft of overburden.

Successful retreat mining under deep overburden is an orchestrated balance between multiple competing requirements. Frequently in Appalachia this balance is achieved in a multiple seam environment where undermining or overmining is present. Successful retreat mining layouts typically address the following issues:

Pillar centers must

- support the overburden stress on development and the front and side abutment stresses on retreat
- be an integer multiple of the MSHA approved cut depth (20 to 40 ft dependent upon roof conditions) so that the pillar can be cut through from one or two sides using the "Christmas tree" retreat mining plan. Longer cuts may be permitted on retreat where mine personnel do not pass inby.
- satisfy the reach limitations of continuous haulage systems

Barrier Pillars must

- be wide enough to support the side abutment stresses of a retreat mined panel(s) so that the panel is separated and isolated from adjacent panels
- be sufficiently wide to avoid bumps or out bursts of coal

Panels should

- be wide enough to promote caving
- be wide enough to permit one pillar row to be recovered during two shifts, so that a partially retreated pillar line is not left to stand during third shift
- be restricted in length to the head drive capacity for a single conveyor belt

A case history is presented to illustrate situations where this balance has been achieved and situations where a panel design was modified to avoid bumps.

CASE HISTORY

The case history is located in southwestern Virginia. The mine is a room-and-pillar operation that was developed from the outcrop. It operates under overburden ranging from the outcrop face-up to a maximum depth of 1,860 ft beneath a ridge line. The seam height varies between 30 to 37 in with an average of 34 in. The mining height ranges between 38 and 55 in with the objective of maintaining 48 in throughout the mine for equipment clearance. The case was initially presented (Newman, 2008) when the 2nd Right panel was retreat mined for 24 of 45 pillar rows or a distance of 2,064 of the 3,600 ft long panel without a roof fall. Although small "draw rock" falls occurred, there was no significant collapse or caving of the immediate or main roof.

The mine has had multiple owners that influenced the approach to mining. A nine entry main was driven from the outcrop with pillars initially spaced on 70 x 70 ft centers. A change to 90 ft x 90 ft centers was made once the mine had progressed under deep (1,700 ft) overburden and the first mine management group recognized that larger centers were needed. An eight to nine entry submain developed on 70 ft x 70 ft pillar centers was driven off the main. Two panels with pillars spaced on 70 ft x 80 ft centers were developed off the submain. The mine layout is shown in Figure 1. An enlarged section in Figure 2 illustrates the size of the inby and outby remnant pillar stumps that were left after pillar recovery. The immediate and main roof consists of competent rock. In the first 100 ft of rock above the seam, 84 ft are either sandstone or sandy shale.

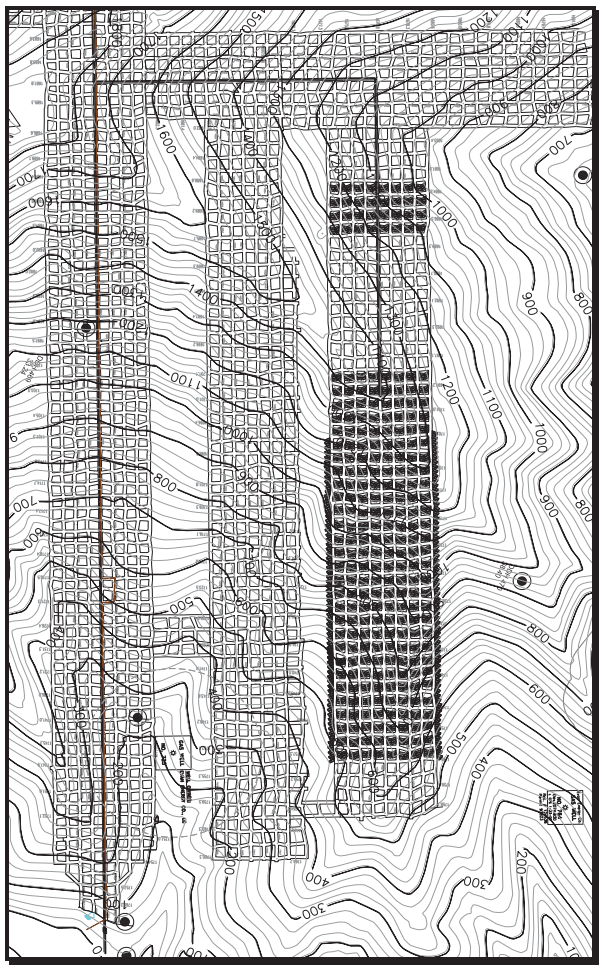

Figure 1. A portion of mine no. 2 illustrating the main, submain, 1st right, and 2nd right panels.

Based upon analytical and numerical analysis it was decided to abandon pillar recovery as the panel approached a ridgeline with 1,450 ft of overburden. Ten pillar rows were skipped and the panel was completed by mining four pillar rows adjacent to the panel mouth. This enabled submain development to clear the future 3rd Right panel that was driven parallel to the 2nd Right panel.

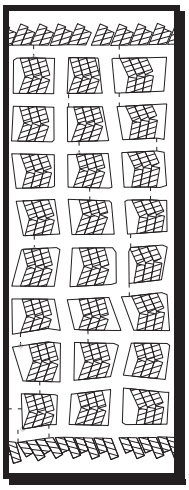

Figure 2. View of inby and outby pillar remnants left after retreat mining.

The most important conclusion was that a potential large collapse, coal bump, and the resulting airbast from either was averted by discontinuing retreat mining in the 2nd Right panel. Remnant stumps created from retreat mining are assumed to have provided the internal support to prevent roof caving in the gob. However, the failure of one or more of the remnant stumps could have initiated a large scale main roof collapse. Similarly, if retreat mining continued under the ridgeline at 1,450 ft of overburden, a bump in the active pillar line could have been initiated by the front abutment pressure from the hanging gob.

The experiences of the 2nd Right panel were incorporated into a revised pillar plan to be used in another area of the mine under high overburden. The initial panel of the new area, 1st Left is located adjacent to a set of mains where the barrier between the first panel and mains had been driven prior to the ground control knowledge obtained from the 2nd Right panel study. The 1st Left panel is shown in Figure 3. The initial change between the previous pillar plan and that used on the 1st Left panel is that the pillar remnant size was decreased in order to promote crushing and roof caving.

The concern was whether the 90 to 95 ft wide barrier pillar separating the 1st Left panel from the mains would be adequate to prevent side abutment pressures from transferring abutment stress onto pillars in the mains. As can be seen in Figure 3, the panel passes adjacent to a ridge where the overburden ranges from 1,840 ft close to the panel mouth and decreases to 1,300 ft at the head end of the panel. A core hole located near the bleeder showed a 67 ft thick interval of sandstone and sandy shale as the immediate/ main roof. A second core hole located immediately to the north of the submain had 80 ft of sandstone and sandy shale above the coal. The panel was developed as a seven entry system on 70 x 90 ft centers with a 48 in +/- 3.45 in mining height. The adequacy of the barrier pillar was addressed using ARMPS and four LaModel scenarios. ARMPS indicated that the panel pillars were adequate with a minimum 1.72 development stability factor under the maximum overburden.

The LaModel scenarios were run because ARMPS does not have a situation comparable to the 1st Left panel geometry where there

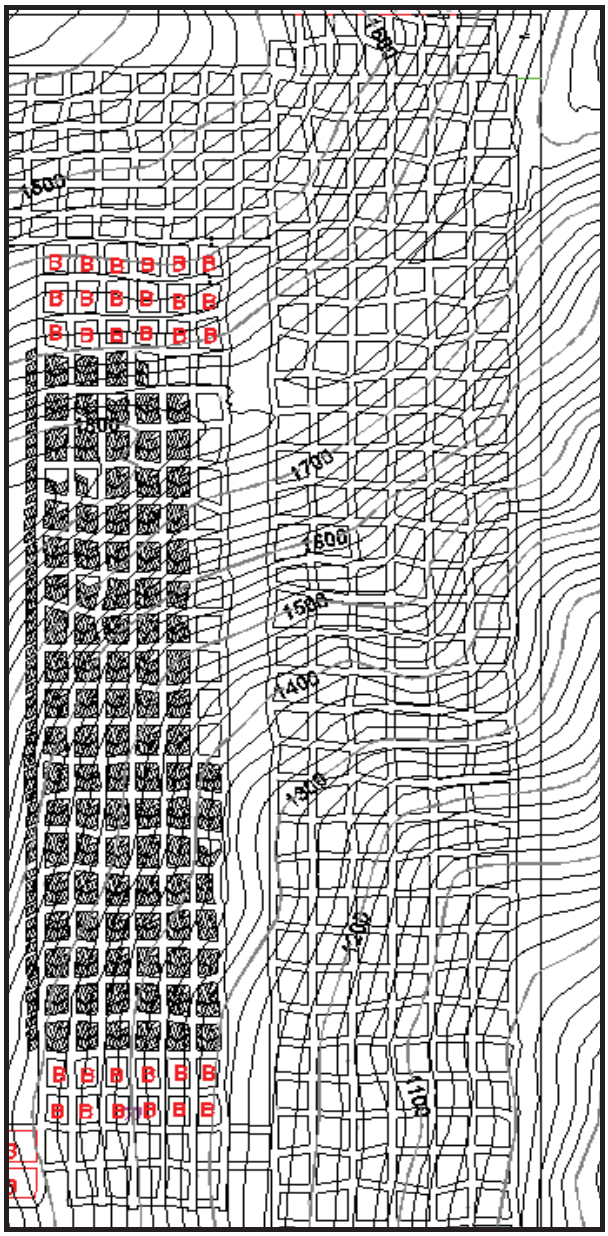

Figure 3. 1st left panel against the mains.

is no adjacent gob and a set of mains are present in lieu of solid coal. If it was determined that if the barrier pillar was insufficient to protect the mains, the pillar row against the barrier would be left as a bleeder pillar row. The LaModel scenarios were:

- No caving in the 1st Left panel, bleeder row taken,
- No caving in the 1st Left panel, bleeder row not taken,
- Caving in the 1st Left panel, bleeder row taken, and
- Caving in the 1st Left panel, bleeder row not taken.

The focus of the LaModel runs was to determine the condition of the barrier pillar with respect to rib sloughing and stress concentration. Convergence and deterioration of the mains is a concern if the barrier pillar was insufficient and side abutment stresses were transferred onto the mains. The LaModel material

properties were identical to those used in the earlier study. No convergence measurements were taken during the prior study on the 2nd Right panel. This was due to the short time frame in which a decision was required to continue or abandon pillar recovery. Consequently, for the 1st Left panel study, pogo stick convergence meters were placed in the mains in the entry adjacent to the barrier pillar. Concurrent with the pogo stick readings, observations of pillar behavior (sloughing, spalling) were recorded.

As anticipated the "no caving" LaModel scenarios showed spalling on the 1st Left side of the barrier pillar. Because the element size was 5 ft, the spalling ranged between 5 and 10 ft. The decision was to take all the pillars and see whether the immediate roof would cave. If it did cave prior to the 1,400 ft overburden contour, the remainder of the bleeder pillars would be taken, if no caving occurred the bleeder row would be left.

No caving, with the exception of minor "draw rock" falls occurred in the 1st Left Panel. At the time the active pillar line reached the 1,400 ft contour, looking into the gob from the bleeder line and from the pillar line, isolated blocks of rock had fallen but the remainder of the gob was open. The immediate roof was observed to be sagging. No floor heave occurred on the section.

The decision was made to leave the bleeder row and retreat mine the remainder of the panel. All pillars were recovered cleanly, with the exception of two pillars in the seventh row from the panel mouth. The pillar line was typically in very good condition. Active and continual pillar spalling occurred on the outby pillar row without rib rolls or violent ejection of coal from the rib. Timber posts were used because the mining height is too low for MRS units.

During the retreat mining of the 1st Left panel, plans were devised for the mining of the 2nd Left panel. The 2nd Left Panel, shown in Figure 4, lies beneath a ridge top under 1,860 ft of overburden. The barrier pillar width was the most significant concern followed by the adequacy of the pillar centers under the higher overburden. The overburden ranged from 1,600 ft to 1,860 ft. Similar to the 1st Left panel, the analysis focused on initial ARMPS runs for the barrier and panel pillar stability followed by LaModel scenarios to decide on a barrier pillar width.

The ARMPS runs, shown in Table 1, were conducted using the same 70 x 90 ft pillar centers, 4 ft average mining height, and a 165 ft wide barrier pillar with a 31 ft slab cut taken from the 2nd Left panel. The 1st Left panel gob width, including the slab cut, is 465 ft. It is apparent that the ARMPS stability factors exceed the 1.50 threshold for panel pillars during retreat mining and the 2.00 criterion for barrier pillars in bump prone ground. The presence of thick sandstone roof and the bump/bounce experience of another operator in the same seam led to the assessment of being bump prone.

The LaModel runs were focused on confirming that the barrier pillar separating the 1st Left and 2nd Left panels is sufficient to prevent side abutment stress transfer from the 1st Left panel onto the development pillars in the 2nd Left panel. No difference observed between the stress distribution using a 125 or a 150 ft wide barrier pillar to separate the panels. The conclusion was that the 125 ft (134 ft in practice with actual slab cuts taken from both sides) was effective in isolating the adjacent panels. The LaModel

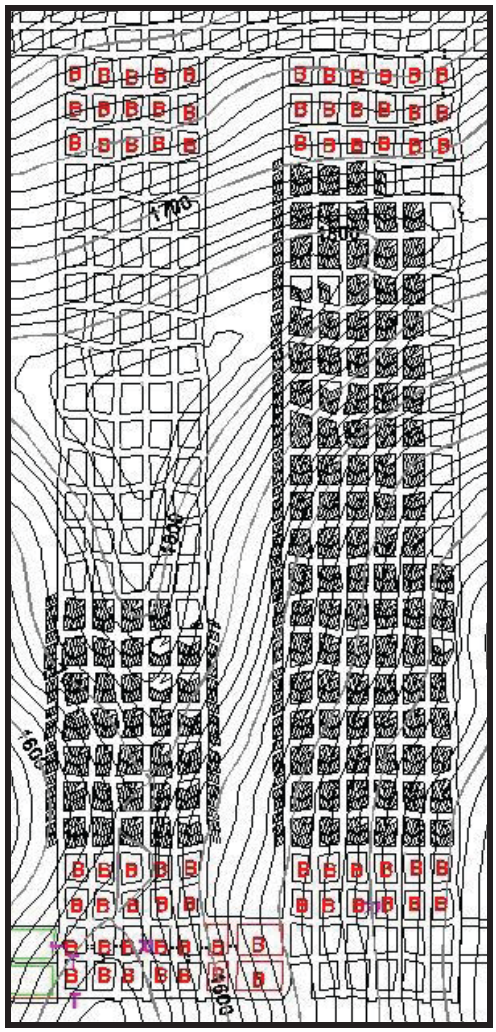

Figure 4. 2nd left panel.

runs confirmed the competency of the panel pillars. Although the front abutment stress on the active pillar row is high and the pillar strain safety factors low, pillars in the outby row had stable cores. The conclusion was that a balance had been achieved between isolating adjacent panels and having panel pillars that are both stable and amenable to retreat mining with the MSHA approved cut depth.

A second series of LaModel runs were done to duplicate the retreat cut sequence. The objectives are to examine changes in pillar stress distribution as the individual cuts are taken. This enables the determination of which cut or cuts are taken into more highly stressed portions of the pillars. These cuts are assumed to be more bounce/bump prone and are compared with the observations of the continuous miner operators.

The ground conditions and observations during development and retreat mining of the 2nd Left Panel are;

- Under the ridge top, pillar spalling was observed on development.

Table 1. ARMPS Stability Factors for the 2nd Left Panel.

Overburden Depth	Stability Factors			
	Panel Pillars		Barrier Pillar	
(feet)	Development	Retreat	Development	Retreat
1,600	2.61	1.88	4.47	4.16
1,650	2.52	1.83	4.33	4.03
1,700	2.48	1.81	4.18	3.89
1,750	2.45	1.79	4.03	3.75
1,800	2.41	1.77	3.90	3.63
1,850	2.39	1.76	3.77	3.51

- The sandstone roof did not fall as the panel was retreated toward the ridge top. However, once the panel was retreated under the highest overburden, roof falls occurred periodically. A large fall would occur after two to three pillar rows were recovered. The amount of rib spalling would increase as the rows were retreated until the roof fall, after which there would be an absence of pillar spalling and the sequence of increased spalling activity culminating in a large fall would be repeated. The conclusion is that the sandstone cantilevered into the gob and eventually failed. The rib spalling and pillar behavior is characterized by coal ejected from the rib and 1 to 2 ft wide blocks periodically rolling off the rib. The rib spalling was continual during retreat mining. The timber supports bowed in response to roof deformation but were not overrun by a roof fall.
- When mining in the vicinity of the "push-out" stump the coal was crushed and was loaded out rather than cut by the continuous miner.
- Once the roof falls began occurring in the 2nd Left panel mine personnel checking ventilation air in the bleeders observed roof falls in the 1st Left panel. The extent of the roof falls is unknown since the view into the gob from the bleeder entries was obscured by the falls.

A second series of LaModel runs were carried out once the roof falls began occurring in the 2nd Left and in 1st Left panels. The objectives were to ensure that the barrier pillar was adequate to handle the abutment stress, and that the panel pillars were adequate for retreat mining under the higher overburden. The purpose of the modeling was to replicate the conditions observed underground. The pillar strain safety factors associated with the geometry of Figure 4 are shown in Figure 5.

The model shows that although the active pillar line has low strain safety factors, the outby pillar row is stable with rib spalling anticipated. This mimics the underground observations by mine personnel. The effect of the ridge top on the pillars is clearly seen in the strain safety factor distribution in the center of the 2nd Left Panel.

CONCLUSIONS

Retreat mining under high overburden is unique to Southern Appalachia and isolated areas of the Western U.S. It is a balance between isolating individual panels between barrier pillars and ensuring that the panel pillars are large enough to withstand the front abutment stress. The panel pillars should be integer multiples of the approved continuous mine cut depth to be efficient during development and to ensure that irregular remnants are not left during pillar recovery.

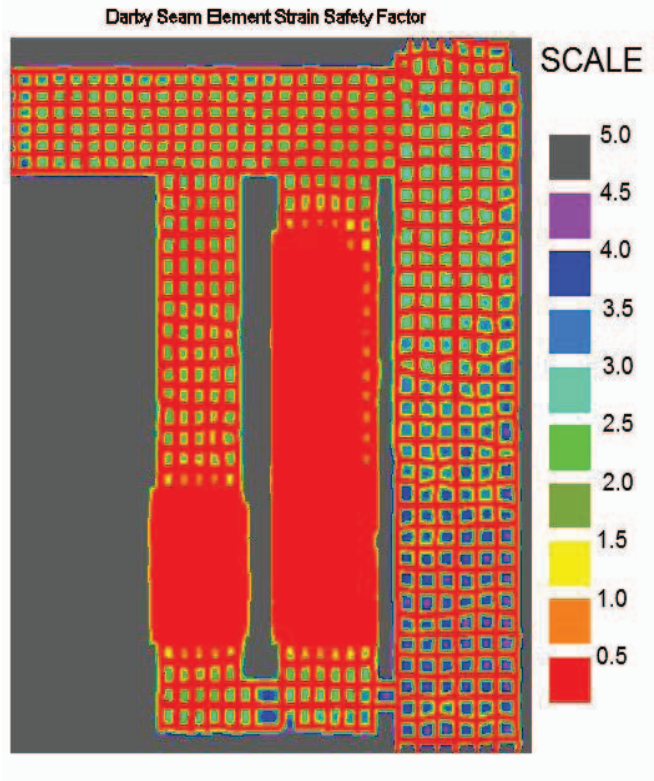

Figure 5. Strain based safety factors determined by LaMODEL.

The case history presented in this paper documents that sequence of events leading from a non-caving situation under deep overburden and competent roof to a planned sequence of development and retreat mining. Changes in the final stump dimensions likely permitted the roof to cave in the 1st Left and 2nd Left panels where the larger inby and outby stumps in the earlier study on the 2nd Right panel supported the roof and inhibited caving. Retreat mining under high overburden is more difficult and the caving less predictable with competent sandstone and sandy shale roof that does not cave as readily as shale.

REFERENCES

Heasley, K.A. (1997). A New Laminated Overburden Model for Coal Mine Design. Proceedings of the New technology for Ground Control in Retreat Mining, National Institute for Occupational Safety and Health, DHHS (NIOSH) Publication No. 97-122, IC 9446, pp. 60-73

Mark, C., Pappas, D.M. and Barczak, T.M. (2009). Current Trends in Reducing Groundfall Accidents in U.S, Coal Mines. SME preprint 09-69, Society for Mining, Metallurgy, and Exploration, Inc.

Mark, C. and Zelanko, J.C. (2001). Sizing of Final Stumps for Safer Pillar Extraction. Proceedings of the 20th International Conference on Ground Control in Mining, Morgantown, WV, pp. 59-66.

Mark, C. and Chase, F.E. (1997). Analysis of Retreat Mining Pillar Stability. Proceedings of the New technology for Ground Control in Retreat Mining, National Institute for Occupational Safety and Health, DHHS (NIOSH) Publication No. 97-122, IC 9446, pp. 17-34.

Newman, D.A. (2008). Coal Mine Bumps: Case Histories of Analysis and Avoidance Proceedings of the 27th International Conference on Ground Control in Mining, Morgantown, WV, pp. 1-6.

Spatial Variability of Coal Strength and Its Implications for Pillar Design

Murali M. M Gadde, Senior Manager, R&D
Peabody Energy Co.
St. Louis, MO

ABSTRACT

Over the past four decades, much research has been done on the mechanics and design of underground coal mine pillars. Significant insights into factors governing pillar strength and loading were developed during this period. Well-tested empirical and semi-empirical approaches have been developed by all major coal producing countries to size pillars while considering specific local and regional geologies. Because of this, desirably, today's empirical research on pillar design has a narrow focus with the principal aim of refining the standardized pillar design methodology that the industry in each country has adopted. At the same time, new frontiers are being explored with the use of advanced numerical modeling methodologies for pillar design. Despite these advancements, it is not uncommon that such fundamental issues as the validity of using compressive strength of coal for pillar design spur intense debate within the research community. There appears to be two principal reasons for the controversy over the use of compressive strength for pillar design: significant variability seen in the lab tests and ill-developed procedures to compute the in-situ strength. Both these concerns are highly valid as numerous empirical analyses have demonstrated in the past. In this paper, however, it will show that the variability seen in the laboratory compressive strength of coal is not such a big factor in estimating the "average" behavior of a coal pillar as it was thought in the past. Using some lab testing data from a coal mine, it will be shown that the uniaxial compressive strength variability noticed on a pillar-scale is no different from that observed on the mine-scale. Similarly, with the use of numerical modeling it will be demonstrated that accounting for such "local" variability of strength within a coal pillar will lead to similar estimate of pillar strength as that obtained from the average laboratory strength. With the help of some failed and stable pillar cases from the same mine, it will also be shown that significant differences exist between the seam-specific in-situ strength and the "national average" established in the past based on a larger database of case histories. Finally, the pillar cases from the studied mine also demonstrate that the popular Gaddy's equation to estimate in-situ strength of coal is a reasonable first approximation and provides a decent explanation of the conditions noticed at the mine.

INTRODUCTION

The most common approach to design underground coal mine pillars involves two major components: estimation of the average load and computing the strength. In popular empirical methods, the two principal design components are normally linked through a stability or safety factor (SF). All major coal producing countries across the globe have developed databases of stable and unstable pillar performances from local mines and have established desirable performance criteria in terms of the pillar stability factor. Despite its shortcomings, this simple empirical approach has served its purpose across the globe over the years. Today, empirical methods have matured to a stage where very little debate occurs on the overall validity of the popular models in each country. Any new research in these countries appears to focus on refining the popular model than to revamp the whole design approach. Such standardization is highly desirable in certain ways as it minimizes the confusion, which would occur if multiple pillar design models are used based on individual preferences. Further, the standard models provide a common "language" to communicate pillar design results.

When the popular models across the globe are examined closely, for pillar strength estimation two different approaches are in vogue (Mark and Barton, 1996). In the first approach, the seam-specific strength is treated as an independent variable and is included via laboratory uniaxial or triaxial compressive strength (e.g., Sheorey, 1992; Wilson, 1983). The second group considers lab strength as an insignificant factor in the overall pillar behavior and thus ignores it in the design. These later methods, however, include an "average strength" for the entire range of coal mines included in the base database. The popular Salamon and Munro formula (1967), Analysis of Longwall Pillar Stability (ALPS) (Mark, 1992) and Analysis of Retreat Mining Pillar Stability (ARMPS) (Mark and Chase, 1997) fall into this second group. While intuitively it appears that the seam-specific strength must have some influence on the pillar behavior, the following factors are often cited as the reasons for ignoring its effect (Mark and Barton, 1996):

- spatial variability of strength;
- difficulties in sample collection, preparation and testing;
- inaccuracies in estimating the size effect.

When the laboratory compressive strength data from a typical coal mine is examined, it is normal to see very high spatial variability both vertically and horizontally. It is not uncommon to see standard deviations comparable in magnitude to the average value of the strength or higher. Because of the differing depositional environments at the time of coal formation, it is also common to see several "bands" of varying properties from roof to floor (Unrug et al., 1985). These "bands" could be comprised of coal of different quality and strength or extraneous materials like shale. Therefore, the general contention is that when such variability in compressive strength exists both laterally and vertically in the coal seam, which statistic of compressive strength (e.g., mean, minimum or some other percentile value) should be used for pillar design? In fact Mark and Barton (1996) summarized one prevailing view by saying, "Some have held that these difficulties [the three mentioned above], and the resulting high variability in results, are enough to largely invalidate laboratory testing." This is a valid problem and will be discussed extensively in this paper.

Coal is notorious for the difficulties it poses for sample collection and laboratory preparation. Because of the high density of cleating, coal samples typically contain numerous small discontinuities even at the laboratory scale. Consequently, sample preparation for lab testing is far from perfect in a majority of cases. Such "imperfect" specimen testing obviously adds to the high degree of variability seen in the lab results. Even though this problem may be minimized by taking extreme care in sample collection and preparation, in reality, handling imperfections will remain. In this context, it may be mentioned that while the quality of coal test specimens has attracted greater attention, several other rocks also pose similar difficulties for lab testing. For example, the weak laminated "stackrock" and underclay floors of the Illinois Basin are well known for the difficulties in sample collection and preparation. Despite the imperfect sampling and testing, the critical question to ask from the pillar design viewpoint is, will this factor cause any more variability in the lab compressive strengths than would be seen due to the inherent material variability on a pillar-scale? Within the knowledge of the authors, no such systematic research had ever been conducted to separate the strength variability into natural and testing factors. However, when data from in-situ testing is examined, similar variability in strength is seen as is normally noticed with laboratory compressive strength (e.g., Unrug et al., 1985; Unrug and Turner, 2005; Unrug et al., 2009). The in-situ tests are supposed to minimize the sampling and preparation problems and thus are perhaps more reflective of the natural material variability (Unrug et al., 2009).

Estimating the in-situ strength from laboratory samples is a highly complex problem. Despite a significant pool of research on this topic, difficulties remain. There is some evidence to show that the scale-effects of different coal seams could be different depending on the seam structure (Mark and Barton, 1996). Therefore, the popular Gaddy's (1956) equation may not work well in every situation. Research, however, shows that unlike coal's laboratory compressive strength, its in-situ counterpart may fall within a narrow range of values between 780 and 1,070 psi (Mark and Barton, 1996). The case histories presented later in this paper will demonstrate that if site-specific experience is available, then reliable approximations to in-situ strength could be made. Further, the case histories to be discussed will also show that the Gaddy's equation provided a reasonable first-approximation to the in-situ strength at the studied mine.

SPATIAL CORRELATION LENGTH

As the discussions above indicate, one of the contentious issues in coal pillar design is the use of laboratory compressive strength. It was also mentioned that the very high spatial variability displayed by the strength is one of the main reasons for rejecting its value in site-specific pillar design. In this section, a systematic attempt will be made to fully characterize the spatial variability of coal strength using some standard parameters borrowed from the random field theory (VanMarcke, 1984). Later, the effect of spatial variability on coal pillar strength will be examined using numerical modeling. In order to completely characterize the spatial variability of geotechnical materials (soils and rocks), three parameters are needed (VanMarcke, 1984):

- the mean, μ;
- the standard deviation, σ;
- the spatial correlation length or scale of fluctuation, δ.

In the mainstream coal mine ground control publications, only the first two factors are normally used for describing the variability. It is the authors' opinion that the incomplete description of the spatial variability of rock properties and the consequent inadequate analysis has in someway contributed to the apparent underestimation of the value of site-specific coal strength for pillar design.

When used in conjunction with the mean (μ), the standard deviation (σ) provides an idea on the degree to which the actual values differ from the average. Estimating the mean and standard deviation from a suite of uniaxial compressive strength (UCS) tests, however, will have limited value with the empirical pillar design models. Even if the pillar strength equation has a provision to include the UCS, it is not always clear whether the mean or the minimum or some other percentile value be substituted in its place. If the minimum laboratory strength value is significantly lower than the average, then one might think that using the minimum is "safer" thus resulting in conservative pillar sizing. To overcome this limitation with the deterministic approach, it is possible to apply probabilistic models to design coal pillars. In these random models, the standard deviation can be used along with the mean to generate a distribution function of stability factors, which eventually can be used to compute the probability of pillar failure. While the probabilistic models are one-step ahead in including the strength variability, they also fall short in reflecting the reality. For each of the individual probabilistic simulations, it is necessary to assume that the coal strength across the entire pillar is the same. In essence, whether it is a deterministic or a probabilistic model, use of only the mean and standard deviation values with empirical pillar strength equations will not reflect the reality.

In order to realistically include the true spatial variability of coal strength in the analysis, another random variable is needed. This additional parameter is called the "spatial correlation length" or "scale of fluctuation" (VanMarcke, 1984). Using this parameter, it is possible to compute the distance over which compressive strength shows strong correlation in horizontal or vertical direction (Wickremesinghe, 1989). If two points are separated by a distance less than the spatial correlation length, then the compressive

strength at those two points are correlated and will be on the same side of the mean (either higher or lower). Similarly if the points are spaced more than the scale of fluctuation, then the strength at the two points are uncorrelated and could be considered as random values. A low value of spatial correlation length means very high variability of the property about the mean and a high value indicates lower spatial variability. In other words, a large value of spatial correlation length will imply a smoothly varying field while a smaller value, a ragged field (Griffiths and Fenton, 2001).

Several approaches are available to calculate the spatial correlation length from field data of a chosen material property (VanMarcke, 1984; Wickremesinghe, 1989; Fenton, 1990). For this paper, however, the procedure suggested by Weickremesinghe (1989) has been adopted for its simplicity. The following discussion is a summary reproduction of the procedure suggested in Wickremesinghe's Ph.D. dissertation. Because of the practical constraints that restrict the number of samples that could be tested in a given volume of coal seam, and also the physical requirement of the test to have a coal sample of finite volume, some local averaging of properties occur in reality. Therefore, the suggested procedure to estimate the spatial correlation length is in terms of the so called "variance function", which accounts for the inevitable local averaging that occurs in practice.

Let us assume that there are N number of tests conducted in a finite volume (say, a coal pillar). Let us also assume that the N tests are conducted at an average S spacing. In order to compute δ, the data are first considered in pairs (n = 2) and a new series of data is created comprising the moving average of two tests considered at a time. Similarly, the length of averaging (Z_2) for this set is computed, which will be equal to the average spacing of the data points. For this new series, the standard deviation (σ_2) is also calculated. It may be noted that σ_2 will be smaller in magnitude as compared to the standard deviation (σ_1) of the original data because of the spatial averaging. The same procedure is repeated for n = 3, where the moving average of three adjacent points is used to generate a new series. The corresponding standard deviation (σ_3) is calculated along with the spacing, Z_3, which is equal to twice the average spacing between tests. This process is repeated for n = 4, 5, 6,……, N. For each n, the variance function, $\Gamma^2(Z_n)$ is calculated as

$$\Gamma^2(Z_n) = \frac{\sigma_n^2}{\sigma_1^2} \tag{1}$$

where σ_n^2 is the variance of the derived moving average series of degree n and σ_1^2 is the variance of the original data. If the average spacing of the original data is S, then Z_n in equation (1) is equal to (n – 1) S. When the variance function $\Gamma^2(Z_n)$ is plotted against different lag distances, Z, a decaying function like that in Figure 1 is generated (Wickremesinghe, 1989). For large values of Z (very large n), the variance function will become inversely proportional to Z and can be expressed as,

$$\Gamma^2(Z) = \frac{\delta}{Z} \tag{2}$$

or

$$\Gamma^2(Z).Z = \delta \tag{3}$$

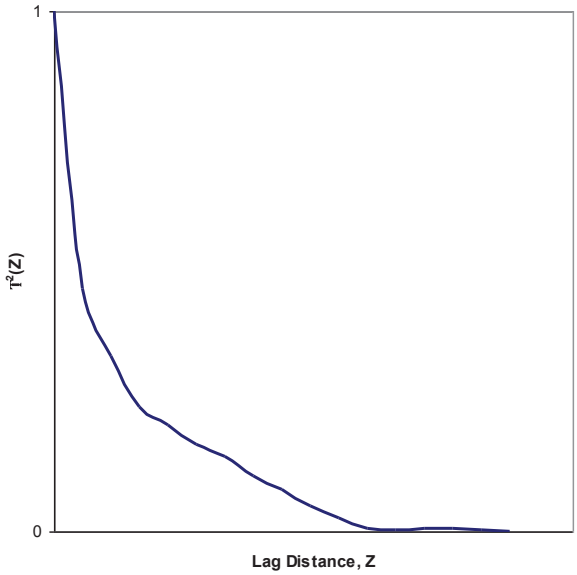

Figure 1. Variance function plotted against lag distance.

VanMarcke (1984) suggested that from a plot of $\Gamma^2(Z_n)$ versus Z, obtain the value of $\Gamma^2(Z_n)$ at the point of inflection and its corresponding Z. Substituting these values in equation (3) would provide an estimate of the spatial correlation length for the data set.Wickremesinghe (1989), however, noted that a more computationally efficient method would be to create a plot of $\Gamma^2(Z_n)$. Z against the lag distance, Z and pick the lag distance corresponding to the peak of the curve to represent the spatial correlation length. Some studies were conducted by Wickremesinghe to estimate the differences in the calculated spatial correlation length obtained by equation (3) and his procedure. The differences were found to be negligible and hence Wickremesinghe's procedure is used for this paper as discussed in the next section.

CASE STUDY

The spatial variability of compressive strength of coal can be established in two different ways. One, test a huge number of samples on very small spacing and establish a map of strength variability across the mine. Two, conduct a decent number of reasonably close-spaced tests and use the random field theory to characterize the variability. Obviously, the first option is cost-prohibitive, time-consuming and thus is impractical. As discussed in section "Spatial Correlation Length" above, the random field theory offers a valuable means to characterize the spatial variability of strength from a finite number of tests. Because of the elegant way in which the random field theory characterizes the variability, it is possible to incorporate the output in numerical models to understand the effect of the variability on pillar strength. To generate the data needed to apply the random field theory, a detailed field testing program was undertaken at an underground

mine in Colorado. This is a longwall operation that extracts the Wadge seam at a depth between about 600 and 1,700ft. The coal seam is about 9 to 10ft thick in a major portion of the mine. The mine is located on the southern flank of the Twentymile Park structural basin. The coal bearing strata at the mine are confined to Mount Harris member of the Upper Cretaceous Williamsfork formation. Structurally, the seam is very regular and has very few rolls. The average coal seam dip within the longwall development area is close to 6%, however, the direction of dip varies because the panels are cutting across a bowl shaped structure with dip radiating inward towards the center of a syncline axis.

One prominent feature of the Wadge seam at the study mine is the persistence of face cleats. The strike of these cleats at the mine falls in a narrow range between N30˚W and N40˚W. While variable, it is not uncommon to see about four to six well-developed face cleats per linear foot of entry. The dip of these well-developed cleats is near vertical with angles between 85 and 90°. In contrast, the butt cleats are poorly developed and where seen have a strike of about N60˚E. No prominent bands of rock or coal of significantly different quality are seen in the seam. However, a few high ash bearing dull looking thin bands are sporadically noticed within the seam. Otherwise, the seam is vertically consistent in its quality throughout the mine.

Since coal strength has relevance mainly for pillar design at this mine, the testing program was designed to characterize the spatial variability on a pillar-scale. For this purpose, two different sites were selected at the mine. The first site was in an area where some failed pillars (which are in stable, post-failure state) exist in the mine as shown in Figure 2. The stable pillar at this location, from which the close-spaced samples were collected, was about twenty years old. Given this long time gap since development, some physical disintegration of coal at the ribs was expected. To represent fresh coal condition, the second site was chosen in an area that was recently developed. Based on the testing experience from the first site, which did not produce a large number of samples, it was decided to test two adjacent pillars at the second site as shown in Figure 3.

In order to expedite the testing process and to conduct the tests at the mine site, point load testing was utilized to estimate the coal

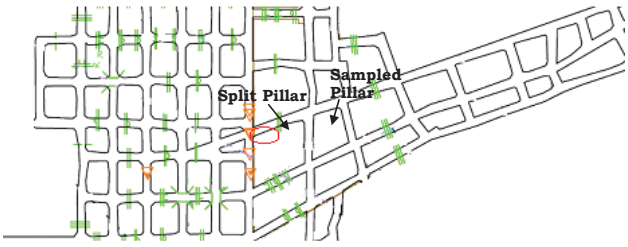

Figure 2. Pillar from which samples were collected at site 1 (notice the two small failed pillars next to the sampled pillar).

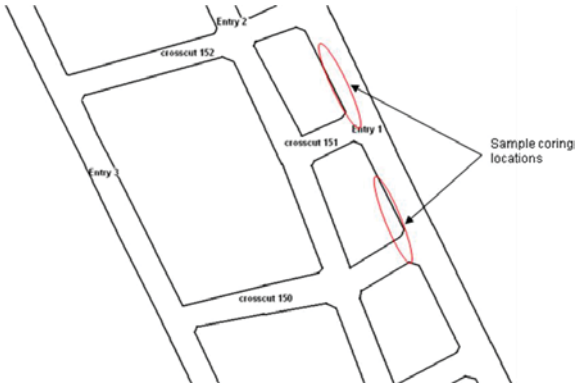

Figure 3. Pillars from which samples were collected at site 2.

strength in this study. Since cylindrical shaped specimens provide the best results from point load tests, the Hilti battery powered portable drill TE 6A 36V shown in Figure 4 was used for sample collection. With this core drill, samples that were 2 inches in diameter and 2-3 inch long were obtained. As mentioned before, the coal seam at the mine did not have any prominent rock or other bands. Therefore, it was planned to collect the coal samples on a random pattern from each pillar side. Even though the tested samples were taken on a reasonably random pattern, some bias was inevitable towards stronger coal in each pillar. This bias was somewhat more prevalent at site 1 because of the time-dependent deterioration of the pillar ribs. The sampling in fresh coal at site 2 went a lot more smoothly than at site 1. Some views of the coal pillars showing the location of test samples are shown in Figure 5 and Figure 6. In addition to the cylindrical samples, from site 1, a large lump of coal was also collected. From this lump six irregular coal samples were tested to see what kind of variability is obtained from such an ultra close-spaced sampling.

The point load tests were conducted using GCTS PLT-110 tester manufactured by GCTS, Phoenix, Arizona. This machine was built to ISRM specifications for point load testing. Data collection was automated using pressure and displacement transducers, which can be directly imported to a laptop for processing. A pressure gauge was also provided in the tester for manual reading of the maximum pressure in the test. Among the test samples collected from the two sites, only those that satisfied the ISRM size requirements were chosen for testing. Each specimen was photographed before and after the test and was systematically labeled for proper identification. In Figure 7, some axial, diametral and irregular test samples are shown before and after the test. The location of all the samples that were finally tested are shown in Figure 8. Also shown in this figure are the compressive strength values estimated from the point load tests. The pillars and the sample locations are shown to the scale in Figure 8. The conversion factors used to calculate the compressive strength from point load data are discussed next.

For the U.S. coal measure rocks, empirical correlation have been developed by Rusnak and Mark (2000) to estimate the compressive strength from point load data. While this generic relation is a good starting point, experience has shown that significant departures might exist when site- and rock-specific data are available. For this reason, the available data from the case study mine were collected to see if the Rusnak and Mark relationship could be used for compressive strength estimation. A total of 22 pairs of UCS and

Figure 4. Coring using the Hilti portable drill.

Figure 5. Partial view of the sample locations at Site 1.

point load test data were available for coal from the same boreholes at this mine. The data is plotted in Figure 9. The best-fit curve for this data showed that the coal's compressive strength could be estimated by

$$UCS = 45\, I_{s50} \qquad (4)$$

where I_{s50} is the axial point load value and the compressive strength is estimated in psi. Equation (4) clearly shows that site-specific conversion factors could be significantly different from the generic value suggested by Rusnak and Mark.

Spatial Correlation Length

As explained in section 2.0 above, the procedure suggested by Wickremesinghe (1989) is computationally more efficient to calculate the spatial correlation length (δ). Using this procedure, the spatial correlation length at the two study sites was calculated. The results are plotted in Figure 10. In this figure, it may be noted that the two pillars at Site 2 were analyzed together. When the compressive strength values from the two pillars at Site 2 were analyzed, it was found that there was no statistically significant difference between the two. Consequently, in order to have more data points for the estimation of δ, the data was combined.

From Figure 10, it can be seen that at the two test sites, the spatial correlation length was 9.9 ft and 7.2 ft, respectively. While creating the plots in Figure 10, it was noted that the calculated spatial correlation length value changed depending on which end of the test-pillar was chosen as the starting test location. The change in δ, however, was not significant. For calculating δ, the pillar end towards split pillar in Figure 2 was chosen as the starting test for Site 1. Similarly, for site 2, the inby most test was chosen as the starting point. Even though the computed spatial correlation length values for the two test sites were much smaller than the pillar size, it is likely that these values may not be a true reflection of the actual δ. Research shows that if the sampling interval is greater than the true δ, then the computed spatial correlation length will tend to be significantly greater (Wickremesinghe, 1989; Fenton, 1999). Further evidence that the computed δ in Figure 10 may not be the true value comes from the compressive strength data obtained from a large coal chunk collected from site 1. An irregular coal chunk measuring about 18 x 12 x 8 inches was collected for some ultra-close spaced testing. Six irregular samples tested from this chunk gave compressive strengths of 6,300, 2,250, 2,700, 4,050, 4,950 and 4,500 psi. The UCS values were calculated using equation (4). Given this wide variability of the strength shown by the samples from a very small coal chunk (compared to the pillar size), it can only be deduced that the true spatial correlation length at the study mine might be much smaller than the calculated average 8.5 ft. Obviously, this outcome was not anticipated when the testing program was planned. Based on this hindsight, some future field work is planned to conduct ultra-close spaced testing on a pillar-scale to estimate a more realistic δ.

Uniaxial Compressive Strength

Even though the testing program did not produce a satisfactory outcome for spatial correlation length, the data provided useful insights on the compressive strength at pillar-scale. Some key statistics for the computed uniaxial compressive strength using equation (4) for the two test sites are given in Table 1. Over the twenty plus years of operating life of the case study mine, several UCS tests were conducted on cylindrical coal samples recovered from coreholes. Such data was available from 53 coreholes for a total of 378 individual tests. Key statistics for this large UCS data are also included in Table 1. As a part of a major study, Mark and Barton (1996) collected a large amount of UCS data from several major U.S. coal seams. From this database, individual test values were available for 2 251 samples. For comparison, the same key statistics for this large representative U.S. coal database are also included in Table 1.

Figure 6. Partial view of the sample locations at Site 2.

At both test sites, some axial and diametral point load tests were conducted to see if the coal exhibited any strength anisotropy. However, for Site 1, the data obtained from axial point load tests were not included in Table 1. As mentioned before, the pillars at site 1 were developed over twenty years ago and some time dependent deterioration of pillar ribs had occurred at this site. When the test data was analyzed, it was found that the axial point load strength was smaller than the diametral one at this site (statistically significant at 95% confidence level by a t-test). Such difference between the axial and diametral strengths was not found at the recently developed site 2. Given that the diametral point load is more meaningful for pillar design (because of the way coring was done as shown in Figures 4-6), the data obtained from axial point load tests from site 1 was excluded for all analyses in this paper. Interestingly, despite the significant time difference, there was no statistically significant difference (from t-test) in the diametral strengths at both study sites.

To understand the significance of the results in Table 1, several t-tests were conducted. These results showed that at 95% confidence level, there was no difference in the average compressive strength of coal at Sites 1 and 2. Similarly, the strength of coal at the two study sites was no different from the average behavior of coal seen at the entire mine. This later conclusion is extremely significant for practical pillar design. Even though there is a very high variability of coal strength when a large number of tests are done for the entire mine, the mean strength of coal is statistically similar to the average strength obtained from reasonably close-spaced testing done on a single pillar. The implication of this conclusion is that it is perhaps possible to get an idea of the mean value of the UCS and its variability on a pillar-scale by studying the coal strength data obtained from sparsely distributed coreholes throughout the mine. This conclusion thus provides some justification and validates the current practice of using the mine-wide average compressive strength for design. However, such mine-scale database only provides an idea of the pillar-scale strength average and variability, not the spatial correlation length, which is an equally important parameter for pillar strength determination as discussed in the next section.

The results in Table 1 also show that the average compressive strength of coal at the study mine is significantly higher than the national average obtained from the National Institute for Occupational Safety and Health (NIOSH) database. Even at 99% confidence interval, the coal at the study mine is statistically stronger than the average U.S. coal. This determination provides a solid base and explanation for the significantly higher in-situ coal strength needed to explain the behavior of some failed and stable coal pillars at the study mine. With the standard 900 psi in-situ strength, the field behavior of pillars at the mine could not be well explained as discussed later in this paper.

EFFECT OF D ON PILLAR STRENGTH

The random field theory provides an elegant way to completely describe the spatial variability of geotechnical materials. As discussed in section 2.0, this variability can be captured through the mean (μ), standard deviation (σ) and spatial correlation length (δ). When the spatial variability is described using these three parameters, it is also very convenient to study its effect on pillar strength using the so-called random numerical modeling (*RaNuM*) methodology. Vaughan Griffiths and Gordon Fenton pioneered this approach for geotechnical materials through random finite element method and conducted research on such diverse topics as soil bearing capacity, slope stability, pillar strength and several other topics (Fenton and Griffiths, 2008). Even though Griffiths and Fenton (2002) conducted some preliminary random finite element studies on coal pillars, their study lacked any field data and was restricted to two-dimensional space. However, their parametric studies provided some useful insights into the effect of spatial variability on pillar strength.

In a nutshell, the *RaNuM* approach works the following way. Once the variability of material properties are captured from field tests by μ, σ and δ, a representative numerical model of the problem domain (e.g., coal pillar and surrounding strata) is constructed. Within the numerical model, the element or zone material properties are assigned as random samples drawn from a large population of the property. The shape of the property distribution function for the population can be determined from field data if enough testing is done, or in a majority of cases can be

a. Diameteral test

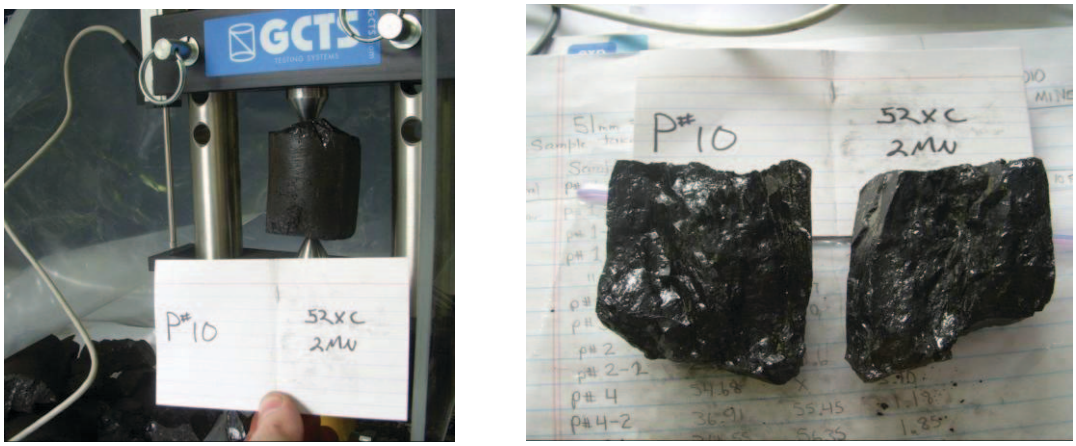

b. Axial test

c. Irregular test

Figure 7. Some samples before (left) and after (right) test.

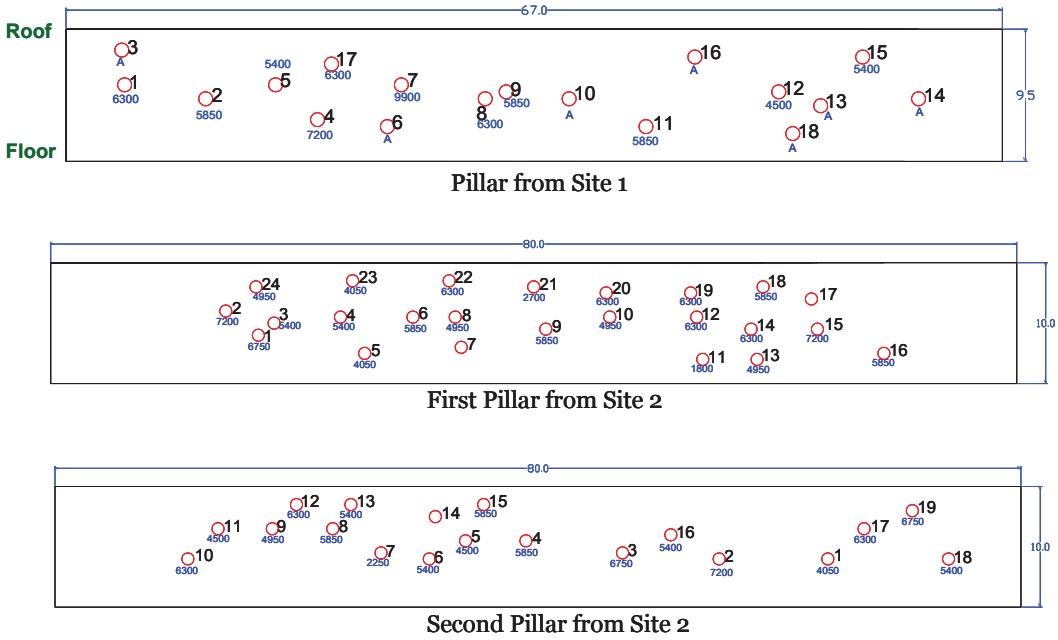

Figure 8. Sample locations and the corresponding coal strength from the two sites (smaller font used for strength and the larger font for the test number).

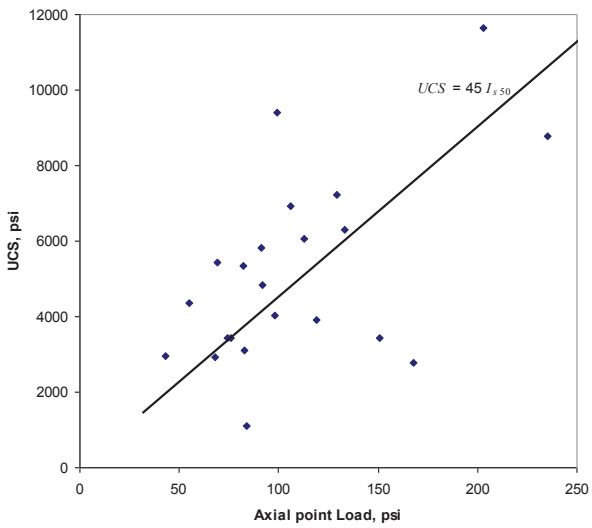

Figure 9. Correlation between the UCS and point load strength for coal at the study mine.

assumed Gaussian. To simulate the variability of rock strength in the numerical models accurately, one could use such sophisticated procedures as the Local Area Subdivision (LAS) method (Fenton, 1990) which produces local arithmetic average of the property for each element or zone. With LAS, the assigned element property in the model accurately reflects the variance reduction due to local averaging over the size of the element as well as the cross-correlation structure dictated by δ. Further details on *RaNuM* can be found in Fenton and Griffiths (2008).

After the individual element properties are assigned, models are then solved to estimate the pillar strength. Use of numerical modeling for pillar strength determination has been explored by several researchers in the past (e.g., Gadde et al., 2001; Morsey and Peng, 2001; Dolinar and Esterhuizen, 2007). All these researchers used displacement controlled loading to obtain numerical average stress-strain curve for the pillar to define its peak strength. This standardized approach is used to compute pillar strength in this paper. Since the main purpose here is to study the influence of δ, no attempt was made to be highly realistic in representing the pillar boundary conditions seen in the real world (e.g. contact conditions at roof and floor). Rather, simple friction free boundaries were assigned at the roof and floor. This assumption eliminated the need to model the roof and floor thus reducing the model size significantly (besides, spatial variability of roof and floor strength might have their own impact on pillar strength, which is a topic for future research). Further, to simplify the task, it had been assumed that the same random strength can be assigned to all elements within a volume represented by a cube whose dimensions were equal to the spatial correlation length, δ. In essence, no attempt was made to apply the LAS method to assign material properties. These simplifications have little bearing on the value of the model outcome, as the main goal here is to study the difference in the pillar strength estimated using "average uniform" versus "spatially varying" coal strength properties with everything else remaining the same.

When element or zone properties are assigned as random numbers drawn from a population, even for the same μ, σ and δ, every realization of the numerical model will have a different spatial distribution of the element properties. In such a situation,

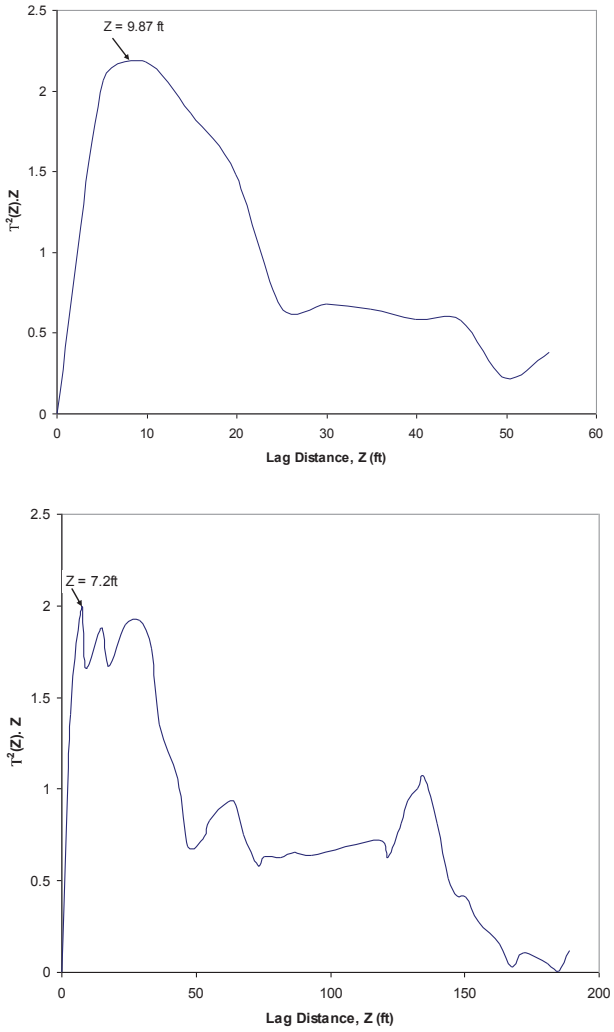

Figure 10. Plot of. Z against Z for Site 1 (above), and Site 2 (below).

normal practice of using the average coal strength for the entire pillar. For this purpose, only a few handful realizations of the element properties were necessary.

Using the μ and σ values in Table 1 and information on δ for the study mine, a random numerical model was constructed for one of the failed pillars at the study mine as shown in Figure 11. The modeling tool used for the current research was the popular FLAC3D explicit numerical modeling code (Itasca, 2009). The assignment of material properties described by a set of μ, σ and δ was accomplished using a FISH routine developed within FLAC3D. Models were also run assigning uniform strength properties for all zones in the coal pillar, as is the normal practice. For both the random and uniform-property models, the in-situ strength of coal was calculated using the Gaddy's equation. Except for the way individual element properties were assigned, everything else was kept the same for both the "random" and "uniform" numerical models.

The modeling results are given in Table 2 in terms of the peak pillar strength estimated for the uniform-property model and ten different realizations of the random model. The deformed states of the pillar for two different realizations of the random model are shown in Figure 12. From these plots, it can be seen that when spatial variability of coal strength exists, the deformation pattern of the pillar is different from the normal regular shape expected for the uniform-property model. As discussed in section 3.1, the ultra-close testing from the irregular coal chunk indicated that the 8.5 ft spatial correlation length is perhaps much greater than the real value. Therefore, to be more realistic, the modeling was conducted for a spatial correlation length equal to the element size (1.5ft) for the random models in Table 2.

From the results given in Table 2, it can be concluded that given the high spatial variability of coal properties on a pillar-scale, the pillar strength estimated by using the average coal strength is not significantly different from that obtained by realistically considering the variability. Such similarity in the limit values is because of the fact that as the scale of fluctuation decreases, the weakest path of failure becomes increasingly tortuous and its length correspondingly longer. Consequently, the failure path will take the shorter route cutting through the harder materials.

Table 1. Key statistics for the uniaxial compressive strength (in psi) data.

Statistic	Site 1	Site 2	Entire case study mine data	NIOSH U.S. data
Mean	5,432	5,436	5,196	3,837
Number of Tests	28	62	378	2,251
Median	5,625	5,400	4,265	2,988
Standard Deviation	1,596.54	1,388.31	3,202.08	3,331.77
Skewness	-0.02	-1.18	1.07	2.93
Minimum	1,800	450	124	68.1
Maximum	9,900	8,100	15,251	27,304

if one were interested in making probabilistic interpretations of the pillar strength, then approaches like Monte-Carlo simulation will be necessary. In this initial research, however, the objective is limited to examining the effect of pillar-scale spatial variability of coal properties on the pillar strength and draw contrasts with the Griffiths and Fenton (2002) note that in the limit, when δ becomes zero, the optimum failure path will look the same as in a uniform material with strength equal to the mean value. The modeling outcome in Table 2, for the first time, provides an insight into the reason why the traditional approach of

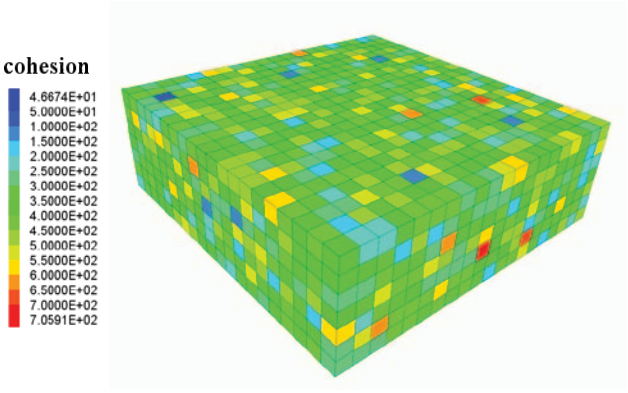

Figure 11. Spatial distribution of cohesion within the coal pillar in a model.

Table 2. Pillar strength obtained from numerical modeling.

Peak strength of the pillar, psi	
Uniform strength for all pillar elements	Random input strength assigned to each element
1,290	1,243
	1,243
	1,253
	1,250
	1,253
	1,255
	1,250
	1,253
	1,259
	1,254

using the average coal strength for pillar strength estimation has been providing satisfactory results over the decades. However, parametric studies by Griffiths and Fenton (2002) indicate that the effect of spatial variability may only be ignored for very small or very high spatial correlation lengths (as compared to the pillar size). For intermediate values, the normal "uniform-strength" approach may overestimate the pillar strength and thus may lead to unconservative designs.

Drawing on the preliminary field and modeling work discussed thus far, the authors conclude that coal is highly likely to exhibit extreme variability at ultra-close distances and thus the traditional approach of using the average compressive strength for pillar design is perhaps accurate enough for routine use. It is also concluded that the high variability of strength seen in laboratory testing of coal has very little consequence for practical pillar design. While sounds surprising, it appears that the higher spatial variability of coal strength is the very reason why the traditional strength "averaging" is working well and thus, after all, the high variability is not all that undesirable for pillar design purposes.

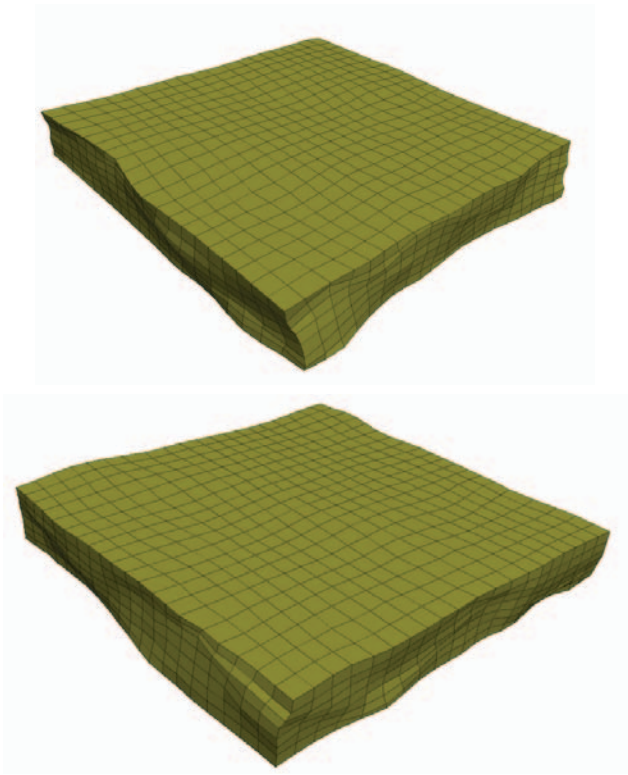

Figure 12. Exaggerated deformed shape of pillars from two different random models.

IN-SITU COAL STRENGTH

As mentioned before, another controversial aspect of using site-specific coal strength for pillar design is related to the estimation of in-situ strength. The most popular approach to link the laboratory and in-situ strength of coal was developed by Gaddy (1956). Later, Hustrulid (1976) extended Gaddy's work and showed that the following equations will provide a reasonable estimate of in-situ coal strength:

$$\sigma_{in-situ} = \frac{\sigma_c \sqrt{D}}{\sqrt{h}} \qquad \text{if } h < 36 \text{ inches} \qquad (5)$$

$$\sigma_{in-situ} = \frac{\sigma_c \sqrt{D}}{\sqrt{36}} \qquad \text{if } h \geq 36 \text{ inches} \qquad (6)$$

where σ_c = laboratory compressive strength of coal (in psi) obtained from a cylinder of diameter D or cube of edge length D (inches);

h = pillar height, inches.

When a large database of satisfactory and unsatisfactory pillar case histories from several U.S. coal mines was studied by Mark

and Barton (1996), it was found that the ability to explain the field performance decreased when site-specific in-situ strength estimated by equation(6) was considered in the analysis. In fact, the same analysis showed that a better explanation of case histories was obtained if the in-situ strength was assigned a constant 900 psi value across the board. Subsequent to this research, in the U.S., site-specific coal strength has largely been ignored for pillar design purposes. Even though some researchers (Unrug et al., 2009) question the validity of using the same in-situ coal strength for every coal mine in the U.S., currently site specific data is not considered for pillar design purposes in a majority of cases.

As mentioned before, at the case study mine, some failed pillar cases are available to examine which method of in-situ coal strength approach makes sense in explaining the conditions at the mine. The location of these failed pillars (FP-1, FP-2 and FP-3) is shown in Figure 13. It may be mentioned that the failed pillars in Figure 13 were initially developed to be much larger and subsequent operational needs required splitting them into smaller pillars. The pillars exhibited failure after the splitting was done. The current condition of one of the failed pillars is shown in Figure 14. In addition to the failed pillars, some stable pillars (SP-1, SP-2 and SP-3) were also picked from this part of the mine as shown in Figure 13. Since the failed pillars were slightly irregular in shape and were adjacent to larger pillars, the average vertical stress cannot be accurately estimated with the tributary area method. Therefore, the boundary element based LaModel program (Heasley, 1998) was used to calculate the pillar loads. For this purpose, the default inputs of LaModel program were used except for the geometric and depth information. Also, in the LaModel analysis, the pillars were assumed to be elastic for the stress determination.

The pillar stability factors computed for both the stable and unstable pillars identified in Figure 13 are given in Table 3. The strength of these pillars was estimated using the Mark-Bieniawski equation (Mark and Chase, 1997). For all these irregular pillars, an equivalent width was computed using the Wagner's formula (1974) for use with strength estimation. The pillar stability factors in Table 3 were computed using both the 900 psi value and the in-situ coal strength estimated by equation (6). Given that the core samples obtained from this mine were 3 inches in diameter and using the average laboratory compressive strength of 5,196 psi from Table 1, equation (6) produced in-situ coal strength equal to 1,500 psi. Even though there are several stable pillars in Figure 13, only the smallest of the stable pillars was picked for Table 3. If the coal strength can explain the condition of the smallest stable pillar, then the larger pillars are automatically accounted for.

The results in Table 3 clearly show that the use of 900 psi in-situ strength can not explain the conditions noticed at the mine. On the other hand, the stability factors computed using the in-situ strength estimated by equation (6) appear to explain the conditions well. While the stable pillars can have any stability factor value above 1.0, given that barring some rib spalling these pillars were stable in their over two decades of life, the stability factors in Table 3 for 1500 psi in-situ strength appear realistic. If it was assumed that the stable pillars in Table 3 had pillar stability factors slightly above 1.0, then the required in-situ coal strength was about 1,100 psi. Therefore, it is possible that the actual in-situ strength of coal at the study mine is somewhere between 1,100 and 1,500 psi. Even though not provided here, analysis done on longwall chain pillars at this mine using 900 psi in-situ strength showed that under the tailgate loading condition, the computed pillar stability factors were as low as 0.26 in areas that were mined successfully in the past. In fact, the back analysis of successful longwall chain pillars at this mine demonstrated that much lower ALPS stability factors than recommended values provided satisfactory performance over the two decades plus operating life of the mine. The analysis in Table 3 and the long operational experience at the mine clearly demonstrate that the 900 psi "national average strength" could not explain the field conditions well. On the other hand, the in-situ strength estimated using the Gaddy's equation provided acceptable results for the geologic conditions at this mine. It is also interesting that when the 2,251 individual laboratory UCS values collected by NIOSH were analyzed using equation (6), the national average in-situ strength obtained was 1,007 psi which is only about 12% higher than the 900 psi value used in ALPS and ARMPS.

Even though the developers of the ALPS and ARMPS models never suggested using the 900 psi in-situ coal strength indiscriminately, in practice, this number has been used for any rock mechanics analysis involving coal. If the original publications are carefully read, it becomes obvious that the 900 psi value may be interpreted as another empirical constant that provided the best explanation of the case histories using the ALPS and ARMPS models. Any other interpretation will imply that the underlying loading and pillar strength calculation models in ALPS and ARMPS are accurate for all the case histories in the database, which obviously is not known. Despite this clarity, it is unfortunate that indiscriminate use is being made of this number. It is perhaps not out of context to reiterate that the 900 psi value may only be used if the mine under consideration falls within the bounds of the NIOSH case histories and the mine is planning to use the recommended NIOSH stability factors for pillar sizing. As the experience at the case study mine in this paper demonstrated, exceptions to ALPS – and possibly ARMPS – predictions are possible, and in such an event, the local experience should be the driving factor in proper pillar design. If the general ALPS/ARMPS recommendations are not fine-tuned to local conditions, then the possible unsatisfactory pillar design may have safety consequences or sterilize valuable reserves depending on whether the actual coal strength is smaller or greater than 900 psi.

DISCUSSION AND CONCLUSIONS

The random field theory provides an elegant way to fully characterize the spatial variability of geotechnical materials. In addition to the traditional mean and standard deviation values, estimation of the spatial correlation length is necessary to completely describe the variability. With the use of random numerical modeling, the spatial variability can be easily included in a stability analysis. The field investigations described in this paper show that the compressive strength of coal exhibits extreme variability on very small length-scales. In fact, the data showed that the mean strength of coal on a pillar-scale was not statistically different from that obtained through sparse drilling covering the entire mine. This conclusion is significant for practical pillar design and in a way validates the current practice of using the average compressive strength obtained from mine-wide core drilling. The results of the random numerical modeling showed that given the high spatial variability of coal strength over short distances, the "average" pillar behavior obtained by realistically considering the spatial variability was not significantly different

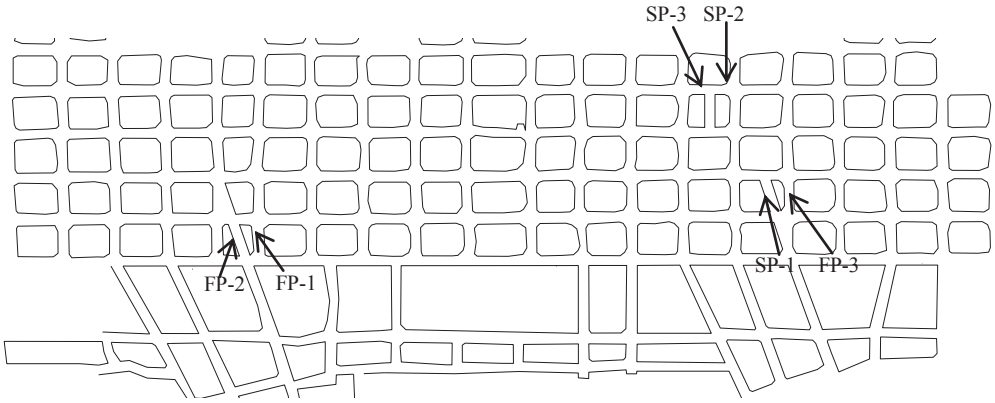

Figure 13. Location of stable and unstable pillars at the case study mine.

Figure 14. Condition of failed pillar FP-1 at the case study mine.

variability of coal strength is the very reason why the traditional strength "averaging" is working well in practice.

The practical experience at the case study mine showed that the 900 psi in-situ coal strength could not provide satisfactory explanation of the conditions at the mine. This analysis also showed that the Gaddy's in-situ strength equation provided a reasonable first approximation to the field strength at the mine. Based on this experience, it is suggested that the 900 psi value should only be used if the mine under consideration falls within the bounds of the NIOSH database, and is planning to use the recommended pillar stability factors derived from the large case history database. One way to check if the coal at a particular mine is stronger or weaker than the U.S. average is by "statistically" comparing the mine-specific laboratory coal strength with the national strength database put together by NIOSH. If the laboratory strength data shows no statistical difference, then perhaps the 900 psi value could be used as the starting point. If the coal is weaker or stronger, then the Gaddy's in-situ strength equation may be used to estimate the site-specific strength. In either situation, the pillar design must be refined as more field

Table 3. Pillar stability factors for different in-situ coal strengths.

Pillar	Mining height, ft	Depth, ft	Equivalent pillar width, ft	Average vertical stress from LaModel, psi	Pillar stability factors for different in-situ coal strengths		
					900 psi	1,500 psi	1,100 psi
FP-1	9.7	1,100	24	2,815	0.49	0.81	0.59
FP-2	9.7		30	2,685	0.59	0.98	0.72
FP-3	9.65		24	2,495	0.55	0.92	0.68
SP-1	9.65		54	2,218	1.08	1.79	1.32
SP-2	9.65		40	2,259	0.84	1.40	1.03
SP-3	9.65		42	2,265	0.88	1.47	1.08

from that produced using uniform coal strength for the entire pillar. Again, this insight provides an explanation for the satisfactory practical results obtained over decades by using average coal strength for pillar design. Based on the research in this paper, it is concluded that the high variability of strength seen in laboratory testing of coal has very little consequence for practical pillar design. While sounds surprising, it appears that the high spatial

experience is gathered to reflect the local geology and operational conditions. Even if in a majority of situations the 900 psi value works for pillar design, estimation of site-specific in-situ coal strength is essential for such applications as yield pillar design, rib support design and for studying roof or floor stability in thick coal seams.

It is not uncommon to find coal seams with several "bands" of differing properties from roof to floor. At the case study mine, the coal seam was reasonably uniform and no apparent bands were found. Consequently, the field testing program could be conducted the way it was done. However, if different layers of materials exist in a coal seam, it is necessary to plan the field investigations such that enough data is obtained to identify the bands that are "statistically different" in strength from others. Once such significant layers are identified, it may be necessary to compute the spatial correlation lengths for each band individually for use with random numerical modeling to compute the pillar strength. It is inappropriate to partition the coal seam into several bands "visually" and based only on a handful of strength tests that can not be subjected to statistical tests for significance. From the experience discussed in this paper, it appears that a possibility exists where the strength variability identified by a "handful" of tests on "visually" different coal bands may not be statistically different from the variability that would be obtained within a "uniform" single layer of the same seam.

It may be cautioned that the very high variability of strength on small distances was inconsequential only when the "average" behavior of the structure was important. Therefore, the high coal strength variability did not materially affect the peak capacity of the coal pillar. However, when the spatial distribution of instability is important (e.g. localized rib spalling, cutter roof failures), then the strength variability will have significant bearing on the performance of the structure and thus cannot be ignored. In fact, it appears that proper use of random field theory and *RaNuM* approach offers promise to address several outstanding problems in coal mine ground control. With this combination of new tools, it seems likely that some progress can be made in finding an explanation for the eternal ground control problem, "why instability only here, not right next to it?"

ACKNOWLEDGEMENTS

The authors would like to formally recognize the assistance received from Casey Huber, Rocky Thompson, and Eileen Sullivan in conducting the field work described in this paper. Grateful appreciation is also due to John Rusnak for his encouragement during this research.

REFERENCES

Dolinar, D.R. and Esterhuizen, G. (2007). Evaluation of the Effects of Length on Strength of Slender Pillars in Limestone Mines Using Numerical Modeling. Proceedings of the 26th International Conference on Ground Control in Mining, Morgantown, WV, pp. 304-313.

Fenton, G.A. (1990). Simulation and Analysis of Random Fields. Ph.D. Thesis, Princeton University.

Fenton, G.A. (1999). Random Field Modeling of CPT Data. J. Geotech. Geoenvi. Eng. *125*(6):486-498.

Fenton, G.A. and Griffiths, D.V. (2008). Risk Assessment in Geotechnical Engineering, John Wiley & Sons, Inc..

Gadde, M.M. Sheorey, P.R. and Kushwaha, A. (2001). Numerical Estimation of Pillar Strength in Coal Mines. Int. J. Rock Mech. Min. Sci. *38*:1185-1192.

Gaddy, F.L. (1956). A Study of the Ultimate Strength of Coal as Related to the Absolute Size of Cubical Specimens Tested. Virginia Polytechnic Bulletin No. 112, pp. 1-27.

Griffiths, D.V. and Fenton, G.A. (2001). Bearing Capacity of Spatially Random Soil: the Undrained Clay Prandtl Problem Revisited. Geotechnique *51*(4):351-359.

Griffiths, D.V., Fenton, G.A. and Lemons, C.B. (2002). Probabilistic Analysis of Underground Pillar Stability. Int. J. Numer. Anal. Meth. Geomech. *26*:775-791.

Heasley, K.A. (1998). Numerical Modeling of Coal Mines With Laminated Displacement-Discontinuity Code. Ph.D. Dissertation, Colorado School of Mines.

Hustrulid, W.A. (1976). A Review of Coal Pillar Strength Formulas. Rock Mech. *8*(2):115-145.

Itasca Consulting Group (2009). Fast Lagragian Analysis of Continua in 3-Dimensions. Minneapolis, Minnesota, USA.

Mark, C. (1992). Analysis of Longwall Pillar Stability: An Update. Proceedings of the Workshop on Coal Pillar Mechanics and Design, Santa Fe, NM, USBM IC 9315, pp. 238-249.

Mark, C. and Barton, T. (1996). The Uniaxial Compressive Strength of Coal: Should It Be Used To Design Pillars? Proceedings of the 15th International Conference on Ground Control in Mining, pp. 61-78.

Mark, C. and Chase, F. (1997). Analysis of Retreat Mining Pillar Stability. Proceedings of the New Technology for Ground Control in Retreat Mining, NIOSH IC 9446, pp. 35-48.

Morsy, K. and Peng, S.S. (2001). Typical Complete Stress-Strain Curves of Coal. Proceedings of the 20th International Conference on Ground Control in Mining, pp. 210-217.

Rusnak, J.A. and Mark, C. (2000). Using the Point Load Test to Determine the Uniaxial Compressive Strength of Coal Measure Rock. Proceedings of the 19th International Conference on Ground Control in Mining, pp. 362-371.

Salamon, M.D.G. and Munro, A.H. (1967). A Study of the Strength of Coal Pillars. J. S. Afr. Inst. Min. Metall. *68*:55-67.

Sheorey, P.R. (1992). Pillar Strength Considering In Situ Stresses. Proceedings of the Workshop on Coal Pillar Mechanics and Design, Santa Fe, NM, USBM IC 9315, pp. 122-127.

Unrug, K.F., Nandy, S. and Thompson, E. (1985). Evaluation of the Coal Strength for Pillar Calculations. SME Transactions *280*:2071-2075.

Unrug, K.F. and Turner, D. (2005). Seam Structure – An Important Criterion for Coal Pillar Design. Proceedings of the 24th

International Conference on Ground Control in Mining, pp. 121-129.

Unrug, K.F., Thacker, E. and Waggett, J. (2009). Determination of Coal Pillar Strength Based on In Situ Testing Method – Case Studies of Successful Pillar Performance. Proceedings of the 28th International Conference on Ground Control in Mining, pp. 17-20.

VanMarcke, E.H. (1984). *Random Fields: Analysis and Synthesis*, The MIT press, Cambridge, MA.

Wagner, H. (1974). Determination of the Complete Load-Deformation Characteristics of Coal Pillars. Proceedings of the 3rd International Soc. Rock Mechancis, Denver, CO, pp. 1076-1081.

Wickremesinghe, D.S. (1989). Statistical Characterization of Soil Profiles Using In-Situ Tests. Ph.D. Dissertation, The University of British Columbia, Vancouver, Canada.

Wilson, A.H. (1983). The Stability of Underground Workings in Soft Rocks of the Coal Measures. Intl. J. of Min. Eng. *1*:91-187.

An Evaluation of Time to Failure of Coal Pillars in Australia

Ismet Canbulat, Principal Geotechnical Engineer
Anglo American Metallurgical Coal
Brisbane, Australia

ABSTRACT

Following the Coalbrook Colliery disaster in 1960, Salamon and Munro (1967) established the well know empirical coal pillar strength formula in South Africa. This formula has prevented further violent multiple pillar failures. In 1996, a back analysis of the collapsed and uncollapsed cases in Australia led to the development of the Australian empirical coal pillar strength formulae. The original collapsed and uncollapsed coal pillar database of Salamon and Munro (1967) was updated in 2006. This study introduced strength formulae for different coalfields and seams in South Africa through back analyses of collapsed and uncollapsed cases.

Today, the resultant pillar strength formulae from these previous studies and the behaviour of the coal pillars are mostly well understood and applied with confidence. However, it was assumed in the previous studies that the behaviour of pillars is not time dependent; therefore, the formulae established do not provide an associated time to failure of coal pillars. This paper attempts to evaluate the so called "Geometrical Limits" concept to provide the Australian coal mining industry with a tool to assess the long-term behaviour of bord and pillar workings where the pillars are prone to failure due to spalling of ribs. In order to achieve this outcome, the principles of safety factor and the probability of failure calculated using the coal pillar strength formulae have also been evaluated and the results are presented in this paper.

INTRODUCTION

Since the turn of the previous century, a number of investigators have studied the effects of sample size and shape on the compressive strength of coal specimens in the laboratory. General trends, such as increasing height decreases the strength and increasing width increases the strength, were quickly established. These tests were inexpensive and easy to conduct; however, wide scatter of the results and the size effect made the extrapolation of strength results to full size pillars difficult. In order to overcome the limitations of the laboratory tests, testing of large *in situ* samples was initiated. These experiments were more expensive and difficult but had the advantage of being conducted in the underground environment and yielded valuable information regarding the stress-strain behaviour of coal pillars. Following the Coalbrook disaster in South Africa efforts went into statistical analyses of collapsed and uncollapsed cases using the Maximum Likelihood (ML) method. This led to establishment of the well known empirical coal pillar strength formula of Salamon and Munro (1967). Over 2. 5 million coal pillars have been developed in South African coal mines since the establishment of this formula (Salamon et al. , 2006), which has certainly been successful and prevented further violent multiple pillar failures.

In 1996, a back analysis of the collapsed and uncollapsed cases led to the development of the Australian empirical coal pillar strength formulae in the form of power and linear functions (Salamon et al., 1996). During the intervening years, this formula has also been proven to be successful in most instances.

An obvious disadvantage of the original study of Salamon and Munro (1967) was that the databases used in the analysis had a limited number of collapsed and uncollapsed cases. A recent study by Salamon et al. (2006) overcame this problem and introduced a series of formulae for different coalfields and seams in South Africa using the same principal of statistical back analysis of collapsed and uncollapsed cases. The limitations associated with computing power were also overcome in the study and different distributions and formulae in the form of power, linear and none-linear functions were established.

Today, the resultant pillar strength formulae from these previous studies as well as the behaviour of the coal pillars are well understood. However, an important assumption made in these previous studies was that the behaviour of the pillars is not time dependent; therefore, the formulae established do not provide an associated probability of survival for the life of coal pillars. In order to achieve this outcome, a study was conducted using the so called "Geometrical Limits" concept. It is postulated in this model that:

- the failure of a pillar is controlled by the volume of space available underground to allow sufficient spalling for failure,
- the underlying strength of pillars remains unaltered and the changes come about merely as a result of time-dependent reduction in pillar width,
- the pillar will fail when the safety factor reaches the critical safety factor, and

- the nominal safety factors at failure are distributed according to the same lognormal distribution obtained in the derivation of the empirical pillar strength formulae.

It is evident from the above assumptions that this model is only applicable in areas where the pillars are prone to failure due to spalling of ribs and does not consider the long term pillar failure associated with floor failure.

In this paper, an attempt will be made to adapt this model to Australian conditions and provide a tool to assess the long-term behaviour of pillars. The principles of safety factor concept and the probability of failure calculated using the coal pillar strength formulae has also been evaluated and the results are presented herein.

GENERAL REMARKS

The methodology used in the studies of Salamon and Munro (1967) in South Africa and Salamon et al. (1996) in Australia are identical. In both studies it was postulated that (i) the strength of a pillar can be expressed as a function of the linear dimensions of the pillar, (ii) the mean stress acting on a pillar is the tributary area load and (iii) failure occurs when the true load exceeds the actual strength, which can be expressed in terms of the conventional safety factor (*SF*):

$$SF = \frac{Strength}{Load} \qquad [1]$$

The general 'power' formula for strength (σ_p) was defined by Salamon et al. (1996) as:

$$\sigma_p = K\frac{(w\Theta)^{\alpha}}{h^{\beta}} \qquad [2]$$

Where *K*, α and β were determined by a statistical analysis of collapsed and uncollapsed pillar geometries, *w* and *h* are pillar width and mining height, in metres. Θ is a dimensionless 'aspect ratio' factor to account for pillar length. Salamon et al. (2006) determined the values for *K*, α and β to be 8. 6 MPa, 0. 51 and –0. 84 respectively.

The dimensionless aspect ratio is a modification of hydraulic radius concept (effective pillar width) of Wagner (1974) and as follows:

When pillar width to height (w/h) ratio <3:

$$\Theta = 1 \qquad [3]$$

When 3 ≤ w/h ≤ 6:

$$\Theta = \left[\frac{2l}{w+l}\right]^{\frac{(w/h)-3}{3}} \qquad [4]$$

where *l* is pillar length.

When w/h >6:

$$\Theta = \left[\frac{2l}{w+l}\right] \qquad [5]$$

Salamon (1982) proposed an extension to his original pillar strength formula to account for the increased strength "squat" pillars with large width to height ratios. Laboratory tests, field trials and *in situ* measurements were conducted to observe the performance of squat coal pillars. This was achieved by examining the extent of fracturing on the pillar sides as well as monitoring pillar dilation and the stress profile of pillars designed according to the squat pillar formula, with the assumptions that the critical width to height ratio (R_0), where deviation from Salamon and Munro's (1967) original formula occurs, is 5. 0 and that the rate of strength increase (ε) is 2. 5. The assumption that the critical width to height ratio be equal to 5. 0 was also partly based on the fact that no pillar had collapsed with a width to height ratio greater than 3. 75 until 1988 (Madden and Canbulat, 1997).

Salamon et al. (1996) proposed the following squat pillar formula in Australia:

$$\sigma_s = \frac{27.63\Theta^{0.51}}{w^{0.22}h^{0.11}}\left\{0.29\left[\left(\frac{w}{5h}\right)^{2.5}-1\right]+1\right\} \qquad [6]$$

where σ_s is the strength of a squat pillar.

Salamon et al. (1996) also introduced a linear pillar strength (σ_L) formula, which is defined as:

$$\sigma_L = 5.1[0.56 + 0.44w/h] \qquad [7]$$

The linear formula does not include an explicit 'squat pillar' provision. The constants in this formula were also derived from the ML method. An important design consideration in these formulae is that as the standard deviation of the power formula (0. 157) is relatively smaller than the linear formula (0. 207), the power formula recommends relatively lower safety factors than the linear formula for a given probability of stability. It is therefore that the power formula has generally been accepted and utilised in the design of coal pillars in Australia.

As mentioned above, in the analyses, the load acting on pillars was calculated using the Tributary Area Theory (TAT), which

assumes that each pillar carries a proportionate share of the full overburden load. Assuming H is depth to the seam floor, b is roadway width, w is pillar width, C is centre distance, then for a square pillar layout the pillar load (q_m) can be estimated in MPa units as:

$$q_m = \frac{\gamma H C^2}{w^2} \qquad [8]$$

where $C=w+b$ and γ is the average specific weight of the overburden rocks.

Maximum Likelihood Method

In all three the above mentioned studies, the ML method was utilised to estimate the unknown variables in the strength formulae.

The ML method is a well known and frequently used statistical procedure for parameter estimation, K α and β in pillar strength formulae. The estimation begins with the mathematical expression known as the likelihood function of the sample data (Salamon et al., 2006).

In pillar strength studies, the starting point in the ML method is to write down the critical safety factor S_c of a given pillar (the safety factor at which a collapse actually occurs), as in Equation [1].

The strength is given by some assumed expression which is a function of pillar geometry and a set of unknown strength parameters; while the load q_m is known from TAT and is given by Equation [8].

A probability density distribution, *f(S)*, with corresponding cumulative distribution, *F(S)*, also has to be assumed in order to describe the spread of critical safety factors about the median of 1. 0. The standard deviation of these distributions is another unknown parameter which has to be estimated by ML analysis.

Next, a 'likelihood function' is set up, which is simply the product of the probabilities of observing the given instances of collapsed and uncollapsed pillars. An optimum set of unknown parameters is then chosen such that this 'likelihood function' is maximised. To simplify the calculations, it is usual to maximize the natural logarithm of the likelihood function, so that the ML formulation finally takes the form:

$$Maximise\, L_L = \sum \ln(f(S_c)) + \sum \ln(F(S_u)) \qquad [9]$$

where $f(S_c)$ = probability of collapsed cases

$F(S_u)$ = probability of uncollapsed cases

Note the summations are taken out over the collapsed set c and over the uncollapsed set u. Maximisation of L_L is accomplished by means of a comprehensive search through the space of unknown parameters, starting with a set of arbitrary initial values.

Thus, to develop the maximum likelihood approach, it is necessary to postulate that the pillar strength and statistical probabilistic distributions assume a specific form.

Density Functions of the Critical Safety Factor

Any probability density function, *f(s)*, describing the spread of critical safety factor values, should have the property of median centred at SF_c=1 (i.e., satisfying $F(1)$=50%) and should be zero for negative values of the critical safety factors. Such distributions are inherently skewed. Three distributions, namely lognormal, Weibull and Gamma, were evaluated in the study of Salamon et al. (2006) in South Africa. This study indicated that the lognormal distribution provides results at least as robust and consistent as those produced by the Gamma and Weibull distributions. Therefore lognormal distribution is considered to be appropriate to describe the critical safety factors.

This distribution is symmetric in the logarithmic scale, and the standard deviation (σ) is simply a measure of the scatter about the central value of zero. An increase in the logarithmic standard deviation indicates a wider (more scattered) distribution of the data.

The frequency distribution of S_c itself is given by:

$$f(S_c) = \frac{1}{\sqrt{2\pi}\,\sigma\, S_c} \exp\left[-\frac{1}{2}\left(\frac{\ln S}{\sigma} \right)^2 \right] \qquad [10]$$

The corresponding cumulative distribution function, $F(S_c)$, is the integral of $f(S_c)$ between the limits zero and S_c, and:

$$F(S_c) = \Phi\left(\frac{\ln S_c}{\sigma} \right) \qquad [11]$$

where Φ is the cumulative normal distribution function.

SAFETY FACTOR CONCEPT

The standard notion of the safety factor is given in Equation [1]. In order to achieve an exact safety factor, it is necessary to use the exact values of strength and load. For a perfectly stable design, it is also necessary that the safety factor should be greater than unity (i. e. , 1) in *all* circumstances. However, in mining situations the strength and load assumed in safety factor calculations are only approximations which are subject to error due to (i) inexactness of specified mining dimensions, (ii) uncertainties and unpredictability nature of geological materials and (iii) human error in the geometrical data. Therefore, in most instances the exact values of strength and load cannot be determined.

The concept of safety factor has been used in all engineering disciplines; it is conceptually sound and acceptable. However, it does not provide an indication of appropriateness of the safety

factor; it only suggests that the safety factor should be greater than unity for a stable design.

Therefore, in order to achieve an adequate design, with a reasonable certainty, an appropriate safety factor should be used to ensure that the pillars will neither fail nor be over-designed. This design is no longer deterministic; it is probabilistic.

There are two probabilistic interpretations of the traditional concept of safety factor. The first of these is widely used in civil engineering and called stochastic modelling (a technique of presenting data or predicting outcomes that take into account a certain degree of randomness or unpredictability). In this interpretation the input parameters are taken as probability distributions rather than single values using the well known Monte Carlo simulation method. The probability density functions of the strength and load and the probability of survival of the structure is determined by estimating the interference between the two distributions. An advantage of this approach is that it can be employed without any historical data concerning failures; a deterministic problem is solved a large number of times to build a statistical distribution of strength and load.

The second probabilistic interpretation was motivated by the realization that in mining the probability density functions of load and strength are at best can only be guessed at and it is of questionable value to base a design procedure on such a weak foundation. This approach involves the introduction of functions purporting to describe the variation of load and strength as functions of the mining dimensions. In the case of bord and pillar workings, the pillar load is given by the tributary theorem, hence only the strength requires a predictor. Conceptually, any empirical formula involving a set of unknown constants could be used for this purpose. The constants in the strength expression are determined by an appropriate back-calculation. A necessary requirement of the application of the second approach to the probabilistic safety factor is the documentation of a sufficient number of case histories concerning failures in the field. The power of the method is enhanced if case histories involving non-collapsed cases are also documented (Salamon, 2003). This approach was utilised in development of the empirical coal pillar strength formulae with the aid of field data. Since this methodology takes into account the variation of the size and the shape of the pillars (as the input parameters were based on the *design* dimensions not *actual dimensions*) a stochastic modelling approach to deal with the variation between the design and actual dimensions is not required.

In the second approach, the strength and load are approximations; calculations based on them can yield only an approximate or nominal value for safety factor, SF_N, that is:

$$SF_N = \frac{S_N}{L_N} \qquad [12]$$

where S_N and L_N are nominal strength and load respectively.

The *nominal* values of strength and load can be written with their true (exact) values of strength (S), load (L) and their relative errors as (Salamon, 2003):

$$S_N = (1 + e_S)S \qquad [13]$$

$$L_N = (1 + e_L)L \qquad [14]$$

Where e_s and e_L represent the *relative errors* in the true values of strength and load respectively. Using these new notations, the nominal factor of safety can be written in the following form:

$$SF_N = \frac{1 + e_S}{1 + e_L}\frac{S}{L} \qquad [15]$$

If the definition of the true safety factor from Equation [1] is recalled, then the exact value of nominal safety factor is expressed as:

$$SF_N = \frac{1 + e_S}{1 + e_L}SF \qquad [16]$$

When failure occurs, by definition, the true safety factor must be unity, that is, the true strength must be equal to the true load, therefore, SF=1. If the nominal safety factor at failure is the *critical* safety factor, SF_c, the substitution of SF=1 into Equation [16] yields:

$$SF_c = \frac{1 + e_S}{1 + e_L} \qquad [17]$$

This expression reveals that, in general, the critical safety factor at failure will be less or more than unity, and if the dimensionless relative errors remain small, the value of the critical safety factor will be around unity.

In order to validate the critical safety factor concept, Monte Carlo simulation can be employed using Equation [17] to demonstrate hypothetical relative errors in strength and load by the histogram of the critical safety factor.

For the sake of simplicity, it is assumed that the errors in strength and load are lognormally distributed using a mean (m_s) and a standard deviation (σ_s) of 0. 07 and 0. 1 for relative error in strength and 0. 1 and 0. 2 for load respectively. Note that these assumptions may be varied; however considering the fact that the empirical strength formula developed in South Africa four decades ago has been successful, these error margins are considered to be reasonable for the purpose of this demonstration. Figure 1

shows the assumed distribution of the errors in strength and load following 10,000 Monte Carlo simulations.

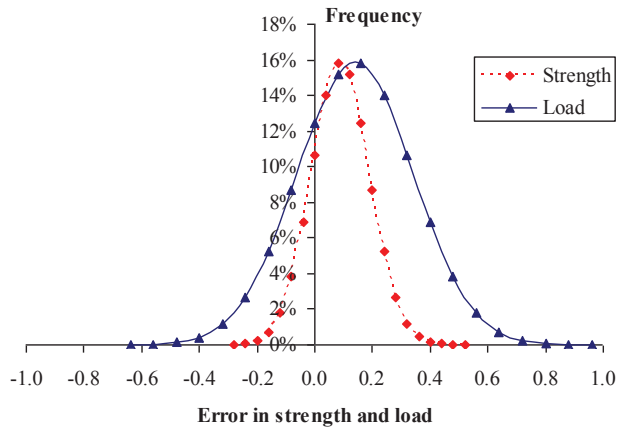

Figure 1. Distributions of errors in strength and load.

The distribution of the resultant critical safety factor is depicted in Figure 2. It is evident from this figure that despite the variations in relative errors this histogram appears to be reasonable with the mean, median and standard deviation of 1. 009, 0. 97 and 0. 23, respectively.

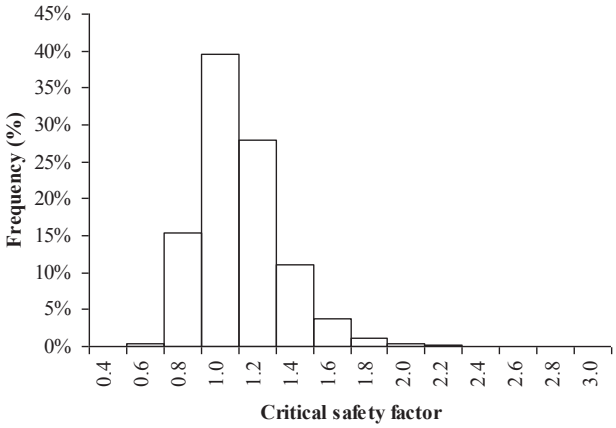

Figure 2. Distributions of critical safety factor.

For the purpose of this study and estimation of time to failure of coal pillars in the next section, this brief demonstration of the principle of the critical safety factor and its probability density function used in the development of pillar strength formulae is considered to be realistic.

TIME TO FAILURE OF COAL PILLARS

As mentioned above, an assumption made in the development of the pillar strength formulae was that the behaviour of the pillars, for practical purposes, is not time dependent. It has however been reported in the past (van der Merwe, 1993 and Salamon et al., 2006) that the strength of pillars may reduce over time by a spalling process that starts at the pillar edges and works its way into the pillar core. As the pillar sides get weaker, spalling occurs and the effective size of the pillar is decreased. Eventually it reaches the stage where the loss of strength is sufficient to result in failure of the pillar (van der Merwe, 1993). This failure mechanism is however controlled by the volume of space available underground to allow sufficient spalling for failure, which also implies a maximum depth of spalling. This limitation is referred to as "Geometrical Limits" in this paper. This concept of spalling was first suggested by Salamon et al. (1998). A further study conducted by Canbulat and Ryder (2002) somewhat simplified the model (i. e. , a cubic equation was simplified based on Newton iteration); this method is utilised in this current study.

Using the observations of van der Merwe (1993), Salamon et al. (1998) examined the mechanism of pillar failure when the pillars are spalling. In their study, the pillar strength was based on the original model of Salamon and Munro (1967) and the time dependency was introduced through a simple model of time dependent spalling. This combination of effects yields a situation where the pillar width decreases with increasing time. This approach has facilitated the estimation of pillar life expectancy, probability of survival for a specified number of years or indefinitely and to a methodology of designing pillars with a specified probability of survival and of life. While the model given in their study was substantiated only by very limited observations, the outcomes of numerical experimentations presented in the publication appear to be reasonably realistic. It would appear on the basis of this work that the time dependent spalling of pillar sides could be an explanation of the failures observed at relatively high nominal safety factor values. This study was conducted exclusively for South African coal pillars; this methodology is adapted to Australian conditions in this current paper.

Geometrical Limits

In their study Canbulat and Ryder (2002) assumed that a spalling pillar (Figure 3), of original width w and height h, continues to scale until a width w_1 is reached at which the 'apron' of scaled material forms a fully confining rim of height h and width c given by:

$$c = h \cot \varphi \qquad [18]$$

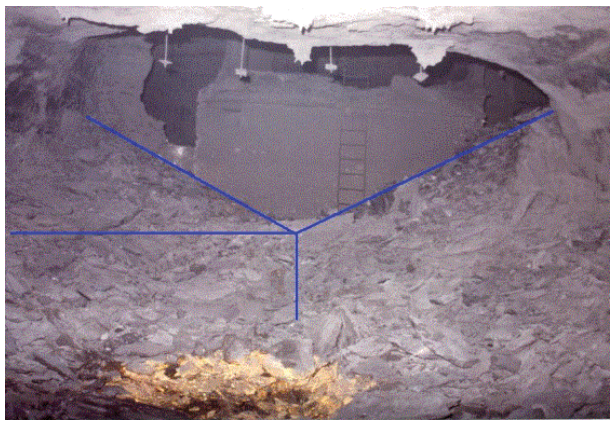

Figure 3. A scaled pillar indicating the angle of repose and the height of the rubble (after Canbulat and Ryder, 2002).

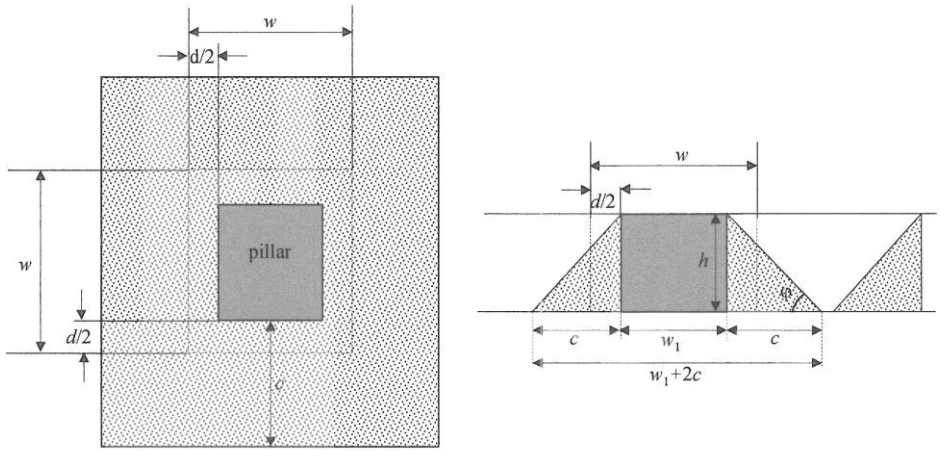

w = original pillar width (m)
b = bord width (m)
c = spalled off material width (m)
φ = angle of repose (35°)
h = mining height (m)
w_1 = pillar width after scaling (m)
d = amount of scaling on one side (m)

Figure 4. Plan and section of a spalled pillar (aprons not touching).

where φ = angle of repose.

Figure 4 illustrates the geometry involved. (It may be that the total width of the spalled apron w_1+2c exceeds the centres spacing "C" of the pillars, and overlap occurs with the aprons around the neighbouring pillars. This case is examined later.)

The volume of apron must equal the volume of scaled coal, allowing for a bulking factor B. The volume of a truncated pyramid is given by $V = (h/3)[A_1 + A_2 + \sqrt{A_1 A_2}]$, where A_1 is the area of the base, A_2 is the area of the top, and h is the height. Thus, for square pillars, the volume of scaled material is given by:

$$V = \frac{h}{3}[(w_1 + 2c)^2 + w_1^2 + (w_1 + 2c)w_1] - hw_1^2 \qquad [19]$$

This must equal the volume of bulked material from the pillar:

$$V = Bh(w^2 - w_1^2) \qquad [20]$$

Equating, and solving this quadratic equation for w_1, the result is

$$w_1 = -\frac{c}{B} + \sqrt{w^2 - \frac{c^2}{B^2}\left(\frac{4B}{3} - 1\right)} \qquad [21]$$

The total depth of spalling d is then given by:

$$d = w - w_1 \qquad [22]$$

For validity of Equation [21], it is obviously necessary that w_1>0. For this to be true, it can be shown that:

$$\frac{w}{h} > \sqrt{\frac{4}{3B\tan^2\alpha}} \qquad [23]$$

That is, provided the original w/h ratio of the pillar exceeds about 1. 5, the pillar can still spall to the limit set by Equation [21] and will be left with an uncollapsed core of width w_1>0.

A further limit to the validity of Equation [21] is that the edges of the spalled aprons do not touch or intersect; that is, that

$$w_1 + 2c < C \qquad [24]$$

where C is the centre distance. For high mining heights (i. e. , h>2. 5m), this relationship may not be satisfied, and the following more complicated situation has to be analysed (Figure 5).

$$V_0 = \left(\frac{X^2 h}{2c}\right)\left(C + \frac{X}{3}\right) \qquad [28]$$

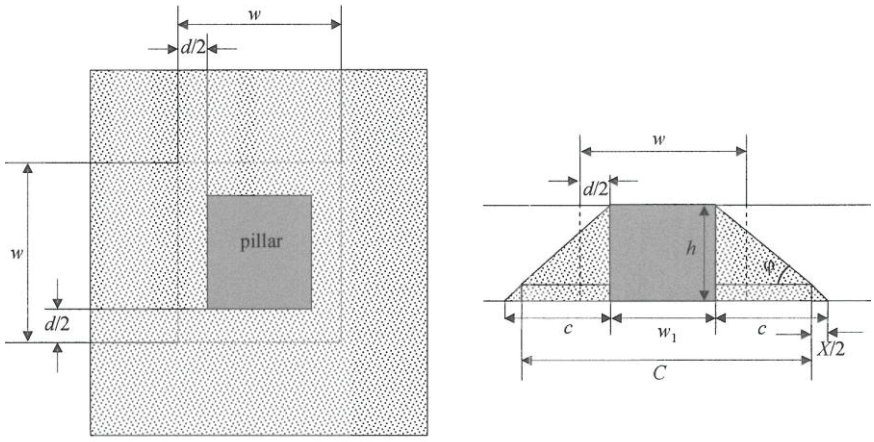

(a) Plan view (b) Section view

w = original pillar width (m)
b = bord width (m)
C = centre distance
c = spalled off material width (m)
φ = angle of repose (35°)
h = mining height (m)
w_1 = pillar width after scaling (m)
d = amount of scaling on one side (m)

Figure 5. Plan and section of a spalled pillar (aprons overlapping).

The actual total width of the apron is now C, and the amount X of overlap is given by:

$$X = w_1 + 2c - C \qquad [25]$$

The height of overlap h_0 is given by:

$$h_0 = \frac{1}{2} X \tan\varphi = \frac{Xh}{2c} \qquad [26]$$

The volume, V_0, of the overlapped portion of the apron has now to be subtracted from Equation [19], where:

$$V_0 = \frac{1}{3} h_0 \left[(C+X)^2 + C^2 + (C+X)C\right] - C^2 h_0 \qquad [27]$$

After substituting Equation [25], this leads finally to a *cubic* equation for w_1. The exact form of Equation [21] for this case now reads:

$$w_1 = -\frac{c}{B} + \sqrt{w^2 - \frac{c^2}{B^2}\left(\frac{4B}{3} - 1\right) + \frac{X^2(C + X/3)}{2cB}} \qquad [29]$$

Given an initial estimate of w_1 from Equation [21]; Equations [25] and [29] are evaluated and give an improved estimate for w_1. This process is repeated until the change in w_1 becomes negligible; generally, only a few iterations will be required. Alternatively, the following formula, based on Newton iteration, allows a single step to the final solution:

$$w_1^{final} \approx w_1 + \frac{X^2(C + X/3)}{4c(c + Bw_1) - X(2C + X)} \qquad [30]$$

where w_1 is from Equation [21] and X is from Equation [25].

As before, the total depth of spalling d is then given by:

$$d = w - w_1^{final} \quad [31]$$

Canbulat and Ryder (2002) identified the following limitations in this model:

- This model assumes a vertical rib profile. In reality, in the early stage s of spalling the lower portions of a pillar are probably protected by the spoil pile of scaled material, and only the upper portions of the pillar are susceptible to further scaling. This possible indicates a stepwise rib profile. Although the difference may be insignificant in terms of change in volumes, this is an issue that needs to be resolved.
- The strength of the spalled pillar would possibly be greater than that normally associated with a freshly-cut pillar of width, *w1*, due to the strengthening effect of the spalled material.
- In certain circumstances, the roadway width can enlarge significantly due to assumed spalling. These large roof spans may be prone to instability in their own right, especially after years of potential deterioration.

Spalling of Pillar at Failure

In order to determine the required spalling distance to reduce the safety factor to the critical safety factor (i. e. ,*SF*=1), the approach developed by van der Merwe (1993) can be used. In this approach, it is assumed that the original pillar width spalls by an amount, d_c, then the effective pillar width at critical safety factor is w-d_c. The critical spalling depth at failure can be solved in Equations [1], [2] and [8] by assuming that the centre distance is constant; that is:

$$d_c(S_c) = \frac{1}{2}\left[w - \left(\frac{\gamma H S_c h^{\beta} C^2}{K} \right) \right]^{\frac{1}{2+\alpha}} \quad [32]$$

Once the critical spalling depth is known, the time elapsed to failure can then be calculated using the following simple formula:

$$t_c(S_c) = \frac{d_c(S_c)}{r} \quad [33]$$

where r is the rate of spalling in m/year.

Note that the frequency of the critical safety factor at failure is represented by a lognormal distribution. The standard deviation of this distribution was determined in the Australian study by Salamon et al. (1996) as to be 0. 157.

Pillar Life Expectancy and Probability of Survival

Salamon et al. (1998) stated that it is not possible, due to the probabilistic definition of pillar strength, to determine unequivocally whether a pillar will or will not fail and that no unique relationship exists between the initial mining geometry and pillar life. This is evident in Figure 6, which shows the safety factor and life of collapsed South African pillar cases in the database presented by Salamon et al. (2006).

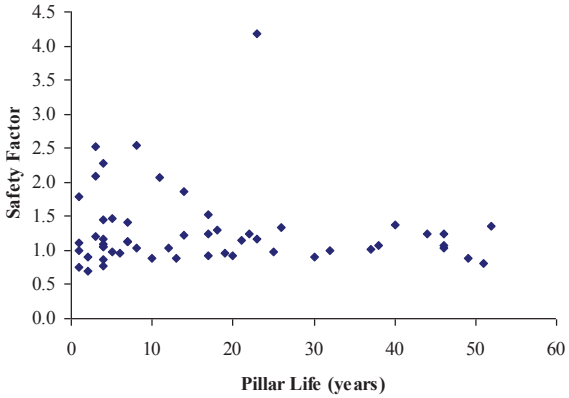

Figure 6. Design safety factor versus time interval. Data from South African collapsed cases using the original Salamon and Munro (1967) pillar strength formula.

Salamon et al. (1998) also stated that although no relationship can be established between pillar life and the initial mining geometry, the probability that failure will or will not occur can be determined. However, if pillar spalling occurs, the situation becomes complex. The effect of spalling reduces the pillar width and, therefore, may cause the failure of a pillar at some later time. The Monte Carlo technique can be employed to evaluate this phenomenon and the expected life of pillars.

To demonstrate this, three examples are given in this section assuming that:

Angle of repose, $\varphi = 35^{o}$

Bulking factor, B= 1. 35 [34]

Spalling rate, r= 0. 2m/year

The dimensions of the panels are given in Table 1.

Table 1. Dimensions of layouts used in examples.

Dimensions	Case 1	Case 2	Case 3
Pillar centres (m)	15	18	21
Roadway width (m)	5.5	5.5	5.5
Depth (m)	130	130	130
Mining height (m)	3.5	3.5	3.5
Pillar with to height ratio	4.3	5.1	6

Table 2 summarises the safety factors and the probabilities of failure and stability of the above examples.

Table 2. Safety factors and the associated probabilities of failure and stability.

	Case 1	Case 2	Case 3
Pillar safety factor	1.2	1.6	2.3
Probability of failure	0.161	0.001	7.1E-08
Probability of stability	0.839	0.999	1.0E+00

The pillar life histograms (frequency of collapses as a function of time) of the three cases resulting from 10,000 Monte Carlo simulations are summarised in Figure 7.

In Figure 8, the resulting estimate of the survival probabilities are plotted. The probability in this figure is an approximation of the probability that the pillars in this panel will survive without collapse to time.

The following conclusions are evident from these figures:

- As the pillar width increases, the safety factor increases and the life expectancy of pillars increases,
- Approximately 1,600 cases fail instantaneously (16%) and none of them survive permanently in Case 1. Therefore, the probability of survival curve in Case 1 is approximately 84% at the 'instant' of forming the panels and rapidly reduces with time and at six years, the survival probability is zero.
- In Case 2, during the first year or so after the formation of the panels only a few panels collapse, but later the rate of failure increases significantly and all pillars fail within approximately 10 years.
- In Case 3, the probability remains virtually unity up to almost five years; within 5 to 10 years only a few collapses (11% probability of survival) occur and then gradually reduces to 89%; after 10 years the probability remains unaltered indefinitely at 89%.

From these results and experience gained over the years, it is possible to conclude that using this methodology, it is possible to design layouts (especially beneath the critical surface structures) when there is a high probability that the pillars will remain *indefinitely* stable in areas where the pillars are prone to excessive spalling and collapse. For example, (i) a design safety factor of 2. 56 of a spalling pillar system would survive for an unlimited period of time with a probability of 0. 99 and (ii) for an increased probability of 0. 9999, a design safety factors of 2. 97 is required.

The histogram of critical safety factor utilised in these examples is shown in Figure 9.

Evaluation of Spalling Rates

Since an important assumption in the above calculations is the spalling rate, an estimate of the rate of spalling should be known. Figure 10 demonstrates the effect of spalling rate on the expected life of pillars using the above dimensions given for Case 2. In these examples, two spalling rates, 0. 2 m/year and 0. 1 m/year, were evaluated. It is evident from this figure that the spalling rate has a significant impact in determining the life and probability of

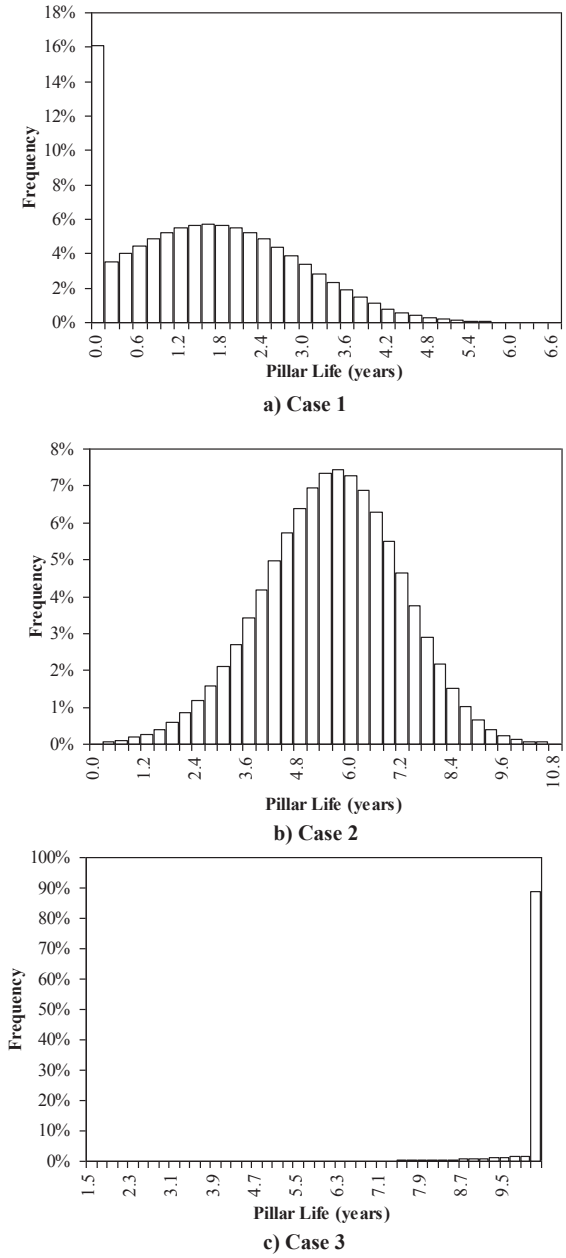

Figure 7. Histograms of pillar life for Cases 1, 2 and 3.

survival of coal pillars; the higher the spalling rate, the earlier the majority of pillars will collapse.

Salamon et al. (1998) evaluated 13 documented cases of collapse that have occurred in collieries mining the No. 3 Seam in the Vaal Basin. The aim of this evaluation was to estimate the rate of spalling which could have prevailed in the recorded cases and seemingly caused the collapse of the pillars.

The methodology adapted by Salamon et al. (1998) involved the adoption of the Monte Carlo method to create a large number of nominal safety factors as was done earlier in this paper. From these values, through the use of the relationship in Equation [32], a set of critical spalling depths was generated and stored as a vector, which

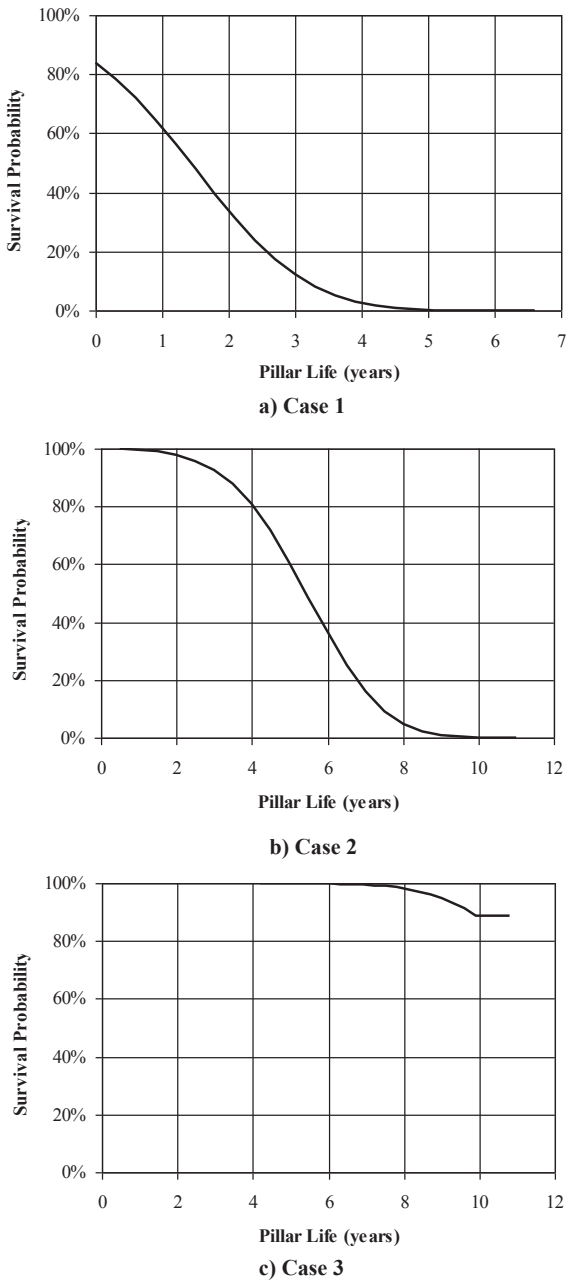

Figure 8. Survival probability and pillar life for Cases 1, 2 and 3.

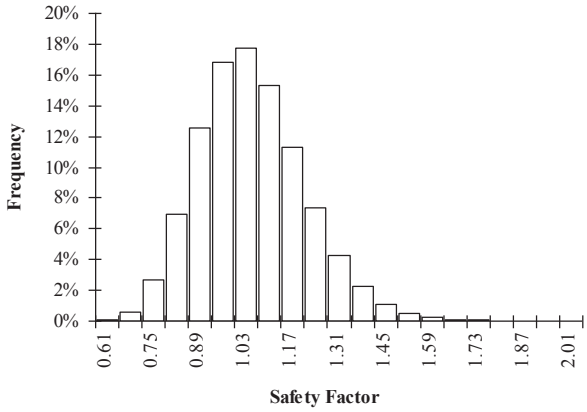

Figure 9. Histogram of critical safety factor.

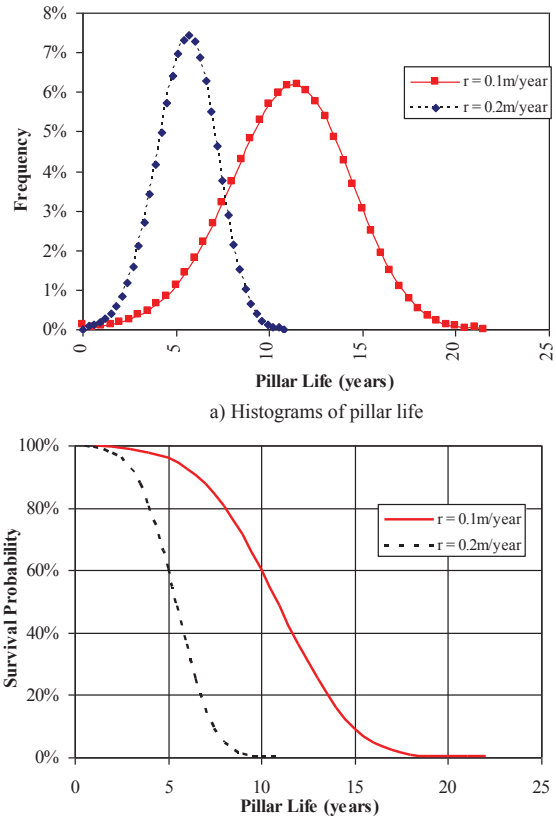

Figure 10. Effect of rate of spalling on the life expectancy of pillars.

was in turn sorted in ascending order. Using all the usable values of spalling depth, spalling rates were computed for each case and the distributions of spalling rates were obtained and averaged. This study estimated an average spalling rate of 0. 197m/year for the Vaal Basin. Considerably lower rates in the order of 0. 02–0. 07 m/year were also reported for the Witbank Coalfield (Madden and Canbulat, 1996).

Using the South African pillar collapse database, van der Merwe (2003) also conducted a study to establish the spalling rates of coal pillars by calculating the minimum pillar widths which corresponded to a minimum safety factor within the pillar collapse database. He concluded that (i) there is a strong inverse relationship between spalling rate and time, (ii) a less well developed relationship with the mining height and (iii) the average spalling rate decreases with observed lifetime.

In 2004, van der Merwe conducted a further investigation to verify the findings of his 2003 study. This study involved underground measurements of over 350 pillars at 13 sites on 6

mines. The results confirmed the pillar scaling rates inferred in 2003 within certain limits of confidence.

In order to obtain relevant spalling rates, the Australian collapse pillar database was evaluated using the pillar collapse database of Salamon et al. (1998). This database is summarised in Table 3. It is evident from this table that most of the Australian failed cases had relatively low safety factors at failure. The life spans of the collapsed cases were also relatively short with an average of 2. 68 years; 11 of 15 known cases collapsed within the first year of mining and the remaining four cases at life spans of 2 to 18 years. It is therefore concluded that the Australian database is not suitable for this methodology and that spalling rates cannot be calculated. It is recommended that a study into the spalling rates of coal pillars be conducted, which should involve measuring the amount of spalling in new and old panels. The methodology proposed by van der Merwe (2004) to measure the spalling rates can be used for this purpose.

estimation of time to failure of coal pillars, the principle of the critical safety factor and its probability density function used in the development of pillar strength formulae is a realistic concept.

One of the assumptions made in the development of the empirical pillar strength formulae was that the behaviour of pillars, for practical purposes, is not time dependent. It has however been reported in the past that coal pillars may fail due to spalling process that starts at the pillar edges and works its way into the pillar core. In order to overcome this weakness of the coal pillar strength formula developed in Australia (Salamon et al., 2006), an evaluation of the geometrical limits concept was conducted. This model is applicable in areas where the pillars are prone to failure due to spalling and was previously suggested by Salamon et al. (1998) and somewhat simplified by Canbulat and Ryder (2002) to estimate a maximum depth of spalling that would be used to determine if the spalling process would be arrested should the coal rubble around the pillar reach a critical height.

Table 3. Australian collapsed pillar cases (after Salamon et al. 1996).

Case	Depth (M)	Pillar Dimensions (m)	Pillar Height (m)	Bord Width 1 (m)	Age At Collapse (Yrs)	Nominal Safety Factor
FC1	140	15 x 15	5.0	7.0	2.0	1.18
FC2	80	7.5 x 18	7.0	7.0	0.5	0.87
FC3	80	6 x 7.5	3.0	7.0	0.5	1.02
FC4	135	7 x 20	5.0	6.0	0.5	0.74
FC5	100	10 x 10	6.0	5.5	1.0	1.03
FC6	120	10 x 20	3.2	7.0	18	1.53
FC7	95	3.5 x 12	1.75	6.2	unknown	1.02
FC8	70	9 x 9	6.0	8.0	0.25	0.94
FC9	250	15 x 27	3.0	5.0	0.5	0.76
FC10	115	10.5 x 22	5.0	8.0	0.25	1.07
FC11	145	11.3 x 22.5	7.0	6.3	4.0	0.80
FC12	336	13.5 x 28.5	3.0	6.3	0.5	0.93
FC13	185	21 x 21	4.9	6.1	unknown	1.39
FC14	240	22 x 22	4.9	6.1	unknown	1.12
FC15	152	25 x 30	9.2	5.5	10	0.66
SC1	75	8 x 8	4.5	6.5	1.0	1.14
SC2	58	3.6 x 54	2.7	7.3	1.0	1.44
SC3	170	20 x 20	2.45	55 x 70	0.25	1.43
FC16	170	8.2 x 32	2.8	8.5 x 8.0	unknown	0.98

CONCLUDING REMARKS AND RECOMMENDATIONS

The aim of this study was to evaluate the "Geometrical Limits" concept to provide the Australian coal mining industry with a tool to assess the long-term behaviour of pillars where they are prone to failure due to spalling of ribs.

A demonstration of the critical safety factor and the probability of failure concepts utilised in the original study of Salamon and Munro (1967) (and also the subsequent studies in Australia and South Africa) was also conducted using the stochastic modelling of hypothetical relative errors in strength and load. This simple demonstration indicated that for the purpose of this study and

Based on the examples given in this study, it is considered that despite its limitations, this method of calculating the life expectancy of pillars is reasonable and may be evaluated further. This will enable the designers to evaluate the long-term stability of pillars beneath critical surface structures. In order to take this method further, a detailed study into the pillar spalling rates in Australian coal mines is required.

An evaluation of the spalling rates in South Africa was conducted by Salamon et al. (1996). A pillar collapse database from the Vaal Basin was used in the analysis. The results indicated an average spalling rate of 0. 197 m/year. Considerably lower rates in the order of 0. 02–0. 07 m/year were also reported for the

Witbank Coalfield (Madden and Canbulat, 1996). A similar study was also conducted for the Australian pillar collapse database in this paper. The results revealed that the collapsed cases included in the Australian database of Salamon et al. (1996) were due to low nominal safety factors and there is no indication of that these pillars collapsed due to high levels of spalling. Therefore, a spalling rate for Australian mines could not be obtained.

ACKNOWLEDGEMENTS

Anglo American Metallurgical Coal is acknowledged with gratitude for the permission to publish this paper.

REFERENCES

Canbulat, I. and Ryder, J. A. 2002. Prediction of Surface Subsidence and Sinkholes. Proceedings of the SANIRE Symposium: Re-Defining Boundaries, Vereeniging.

Harr, M. E. (1987). Reliability-Based Design in Civil Engineering. McGraw-Hill Inc.

Madden, B. J. and Canbulat, I. (1996). Reassessment of Coal Pillar Design Procedures. Proceedings of the Safety in Mines Research Advisory Committee (SIMRAC) Symposium. Mintek, Johannesburg.

Madden, B. J. and Canbulat, I. (1997). Practical Design Considerations for Pillar Layouts in Coal Mines. Proceedings of the 1st Southern African Rock Engineering Symposium (SARES 97), Johannesburg, South Africa.

Salamon, M. D. G. (2003). Review of Initial Study on the Development of Seam-Specific Strength Formulae for South African Collieries. Unpublished study notes/personnel communication, Coaltech Project, Task 2. 16.

Salamon, M. D. G, Ozbay, M. U. and Madden, B. J. (1998). Life and Design of Bord and Pillar Workings Affected by Pillar Spalling. J. of S. Afri. Min. and Metall. *98*:135-145.

Salamon, M. D. G. (1982). Unpublished report to Wankie Colliery. Zimbabwe.

Salamon, M. D. G. and Munro, A. H. (1967). A Study of the Strength of Coal Pillars. J. of S. Afri. Min. and Metall. *68*(2):55-67.

Salamon, M. D. G. , Galvin, J. M. , Hocking, G. and Anderson, I. (1996). Coal Pillar Strength From Back-Calculation. Strata Control for Coal Mine Design, UNSW Final Project Report, No: RP 1/96, Joint Coal Board.

Salamon, M. D. G. , Canbulat, I. and Ryder, J. A. (2006). Seam-Specific Pillar Strength Formulae for South African Collieries. Proceedings of the 41st U. S. Rock Mechanics Symposium, Golden, CO.

van der Merwe, J. N. (2004). Verification of Pillar Life Prediction Method. J. of S. Afri. Min. and Metall. *93*:71–77.

van der Merwe, J. N. (2003). Predicting Coal Pillar Life in South Africa. J. of S. Afri. Min. and Metall. *103*:293–301.

van der Merwe, J. N. (1993). Revised Strength Factor for Coal in the Vaal Basin. J. of S. Afri. Min. and Metall. *104:*667–676.

Wagner, H. (1980). Pillar Design in Coal Mines. J. of S. Afri. Min. and Metall. *80*:37-45.

Pillar Design for Deep Cover Retreat Mining: ARMPS Version 6 (2010)

Chris Mark, Principal Mining Engineer
NIOSH Ground Control Branch
Pittsburgh, PA

ABSTRACT

In the wake of the Crandall Canyon mine disaster, the National Institute for Occupational Safety and Health (NIOSH) revisited the issue of pillar design for deep cover retreat mining. Studies conducted at 30 mines added more than 200 new case histories to the Analysis of Retreat Mining Pillar Stability (ARMPS) database. Extensive statistical analyses were supplemented with numerical modeling using Boundary Element and Finite Difference techniques.

The analysis focused on the development of a "pressure arch" loading model for ARMPS. A previous study, published in 2002, had found that pillar designs under deep cover could be successful with lower ARMPS stability factors. The current study concluded that the most likely explanation is that a pressure arch forms above a deep panel, transferring some of the load from the production pillars to the barrier pillars. The analysis showed that the statistical "best fit" pressure arch algorithm results in recommended pillar sizes that are very similar to those suggested by the 2002 guidelines. It represents a significant improvement, however, because:

- It provides a rational explanation for the observed success of smaller pillars at depth, and
- It recognizes the inherently greater stability of narrow panels at depth, and incorporates panel width into the design guidelines.

The revised loading model has been implemented in an updated version of the ARMPS computer program, called ARMPS Version 6 (2010). For most shallow cover situations, where the panel width exceeds the depth of cover, ARMPS Version 6 (2010) is identical to ARMPS 2002.

Other statistical analyses explored the effects of roof strength, coal strength, and geographic location on the likelihood of pillar design success. None of these factors was found to be highly significant. New guidelines for determining ARMPS input values for the depth of cover and the mining height are included as an appendix.

BACKGROUND

On August 6, 2007, a widespread pillar failure occurred at the Crandall Canyon mine near Price, Utah. Six miners working in the South Barrier section of the mine were presumed trapped by the coal bursts and mine collapse that accompanied the pillar failure. Rescue efforts were abandoned after three rescuers were killed in a second burst event ten days later.

At the time of the incident, the Crandall Canyon miners were engaged in retreat mining in the South Barrier section. With cover that exceeded 2,200 ft at its deepest point, these were some of the deepest pillar retreat operations ever attempted in the U.S.

The Mine Safety and Health Administration (MSHA) report on Crandall Canyon (Gates et al., 2008) emphasized the role of the flawed pillar design in the disaster. In the report's words, the "pillar dimensions were not compatible with the deep overburden and high abutment loading that existed in the South Barrier section," and as a result the "stress level exceeded the strength of a pillar or group of pillars near the pillar line, and that local failure initiated a rapid and widespread collapse that propagated outby through the large area of similar sized pillars."

Following the disaster, Congress asked NIOSH to study the safety of retreat room and pillar mining. As part of that study, NIOSH revisited the ARMPS methodology, with the goals of:

- Enlarging and updating the deep cover case history data base;
- Conducting statistical and other analyses to identify any potential improvements to the ARMPS program;
- Developing an enhanced version of the program reflecting the latest research findings.

ANALYSIS OF RETREAT MINING PILLAR STABILITY (ARMPS)

The original version of ARMPS was developed by NIOSH in the mid 1990's (Mark and Chase, 1997.) Its purpose was to help prevent three types of pillar failures:

- *Squeezes*, which are non-violent events that may take hours, days, or even weeks to develop. Squeezes are the most

common type of pillar failure, and they commonly cause roof instability, floor heave, and rib falls. Because they develop slowly, however, the affected area is usually abandoned before there are any injuries to miners.

- *Collapses*, which occur when a large number of overloaded pillars fail almost simultaneously, usually resulting in a destructive airblast. Most collapses in the U.S. have occurred under low cover (less than 500 ft), and they have been associated with the slender pillar remnants that have been left in worked-out gob areas after partial pillar recovery operations.
- *Bursts*, which can affect just a small portion of a single pillar, or may destroy many pillars at once. While bursts (sometimes referred to as "bumps" or "bounces") have many causes, and not all of them can be eliminated by pillar design, the likelihood of large bursts affecting multiple pillars can be greatly reduced when properly sized pillars are used.

Like most pillar design methodologies, ARMPS consists of three basic steps:

- Estimate the applied loads, including any abutment loads;
- Estimate the load bearing capacity of the coal pillars;
- Compare the load to the capacity, and employ engineering criteria to determine whether the design is adequate.

To estimate the development loads, ARMPS starts with the "tributary area" approximation, which assumes that each pillar supports the rock directly above it all the way to the surface. The "abutment angle" concept is used to estimate the loads transferred to the pillars during the various stages of the pillar extraction process (Figure 1). To calculate the strength of the pillars within the "Active Mining Zone" (AMZ) as shown in Figure 2, ARMPS uses the Mark-Bieniawski formula (Mark and Chase, 1997). Each pillar's load bearing capacity is simply its strength multiplied by its load bearing area. A "Stability Factor" (SF) is then calculated by dividing the total load-bearing capacity of all the pillars within the AMZ by the total load. ARMPS also calculates a SF for each barrier pillar that is part of the design, and if the barrier pillars are too small, transfers additional loads to the AMZ. ARMPS is flexible enough to consider such design variations as angled crosscuts or slab cuts into the barrier pillars (Figure 2).

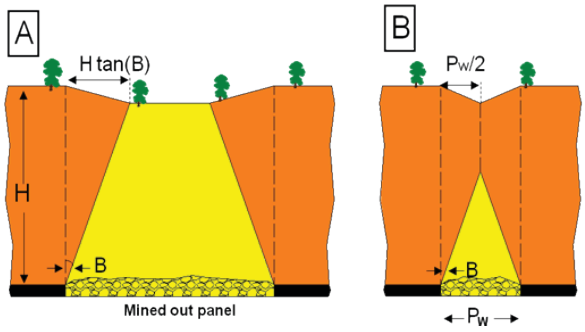

Figure 1. The "abutment angle" concept used to estimate loads in ARMPS. A: Supercritical panel. B: Subcritical panel.

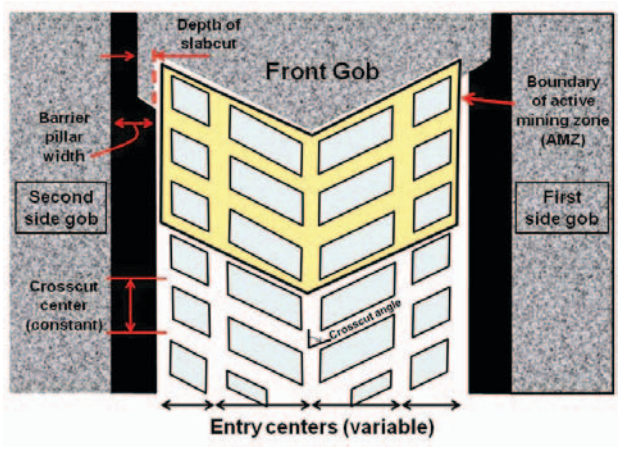

Figure 2. Mining geometry parameters used in the ARMPS program.

The power of ARMPS is not derived from the accuracy of its calculations, but rather from the large data base of retreat mining case histories that it has been calibrated against. Statistical analysis has been used to help derive guidelines for selecting an appropriate ARMPS SF for design. The empirical, case history approach employed by ARMPS is similar to the quantitative statistical techniques used in other scientific disciplines, such as epidemiology or economics. In the recent past, statistical analysis of large ground control case history data bases has led to the development of methods for longwall pillar design (Mark et al., 1994; Colwell et al., 1999), roof bolt selection (Mark et al., 2001), the design of rib support (Colwell and Mark, 2005), and multiple seam mine planning guidelines (Mark et al., 2007). Because they are firmly grounded in real world mining experience, empirical methods can also provide valuable insights into the performance of very complex rock mechanics systems.

The original ARMPS data base consisted of approximately 150 case histories, representing a broad range of cover depths (Mark and Chase, 1997). About half of these were considered "successful" because the entire panel was recovered without significant ground control incident. Analysis indicated that when the depth of cover was less than 650 ft, an ARMPS SF of about 1.5 was a reasonable starting point. However, for deeper cover cases, two conclusions were drawn:

- Many panels with an ARMPS SF well below 1.5 were successful, and;
- No single ARMPS SF was able to separate the successful from the unsuccessful cases.

Accordingly, a follow-up study was conducted which focused on deep cover pillar recovery (Chase et al., 2002). During this study, an additional 100 case histories were collected from mines in Central Appalachia and the West where the depth of cover exceeded 750 ft. The analysis indicated that squeezes were the most likely failure mode when the depth of cover was less than 1,250 ft, but bursts predominated in the deeper cover cases. Design guidelines, including suggestions for barrier pillars to isolate active panels from nearby gobs in burst prone ground, were also presented (Table 1, Figure 3a and Figure 3b).

Table 1. Recommended ARMPS Stability Factors (Chase et al., 2002).

	Depth of Cover (H)	Weak and Intermediate Strength Roof	Strong Roof
ARMPS SF	H<650 ft	1.5	1.5
	650 ft ≤ H ≤ 1,250 ft	1.5 - [H-650] / 1000	1.4 - [H-650] / 1000
	1,250 ft ≤ H ≤ 2,000 ft	0.9	0.8
Barrier Pillar SF	H > 1,000 ft	≥ 2.0	≥ 1.5* (≥ 2.0**)
	H < 1,000 ft	No Recommendation	

*Non-burst-prone ground

**Burst-prone ground

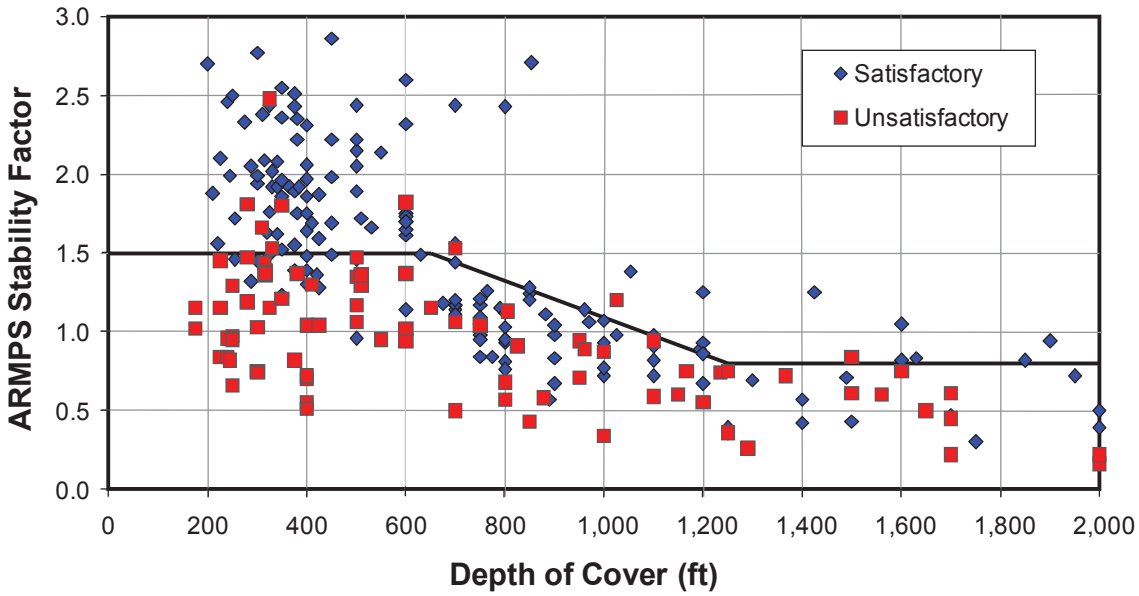

Figure 3A. Recommended ARMPS production pillar SF from 2002 deep cover study (see also Table 1).

Figure 3a shows that a central finding of the 2002 study was that the required ARMPS SF for the production pillars declined as the depth of cover increased, from 1.5 at 650 ft of cover to 0.8 at 1,250 ft of cover (for strong roof). While acceptable from a practical standpoint, this "depth adjusted recommended SF" raised some theoretical issues. The two most likely explanations for the depth adjustment are that:

- The ***pillar strength*** actually increases with depth, so that the strength formula used in ARMPS underestimates the strength at greater depths, or;
- The ***pillar loading*** model used in ARMPS actually overestimates the load applied to the pillars within the AMZ at greater depths.

While these two explanations are not mutually exclusive, there are several reasons to believe that the second is more likely. Most importantly, the reduction in the recommended SF with depth was only found for the production pillars, not for barrier pillars. As Table 1 shows, the recommended SF for barrier pillars was 1.5 or 2.0, even as the recommended production pillar SF was less than 1.0. There is no reason to believe that the strength of the smaller production pillars increases with depth, while the strength of the larger barrier pillars is unaffected. In addition, the analysis also indicated that narrow panels were more likely to be successful than wider ones, though the effect was only statistically significant at the 75% confidence level. This "panel width" effect would be expected if the loading on the production pillars was being reduced by the formation of a "pressure arch."

THE PRESSURE ARCH MODEL OF PILLAR LOADING

The pressure arch concept is illustrated in Figure 4a and Figure 4b. The phenomenon was first observed in coal mines in the UK during the 1940s, and subsequently popularized in the U.S. by Professor C.T. Holland (1973). According to Holland, "If the pressure arch is supported on both flanks by broad abutment or

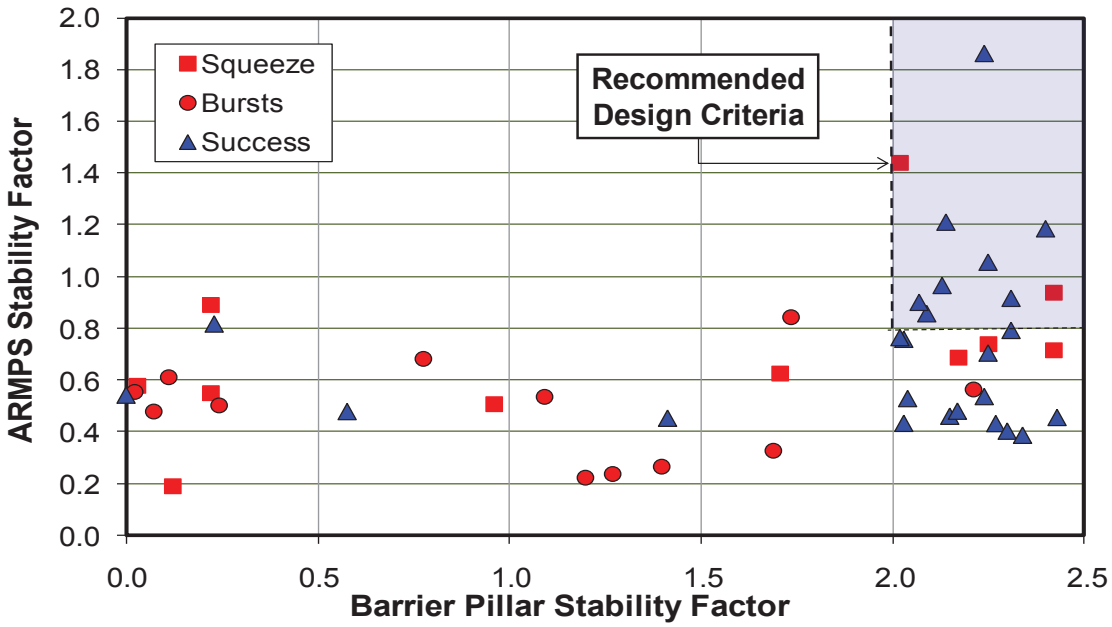

Figure 3B. Recommended ARMPS production and barrier pillar SF from 2002 for deep cover case only (see Table 1). (Note that a graphical technique called "jittering" has been used to create figure 3B. There are a number of cases in which no barrier pillar was used, and these were randomly assigned barrier pillar SF between 0 and 0.2. Similarly, when the barrier pillars were very large, SF between 2.0 and 2.5 were randomly assigned.).

barrier pillars, and entries are developed within the pressure arch using comparatively narrow pillars that can yield, the load that formerly rested on these pillars will, in large part, be transferred to the abutments."

The clearest evidence of the formation of pressure arch loading situations is the widespread use of yield pillars in the longwall mines, particularly in Utah and Alabama. When 20- or 30-ft-wide yield pillars are developed under 2,000 ft of cover in these mines, the pillars are clearly not carrying the tributary area overburden load all the way to the surface. In Alabama, 2-, 3-, and 4-entry yield pillar systems have been employed routinely (Carr, 1992). In Kentucky, an experimental 5-entry yield pillar system was developed successfully, even though as much as 5 in of entry convergence occurred (Mark and Barton, 1988).

Some multiple seam interaction cases also strongly imply the existence of pressure arches. In at least three cases, interactions have been documented where the interburden thickness was at least 75 ft, and the previous mining was development only (Heasley and Chekan, 1999; Newman, 2002; Gauna and Phillipson, 2008). In each of the three cases, a serious interaction occurred directly above or beneath a larger pillar that was surrounded by smaller ones. Clearly, the smaller pillars had transferred a considerable portion of their load to the larger one.

While it is easy to conceptualize how a pressure arch can be formed above yielded pillars, it might not be expected when full-size production pillars are involved. For loads to be transferred from the pillars to the adjacent abutments, the overburden must be fairly rigid, and there must be a "stiffness contrast" between the

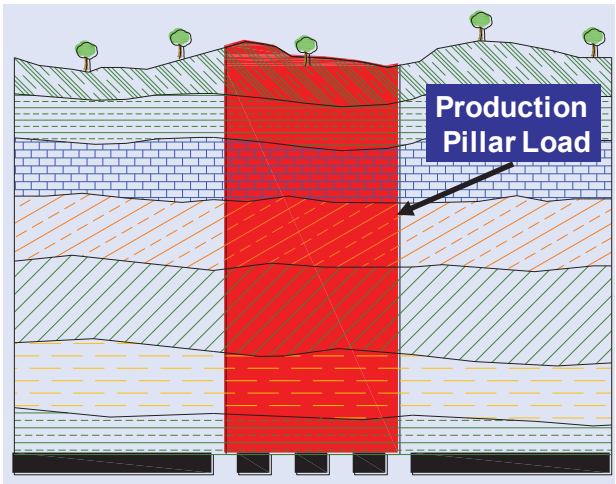

Figure 4A. Tributary area loading models for development mining.

pillars and the abutments. The requirement of "rigid" overburden is clearly met in the Central Appalachian and most Western coalfields, where massive sandstones often constitute 25 to 50% of the rock between the coal and the surface. But it is not evident that typical production pillars with width-to-height ratios (w/h) of 5, 10, and even greater are much less stiff than barrier pillars. Furthermore, if the pillars are assumed to behave in a linear-elastic manner, even pillars within narrow panels might carry loads near the tributary area approximation, so long as the extraction ratio was low (Coates, 1967).

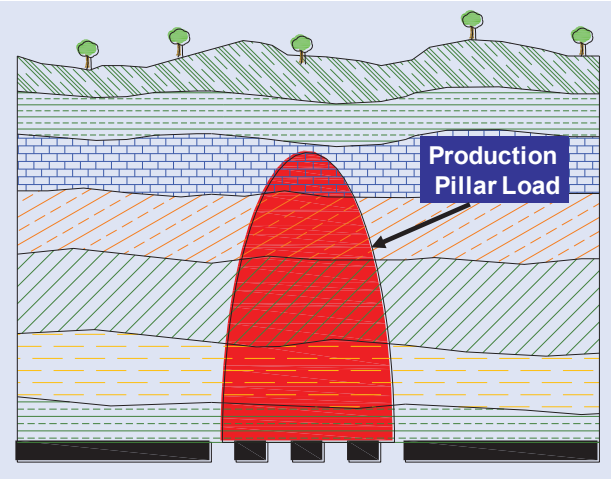

Figure 4B. Pressure arch loading models for development mining.

Nonetheless, the trends within the ARMPS deep cover data base strongly imply that pressure arch behavior is fairly common even with typical production pillars. A recent Australian study similarly concluded that the load carried by many main heading panels in the deep mines of the Southern NSW coalfields is reduced due to pressure arch behavior (Hill and Canbulat, 2008). These main heading panels typically consist of 5 entries, are about 350 ft wide, and are about 1,500 ft deep. The analysis indicated that the pillar loading in such panels might be less than half of the tributary area prediction.

One explanation is that coal pillars with a w/h in excess of 4 do not, in general, fail in a "brittle" manner that causes them to lose their entire load bearing capacity. Instead, they may be strain-softening, elastic plastic, or even strain hardening (Mark, 2006). Indeed, such pillars may soften considerably even before reaching their peak strength. For example, Esterhuizen and Mark (2009) concluded that a coal pillar with w/h = 6 would undergo only 0.25% vertical strain at 50% of its peak capacity, but the strain would be about 1% at peak load (Figure 5).

Underground along the pillar perimeter, it is not unusual to see several inches of sliding on bedding planes within the pillar or at the roof-coal interface. Such deformations indicate that the pillars may have undergone significant vertical deformations without losing load bearing capacity or adversely affecting roof stability. Such deformations could be enough to allow the formation of a pressure arch.

To help explore this issue further, two series of numerical model studies were conducted. In the first, the software package LaModel was used to model a series of 29 deep cover pillar retreat case studies taken from the ARMPS data base (Heasley et al., 2010). The depth of cover for the case study sites ranged from 750 to 1,500 ft, with an average of 1,035 ft. The panel widths averaged about 425 ft, so the depth-to-width ratio averaged about 2.5. Care was taken to match the pillar strengths in LaModel to those used in ARMPS. However, the yielding coal elements used in LaModel allow the pillars to soften in a realistic manner as they become more heavily loaded.

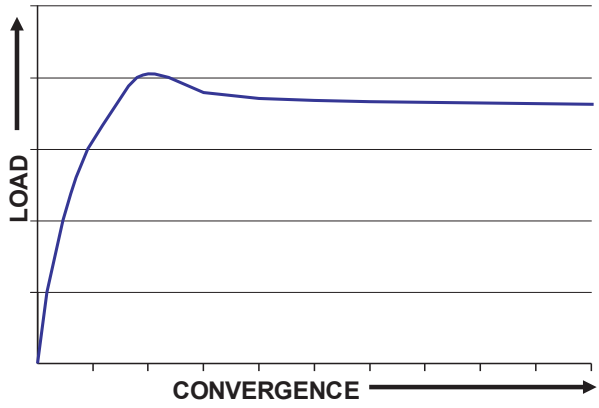

Figure 5. Load-convergence curve for a single modeled coal pillar with width-to-height ratio of 6.0 (after Esterhuizen and Mark, 2009).

The analysis showed that, on average, the loads that LaModel applied to the AMZ were about 25% lower than the loads calculated by ARMPS. Moreover, the proportion of the load that transferred away from the AMZ was highly dependent on the panel width. With the narrowest modeled panels, more than 50% of the load was transferred away from the AMZ.

The second study employed the three-dimensional finite difference code FLAC. The advantage of FLAC is that it can explicitly model the complexity of the geometry, geology, and rock failure associated with pillar retreat mining. In order to model the mined areas without sacrificing the important local details of pillar, roof and floor response, the method of "equivalent pillar elements" was employed (Esterhuizen and Mark, 2009). The equivalent pillar elements incorporate the effect of bedding plane interfaces and the effects of any local floor heave or roof damage. The overburden was modeled using the strain-softening ubiquitous joint elements that can simulate both bedding plane shearing and the failure of intact roof strata.

The FLAC models showed that the development of the pressure arch depends primarily on two factors:

- **Overburden properties:** Thick, strong, massive rock layers enhance the development of a pressure arch.
- **Mining geometry:** For a given depth of cover, narrower panels and deeper cover both assist the formation of a pressure arch.

With weak overburden materials, the models showed that failure is more likely to develop within the overlying rock layers. When this occurred, the overburden acted almost as a "dead weight" on the pillars, and the modeled FLAC loads approximately matched the tributary area loads. Strong overburden formed a more successful arch, particularly when the cover was deep. In one example, the model indicated that the ARMPS calculations overestimated the development load by 9% and the load during

retreat mining by 28% (Esterhuizen et al., 2010; Esterhuizen and Mark, 2009)[1].

In the Western and the Central Appalachian coalfields, where deep cover pillar recovery is practiced in the U.S. (Mark, 2009), the overburden almost always includes several thick, strong, and stiff rock units. As a result, the overburden properties apparently do not vary enough from mine to mine to have a significant effect on ground conditions (Mark et al., 2007). Therefore, from a practical standpoint, it makes sense to focus on mining geometry, in particular the ratio between the depth of cover and the panel width (H/Pw).

One of the goals of the current research was to explore different pressure arch loading functions, and to determine whether any could provide better estimates of the likelihood of success of deep cover pillar designs. This was accomplished using the ARMPS 2010 case history data base. Before discussing the development of the pressure arch loading function, however, it is necessary to describe the data base in some detail.

DEVELOPMENT OF THE ARMPS 2010 DATABASE

As part of the Congressionally-mandated study, NIOSH visited a total of 30 mines located in the Central Appalachian and Western coalfields (Figure 6a and Figure 6b). The mines were initially identified as "deep cover" (depth > 1,000 ft) by the MSHA Roof Control Supervisors in each District. The key goal of each mine visit was to develop a history of retreat mining experience for the operation. Care was taken to collect successful case histories as well as unsuccessful ones. Mine maps, showing the depth of cover, past workings above and/or below, and other important features, were reviewed with experienced mine officials who had first-hand experience of the conditions encountered. The officials also provided their best recollection of the support used and other relevant information. These discussions resulted in a preliminary list of case histories for that mine.

Underground investigations were also conducted at 17 of these mines. It was seldom possible to access more than a few of the historical mining sites because many were in sealed or otherwise inaccessible areas. However, underground observations provided a sample of the ground conditions associated with that mine. The underground visits also provided raw data on roof geology and strength for determination of the Coal Mine Roof Rating (CMRR).

The mine officials were also asked to provide Autocad files with mine maps, together with exploratory bore logs. These data were subsequently analyzed by NIOSH to complete the data base.

Cases included in the older NIOSH data base were also re-evaluated for inclusion in the 2010 data base. The field notes, maps, and other documentation were reviewed to ensure that the data were accurate and met current standards. In addition, the data

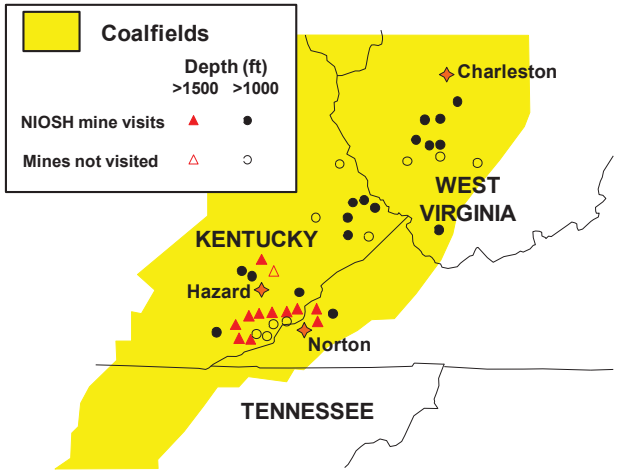

Figure 6A. Location of the U.S. deep cover pillar recovery mines in 2008. Mines visited by NIOSH are noted (Central Appalachian deep cover retreat mines).

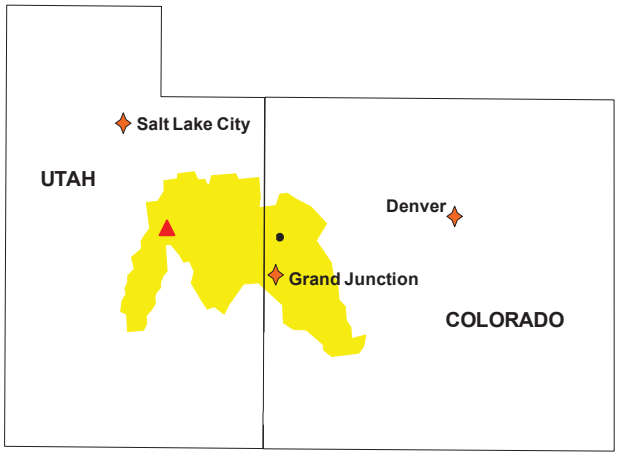

Figure 6B. Location of the US deep cover pillar recovery mines in 2008. Mines visited by NIOSH are noted (Western deep cover retreat mines).

on some cases involving multi-pillar bursts were obtained from reports prepared by others.

Parameters in the Database

In any empirical study, the most important parameter is the "outcome" for each case history. The deep cover retreat study employed a combination of reported conditions and evidence from the mine map to rate the outcome. In general, a case history was considered a "success" only if the map showed that all of the pillars in the panel were recovered completely, leaving only planned bleeder pillars, fenders, and stumps. If, on the other hand, the map showed that under deeper cover several rows of pillars were abandoned, then the knowledgeable mine officials were asked about the conditions there. If the description clearly implied a pillar failure had occurred, the case would be designated as "unsuccessful." If water, a steep dip (swag), too much rock

[1] The pressure arch concept is actually closely related to another fundamental rock mechanics hypothesis, the Ground Response Curve (GRC). The GRC concept as applied to pillars was first developed by Salamon in 1970, and further developed by Zipf (1999). Esterhuizen et al (2010) provide a detailed discussion of the concept and its application to pillar design.

in the coal, or some other non-ground control circumstance was responsible, then the case was not included in the data base.

It is important to note that the ARMPS data base contains only a very small fraction of the total number of successful retreat mining pillar designs. The reason is that the NIOSH data collection effort has always focused on the most extreme case histories. These include the cases that are known to have failed, and those successful cases that had similar depth of cover and pillar dimensions of the failed cases. Mines working under deep cover or with histories of problems with pillar design have been particularly sought out for study. Moreover, each panel is evaluated at its deepest point, which further biases the data towards lower stability factors. The result is that for every successful case that is included in the data base, there are many more with higher ARMPS stability factors that are not included.

In addition to the outcome variable, each case history also includes a number of geometric variables that are used to calculate the ARMPS SF. Most of these, such as the pillar dimensions, entry widths, and widths of worked-out "gob" areas are self-evident. The "entry height" and the "depth of cover" are often less straight forward. Some new guidelines for determining these two parameters were developed for this study, and they are described in Appendix A. Figure 7 plots the distribution of H/Pw ratios within the ARMPS data base. Figure 8 shows that the median panel width is 420 ft, with 540 ft and 320 ft panel width at the 75th and 25th percentiles, respectively.

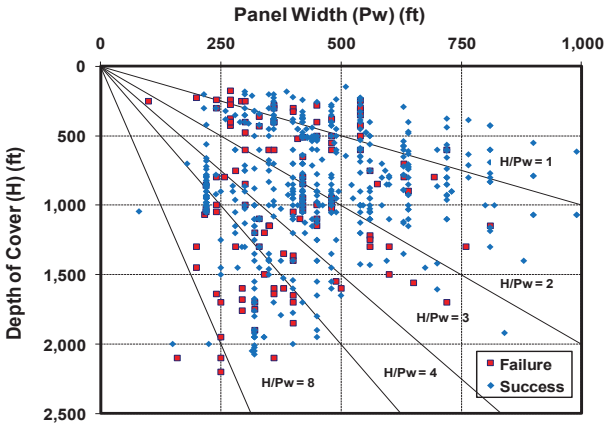

Figure 7. Range of depth-to-panel width ratios in the ARMPS 2010 data base.

Each case history in the data base is also defined by several "explanatory" or "independent" variables that were thought might possibly contribute to the outcome. Values for some of these variables were easily calculated, including the H/Pw, and the pillar width-to-height ratio (w/h). Others, including the roof strength, the coal strength, and the mining region required more effort.

The competence of the immediate roof above the workings was initially measured using the Coal Mine Roof Rating (CMRR). The CMRR was normally determined underground, and then checked against the available core log and other geologic data. In many cases, however, the mine was closed or the relevant areas were otherwise inaccessible, so it was not possible to determine a precise

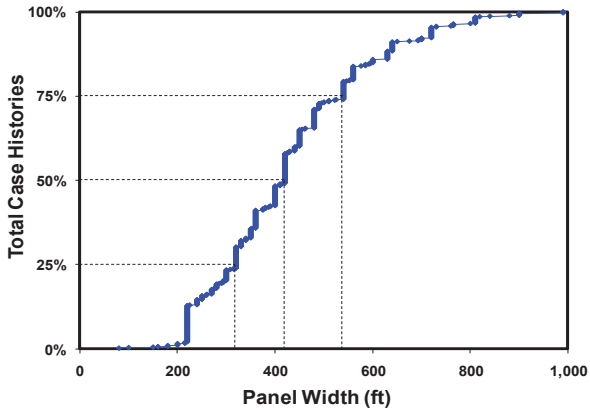

Figure 8. Cumulative distribution of panel widths in the ARMPS 2010 data base.

CMRR. Therefore, a simpler roof strength rating scale (RS) was devised as follows:

- Strong Roof (RS=5): CMRR greater than 63
- Moderate-Strong Roof (RS=4): CMRR between 53 and 63
- Moderate Roof (RS=3): CMRR between 45 and 53
- Moderate Weak Roof (RS=2): CMRR between 38 and 45
- Weak Roof (RS=1): CMRR less than 38

Past empirical studies have indicated that the coal strength measured in the laboratory does not influence the strength of full-scale coal pillars (Mark and Barton, 1996; Galvin et al., 1999). Nonetheless, two coal strength parameters were included in the database. Data on the uniaxial compressive strength (UCS) from laboratory testing was obtained for 38 seams from the NIOSH database. These data covered 73% of the cases in the ARMPS data base. The Hardgrove Index (HGI) has been shown to correlate with the UCS (Mark and Barton, 1996), and it is almost universally available. For this study, HGI values were obtained by seam and county for nearly every case history. In just a handful of cases, it was necessary to infer the HGI from the values available for other seams in the same county.

Finally, each case history was assigned to a "region" based on its location and seam. The goal was to determine if there are regional trends in pillar strength, due to some unknown geologic or stress factors that may be acting at a regional scale. Dummy variables[2] were used in the analysis of regional trends.

Statistical Analysis

The final 2010 ARMPS data base includes 692 case histories from 127 different coal mines. The cases are from 42 counties in 10 states, covering all the U.S. coalfields. A total of 67 different coal seams are represented. The two largest groups of case histories are from the Cumberland coalfields of Harlan County, KY and Wise County, VA, and the Kanawha/Logan/Mingo Coalfields of southern WV. About 90 cases, or 13% of the total, are from UT and CO.

2 "Dummy" is a statistical term used to describe a variable that can only have a value of 1 or 0. For example, the dummy variable "Utah" takes on a value of 1 if the case history is from Utah, and 0 otherwise.

The sources of the case histories are as follows:

- 128 from the original 1997 ARMPS data base
- 122 from the 2002 deep cover ARMPS data base
- 152 from the Analysis of Multiple Seam Stability (AMSS) data base (Mark et al., 2007)
- 272 collected during this study
- 18 new cases from the literature

Of the 692 cases in the data base, the conditions in 42 of them were considered "borderline," and these were excluded from the analysis. An additional 10 failed cases were excluded because the problems were clearly attributable to floor heave rather than pillar failure or bursting. As a result, the analysis was based on 640 cases histories.

Prior to the regression analysis, the database was evaluated using the existing deep cover ARMPS design criteria. As shown in Figure 9a and Figure 9b, the results were very similar to those obtained by Chase et al. in 2002:

- Of the 520 successful cases, 318 (61%) met or exceeded the suggested design criteria, while 202 plotted as "false positives" meaning they had ARMPS SF below the recommended design criteria. For the 121 unsuccessful cases, only 21 plotted as "false negatives" that exceeded the design criteria, while 99 of the unsuccessful cases (82%), including all of the multi-pillar burst and massive collapse cases, properly plotted as not meeting design criteria.
- A total of 138 cases involved the extraction of a panel adjacent to a previously mined panel at a depth of 1,000 ft or greater. Fifty-six of these multi-panel retreat cases employed barrier pillars (BP) with a BP SF>1.5, just 10% of which were failures. For the 72 cases where the BP SF< 1.5, 47% were failures (see Figure 9b).
- At depths greater than 1,500 ft, 16 of the 20 failures are bursts, while only 4 were squeezes. Between 1,000 and 1,500 ft the proportions are nearly reversed, with 24 squeezes and 4 bursts (Figure 9a).

The statistical analysis employed the technique of logistic regression (LR). LR is the most common multivariate statistical technique when the outcome variable is binary (i.e., there are two possible outcomes, as "success" or "failure"). The goal of LR is to develop an equation that can predict the "outcome" using a combination of the explanatory variables. To compare the goodness-of-fit of different models, logistic regression employs the "Receiver Operating Characteristic" (ROC). The ROC is analogous to the R-squared parameter in linear regression (Hosmer and Lemeshow, 2000). An ROC value of 1.0 means that the model achieves perfect discrimination between the two possible outcomes. Further details on LR modeling and its application to ground control research can be found in Mark et al. (2007).

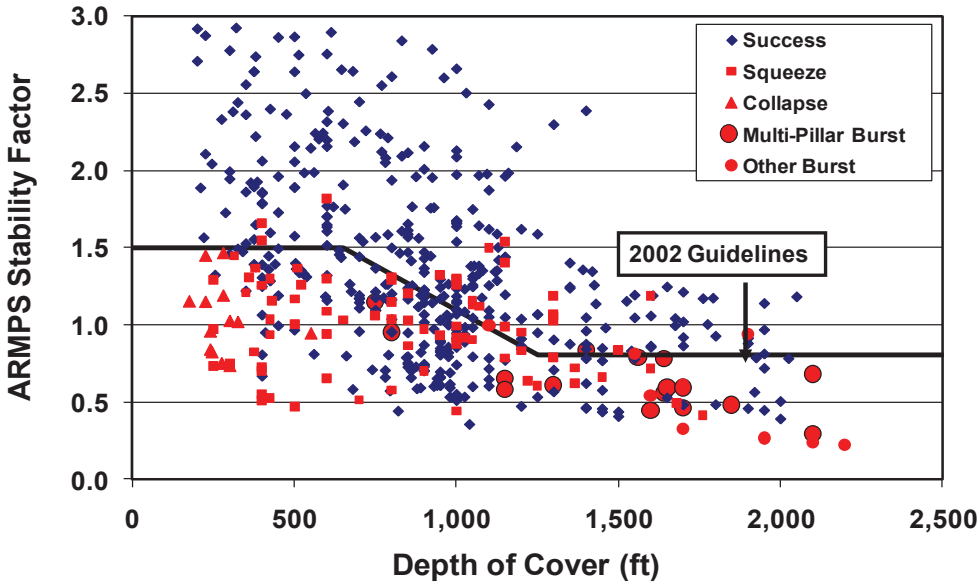

Figure 9A. The 2010 ARMPS deep cover data base, showing the recommended ARMPS production pillar SF from the 2002 deep cover study (compare with figure 3).

The cases were weighted for the statistical analysis because some mines provided a large number of case histories, while others provided only a few. To fairly represent all these cases, without allowing the data base to be overwhelmed by a few mines that contributed many cases, the following equation was used:

$$case\ weight = \frac{1}{\sqrt{N_m}} \quad (1)$$

where: N_m = the total number of cases from this mine.

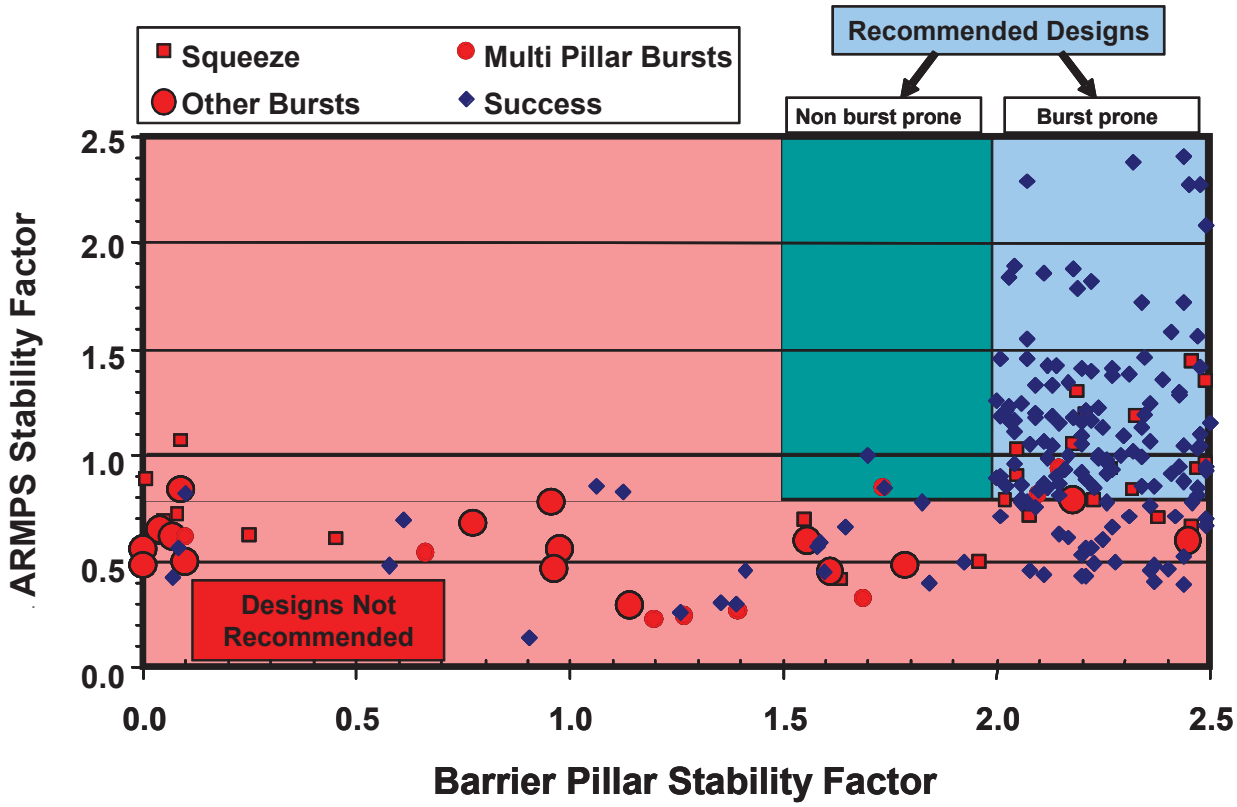

Figure 9B. The 2010 ARMPS Deep Cover data base, showing the recommended ARMPS production and barrier pillar SF from 2002 deep cover study (Jittering was used to present the barrier pillar SFs) (compare with figure 3).

In other words, the more cases there were from an individual mine, the smaller the weight of each individual case, but the greater the weight of the mine's total experience. In addition, because there were approximately four times as many successes than failures in the data base, the failures were each given a statistical weighting of 4.0.

DEVELOPMENT OF THE ARMPS 2010 SUGGESTED DESIGN CRITERIA

The first series of logistic regression analyses were conducted using the original ARMPS SF calculation. Some results are:

- When the whole data set was analyzed, in addition to the *ARMPS SF*, either the *depth of cover* or the *H/Pw ratio* was also significant at greater than the 98% confidence level. The ROC for these models is approximately 0.78 (see Appendix B, Tab. B1).
- When only the shallow cover (depth < 650 ft) subset of the data was analyzed, the only statistically significant variable was the *ARMPS SF*, and the ROC is 0.93.
- When just the deeper cover (depth > 650 ft) data is analyzed, the *ARMPS SF* and the *barrier pillar SF* are highly significant. The ROC is only 0.72, however.

The next phase of the analysis investigated the performance of different pressure arch loading models. In each model, the "Pressure Arch Loading Factor" (F_{pa}) was used to estimate the percent of the load that would be applied to AMZ. The procedure for implementing the pressure arch loading model is as follows:

1. The panel geometry is checked to see if a pressure arch is formed. If the H/Pw does not exceed the minimum threshold (which varied depending on the model), then the traditional tributary area loading is assumed to apply. The threshold for the implementation of the pressure arch was typically a H/Pw ratio of about 1.0.
2. If the H/Pw is such that a pressure arch is formed, then the loads applied to the AMZ are initially reduced by the F_{pa}. For example, if the F_{pa}=0.8, then the initial AMZ loads are reduced by 20%, and the excess "pressure arch loads" that are removed from the AMZ are applied to the barrier pillars.
3. If the barrier pillars are too small to carry all the loads that are applied to them, then the pressure arch loads are transferred back to the AMZ.

Figure 10a and Figure 10b shows conceptually how the process works.

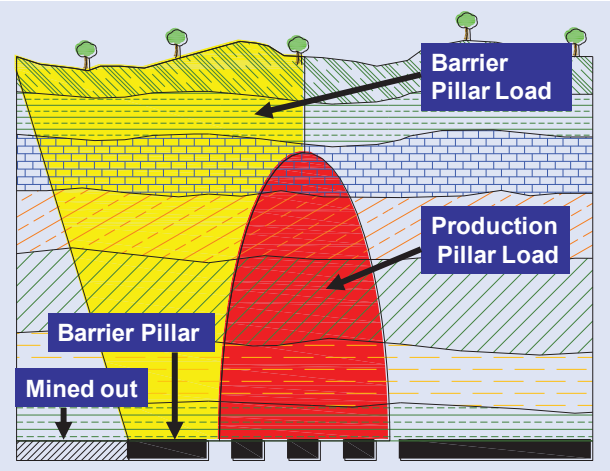

Figure 10A. Implementation of pressure arch loadings in ARMPS. Transfer of pressure arch loads from the production pillars to the barrier pillar.

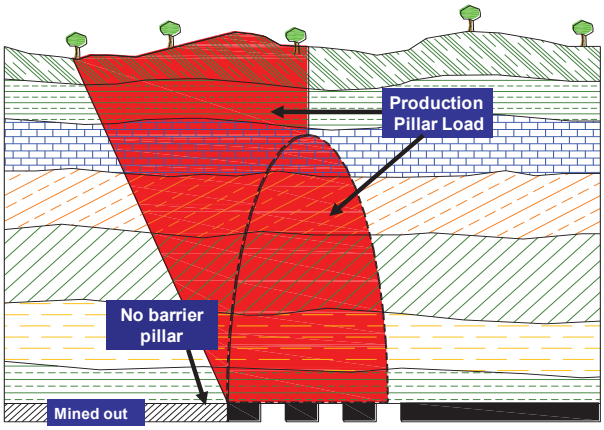

Figure 10B. Implementation of pressure arch loadings in ARMPS. Transfer of pressure arch loads back to the production pillars takes place if the barrier is inadequate or removed completely.

In each model, F_{pa} is a function of the H/Pw ratio. Three different types of models were tested: An ellipse, a linear model, and a logarithmic model. Different versions of each of these models were employed, and statistical analysis was used to determine which did the best job of distinguishing the successes from the failures in the database. The analysis showed that the logarithmic model, which shifts more load to the barriers at smaller depth-to-panel width ratios, gave the best results. The final, "best fit" formula for the pressure arch loading factor (F_{pa}) was:

$$F_{pa} = 1 - 0.28\left[\ln\left(\frac{H}{pw}\right)\right] \qquad (2)$$

where H/Pw > 1.0. Equation 2 is illustrated in Figure 11.

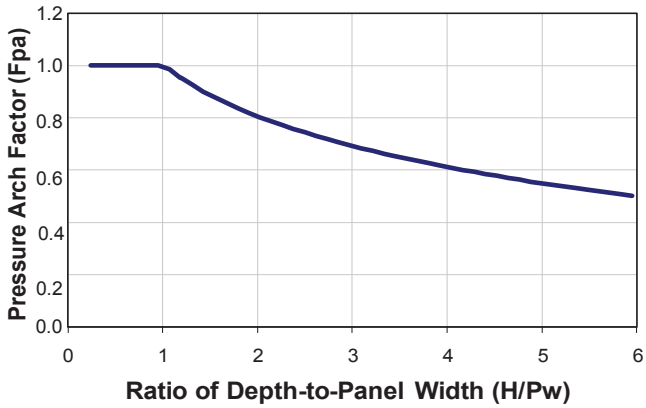

Figure 11. The final pressure arch loading function obtained from the statistical analysis (equation 2). The Pressure Arch Factor (Fpa) expresses the pillar loading as a percent of the full load if no pressure arch was formed.

The best threshold for implementing the pressure arch loading function was found to be when the depth of cover exceeds the panel width plus 80 ft.

Figure 12 shows the ARMPS data base using the new pressure arch loading model to calculate the ARMPS SF_{2010}. It can be seen that the reduction in the suggested SF, that was so evident when the ARMPS 2002 loading model was employed (Figures 3a and 9a), has been eliminated. Using the criterion of ARMPS SF_{2010} = 1.5 regardless of depth, a discrimination between successes and failures is achieved that is almost identical to that obtained with the more complicated Chase et al. (2002) criteria (39% "false positives" and 18% "false negatives"). Moreover, a single design criterion of SF = 1.5 is now employed for both the barrier pillars and the production pillars. These suggested design guidelines are shown in Table 2.

Table 2. ARMPS 2010 suggested design criteria.

Depth of Cover (ft)	ARMPS SF	Barrier Pillar SF
<650	1.5	No recommendation
>650	1.5	1.5

Logistic regression of the complete data set, using just the *ARMPS* SF_{2010} as the only predictor variable, achieved the same ROC of 0.78 as the model that contained the two parameters *ARMPS* SF_{2010} and *depth of cover* (Appendix B, Tab. B2). The pressure arch loading model has almost no effect on the analysis of the shallow cover cases, because most of them have relatively small H/Pw ratios (compare Figures 12 to 9a).

For the deep cover cases, the *barrier pillar SF* is still highly significant, and the ROC of the model with it and the new ARMPS SF_{2010} is 0.74. Figure 13a shows the deep cover case histories in

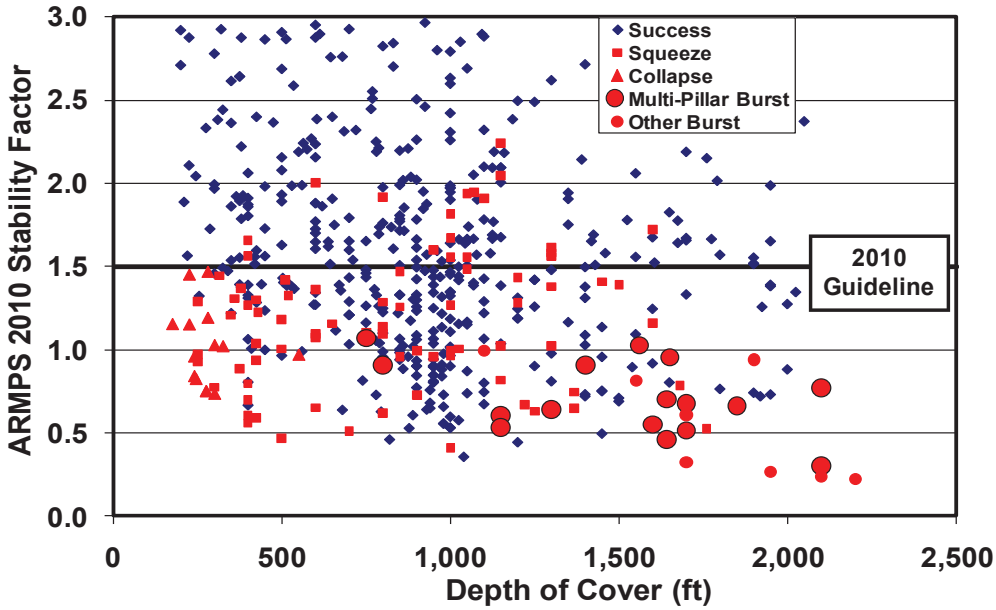

Figure 12. ARMPS 2010 case history data base, showing the recommended ARMPS 2010 SF of 1.5 for production pillars (A SF of 1.5 is also recommended for barrier pillars – see Table 2).

which the barrier pillar SF was less than 1.5, and Figure 13b shows those where the BP SF exceeded 1.5. The following observations can be made about the inadequate barrier pillar cases shown in Figure 13a:

- There are very few cases, successful or unsuccessful, where the production pillar ARMPS SF_{2010} exceeded 1.5.
- Overall, about 1/3 of the cases are failures, including 14 multi-pillar bursts.
- Of the 33 cases where the depth exceeds 1,100 ft, 26 (79%) are failures.

Conversely, Figure 13b shows that when deep cover panels are adequately shielded from side abutment loads,[3] the overall likelihood of success is greatly increased (approximately 90% of the cases are successes). Moreover, there are only two multi-pillar burst cases, both with low production pillar ARMPS SF values. Therefore, it seems that alternative suggested design critieria are justified as shown in Table 3. To provide added assurance that the pressure arch is functioning effectively, it is recommended that these alternative criteria only be used where the panel width is less than 425 ft, and where the barrier pillar has been enhanced by increasing its SF to at least 2.0.

The statistical analyses also explored the effects of the other explanatory parameters. Neither the *Roof Strength,* nor either of the two measures of coal strength, *UCS* or *HGI*, was statistically significant in any of the models tested. The results of the regional analysis, presented in Tab. B3, indicate that the apparent pillar strengths in four regions: Harlan/Wise, Kanawha/Logan/Mingo, Utah, and Colorado, are statistically nearly identical. These four regions include almost 60% of the case histories in the data base. Two other regions, Southern WV/Northwestern VA and Central KY, appear to have pillar strengths that are somewhat stronger than the baseline, but the differences are not significant at the 95% confidence level. Pillar strengths in the Northern Appalachian case histories appear to be somewhat lower than the baseline, but again the difference is only significant at the 90% confidence level. The pillar strengths in northeastern KY (Pike County) appear to significantly stronger than the baseline, and the difference is statistically significant at the 98% confidence level. Since it is not clear what physical characteristics may be responsible for these apparent differences in strength, they should only be applied with great caution.

[3] Note that figure 13b includes development and first panel cases in addition to multi-panel cases where adequate barrier pillars were employed.

COMPARISON BETWEEN ARMPS 2002 AND ARMPS 2010

Despite their different loading functions, the ARMPS 2002 and ARMPS 2010 design criteria have almost the identical success rates when tested against the ARMPS data base. In fact, detailed analysis shows that for almost every individual case in the data base, the methods almost always make the same prediction about its performance. For example, of the 120 failures in the data base, in 112 cases (93%) both ARMPS 2010 and ARMPS 2002 make the same prediction (in other words, either both predict failure, or both predict success).

The explanation is that the two criteria are actually quite similar mathematically. In other words, the ARMPS 2002 criteria, with the adjustment for depth, can be considered a "de-facto" pressure arch model.

This can be shown with a few simple equations. In the 2010 model, the *critical* $SF_{2010} = 1.5$, and is determined as:

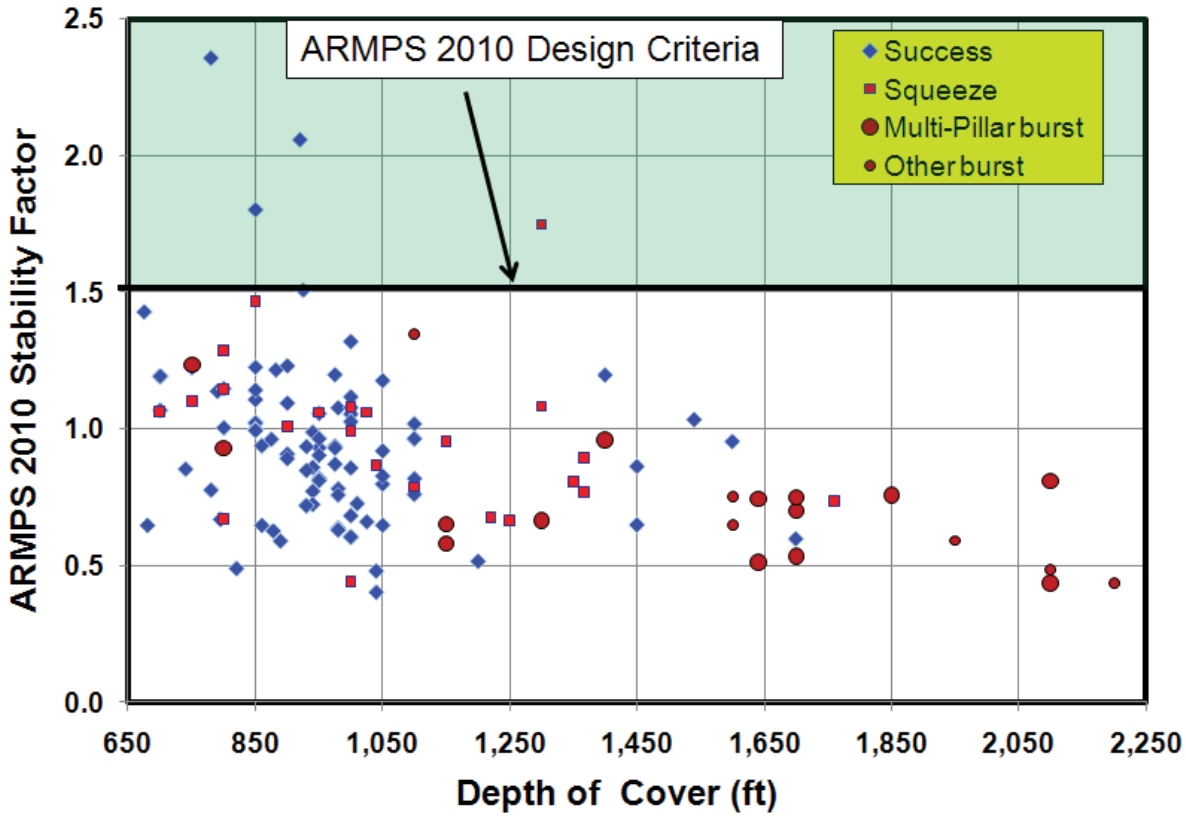

Figure 13A. ARMPS 2010 stability factors vs. depth for the deep cover data base showing case histories with inadequate barrier pillars (barrier pillar SF < 1.5).

$$SF_{2010} = 1.5 = \frac{LBC}{L_{2002} \times F_{pa}} \quad (3)$$

where LBC is the load bearing capacity of the pillars within the AMZ, L_{2002} is the ARMPS load applied to the AMZ if there are no pressure arch loads transferred to the barriers, and F_{pa} is obtained from equation (2).

If it is assumed that the entire apparent reduction in the critical SF in the 2002 model is due to pressure arch behavior, then a similar equation can be written:

$$1.5 = \frac{LBC}{L_{2002} \times F_{2002}} \quad (4)$$

where F_{2002} is the depth adjustment factor for the 2002 model. It can be shown that:

- For H < 650 ft, $F_{2002} = 1$
- For 650 ft < H < 1,250 ft, $SF_{2010} = 1 - 0.47 \times \frac{H - 650}{600}$
- For H > 1,250 ft, $SF_{2000} = \frac{(1.5 - 0.8)}{1.5}$

Unlike F_{pa}, F_{2002} is not dependent on the panel width. Figure 14 plots F_{pa} and F_{2002} against the depth of cover. The similarity between the two is evident.

Although the 2002 and 2010 models have similar success rates, the 2010 model that explicitly includes the pressure arch is superior to the Chase et al. (2002) criteria because:

- The inherently greater stability of narrow panels is recognized, because the pressure arch model transfers proportionately more overburden load from narrow panels to the barrier pillars.
- A single ARMPS SF criterion (SF = 1.5) can be employed across the entire range of cover depths.
- Barrier pillars and the production pillars can employ the same design criterion of SF = 1.5.

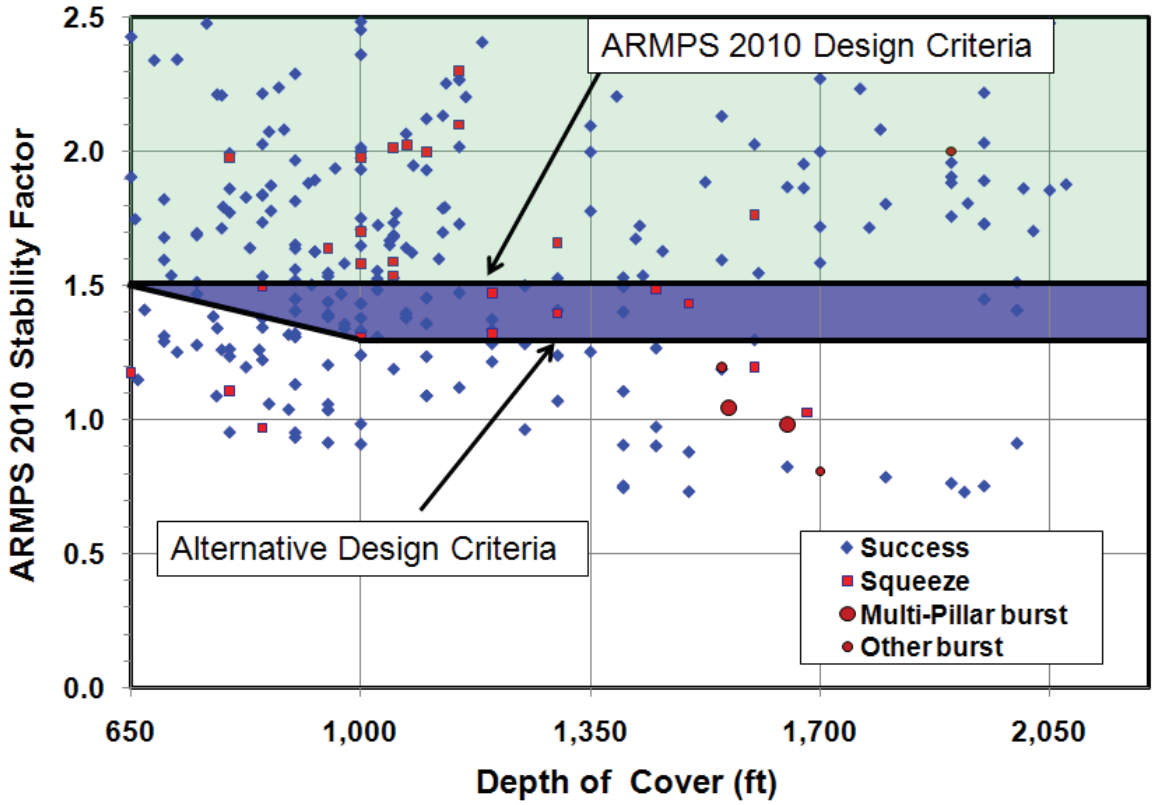

Figure 13B. ARMPS 2010 stability factors vs. depth for the deep cover data base showing case histories with adequate barrier pillars (barrier pillar SF > 1.5) and an alternative design criteria for panel widths < 420 ft (Table 3).

Table 3. Alternative ARMPS 2010 suggested design criteria with narrow panels and enhanced barrier pillars.

Depth of Cover (ft)	Panel Width (ft)	ARMPS SF	Barrier Pillar SF
650-1,000	< 425	1.5-[0.20 x ((Depth-650)/350)]	2.0
> 1,000	< 425	1.30	2.0

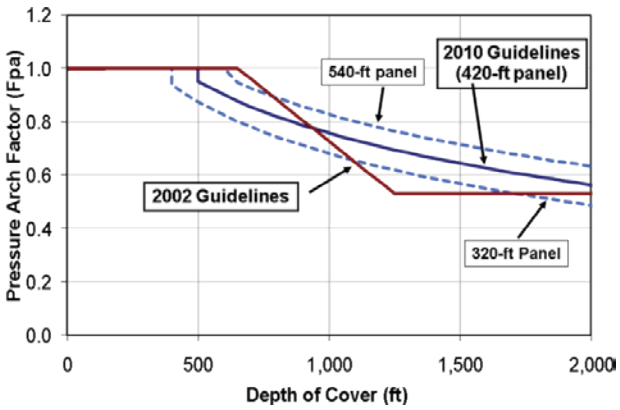

Figure 14. Comparison between the ARMPS 2010 pressure arch loading function, and the implicit pressure arch loading function in the 2002 guidelines.

Moreover, in the ARMPS 2010 model, the barrier pillar behavior is directly linked to the pillars in the AMZ. If the barrier pillars are too small, large loads are transferred back to the pillars in the AMZ (see Figure 10), resulting in reduced ARMPS SF values. Therefore, it is very difficult for a deep cover design to achieve an adequate ARMPS SF without adequate barrier pillars.

One final comment is that both the 2010 and 2002 models misclassify some pillar failure case histories as successes. All of these misclassifications were pillar squeezes, not the more hazardous collapses or bursts. It is significant that the ARMPS data base contains 83 squeezes, yet analysis of MSHA fatality reports shows that no mineworkers have been killed by a pillar squeeze in at least the past 25 years.[4] Pillar squeezes create hazardous situations, but because they develop slowly, the area can almost always be abandoned before injuries occur. Bursts and pillar collapses, on the other hand, represent a much more direct threat to miners because they occur with little or no warning. The pillar

[4] The information included in the MSHA data base is insufficient to determine how many injuries, if any, have been associated with pillar squeezesdetermined

design method should therefore provide a higher margin of safety for bursts and collapses than is necessary for squeezes.

ARMPS 2010 seems to provide a better margin of safety against multi-pillar bursts as shown in a comparison between Figure 9b and 12. While both models correctly predict all 16 multi-pillar bursts in the data base, in the 2002 model there is one case that falls uncomfortably close to the recommended criteria in Figure 9b. In this incident, a crew of Colorado miners was temporarily entrapped by a large burst that affected a number of pillars simultaneously. Because the burst occurred when they were developing a new section, with no nearby worked-out gob areas, the "barrier pillars" were adequate. Using the ARMPS 2002 method, the SF_{2002} was determined to be 0.78, uncomfortably close to the SF_{2002} of 0.80 that was recommended for the depth of cover of 1,560 ft (Table 1). However, the panel was an exceptionally wide 650 ft. Using ARMPS 2010, the F_{pa} for this case is 0.75 (equation 2). Because the estimated pillar load is reduced by 25%, the SF_{2010} increases to 1.03, but this value is well below the recommended SF_{2010} of 1.5 (shown in Figure 12 and Table 2) that applies to any panel with a width greater than 425 ft. If the panel width had been decreased to 380 ft, then the F_{pa} would have been 0.60, and SF_{2010} would have increased to 1.3. This narrow-panel design would have met the alternative ARMPS 2010 suggested criteria shown in Table 3.

CONCLUSIONS

In response to a Congressional request, NIOSH expanded and updated the ARMPS case history data base with almost 450 new case histories. Logistic regression, supplemented by LaModel and FLAC studies, supported the hypothesis that "pressure arch" theory adequately explains the reduced loading experienced by narrow panels under deep cover.

A new, calibrated pressure arch loading model was developed for ARMPS, and it was shown to perform very similarly to the ARMPS 2002 recommended guidelines. The two approaches were made mathematically similar, because ARMPS 2002 actually employed a de facto pressure arch loading model. The new loading model is superior, most importantly because it recognizes the inherently greater stability of narrow panels. New design criteria for both production and barrier pillar are also suggested. The pressure arch loading model and the new design guidelines have been implemented in an updated version of the ARMPS software package. It is called ARMPS 2010 or ARMPS V6.0.

DISCLAIMER

The findings and conclusions in this paper have not been formally disseminated by the National Institute for Occupational Safety and Health and should not be construed to represent any agency determination or policy.

REFERENCES

Carr, F. (1992). Ten Years' Experience of the Wilson/Carr Pillar Sizing Method at Jim Walter Resources, Inc. Iannacchione, A.T., Mark, C., Repsher, R.C., Tuchman, R.J., Jones, C.C., eds. Proceedings of the Workshop of Coal Pillar Mechanics and Design, Bureau of Mines IC 9315, pp. 166-179.

Chase, F.E., Mark, C. and Heasley, K.A. (2002). Deep Cover Pillar Extraction in the U.S. Coalfields. Proceedings of the 21st International Conference on Ground Control in Mining, pp. 68-80.

Coates, D.F. (1967). Rock Mechanics Principles. Mines Branch Monograph 874, Canadian Department of Mines and Technical Surveys.

Colwell, M. and Mark, C. (2005). Analysis and Design of Rib Support (ADRS) - A Rib Support Design Methodology for Australian Collieries. Proceedings of the 24th International Conference on Ground Control in Mining, pp. 12-22.

Colwell, M., Frith, R.C. and Mark, C. (1999). Calibration of the Analysis of Longwall Pillar Stability (ALPS) Chain Pillar Design Methodology for Australian Conditions. Proceedings of the 18th International Conference on Ground Control in Mining, pp. 282-290.

Esterhuizen, G.S. and Mark, C. (2009). Three-Dimensional Modeling of Large Arrays of Pillars for Coal Mine Design. Proceedings of the International Workshop on Numerical Modeling for Underground Mine Excavation Design, NIOSH IC 9512, pp. 37-46.

Esterhuizen, G.S, Mark, C. and Murphy, M.M. (2010). The Ground Response Curve, Pillar Loading, and Pillar Failure in Coal Mines. Proceedings of the Third International Workshop on Pillar Mechanics and Design, in press.

Galvin J.M., Hebblewhite B.K. and Salamon M.D.G. (1999). University of New South Wales Coal Pillar Strength Determinations for Australian and South African Mining Conditions. In: Mark, C., Heasley, K.A., Iannacchione, A.T., Tuchman, R.J., eds. Proceedings of the Second International Workshop on Coal Pillar Mechanics and Design, NIOSH Publication No. 99-114, IC 9448, pp. 63-72.

Gates, R.A., et al. (2008). Report of the Investigation, Fatal Underground Coal Burst Accidents, August 6 and 16, 2007, Crandall Canyon Mine. Available from http://www.msha.gov/Fatals/2007/CrandallCanyon/FTL07CrandallCanyon.pdf.

Gauna, M. and Phillipson, S. (2008). Evaluation of a Multiple Seam Interaction Coal Pillar Bump. Proceedings of the 27th International Conference on Ground Control in Mining, pp. 51-59.

Heasley, K.A., and Chekan G.M. (1999). Practical Boundary-Element Modeling for Mine Planning. Proceedings of the Second International Workshop on Coal Pillar Mechanics and Design, Mark, C., Heasley, K.A., Iannacchione, A.T., Tuchman, R.J., eds., NIOSH Publication No. 99-114, IC 9448, pp. 73-88.

.Heasley, K.A. (2010). Calibrating the LaModel Program for Deep Cover Pillar Retreat Coal Mining. Proceedings of the Third International Workshop on Pillar Mechanics and Design, in press.

Hill, D., Canbulat, I., Thomas, R. and van Wijk, J. (2008). Coal Pillar Loading Mechanisms and Progress in Pillar Design. Proceedings of the 27th International Conference on Ground Control in Mining, pp. 235-240.

Holland, C. T. (1973). Mine Pillar Design. Mining Engineering Handbook, Cummins, A.B. and Given, I.A., eds., SME-AIME, pp. 13-96 to 13-118.

Hosmer, D.W. and Lemeshow, S. (2000). Applied Logistic Regression. Wiley, NY, 375 pp.

Mark, C. (2009). Deep Cover Pillar Recovery in the U.S. Proceedings of the 28th International Conference on Ground Control in Mining, pp. 1-9.

Mark, C. (2006). The Evolution of Intelligent Coal Pillar Design: 1981-2006. Proceedings of the 25th International Conference on Ground Control in Mining, pp. 325-334.

Mark, C. and Barton, T. (1988). Field Evaluation of Yield Pillar Systems at a Kentucky Longwall. Proceedings of the Seventh International Conference on Ground Control in Mining, pp. 1-9.

Mark, C. and Barton, T.M. (1997). Pillar Design and Coal Strength. Proceedings of the New Technology for Ground Control in Retreat Mining, NIOSH Publication No. 97-122, IC 9446, pp. 49-59.

Mark, C. and Chase, F.E. (1997). Analysis of Retreat Mining Pillar Stability. Proceedings of the New Technology for Ground Control in Retreat Mining, NIOSH Publication No. 97-122, IC 9446, pp. 17-34.

Mark, C., Chase, F.E. and Molinda, G.M. (1994). Design of Longwall Gate Entry Systems Using Roof Classification. Paper in New Technology for Longwall Ground Control: Proceedings of the USBM Technology Transfer Seminar, USBM SP 94-01, pp. 5-18.

Mark, C., Chase, F.E. and Pappas, D.M. (2007). Multiple-Seam Mining in the United States: Design Based on Case Histories. Proceedings of the New Technology for Ground Control in Multiple Seam Mining NIOSH Publication No. 97-122, IC 9495, pp. 15-28.

Mark, C., Molinda, G.M. and Dolinar, D.R. (2001). Analysis of Roof Bolt Systems. Proceedings of the 20th International Conference on Ground Control in Mining, pp. 218-225.

Newman, D. (2002). A Case History Investigation of Two Coal Bumps in the Southern Appalachian Coalfield. Proceedings of the 21st International Conference on Ground Control in Mining, pp. 90-97.

Salamon, M.D.G. (1970). Stability, Instability, and Design of Pillar Workings. Int J of Rock Mech Min Sci *7*:613-631.

Zipf, R.K. (1999). Using a Post Failure Stability Criterion in Pillar Design. Proceedings of the Second International Workshop on Coal Pillar Mechanics and Design, Mark C., Heasley K.A., Iannacchione, A.T., Tuchman, R.J., eds. NIOSH Publication No. 99-114, IC 9448, pp. 181-192.

Appendix A. ARMPS Guidelines for determining the "Entry Height" and the "Depth of Cover"

Entry Height: The proper entry height to enter in ARMPS can be complicated because many mines extract significant thicknesses of rock with coal. Currently, the ARMPS Help file provides the following guidelines for entry height:

"The value entered here is the mined height of the pillars, which is not necessarily equal to the seam thickness. Some engineering judgment may be exercised when the seam contains a lot of rock. Quite often partings are weak claystone, whose strength is approximately the same as the coal. In this case, the full mined height should be entered. Where the parting material is significantly stronger than coal, some reduction in the mined height may be justified."

Observations made during the current study indicated that the rock that is mined with the coal usually falls into one of two categories. The first is weak claystone which should be considered part of the entry height, and includes:

- most in-seam rock,
- most floor rock, and
- most draw rock beneath a rider seam.

On the other hand, competent roof rock that that is mined solely for equipment clearance is normally stronger than the coal. The thickness of such competent "cap rock" should be reduced by 50% in the entry height calculation. In other words, if 12 inches of competent cap rock is mined, only 6 inches should be added to the seam thickness to obtain the entry height. This guideline was used in the analysis of the ARMPS 2010 database.

An exception to these rules might include a thick parting that includes some strong rock. In that case, the strong portion of the parting could be subject to the "50% rule." A geologist or ground control professional could help determine how much of the parting is actually competent rock.

Depth of Cover: Determination of the depth of cover to use in ARMPS can be even more troublesome. The ARMPS version 5 Help file suggested that:

"in regions of sharp topographic variation it may be too conservative to use the maximum cover if it is only present over a small portion of the panel, but the average depth might underestimate the load over the deeper sections." Some engineering judgment should be exercised, but in general an appropriate value of the depth of cover for ARMPS is a high average expressed as:

$H = [\{Hmin + (3\ Hmax)\} / 4]$, or (equivalently)

$H = (Havg + Hmax)/2$

Where H_{max} is the greatest depth of cover over the panel, H_{min} is the shallowest, and H_{avg} is the average of H_{max} and H_{min}.

Experience has shown that while this guideline performs adequately in most cases, sometimes the locations of H_{max} and H_{min} are so widely separated that it seems unlikely that they can be related.

To address this topic, a study of the effect of surface topography on seam-level stress was evaluated using the "topographic stress" feature of LaModel. The first step was to determine the pre-mining, in situ vertical stress beneath different topographic features. Using a digitized topographic map typical of the Central Appalachian coalfields, a number of points were classified into three groups:

- Hilltop points beneath topographic highs (hills or ridges)
- Valley bottom points, and;
- Hillside points.

The pre-mining stresses were then determined beneath each point for a range of different seam elevations. The analysis showed that, on average, the stress beneath the hilltops was about 6% less than what would be predicted from the normal depth gradient, while the stress beneath the valley bottoms was about 7% higher. The stress beneath the hillside points was, on average, midway between the two, but there was substantial variation.

The second part of the analysis considered the load actually applied to conceptualized Active Mining Zones that contained a number of LaModel elements. Overall, it appeared that a good estimate of the average AMZ stress could be achieved by computing the average depth of the elements within the AMZ.

Based on this finding, the recommended procedure for estimating depth of cover for an ARMPS analysis is:

1. Locate the point above the panel where the analysis is to be conducted (normally where the depth of cover is greatest.)
2. Draw a perpendicular line across the panel (from rib to rib) that includes the point of the maximum depth of cover.
3. Define a zone that extends 200 ft inby and 200 ft outby of the deepest cover line, and determine the minimum depth of cover within that zone.

The ARMPS depth of cover (H) is then the arithmetic average of those minimum and maximum depths.

Appendix B. Logistic Regression Results

Table B1. Logistic regression output for the 2002 model containing the original ARMPS SF and the depth of cover.

Logistic regression — Number of obs =640

LR chi^2=133.95

Prob > chi^2=0.0000

Log likelihood = -219.00373 — ROC=0.7854

Parameter	Coef.	Std. Err.	Z	P>|z|	95% Conf. Interval
ARMPS SF	2.673421	0.3375929	7.92	0.000	2.011751 — 3.335091
Depth (ft)	0.0013633	0.0002964	4.60	0.000	0.0007823 — 0.0019443
Constant	-4.427077	0.5746138	-7.70	0.000	-5.553299 — -3.300854

Table B2. Logistic regression output for the 2010 model containing the new ARMPS SF calculated using the pressure arch loading model.

Logistic regression — Number of obs = 640

LR chi^2 = 124.01

Prob > chi^2 = 0.0000

Log likelihood = -220.7969 — ROC = 0.7824

Parameter	Coef.	Std. Err.	Z	P>|z|	95% Conf. Interval
ARMPS SF	1.963907	0.2389576	8.22	0.000	1.495559 — 2.432255
_cons	-2.824896	0.3362113	-8.40	0.000	-3.483858 — -2.165933

Table B3. Regional Analyses (Harlan/Wise region is the benchmark, represented by the constant, to which the other regions are compared.).

Logistic regression — Number of obs = 640

LR chi^2 = 147.06

Prob > chi^2=0.0000

Log likelihood = -209.27191 — ROC=0.8205

Parameter	Coef.	Std. Err.	Z	P>|z|	95% Conf. Interval
ARMPS SF	2.150607	0.2609783	0.24	0.000	1.639099 — 2.662115
Utah	0.0362459	0.4511197	0.08	0.936	-0.8479325 — 0.9204242
Colorado	-0.0052166	0.5324366	-0.01	0.992	-1.048773 — 1.03834
Central KY	0.9592073	0.5087713	1.89	0.059	-0.0379662 — 1.956381
Northeast KY	1.365372	0.4747242	2.88	0.004	0.4349299 — 2.295814
SouthernWV/ Northern VA	0.6557758	0.4967568	1.32	0.187	-0.3178495 — 1.629401
Kanawha	-0.0997514	0.3437043	-0.29	0.772	-0.7733995 — 0 .5738967
Northern Ap	-0.8655142	0.4829772	-1.79	0.073	-1.812132 — 0.0811037
Constant	-3.222456	0.4555138	-7.07	0.000	-4.115247 — -2.329665

The Ground Response Curve and Its Impact on Pillar Loading in Coal Mines

Essie Esterhuizen, Senior Research Engineer
Chris Mark, Principal Research Engineer
Michael M. Murphy, Research Engineer
NIOSH-Office of Mining Safety and Health Research
Pittsburgh, PA

ABSTRACT

The response of the surrounding rock mass to the creation of mining excavations determines the ultimate load on a pillar support system. In conditions where the ground is relatively soft and weak, the full overburden weight can be transferred to the pillar system. However, in stiffer and stronger rocks, a greater portion of the overburden load is transferred to the unmined coal barriers or abutments, and the pillar stress is reduced. This paper makes use of numerical models to examine the interaction between typical pillar systems and the surrounding rock mass for weak and strong geological conditions at various spans and depths of cover. The concepts of structural failure and functional failure of pillars are used to assess pillar performance when pillars are deformed beyond their peak resistance. The results show that the span-to-depth ratio is an important factor in determining the pillar stress and the ultimate deformation of pillars. The ultimate pillar strain appears to be closely related to the functional success of pillar systems.

INTRODUCTION

The National Institute for Occupational Safety and Health (NIOSH) was requested by Congress to study the safety of retreat pillar mining following the Crandall Canyon Mine disaster that took place near Price, Utah in August, 2007. As a part of this study, an investigation was made to better understand how the rock mass responds to the creation of mining excavations and how the loads are distributed among the pillars and the surrounding abutments or barriers. The outcome of these investigations contributed to the development of a modified loading model for the ARMPS-2010 (Mark, 2010) method of retreat mining pillar design.

Structural and Functional Failure of Pillars

Pillar design is typically conducted by estimating the pillar strength and stress, and then sizing the pillars so that an adequate margin of safety exists between the expected strength and stress. The pillar strength can be defined as the maximum resistance of a pillar to axial compression (Brady and Brown, 1985). If a pillar is loaded beyond its peak strength, load shedding or yielding can occur, and the pillar is considered to have failed as a structure. Structural failure generally refers to a loss of load-carrying capacity.

Pillars that have a width-to-height ratio of less than 4.0 typically exhibit a clear peak resistance when loaded followed by a rapid decrease in resistance if the loading continues. For these pillars, the point of structural failure can be identified relatively easily on a stress-strain curve. When the width-to-height ratio of pillars becomes large, pillars may yield at a constant stress or may exhibit strain hardening behavior. In these cases, it is difficult to determine a particular "peak" value of the pillar strength and structural failure becomes hard to define.

In some mining applications, structurally failed pillars are desired. For example, yield pillars have been used for many years in deep coal mine layouts (Mark et al., 1988; Iannacchione and Zelanko, 1995) and in hard rock mines (Barrientos and Parker, 1975; Ryder and Ozbay, 1990). Although these pillars may be structurally failed, they are considered to be successful from a "functional" point of view. Functional failure refers to the state of not meeting a desired objective. Yield pillars in longwall gate entries would be considered to be functionally failed if they no longer meet the objective of providing safe access to the longwall face. The evaluation of functional failure usually requires the consideration of an entire system rather than just one component or structure within the system. For example, functional failure of a pillar system may be related to roof damage or floor punching and not only the failure of the pillar as a structure. The Analysis of Longwall Pillar Stability (ALPS) pillar design method for longwalls (Mark, 1993; Mark et al., 1994) and the Analysis of Retreat Mining Pillar Stability (ARMPS) method for retreat mining pillar design (Mark and Chase, 1997; Mark, 2010) both consider pillar stability and local roof geology to evaluate the "functional" success of a pillar design.

Ground Response and Pillar Stiffness

The driver of pillar failure is the response of the surrounding rock mass to the extraction of coal. In flat laying deposits, the pillar stress is related to the weight of the overburden. When the pillar layout consists of a regular array of pillars, the average pillar stress can be estimated using the tributary area method, which assumes the full weight of the overburden is equally distributed over all the pillars. This approach does not consider the fact that a portion of the overburden weight may be transferred to adjacent

unmined barrier pillars or solid abutments. Stress transfer occurs to the relatively stiff barriers or solid abutments as the pillars in the mined area are compressed by the surrounding strata. The amount of pillar compression is determined by the relative stiffness of the pillars and the surrounding strata. Stiffer pillars will develop more stress, while stiffer surrounding strata will deflect less and impose a smaller load on the pillars. The concept of the pillar stiffness and strata stiffness is well established in the field of pillar design and has been used to evaluate the potential for violent pillar collapse (Salamon, 1970; Ryder and Ozbay, 1990; Zipf, 2001).

Understanding the stress and potential failure of pillars, therefore, requires consideration of both the ground response and the pillar response to mining. In this paper, the structural and functional success of pillar systems in coal mines are evaluated for various geological settings, panel spans, and depths of cover. The evaluations are restricted to the overall success, or global stability, of the systems and do not consider local stability issues such the failure of the immediate roof or floor between the pillars.

GROUND RESPONSE CURVE DETERMINATION

The concept of a ground response curve was originally developed by the civil tunneling industry where the timing and method of ground support is determined by monitoring the support pressure and excavation convergence during construction (Rabcewicz, 1965). The ground response approach has found application in both hard rock and coal mining as a method to better understand the interaction between the rock mass and the support system (Brown et al., 1983; Brady and Brown, 1985; Barczak et al., 2005; Medhurst and Reed, 2005).

The ground response curve characterizes the rock mass by plotting the internal support pressure against the excavation convergence, as shown conceptually in Figure 1. If the excavation boundaries are subject to support pressure equal to the stress in the surrounding rock, no convergence will occur (point A). As the support pressure is reduced, the excavation boundaries initially converge in an elastic manner and linear response is observed. As the pressure is further reduced, the response becomes non-linear if rock failure occurs and the self-supporting capacity of the ground is destroyed (point B). A point is reached (point C) where the required support resistance necessary to establish equilibrium begins to increase as the failed ground loosens and its dead weight must be resisted (point D).

The effect of the support system can also be plotted on Figure 1. For example, line PQR represents the stress-convergence response of a support system consisting of pillars. Initially, at zero convergence, the stress in the pillars will be zero. As the overburden is allowed to settle onto the pillars, the pillar resistance will increase. In the figure, the resistance of the pillar is equal to the pressure required to halt the convergence of the overburden at point Q.

Modeling Method to Develop Ground Response Curves for Coal Mine Panels

It is difficult to measure the ground response curve in actual underground excavations because of the significant loads that would have to be applied to balance the original ground pressure. However, numerical models can readily be used to estimate the ground response curve by progressively reducing the internal pressure in a modeled excavation while monitoring the resulting convergence.

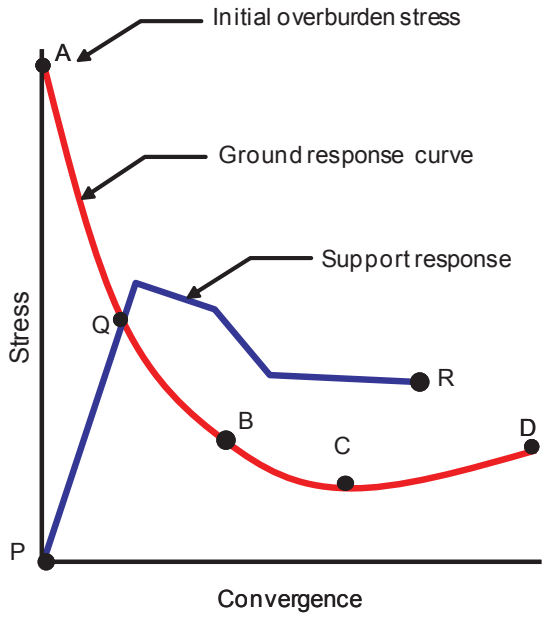

Figure 1. Ground response curve and support line.

The finite difference software FLAC3D (Anon., 2007) was used to develop ground response curves for coal mining excavations that have dimensions typical of longwall and pillar extraction panels in the United States. The software is able to realistically model the overburden behavior from the initial elastic response to the large displacements and deformations that are associated with rock failure and yield. It has the capability to model strength anisotropy found in the bedded coal measures and can simulate the strain-related weakening of failed rock. The software also has a built-in programming language that allows the user to control loads and displacements in the model. This facility was used to apply internal pressure within the modeled panels so that the ground response curve could be determined.

The input parameters used to simulate the coal pillars and the surrounding rock mass were extensively calibrated against field monitoring results to ensure that realistic large-scale behavior of the overburden and coal pillars was achieved (Esterhuizen et al., 2010). The coal was modeled using the Hoek-Brown material type available in the FLAC3D software, while the overburden rocks were modeled as a strain-softening ubiquitous joint material. The ubiquitous joints were used to simulate the bedding weaknesses in the strongly bedded strata. The ubiquitous joints were also used to model vertical joints in massive rock types, such as sandstone or limestone, that did not contain well-developed bedding weaknesses. The gob was modeled as a strain hardening material that follows a hyperbolic stress-strain curve after the results of Pappas and Mark (1993). The horizontal stress in the models consisted of a depth-dependent component and a tectonic component that depends on the stiffness of the strata layers. Details of the input parameters, model calibration, and comparisons

of model results to field measurements are given in Esterhuizen et al. (2010).

The ground response curve for a particular panel was determined by modeling the panel, the unmined coal, and the surrounding strata up to the ground surface. The distribution of support pressure within the panel has an impact on the shape of the ground response curve. Therefore, the internal support pressure in the panels was not modeled as a constant pressure, as one would do when modeling support systems, but rather by simulating an array of pillars in the panel. The resulting "support pressure" distribution in the panel more accurately represented the effect of a system of pillars with higher stress near the center of the panel and lower stresses near the edges. The elastic modulus of the pillars was reduced in stages, simultaneously at all points, to simulate decreasing support pressure in the excavation. The model was run to equilibrium at each stage and the support pressure at the pillar in the center of the panel and the convergence at that location were recorded. This procedure produces the ground response curve at the center of the panel. It is possible to create ground response curves for any pillar location if desired. However, for the single panels modeled here, the pillar at the mid-span is the most critical one because the deformations are the largest at this location. All ground response curves presented in this paper were calculated at the mid-span of the mined panels. The panels were all assumed to be surrounded by an adequately large extent of unmined coal. The potential impacts of adjacent mining and barrier pillar yield were not considered.

EFFECT OF GEOLOGY, DEPTH, PANEL WIDTH, AND PILLAR EXTRACTION OF THE GROUND RESPONSE CURVE

Ground response curves were developed for 300-m (1,000-ft) wide coal mine panels with a mining height of 2.4 m (8 ft) in two different geologies at depths of 150 m and 450 m (500 ft and 1,500 ft). At 150-m (500-ft) depth, the panels are considered to be supercritical, because the span-to-depth ratio exceeds 1.2. At a 450-m (1,500 ft) depth of cover, they are considered to be subcritical, having a span-to-depth ratio of 0.67. The first model simulates "weak overburden" that consists of 75% weak rocks, such as shale or clay stone, and 25% strong rocks, such as sandstone or limestone beds. The gob was modeled as a weak material that followed the "shale" gob response after Pappas and Mark (1993). The weak overburden model is representative of some of the coal measures found in the eastern United States. The second model simulates "strong overburden" containing about 50% strong rocks, typical of the stronger coal measures found in southern Appalachia, Colorado, and Utah. The geology was modeled by simulating alternating layers of weak and strong rocks, having bed thicknesses of between 5 m (16 ft) and 10 m (33 ft), based on actual geological profiles of operating mines in the two geographic areas. The gob was modeled as a stronger "sandstone" material. Figure 2 shows one of the models indicating the general model layout and the geologic layering in the model.

Effect of the Geology and the Depth-to-Span Ratio

Figure 3 shows the resulting ground response curves at mid-span of the panel for the weak and strong geologies at 150- and 450-m (500- and 1,500-ft) depths. Considering the results at a 150-m (500-ft) depth, in which both panels are supercritical (span-to-depth ratio is 2.0), it can be seen that the ground response curves are nearly horizontal and are almost equal to the cover stress of 3.8 MPa (550 psi). There is almost no initial linear section of the curve, because overburden failure starts at an early stage of deformation. This represents a near "dead-weight" loading condition, and, clearly, no arching of the strata is occurring over these supercritical panels. The support system would be required to carry almost the full overburden weight. If pillars are used for support, this situation would approach the classical tributary area loading condition. There is little difference between the weak and strong overburden results because of the near dead-weight loading conditions.

The results for 450-m (1,476 ft) depth show a different picture. Here, the span-to-depth ratio is 0.67 (subcritical), and there is considerable difference between the weak and strong overburden response. The response of the strong overburden is initially nearly linear, followed by a curved section, which is related to the development of failure in the overburden. When the convergence is about 20 cm, the curve flattens out at about 50% of the initial overburden stress. This implies that arching is occurring in the overburden, and about 50% of the weight of the overburden is being carried by the support system, while the remainder is transferred to the solid abutments. The arching mechanism is often referred to as a "pressure arch" in rock engineering practice (Barrientos and Parker, 1975).

In the weak overburden model, the ground response is flatter and arch formation is not as developed as in the stronger rock model. Only about 25% of the overburden load is transferred to the abutments, while about 75% would be carried by the support system. The "support system" might be a system of pillars or the gob if full extraction mining is carried out.

These results clearly show that the geological composition of the overburden and the span-to-depth ratio both have a significant impact on the stress that is carried by the support system, be it pillars or gob. Under weak overburden materials the arching mechanism is not as pronounced and greater load is transferred to the support system, while strong overburden is able to form a more developed arch and a lesser amount of stress is carried by the support system.

Effect of the Span

The strong overburden model was used to further investigate the effect of the mining span on the ground response. Models were created to simulate mining at a depth of 450 m (1,500 ft) and the panel spans were set at various dimensions from 300 m (1,000 ft) (span-to-depth ratio = 0.67) down to 25 m (80 ft) (span-to-depth ratio = 0.06). The resulting ground response curves are shown in Figure 4. It can be seen that as the panel span is decreased from 300 to 25 m (1,000 to 80 ft), the ground response becomes stiffer (steeper slope) and the arching effect becomes more pronounced. For example, when the spans are 150 m (500 ft) (span-to-depth ratio = 0.33) or less the curve flattens at 1–2 MPa (145–290 psi), which is considerably lower than the overburden stress of 11.3 MPa (1,600 psi). This indicates that significant arching of the overburden stress to the solid abutments is occurring.

These results for relatively strong overburden rocks show that the mining span and arching of the roof strata over the excavation

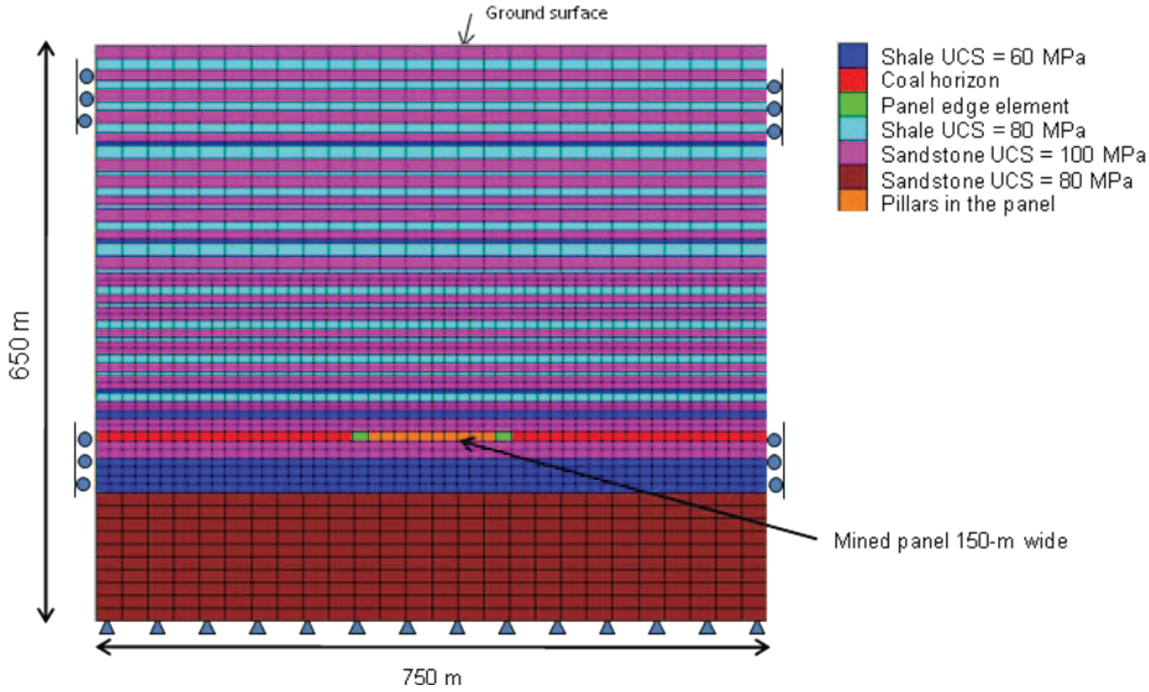

Figure 2. Example of a numerical model layout showing location of mined panel and geological layering.

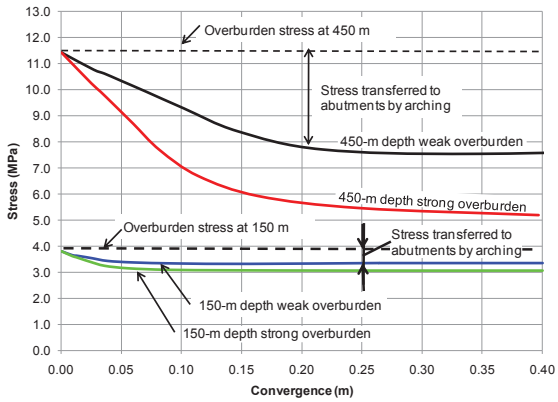

Figure 3. Ground response curves at the center of a 300–m-(1,000 ft) wide panel in weak and strong overburden strata at 150 m and 450 m (500 ft and 1,500 ft) depth of cover.

will have a significant impact on the final stress in the support system. In weaker overburden, the effect of arching is less pronounced and the resulting loading of the support system is likely to be greater.

Ground Response at the Pillar Extraction Line

The ground response curve is dramatically affected if pillar extraction is performed. The prevailing stress is considerably increased and the presence of the adjacent gob will affect the ground response. The results of a fully three-dimensional model that simulated a 150-m (500-ft) wide panel under strong overburden are presented. The ground response curve was determined at the mid-span pillar on the extraction line for a case where the pillars in half of the panel had been extracted. The 600-m (2,000-ft) long extracted portion of the panel was filled with an appropriate gob material, after Esterhuizen et al. (2010). The ground response curve was determined by reducing the pillar stiffness simultaneously in all the remaining pillars in the panel in a stepwise manner and determining the pillar stress and associated convergence at the mid-span pillar on the extraction line at each step. Figure 5 is a schematic diagram showing a partially extracted panel, the pillars, the extraction line and the gob. It also shows the location of the pillar where the ground response was determined. Figure 6 displays the resulting ground response curve at the extraction line and the ground response curve under normal development loading conditions. It can be seen that the ground response curve at the pillar extraction line initiates at a much higher stress because of the abutment loading effects. At the extraction line, the stress required to achieve equilibrium for a given convergence is much greater than under normal development loading conditions. Convergence is also seen to be greater for any given stress value.

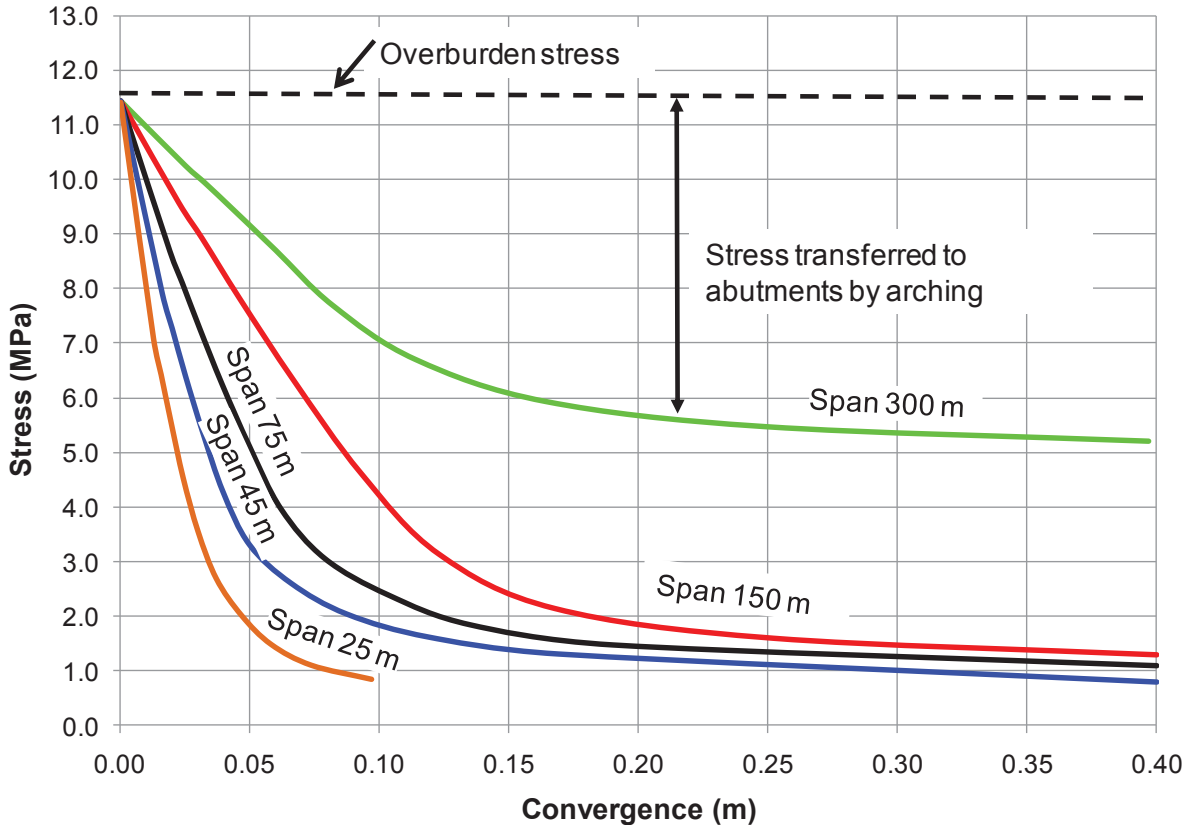

Figure 4. Ground response curves at mid-span of panels with various spans in strong overburden strata at 450-m (1,500-ft) depth of cover.

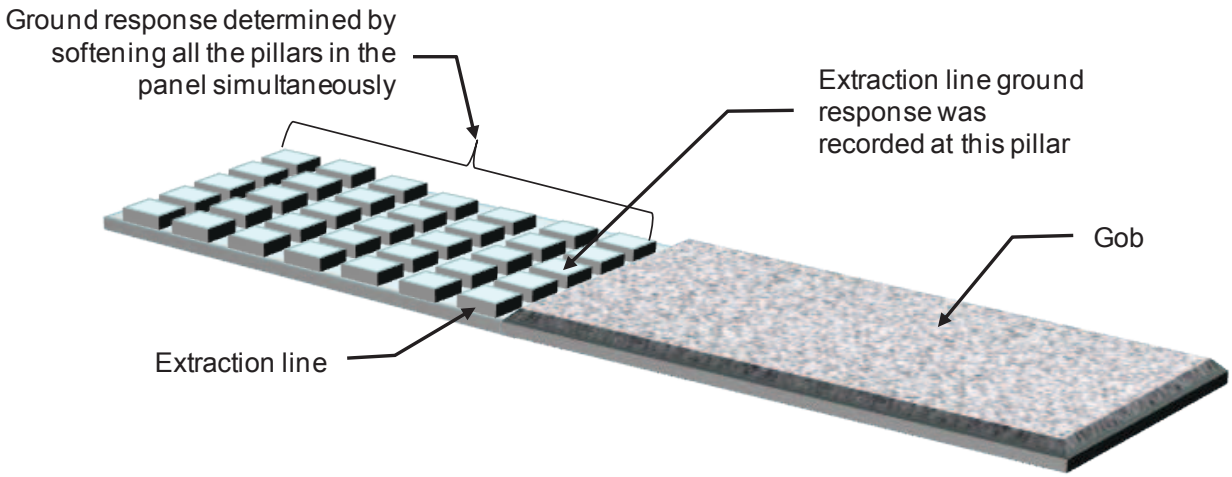

Figure 5. Schematic diagram showing a partially extracted panel and the location of the pillar that was used to determine the ground response at the pillar extraction line.

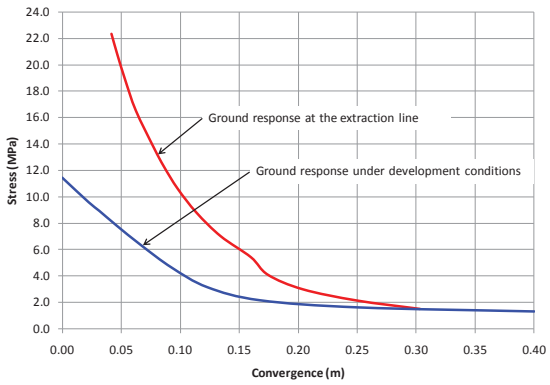

Figure 6. Ground response curves at mid-span of a 150-m- (500-ft-) wide pillar extraction panel, showing the ground response under development conditions and at the pillar extraction line. Depth of cover is 450 m (1,500 ft) under strong overburden strata.

ADDING PILLAR STRESS-STRAIN CURVES

The interaction between the overburden loading system and a system of pillars can be assessed by adding pillar stress-strain curves to the ground response charts to represent the "support system" illustrated in Figure 1. Numerical models were used to generate a representative set of pillar stress-strain curves using adequately calibrated input parameters (Esterhuizen et al., 2010). The models simulated coal pillars that are located between strong roof and floor strata, so that failure or punching into the roof or floor would not occur. Therefore, the resulting pillar strength is based on failure within the coal material only. The models were designed to follow the Bieniawski strength equation up to a width-to-height (W:H) ratio of 8.0. At greater W:H ratios, a clear peak strength is not identifiable, because the pillars become strain hardening.

Equivalent Support Pressure

In order to plot the pillars on the ground response curve, the equivalent "support pressure" of the pillars is calculated. Since the pillars do not contact the full excavation surface, the equivalent pillar stress, P_e, (or "support pressure") is calculated by assuming the pillar stress is applied over the full excavation surface. This can easily be calculated as:

$$P_e = \sigma \times (1 - e) \quad (1)$$

where σ is the average pillar stress and e is the extraction ratio. Figure 7 shows the ground response curve for the strong overburden model at a depth of 450 m (1,500 ft) with the pillar response curves added, after converting the pillar stress to an equivalent support pressure. In this chart, the strain is expressed as ground convergence over the pillar height of 2.4 m (8 ft), to allow the ground response curve and the stress-strain behavior of the pillars to be plotted on the same set of axes.

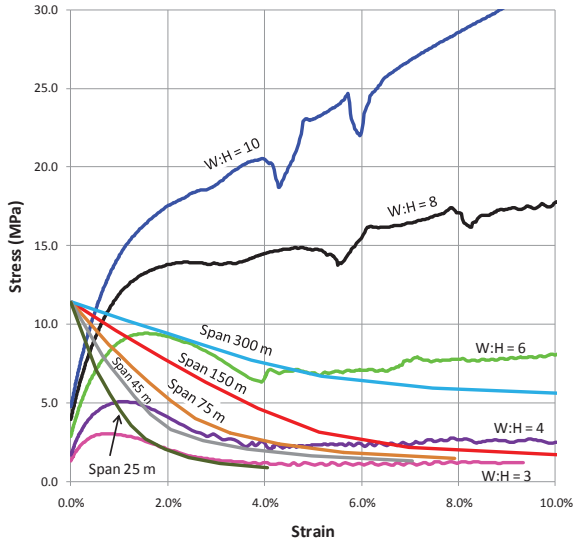

Figure 7. Pillar stress-strain curves and ground response curves at mid-span of panels with various widths at 450-m (1,500-ft) depth of cover under strong overburden strata.

Initial Support Pressure

The pillar stress-strain curves in Figure 7 all have an initial stress value when the strain is zero. This point represents the starting condition of the FLAC3D models, where the convergence is held at zero and the rooms are excavated. At this initial stage, before any convergence takes place, the stress in the pillars is still equal to the original overburden stress. The initial support pressure exerted by the pillars at this stage is calculated using Equation 1 and can be seen to be lower than the overburden stress of 11.3 MPa (1,600 psi). This imbalance causes the roof and floor to converge until the pillar response curve meets the ground response curve and equilibrium is established.

PILLAR PERFORMANCE AND GROUND RESPONSE

The results plotted in Figure 7 can be used to explain pillar performance in a number of situations and can help to explain why pillars can be functionally successful while they may be structurally failed.

Loading of Stable Pillars

Consider the response of the pillar with W:H = 8 in Figure 7. For a span of 300 m (1,000 ft), the pillar and surrounding rock mass will come to equilibrium when the support pressure is 10.8 MPa (1,560 psi), which is 96% of the tributary area stress. The equilibrium point can be seen to occur at decreasing stress values as the span is reduced. For example, when the panel span is 45 m (148 ft), equilibrium is reached when the stress is 9.4 MPa (1,360 psi), which is 83% of the tributary area stress. A similar pattern is seen for the W:H = 10 pillar, but the impact of the span would not be as significant as a result of the increased pillar stiffness.

The W:H = 6 pillar would be considered to be a structurally failed pillar, because its peak resistance is less than the overburden

stress and its safety factor would be less than 1.0 using the tributary area method. However, the ground response curve for the 150 m (500 ft) wide panel is seen to intersect the pillar response curve just prior the peak, which is considered to be a stable, although near critical, situation. As the panel span is decreased, the equilibrium points are located at lower stress values. Therefore, the figure indicates that W:H = 6 pillars might be expected to be stable under the modeled geological conditions if the panel spans are less than about 150 m (500 ft), in spite of a traditional safety factor of less than 1.0.

The figure also shows that when the panel span is 300 m (1,000 ft), the W:H = 6 pillars will be loaded beyond their peak resistance and equilibrium will be reached after about 4.5% vertical strain. In mining terminology, these would be called "yield pillars."

A review of the ARMPS-2010 (Mark, 2010) case history database revealed that a limited number of cases exist where pillars with W:H ratios of between 5.9 and 6.3 have been successfully extracted under strong overburden at depths of 380 to 450 m (1,200 to 1,500 ft). The panel width in these cases varied between 100 and 120 m (330 and 400 ft), similar to the example discussed above. The pillars had calculated stability factors of less than 1.0 on development using the tributary area method. Considering the ground response curve helps to explain why the pillars were in an acceptable condition. The relatively stiff ground response most likely resulted in pillar stresses that were lower than the tributary area estimates.

This assessment shows that assuming pillars carry the full overburden load up to the ground surface can result in over-estimation of the pillar stress, particularly when the spans are small and strong overburden is involved.

Stability of Yield Pillars

In the western United States, two-entry gate road systems with small yielding pillars are often used (Peng, 2008), while in some cases small yield pillars are left adjacent to a wider barrier pillar so that the longwall would be protected from bump events associated with the large barrier (Iannacchione and Zelanko, 1995). These yield pillars may have W:H ratios in the region of 3.0 to 4.0. When mining at depths of cover of 300 to 600 m (1,000 to 2,000 ft), these pillars are likely to be failed on development, yet they are considered to be functionally successful. Referring to Figure 7, which is applicable for mining at a 450 m (1,500 ft) depth, it can be seen that if the excavation span across these pillars (pillar width plus two entry widths) is in the region of 25 m (80 ft), a W:H = 3 pillar would be loaded beyond its peak strength and would be considered to be failed, while a W:H = 4 pillar might actually still be in its pre-peak state. If more than one row of yield pillars were created, the effective span would increase and the ground response will change. If the span across the yield pillars was 45 m (150 ft) for example, the W:H = 3 pillar will yield up to a strain value of about 8% before equilibrium is achieved. This may result in unacceptable rib and roof conditions and the yield pillar system would be considered to be functionally failed. A yield pillar system using W:H = 4.0 pillars would be loaded beyond the peak strength and would be considered to be structurally failed, but since the vertical pillar strain is less than 2%, the conditions may well be acceptable and the system would be considered to be functionally successful.

This evaluation shows that yield pillars can be successfully used if the ground response is such that the pillars are not driven to excessive amounts of strain. The stiffness of the surrounding strata plays an important role in determining how far the pillars are driven beyond their peak strength. When the span-to-depth ratio is small, the ground response is stiffer and yield pillars are more likely to be successful.

The transition of a pillar from a pre-peak to post-peak, or yielded, condition has received much attention in the literature (Salamon, 1970; Ryder and Ozbay, 1990; Zipf, 2001). Comparing the local ground response to the post-peak slope of the pillars can assist in determining whether the transition will occur in a controlled or uncontrolled manner.

Pillars at the Extraction Line

When extracting pillars on retreat, the pillars at the extraction line become even more severely stressed; yet pillars are extracted successfully in spite of the elevated loading. It is possible to gain insight into the performance of the pillars under these conditions by comparing the ground response at the extraction line to the pillar stress-strain behavior and evaluating the likely success of the system using the ARMPS (Mark and Chase, 1997) method.

Figure 8 shows the calculated ground response curves at the pillar extraction line and under normal cover loading conditions, taken from Figure 6. The ground response curves were developed for a 150-m (500-ft) wide panel at a 450-m (1,500-ft) depth under strong overburden, which represents a typical deep pillar extraction layout. The pillar response curves have also been added to the chart. The likely pillar performance of the different pillars plotted on the chart can be examined:

a) The W:H = 3 pillars are likely to be wholly unsatisfactory because their peak resistance is well below the overburden pressure and they would be compressed to a vertical strain in excess of 10% while under development conditions, remote from the extraction line.
b) The W:H = 4 pillars are also likely to be unsatisfactory, the vertical strain will be about 7% when remote from the extraction line, and the ground pressure will drive the pillars to about 9% strain as the extraction line approaches. The ARMPS stability factor for this layout is 0.33, which falls well below the recommended value of 0.76 for mining at 450 m (1,500 ft) in strong rock, indicating that conditions are likely to by highly unsatisfactory.
c) The W:H = 6 pillars will be in a critical state of stability during development; they will be loaded just below their peak resistance, unexpected variation in the stress or pillar strength can result in structural failure of the pillars. As the extraction line approaches, the pillars will fail and equilibrium will be reached at about 5.5% vertical strain. The ARMPS stability factor is 0.55, predicting that it is unlikely that pillar extraction will be successful.
d) The W:H = 8 pillars will be in a pre-peak stress state under development conditions, remote from the extraction line. As the extraction line approaches, the pillars will be loaded beyond their initial peak and post-peak yielding will occur. At these relatively high stress values, the ground response is stiff and equilibrium is reached at a vertical strain value of 3.2%. This level of strain is likely to be acceptable, since several

case histories exist of successful pillar extraction under similar conditions. The calculated ARMPS stability factor for this layout is 0.76, which falls just below the recommended value of 0.8 for mining at this depth in strong roof conditions.

e) The W:H = 10 pillar will also be in a pre-peak state of stress during development and will yield with strain hardening when it is located at the pillar extraction line. The vertical strain will be 2.4%, which is likely to result in satisfactory ground conditions. The ARMPS stability factor for this layout is 1.03, which is well above the recommended value of 0.8.

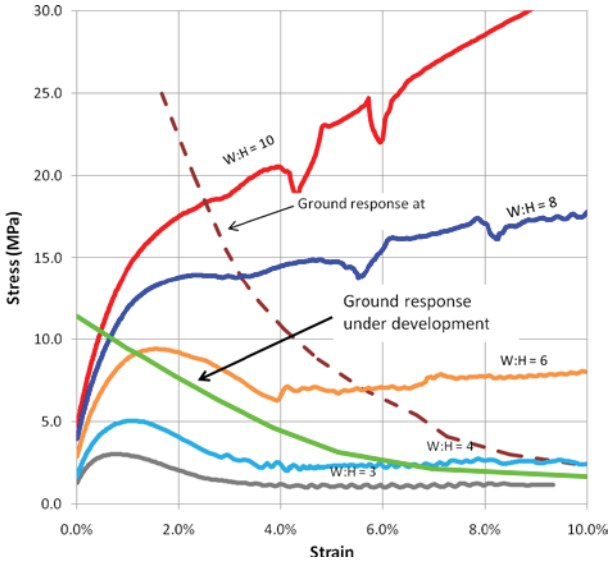

Figure 8. Pillar stress-strain curves and ground response curves at mid-span of a panel that is 150-m (500-ft) wide at 450-m (1,500-ft) depth of cover under strong overburden strata. Ground response curves are shown for development conditions and at the pillar extraction line.

The above results apply for a depth of 450 m (1,500 ft) and an isolated panel with a span of 150 m (500 ft) in strong strata. If the panel geometry, the overburden strength, or the depth-to-span ratio changes, the location of the ground response curve will also change, affecting the final stress and strain condition of the pillars. The importance of the slope of the ground response curve is clearly seen. When the ground response curve is elevated by an increase in the stress at the pillar extraction line, pillars may be driven to excessive strain values, which can result in the functional failure of the system.

Pillar Strain and Functional Failure

The assessment of the various panel layouts and pillar types shows that pillars that have been loaded beyond their peak resistance (structural failure) do not necessarily imply that functional failure has occurred. The ground response determines whether yielding pillars will be driven to excessive strain values and whether the conditions will be acceptable or not.

Comparing the pillar strain values to the ARMPS stability factors shows that for the situation modeled, there appears to be a relationship between the pillar strain and the ARMPS stability factor for yielding pillars at the extraction line. As the ground response drives the yielding pillars to greater strain values, the conditions are expected to deteriorate and successful pillar extraction is less likely to occur. Assessment of the ultimate strain of the pillars provides an improved insight into the likely functional performance of pillar systems. Further investigation of the relationship between the pillar strain and functional failure of pillar systems under various geologies and mining situations needs to be carried out to determine whether the pillar strain can be used as a design criterion for yielding pillars at the extraction line and in longwall mining applications.

CONCLUSIONS

The influence of the ground response curve on ultimate pillar loading and pillar deformation has been demonstrated. When the span-to-depth ratio is small or when the overburden consists of stiff-strong rocks, the ground response is stiffer, and pillar stress will be reduced when compared to the tributary area calculated stress. However, if the span-to-depth ratio increases or the overburden material is weaker and softer, the pillar loading may be closer to the tributary area stress.

The slope of the ground response curve also determines the ultimate deformation to which pillars, and particularly yielding pillars, will be driven. If the ground response is stiff, the ultimate pillar deformation will be smaller and may result in satisfactory mining conditions although the pillars may have yielded and would be considered to be structurally failed. However, if the ground response is soft, the yielding pillars can be driven to excessive deformation values and the mining conditions may become unacceptable.

The study confirmed the importance of the panel span on the ground response curve and the ultimate loading and deformation of pillars in a panel. The span-to-depth ratio has been added as an input parameter in the updated ARMPS-2010 design procedure (Mark 2010).

The ultimate deformation of a pillar provides insight into its likely functional success or failure. A review of pillar strains and calculated stability factors using the ARMPS (Mark and Chase, 1997) method showed that a relationship appears to exist between the ultimate pillar strain and the likely success of retreat mining.

Further research will be required to investigate the relationship between pillar strain and successful pillar layouts for a range of geologies and mining geometries. For example, the pillar stress-strain curves used in this paper assumed failure occurs within the coal only. Factors such as the potential impact of weak roof and floor strata on pillar response, the impact of side abutment loading from adjacent mining, and barrier pillar deformation should also be evaluated.

DISCLAIMER

The findings and conclusions in this paper have not been formally disseminated by the National Institute for Occupational Safety and Health and should not be construed to represent any agency determination or policy.

REFERENCES

Anon. (2007). Fast Lagrangian Analysis of Continua in 3-Dimension (FLAC3D V3.1). Itasca Consulting Group, Minnesota.

Barczak, T. M., Esterhuizen, G. S. and Dolinar, D. R. (2005). Evaluation of the Impact of Standing Support on Ground Behavior in Longwall Tailgates. Proceedings of the 24th International Conference on Ground Control in Mining, pp. 23–32.

Barrientos, G. and Parker, J. (1975). Use of the Pressure Arch in Mine Design at White Pine. Transaction, AIME *256*:1–8.

Brady, B. H. G. and Brown, E. T. (1985). Rock Mechanics for Underground Mining. George Allen and Unwin, London, 527 p.

Brown, E. T., Bray, J. W., Ladanyi, B. and Hoek, E. (1983). Ground Response Curves for Rock Tunnels, J of Geotechnical Eng *109*(1):15–39.

Esterhuizen, G. S., Mark, C. and Murphy, M. M. (2010). Numerical Model Calibration for Simulating Pillars, Gob and Overburden Response in Coal Mines. Proceedings of the 29th International Conference on Ground Control in Mining (to be published).

Iannacchione, A. T. and Zelanko, J. C. (1995). Occurrence and Remediation of Coal Mine Bumps: A Historical View. Proceedings of the Mechanics and Mitigation of Violent Failure in Coal and Hard-Rock Mines. Maleki, H., Wopat, P., Repsher, R., and Tuchman R., eds., USBM Special Publication 01-95, pp. 27–67.

Mark, C. (1993). Analysis of Longwall Pillar Stability (ALPS): An Update. Proceedings of the Workshop on Coal Pillar Mechanics and Design, U.S. Bureau of Mines IC 9315, pp. 238–249.

Mark, C. (2010). ARMPS 2010: Pillar Design for Deep Cover Retreat Mining. Proceedings of the Third International Workshop on Pillar Mechanics and Design, National Institute for Occupational Safety and Health, to be published.

Mark, C., Chase, F. E. and Molinda, G. M. (1994). Design of Longwall Gate Entry Systems Using Roof Classification. Proceedings of the U.S. Bureau of Mines Technology Transfer Seminar, New Technology for Longwall Ground , U.S. Bureau of Mines SP 01-94, pp. 5–17.

Mark, C., Listak, J. and Bieniawski, Z. T. (1988). Yielding Coal Pillars Field Measurements and Analysis of Design Methods. Proceedings of the 29th U.S. Symposium on Rock Mechanics (USRMS), Minneapolis, MN.

Mark, C. and Chase, F. E. (1997). Analysis of Retreat Mining Stability (ARMPS). Proceedings of the New Technology for Ground Control in Retreat Mining, NIOSH IC 9446, pp 17–34.

Medhurst, T. P. and Reed, K. (2005). Ground Response Curves for Longwall Support Assessment, Trans. Inst. Min. Metall. A, Mining Technology, *114*:A81–88.

Pappas, D. M. and Mark, C. (1993). Behavior of Simulated Gob Material. U.S. Bureau of Mines RI 9458.

Peng, S. S. (2008). Coal Mine Ground Control, Third Edition, West Virginia University, WV, 750 p.

Rabcewicz, L. (1965). Die Neue Österreichische Tunnelbauweise, Entstehung, Ausführungen und Erfahrungen, Der Bauingenieur, 40. Jg., Heft 8, 1965.

Ryder, J. A. and Ozbay, M. U. (1990). A Methodology for Designing Pillar Layouts for Shallow Mining. Proceedings of the ISRM International Symposium on Static and Dynamic Considerations in Rock Engineering, Swaziland, pp. 273–286.

Salamon, M. D. G. (1970). Stability, Instability and Design of Pillar Workings. Int. J. Rock Mech. and Min. Sci. *7*:613–631.

Zipf, R. K. (2001). Pillar Design to Prevent Collapse of Room-and-Pillar Mines, In Underground Mining Methods: Engineering Fundamentals and International Case Studies. W.A. Hustrulid, R.C. Bullock, eds., Society for Mining Metallurgy and Exploration, pp. 493–511.

AUTHOR'S INDEX